Viral Modulation of the anti-Glioblastoma Immune Response:

Rewiring Host Immunity to Recognize & Kill Brain Cancer

Nicole Mihelson

University of Oxford

Medical Sciences Division

St John's College

A Thesis Submitted for the Degree of

Doctor of Philosophy

Michaelmas 2022

Abstract

Nicole Mihelson | DPhil Thesis Abstract | St John's College | Michaelmas 2022

Glioblastoma (GBM) is a universally fatal solid malignancy of the central nervous system (CNS), hallmarked by a high mitotic index, intercellular heterogeneity, and low neoantigen burden. Standard of care including surgery, radiation, and chemotherapy has failed to improve life expectancy beyond 15 months. The utility of local therapies is limited by the invasive nature of GBM, its protection behind the blood-brain barrier (BBB), and the absence of a single, druggable pathway. Advancing GBM therapies will likely require immune-based strategies given the ability of immune cells to traverse the BBB and evolve with the changing mutational landscape of the tumor. To this end, we employed a syngeneic murine GBM model, SB28, that recapitulates the highly inflamed environment observed in the brain following surgical resection and that enables tracking by intravital two-photon (2P) microscopy. We uncovered that absent any additional immune stimulus, a negligible amount of tumor antigen is drained to the nodes and virtually no tumor-specific immune response is mounted. To stimulate anti-tumor immunity, we administered a noncytopathic arenavirus (lymphocytic choriomeningitis virus) into circulation that expressed the tumor antigen, Ovalbumin. This infection profoundly altered the tumor immune landscape, led to antigen drainage, tumor-specific lymphocyte expansion in the nodes and trafficking to the tumor milieu, resulting in significant extension on survival.

Acknowledgements

I am grateful to my mentors – Fiona Powrie and Dorian McGavern – and the Rhodes Trust and National Institutes of Health Intramural Research Program, NINDS (Yvette Pittman), and the NIH Ox-Cam PhD program, for the openness to my scientific curiosity, the resources to support my DPhil, the teaching, the mentorship, and the commitment to leadership they've shown me over the course of my studies.

Thank you to my lab mates Patrick Duncker, Monica Buckley, Taz Zhou, and Panos Mastorakos for their collaboration in lab, their experimental support, thought partnership, and meaningful friendship.

I would also like to thank the mentors I've been fortunate to call my own over the years – Hernando Lopez-Bertoni, John Laterra, Sara B. Johnson, and Daniel Reich (and the entire Reich family, especially Walter). I could spend the rest of my career paying forward the debt of gratitude I owe them for their belief in me, the early opportunities, the friendship, and the steadfast support.

My deepest gratitude is to my Family.

Collaborator Contributions

I was fortunate to receive the support of various collaborators for this Thesis. Their specific contributions are outlined below:

Generation of SB28-Ova cell line: Vanja Lazarevic

FACS sorting: Dragan Maric

Single Cell Sequencing Analysis: Kory Johnson

Introduction Figure Illustrations: Alan Hoofring and Ethan Tyler in the NIH Medical Arts Design Section

Table of Contents

1 INTRODUCTION 1

1.1 THE UNIQUENESS OF GBM AND NEED FOR AN IMMUNOLOGICAL PERSPECTIVE 1

1.1.1 THE MYELOID COMPARTMENT 7
1.1.1.1 THE GBM LANDSCAPE IS MYELOID-CELL CENTRIC 7
1.1.1.2 MICROGLIA 8
1.1.1.2.1 MICROGLIA ARE THE MOST COMMON MYELOID CELL AT THE TUMOR MARGIN 8
1.1.1.2.2 MICROGLIA MAY PLAY OPPOSING ROLES IN GBM 10
1.1.1.3 MONOCYTES / MACROPHAGES 11
1.1.1.3.1 MONOCYTIC POPULATIONS ARE DYSREGUALTED IN THE BLOOD OF GBM PATIENTS 11
1.1.1.3.2 THE MYELOD INFILTRATE IN THE GBM CORE IS MOSTLY MACROPHAGES 15
1.1.1.3.3 INFILTRATION BY MELOID CELLS INCONSISTENTLY CORRELATES WITH SURVIVAL 19
1.1.1.3.4 GBM SIGNALS TO THE PERIPHERY TO ATTRACT MONOCYTES 20
1.1.2 NEUTROPHILS 22
1.1.2.1 NEUTROPHILS IN THE TUMOR NICHE ARE LIKLEY DELETERIOUS 22
1.1.2.2 NEUTROPHILIA IS COMMON IN GBM PATIENTS 23
1.1.3 DENDRITIC CELLS (DCs) 23
1.1.4 T CELLS 24
1.1.4.1 EFFECTOR T CELLS 24
1.1.4.1.1 THE PHENOTYPE OF EFFECTOR T CELLS IN THE TUMOR SUGGESTS FEW ARE GBM-SPECIFIC 25
1.1.4.1.2 EFFECTOR T CELLS IN THE PERIPHERY ARE QUANTITATIVELY, BUT NOT QUALITATIVELY DIFFERENT IN GBM PATIENTS 28
1.1.4.2 REGULATORY T CELLS 29
1.1.4.2.1 THE CURRENT LITERATURE SUGGESTS AN OVERSTATE ROLE FOR TREGS IN GBM 29
1.1.5 NATURAL KILLER (NK) CELLS 30
1.1.5.1 NK CELLS HAVE YET TO FULFILL THEIR PROMISE IN KILLING GBM CELLS IN APPRECIABLE NUMBERS 30
1.1.6 B CELLS 31
1.1.6.1 B CELLS HAVE UNTAPPED POTENTIAL IN GBM 31
1.1.7 CONCLUDING REMARKS 32

1.2 VIRUSES IN THE ETIOLOGY AND POTENTIAL TREATMENT OF GBM 34

1.2.1 ENDOGENOUS VIRUSES FOUND IN GBM 35
1.2.1.1 CYTOMEGALOVIRUS (CMV) 35
1.2.1.2 EPSTEIN-BARR VIRUS (EBV) 37
1.2.1.3 HUMAN ENDOGENOUS RETROVIRUSES (HERVs) 38
1.2.1.4 EXPLOITING ENDOGENOUS VIRUSES IN GBM FOR TREATMENT 38
1.2.2 ONCOLYTIC VIRAL THERAPY 44
1.2.3 CONCLUDING REMARKS 50

2 MATERIALS AND METHODS 51

2.1 *IN VIVO* EXPERIMENTS 51

2.1.1 MICE 51
2.1.1.1 MOUSE TRANSGENIC MODELS 51

2.1.1.2 INTRACEREBRAL TUMOR INJECTIONS 52
2.1.1.3 VIRAL INFECTIONS 53
2.1.1.4 SURVIVAL STUDIES 54
2.1.1.5 T CELL ISOLATION AND ADOPTIVE TRANSFERS 54
2.1.2 INTRAVITAL TWO PHOTON MICROSCOPY (2P) 55
2.1.2.1 SKULL THINNING 56
2.1.2.2 INTRAVITAL IMAGING 56
2.2 HIGH-PARAMETER FLOW CYTOMETRY (FACS) 58
2.2.1 CELL ISOLATION FROM THE BRAIN 58
2.2.2 CELL ISOLATION FROM THE SPLEEN AND LYMPH NODES 59
2.2.3 CELL ISOLATION FROM THE BLOOD 60
2.2.4 FACS STAINING 60
2.2.5 FACS ANALYSIS 63
2.3 IMMUNOHISTOCHEMISTRY (IHC) 63
2.3.1 STAINING 63
2.3.2 IMAGE ACQUISITION AND ANALYSIS 64
2.4 SINGLE-CELL SEQUENCING 65
2.4.1 scRNA-SEQ LIBRAY PREPARATION, SEQUENCING, AND ANALYSIS 65
2.5 CELL CULTURE 67
2.5.1 CELL LINE TRANSDUCTION 67
2.6 STATISTICAL ANALYSIS 68
3 CHAPTER 5: THE ANATOMY, IMMUNOLOGY, AND RELATIVE UTILITY OF TWO SYNGENEIC MURINE MODELS OF GBM 69
3.1 THE NEED FOR A HIGHER FIDELITY SYNGENEIC MODEL OF GBM 69
3.1.1 GL261 MODEL BACKGROUND 69
3.1.2 SB28 MODEL BACKGROUND 71
3.2 OPTIMIZATION OF TUMOR MODEL FOR THIS THESIS 72
3.2.1 RECREATING THE POST-SURGERY INFLAMMATORY MILIEU 72
3.2.1.1 INFLAMMATION IN THE IMMEDIATE AFTERMATH OF "SURGERY" 73
3.2.1.2 ENABLING CONSISTENT TUMOR ENGRAFTMENT WITH THE MINIMUM NUMBER OF TUMOR CELLS 75
3.2.2 DEPTH OF INJECTION TO ENABLE CONSISTENT VISIBLITY BY TWO-PHOTON .. 76
3.2.3 OPTIMIZING THE PUNCH BIOPSY FOR EARLY TIME POINT-FLOW CYTOMETRY 78
3.2.4 MODEL SYNTHESIS & EXPERIMENTAL WORKFLOW 81
3.3 HIGH-PARAMETER IMMUNE PHENOTYPING OF SB28 AND GL261 82
3.3.1 EARLY TIME POINT FACS PROFILING: DAY 5 83
3.3.2 MID TIME POINT FACS PROFILING: DAY 10 87
3.3.3 MORPHOLOGICAL DIFFERENCES BETWEEN GL261 AND SB28 90
3.3.3.1 HEMORRHAGE 90
3.3.3.2 ANATOMICAL DIFFERENCES IN THE INTERPLAY BETWEEN TUMOR MODEL AND ITS MILIEU 92
..... 95
3.4 SUMMARY 96
4 CHAPTER 4: MODULATION OF THE ANTI-TUMOR IMMUNE LANDSCAPE BY VIRAL INFECTION 99
4.1 THE PROMISE OF VIROTHERAPY AND THE RATIONALE BEHIND LCMV 99

4.2 SYSTEMIC ADMINISTRATION OF LCMV IN TUMOR-BEARING MICE LEADS TO EXTENDED SURVIVAL AND TUMOR-SPECIFIC VIRAL INFECTION 101
4.2.1 LCMV INDUCES MARKEDLY ALTERS THE SB28 IMMUNE LANDSCAPE..... 104
4.2.2 TUNING THE KINETICS AND STRENGTH OF THE LCMV-SB28 IMMUNE RESPONSE 107
4.2.2.1 TITRATING THE STRENGTH OF VIRAL INFECTION AND CTL RESPONSE.. 107
4.2.2.2 ANTI-VIRAL CTL IN THE BRAIN 108
4.2.2.3 ANTI-PD1 THERAPY DOES NOT INCREASE SURVIVAL..... 110
4.2.3 ANTIGEN PRESENTATION TO COGNATE CYTOTOXIC T CELLS 111
4.3 LCMV FAILS TO PROMOTE SUSTAINED ANTI-TUMOR IMMUNITY 113
4.3.1 LCMV IS CLEARED FROM THE TUMOR MILIEU BY DAY 14..... 113
4.3.2 SINGLE-CELL SEQUENCING OF CONTROL AND INFECTED SB28 TUMORS, AND THEIR IMMUNE COMPARTMENTS 115
4.3.2.1 WITHIN THE INFECTED TUMOR IMMUNE LANDSCAPE, CD8 T CELLS SHOW THE MOST PROFOUND CHANGE IN FUNCTION OVER TIME..... 116
4.4 SUMMARY 122
5 CHAPTER 4: PARADIGM TO SIMULTANESOULY TRACK ANTI-VIRAL AND ANTI-TUMOR IMMUNITY 124
5.1 SB28-OVA ENABLES TRACKING OF THE TUMOR-SPECIFIC T CELL RESPONSE 124
..... 125
5.1.1 SB28-GFP AND SB28-OVA HAVE IDENTICAL SURVIVAL PROFILES..... 125
..... 126
5.1.2 SB28-OVA ENABLES TRACKING OF ANTIGEN DRAINAGE AND PERIPHERAL IMMUNE RESPONSE..... 126
5.1.2.1 ABSENT VIRAL INFECTION, THERE IS VIRTUALLY NO ANTIGEN DRAINED NOR ANTI-TUMOR IMMUNE RESPONSE 126
5.2 LCMV INFECTION POSSESSING A TUMOR ANTIGEN MIMIC 131
5.2.1 rLCMV-Ova INFECTION EXTENDS SURVIVAL IN SB28-OVA-BEARING MICE 132
5.2.1.1 AUGMENTING PRESENTATION OF TUMOR NEOANTIGEN ON THE CELL SURFACE 134
..... 138
5.2.2 MONITORING TUMOR-T CELL ENGAGEMENT IN THE SB28-OVA/LCMV-OVA PARADIGM 138
5.3 SUMMARY 141
6 DISCUSSION.....142
6.1 THE CANCER IMMUNITY CYCLE REVISTED 142
6.2 LCMV AS A TOOL TO OVERCOME GBM-IMMUNE RESPONSE CHALLENGES 145
6.3 FUTURE DIRECTIONS 148
6.4 CLINICAL RELEVANCE 152
6.5 CONCLUDING SYNTHESIS.....154
7 REFERENCES 156

Abbreviations

Glioblastoma	GBM
Central Nervous System	CNS
Immune Checkpoint Therapy	ICT
Glioma Stem Cell	GSC
Vascular Endothelial Growth Factor	VEGF
Tumor Microenvironment	TME
Major Histocompatibility Complex	MHC
Human Leukocyte Antigen	HLA
Myeloid Derived Suppressor Cell	MDSC
Damage Associated Molecular Patterns	DAMPs
Pathogen Associated Molecular Patterns	PAMPs
Programmed Cell Death Protein (Ligand) 1	PD1/PDL1
Antigen Presenting Cell	APC
Days post infection/implantation	dpi

1 INTRODUCTION

Note: Components of this Introduction were adapted from a Review:

Mihelson, N and McGavern DB. 2021. "Viral Control of Glioblastoma." *Viruses* 13 (7).

1.1 THE UNIQUENESS OF GBM AND NEED FOR AN IMMUNOLOGICAL PERSPECTIVE

Glioblastoma (GBM) is a universally fatal solid malignancy of the central nervous system (CNS), and the most common adult brain tumor. It is hallmarked by a high mitotic index, extraordinary intratumoral heterogeneity (Muller et al., 2017; Neftel et al., 2019), and low neoantigen burden (Vogelstein et al., 2013; J. Zhang et al., 2019). Standard of care, including gross total resection, radiation, and chemotherapy, has failed to improve life expectancy beyond 15 months. Drug development efforts against GBM have largely been plagued by a dearth of high-fidelity preclinical models, the diffuse "sand-in-the-grass" nature of the disease, GBM's relative protection behind the blood-brain barrier (BBB), and the absence of a single, druggable pathway due in part to subsets of cancer stem cells that drive the aforementioned intratumoral heterogeneity (Lim et al., 2018; Neftel et al., 2019; Sampson et al., 2020). That the prognosis of GBM has hardly improved over the past two decades is not for lack of trying. Scientists and clinicians have employed various strategies, including but not limited to antisense oligonucleotides targeting immunosuppressive chemokines (e.g. TGFß) (Brandes et al., 2016), wearable tumor treating fields that impair cell division (Stupp et al., 2017), peptide and dendritic cell vaccines (Phuphanich et al., 2013), immune checkpoint therapy (ICT) (Filley et al., 2017; Reardon et al., 2017), and the most promising – oncolytic

virotherapy (Markert et al., 2014; Mihelson & McGavern, 2021). These efforts notwithstanding, GBM is notoriously adept at dodging anti-tumor immunity. Ultimately, the immunology of GBM must be considered within the context of both the tumor itself as well as the unique anatomy of the CNS. Advancing effective therapeutics will likely require that GBM be carefully studied through the lenses of neuroimmunology and neuroanatomy, rather than the cellular biology of single mutations and pathways as has been the case for the past three decades.

Glioblastoma harbors subsets of stem-like cells (GSCs) that are therapeutically resistant and multipotent. Together with highly plastic differentiated tumor cells, GSCs obviate endeavors to target a single pathway or tumor antigen and give rise to incredibly heterogeneous tumors (Dirkse et al., 2019; Lopez-Bertoni et al., 2016; Neftel et al., 2019; Wang et al., 2010; Wang et al., 2018). There is also great inter- and intra-patient heterogeneity at the level of the tumor's infiltrating immune cells, and this landscape changes with selective pressure from therapies such chemo- and radiotherapy (Darmanis et al., 2017; Martinez-Lage et al., 2019; Qianghu Wang et al., 2017). Moreover, the immune landscape of GBM is significantly different from that of brain metastases in comparable niches, suggesting local, tumor-specific shaping of the immune response (Friebel et al., 2020). Additionally, relative to other neoplasms, GBM has fewer neoantigens available to activate the immune system (Vogelstein et al., 2013). While immunotherapies have become prominent in treating many peripheral tumors, the CNS presents unique challenges to the immune system, including its elaborate barriers and restrictive options for lymphatic drainage of tumor antigen.

The described glioblastoma cell-intrinsic challenges are rivaled only by the obstacles conferred by this tumor's intracranial confines. At steady state, the brain is one of a few

unique tissues that does not participate in conventional efferent and afferent modes of immune surveillance (Engelhardt et al., 2017) (**Figure 1-1**). Conventional lymphatic vessels exist along the venous sinuses in the dura mater – the outermost layer of the meninges (Ji Hoon Ahn et al., 2019; Andres et al., 1987; Antoine Louveau et al., 2015; Waggener & Beggs, 1967). These lymphatic vessels are thought to drain cerebrospinal fluid (CSF) found in the subarachnoid space, ventricles, and perivascular spaces of the brain (**Figure 1-1**). The immunological landscape of these compartments is very different, however, from the brain parenchyma. For example, the meninges are inhabited by a plethora of innate and adaptive immune cells, including T cells, B cells, NK cells, innate lymphoid cells, and dendritic cells, among others. By contrast, the brain parenchyma is surveyed almost exclusively by microglia. Microglia do not migrate and present antigen in the cervical lymph nodes, and the degree to which parenchymal antigen drains into the CSF and ultimately to the lymph nodes is quite limited (Morris et al., 2016; Song et al., 2020). Indeed, the anatomy and immunology of these disparate compartments explain findings from nearly a century ago, in which tumors injected into fluid spaces but not into the parenchyma were rejected in animal models (Murphy & Sturm, 1923). These fluid spaces as well as the vasculature of the brain are separated from the parenchyma by various membranes composed of endothelial, epithelial, and/or glial cells (Mastorakos & McGavern, 2019). Therefore, even if immune barriers were to be overcome and proper drainage and presentation of tumor antigen achieved (Song et al., 2020), mounting an efferent immune response capable of penetrating and remaining behind the blood brain barrier (BBB) is a significant challenge (Sarkaria et al., 2018).

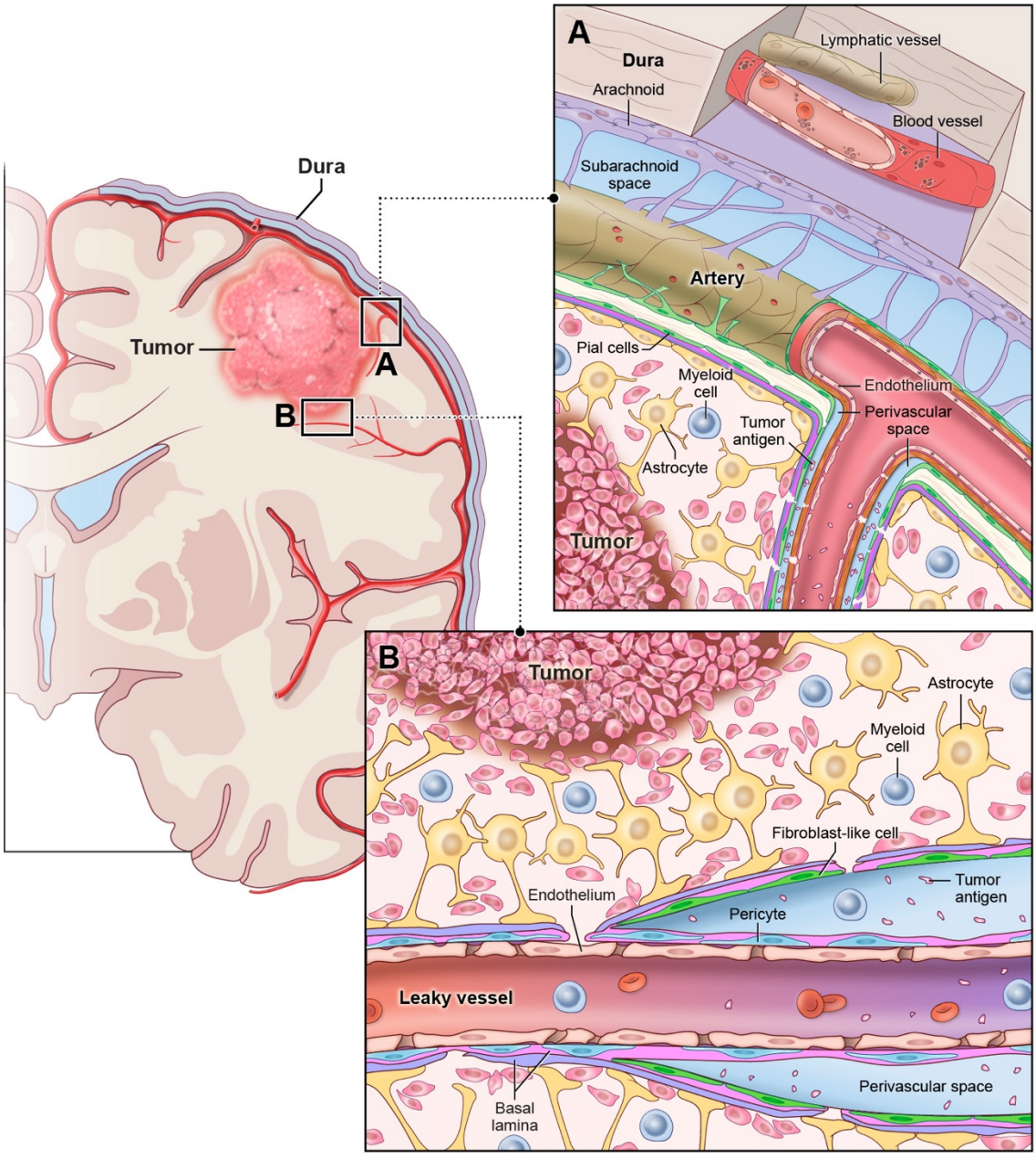

Figure 1-1: Barrier structures prevent the egress of sufficient tumor antigen to the draining nodes. Though the paradigm of a completely immune privileged brain has been recently called into question, the fact remains that the brain parenchyma lacks classic lymphatic drainage, thus making this CNS compartment the ideal cover for neoplasms. Lymphatic vessels in the dura surveil antigen in the outermost layer of the tripartite meninges, but barriers such as the arachnoid and the pia prevent any meaningful sampling of antigen derived from the relatively sealed off brain parenchyma. Data from the Iwasaki lab show that in the absence of supraphysiologic expansion of lymphatic vessels via VEGF-C administration and considerable disruption of barriers via injection, there is minimal tumor antigen drainage (Song et al., 2020). Our own unpublished data show virtually no expansion of tumor-specific T cells in tumor-bearing mice, suggesting that the bits of antigen that do enter the perivascular space and blood stream through disrupted barriers and leaky vessels, respectively, is materially diluted such that the immune response mounted in the cervical nodes is grossly insufficient.

In glioblastoma, and particularly following surgical resection, there is an appreciable violation of the BBB due to GBM-mediated tissue damage and leaky vessels. However, access to the peripheral vascular and lymphatic circulation is still not comparable to that available to other cancers of the body; the brain parenchyma has further evolved ways to compartmentalize insult and injury of all kinds **(Figure 1-2).** This *relative* privilege plays a significant role in shaping the immune response to GBM. At present, relatively little is known about the immune response to glioblastoma, and how it can best be wielded in a therapeutic context. Immunological studies rooted in both the human disease with functional validation in relevant models are lacking. It is also crucial that glioblastoma be studied from a neuroimmunological perspective to advance therapeutic strategies.

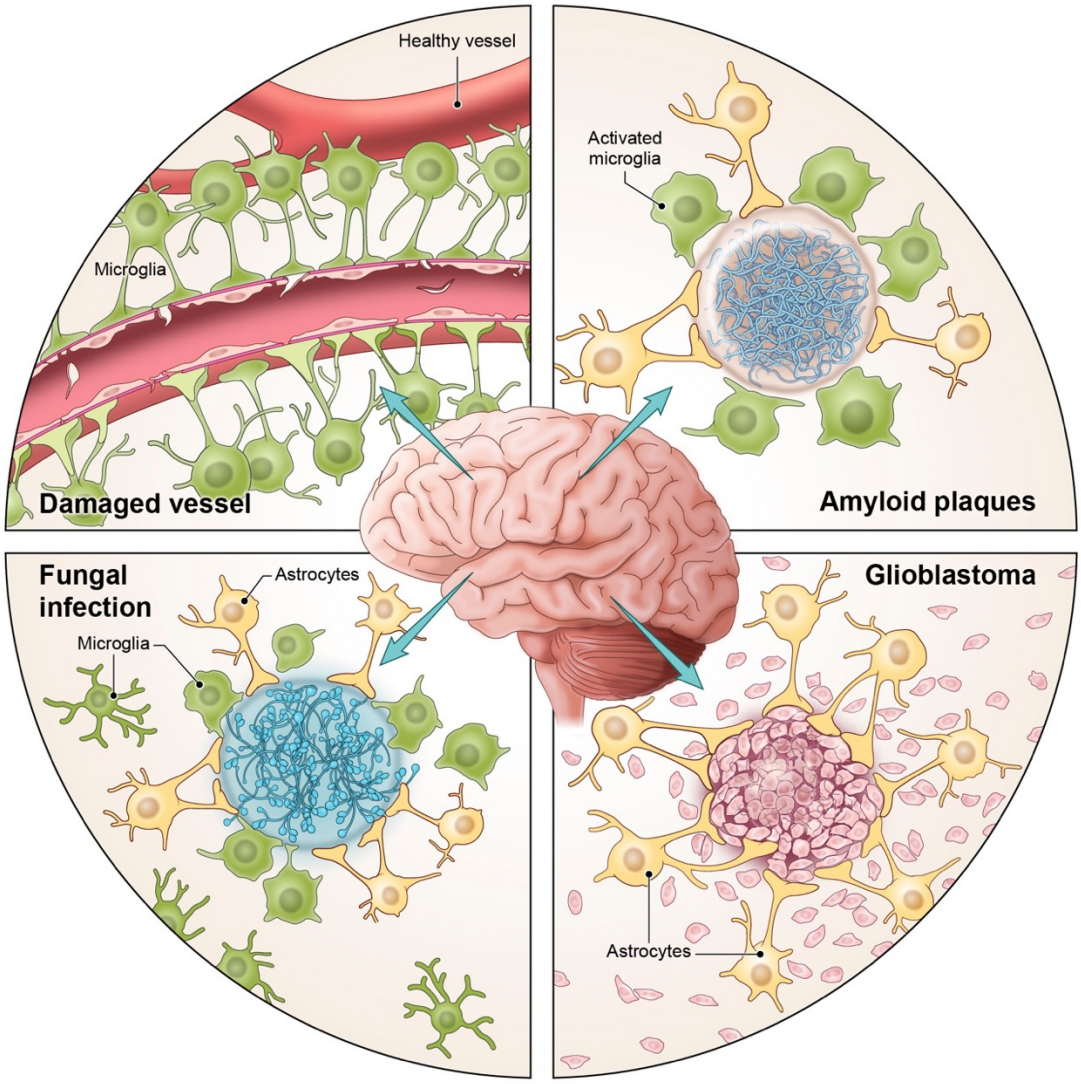

Figure 1-2: Compartmentalization of insult and injury. In the service of self-preservation, the brain has evolved ways to compartmentalize a variety of injuries – sterile and otherwise. These mechanisms of sealing off injury, infection, toxic aggregates, and tumors suggest an effort on the part of brain-resident leukocytes and glial cells to prevent the spread of injury. Our lab and others have shown by intravital two-photon microscopy and immunohistochemistry that in response to cerebrovascular injury, microglia project their processes toward injured blood vessels, forming tubular structures that envelop the vessels and containing leaking vasculature (Mastorakos, Mihelson, et al., 2021). These so-called "rosettes" represent the first line of defense against this injury, the absence of which leads to significantly more hemorrhaging. Similar themes have emerged in the context of infection. The fungus Candida albicans, upon crossing the blood brain barrier (BBB), triggers a neuroinflammatory cascade that the brain then attempts to dampen by sealing off the fungus in granuloma-like structures. In the context of neurodegeneration, several groups have observed the positioning of resident microglia around deposits of disordered protein. We have also observed astrocytes attempting to create a glial scar around intracranial GBM models. In the context of this neoplasm, aggressive growth outpaces the brains capacity to "wall off" the cancer, resulting in both insufficient anti-tumor immune responses and universal fatality.

1.1.1 THE MYELOID COMPARTMENT

1.1.1.1 THE GBM LANDSCAPE IS MYELOID-CELL CENTRIC

The immune infiltrate of GBM ranges from ~8% (de Groot et al., 2020; Goswami et al., 2020) to 50% (Darmanis et al., 2017) of all viable cells. Within the immune infiltrate, 60-95% of cells are microglia/macrophages (Darmanis et al., 2017; Fu et al., 2020). It is worth noting that these two cell populations have been historically reported together, and methods that enable their differentiation are relatively new. Some of the earliest studies on glioma immunology indicated that up to one third of all cells in the tumor microenvironment (TME) were microglia/macrophages (Morimura et al., 1990) and that the extent of microglia/macrophage infiltration increased with tumor grade (Roggendorf et al., 1996). These findings led to the suggestion that microglia/macrophages play a role in promoting immune suppression and tumor invasion (Hussain et al., 2006; Wei et al., 2013). This hypothesis was bolstered by subsequent studies in which the M1/M2 paradigm of macrophage polarization was applied to brain microglia/macrophage populations (Gabrusiewicz et al., 2015; Komohara et al., 2008; Prosniak et al., 2013). Specifically, *in vitro* experiments using tumor-conditioned media were used by several groups to demonstrate that myeloid cells were induced to express "phenotypic M2 markers", were unable to appropriately stimulate T cells, and when co-incubated with tumor cells, further induced tumor cell secretion of immunosuppressive cytokines such as TGF-β and IL-10 (Wu et al., 2010). The widespread adoption of this "immunosuppressive myeloid compartment" hypothesis led in part to the unsuccessful attempts to antagonize tissue resident microglia in GBM patients (Butowski et al., 2016).

Recently, the first comprehensive characterization of the human GBM myeloid infiltrate was published (Gabrusiewicz et al., 2016). This study challenged the preceding dogma that microglia/macrophages were crucial promoters of tumor growth and showed that GBM-associated microglia and macrophages are in fact most closely aligned with a nonpolarized M0 phenotype. This finding underscores the potential to modulate this dominant GBM-infiltrating cell subset with the appropriate therapeutic manipulation.

1.1.1.2 MICROGLIA

1.1.1.2.1 MICROGLIA ARE THE MOST COMMON MYELOID CELL AT THE TUMOR MARGIN

GL261 is the most used syngeneic murine model of glioblastoma, but the model has few parallels to the human disease (Lenting et al., 2017), other than the fact that both GBM and GL261 are fatal glial neoplasms. Nonetheless, this murine model has been used extensively to speculate about the immune infiltrate of glioblastoma. Although studies using GL261 cells indicate that resident microglia represent only 15% of myeloid cells in the TME (Chen et al., 2017), recent profiling studies of human GBM provide a different and more nuanced picture. Specifically, the current consensus is that while only 20-30% of the myeloid cells in the tumor core are microglia, that figure rises to 80% in the tumor margins (**Figure 1-3**) (Pinton et al., 2019). Notably, other studies that have not looked at separate niches within the tumor report that 40-75% of the myeloid compartment in GBM is comprised of microglia (Friebel et al., 2020; Gabrusiewicz et al., 2016; Goswami et al., 2020; Sankowski et al., 2019). It is important to note that GBM harbors numerous microanatomical niches (e.g., necrotic, microhemorrhaging, actively mitotic, core, periphery). Though many of the

immune populations in this thesis are introduced as monolithic groups, their plasticity and response to their environment should not be overlooked. In fact, pronounced transcriptomic differences within immune populations from the same tumor are well-documented (Darmanis et al., 2017).

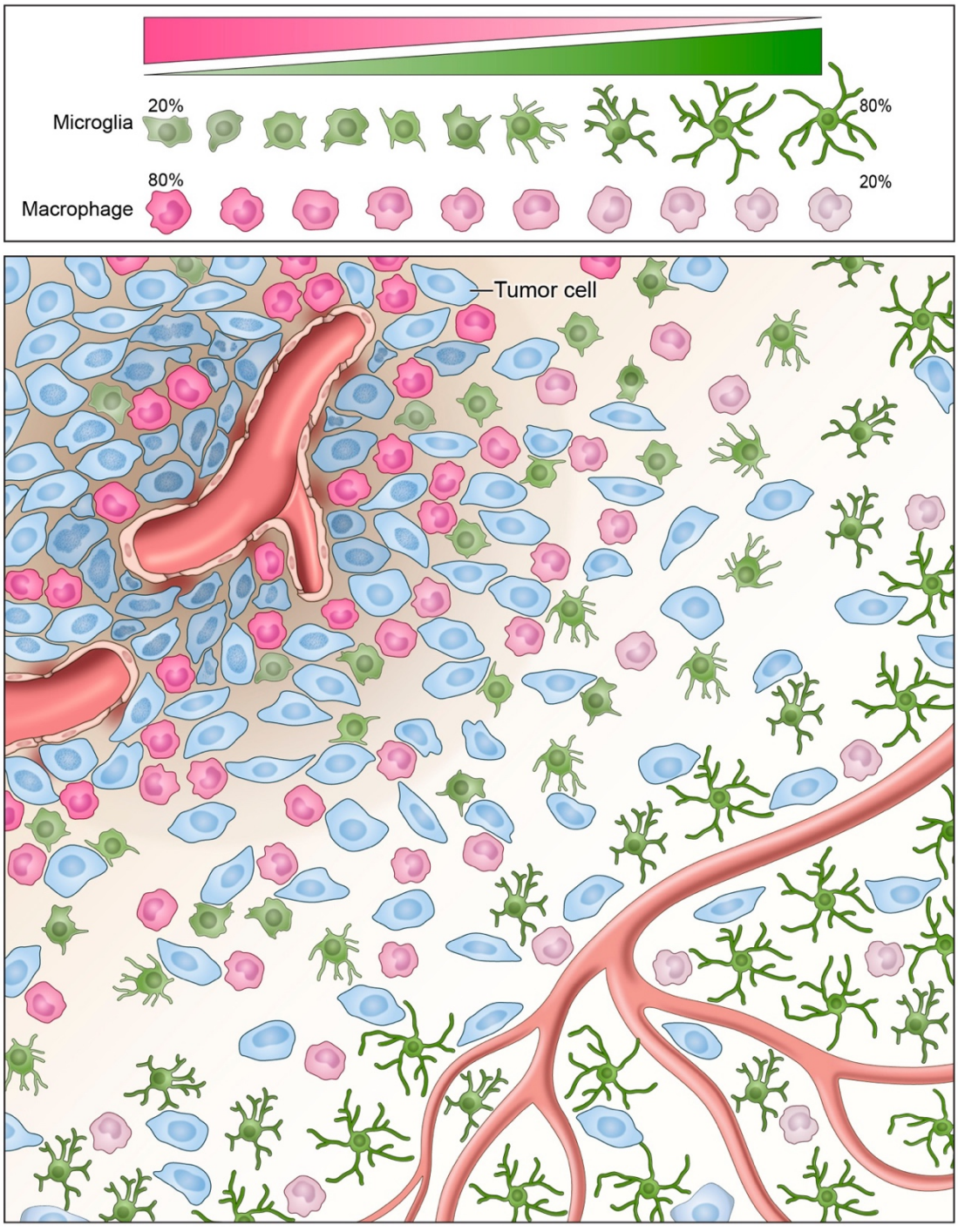

Figure 1-3: The GBM infiltrate is myeloid-centric. 60-95% of the entire tumor immune infiltrate is comprised of peripherally derived macrophages and brain-resident microglia. Indeed, up to one third of all cells in the TME are myeloid. The core of the tumor is made up of primarily macrophages and the periphery, microglia. RNA sequencing has suggested a gradient of inflammation such that the core macrophages are immunosuppressive and the more peripheral microglia are still attempting to mount an anti-tumor response. Indeed, macrophages from the core suppress T cell proliferation *in vitro* significantly more than microglia from the core or either microglia or macrophages from the periphery. These differences underscore the regional heterogeneity and local environmental cues that drive important differences in the immune landscape of GBM.

1.1.1.2.2 MICROGLIA MAY PLAY OPPOSING ROLES IN GBM

In a recent study, single-cell sequencing of microglia from GBM tissue and healthy age matched controls revealed 14 distinct microglial clusters, three of which were enriched in control samples and two of which were almost exclusively derived from GBM microglia (Sankowski et al., 2019). GBM-associated clusters revealed a downregulation of core microglia genes such as CX3CR1 and an upregulation of metabolic, inflammatory, aging, interferon, and angiogenesis-associated genes such as CD163, APOE, IFITM3, and VEGFA. GBM is a highly vascularized tumor that can even transdifferentiate into neoplastic blood vessels and decreasing the formation of new vessels with anti-Ang2/VEGF antibodies or by targeting microglia has been shown to decrease GBM growth in animal models (Atzori et al., 2017; Brandenburg et al., 2016; Kloepper et al., 2016; Ricci-Vitiani et al., 2010; Turkowski et al., 2018). Unfortunately, anti-VEGF antibody therapy in human GBM (Bevacizumab) does not increase overall survival due to a variety of compensatory and resistance mechanisms (Ahn et al., 2016; Kloepper et al., 2016). Thus, a more targeted approach is warranted to abrogate VEGF production in the tumor microenvironment. One option would be to specifically target the pro-angiogenic subset of microglia.

There is an overall lack of functional and mechanistic data pertaining to microglia in human GBM. This is due in part to the fact that human microglia do not survive well *ex vivo*. However, studies conducted in the murine GL261 model support the notion that microglia are 'edited' by GBM. For example, tumor cells secrete extracellular vesicles (EVs) containing functional microRNAs and proteins. These EVs are taken up by microglia and can influence their functional state by promoting proliferation, influencing their cytokine profile, etc. (Abels et al., 2019; Tsui et al., 2012015). GBM also express myeloid checkpoint molecules such as CD47, which engages SIRPα on microglia / macrophages and serves as a 'don't eat me' signal. While inhibiting this interaction increases microglial phagocytosis, it is only modestly efficacious in promoting GBM clearance in mice (Hutter et al., 2019).

In contrast to the microglia-mediated immunosuppression described above, GBM microglia were also shown to highly express transcripts related to TAP-independent cross-presentation, antigen processing, as well as presentation on MHC II (Sankowski et al., 2019). Similarly, another study has shown that microglia displayed an "immunostimulatory" gene signature at the single cell level (Goswami et al., 2020). It is important to note, however, that most microglia isolated from GBM patients cluster with those from healthy patients; only a small fraction display the pro-angiogenic or immunostimulatory transcriptomes described here (Darmanis et al., 2017; Sankowski et al., 2019).

1.1.1.3 MONOCYTES / MACROPHAGES

1.1.1.3.1 MONOCYTIC POPULATIONS ARE DYSREGUALTED IN THE BLOOD OF GBM PATIENTS

Several studies have confirmed that there are elevated numbers of monocytes and myeloid derived suppressor cells (MDSCs) ($CD33^+$, $MHCII^-$ cells) in the blood of GBM patients (Alban et al., 2018; Gabrusiewicz et al., 2016; Gielen et al., 2015; Harshyne et al., 2016) **(Figure 1-4).** Steroids such as dexamethasone, which are often prescribed to GBM patients to manage edema, exacerbate the increase in peripheral MDSC counts but not in monocyte counts (Gabrusiewicz et al., 2016). $CD14^+$ myeloid cells (presumed monocytes) isolated from the blood of GBM patients and compared to those from healthy donors showed elevated expression of transcriptions factors, proteases, and cytokines, including *CEBPB*, *IRF8*, *MYCC*, *NFKB*, *STAT3*, *MMP9*, and *IL10*; by contrast *IRF4*, *KLF2*, *MHCII*, *CCL2*, *IL23*, *TNFα*, *IL1β*, and *MIP1A* were all downregulated (Gabrusiewicz et al., 2016). From this differential gene expression profile, it is difficult to infer the differentiation or activation state of these circulating myeloid cells. However, upregulation of *MMP9* and *IL10* with concomitant downregulation of *TNFα* and *IL1β* may suggest that these cells are poised to execute wound repair or immunoregulatory responses as opposed to immuno-stimulatory ones.

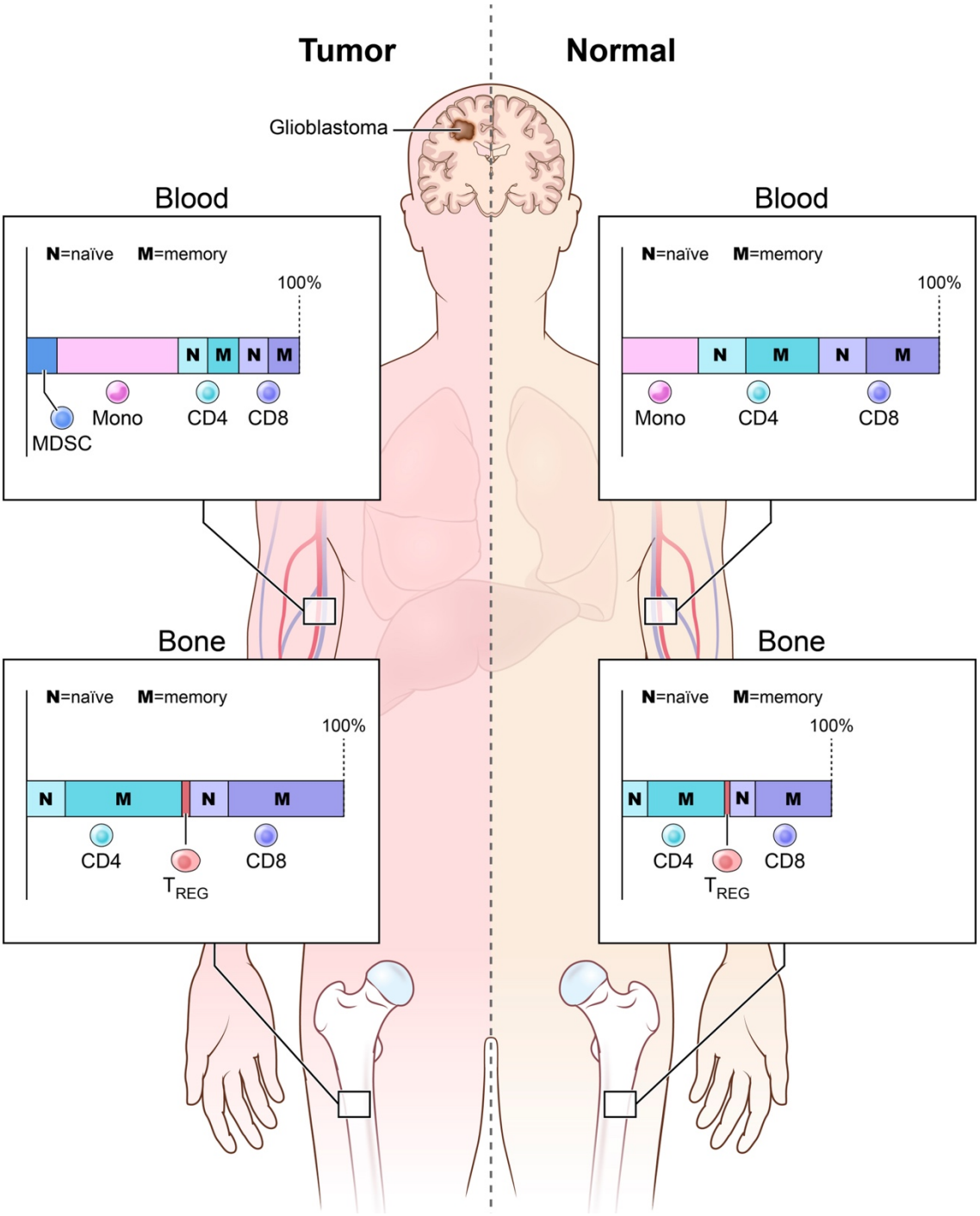

Figure 1-4: GBM disrupts peripheral immunity by manipulating myeloid and lymphoid egress and development. Both GBM-bearing mice and patients harbor aberrant leukocyte levels in both their blood and bone marrow, suggesting that either the tumor (or the brain) releases some signal to prevent an immune onslaught of this compartment. Relative to naïve/healthy controls, the blood of tumor patients shows elevated levels of MHCII- monocytic cells sometimes referred to as MDSCs, elevated levels of blood monocytes, and fewer total T cells. This is thought to be a result of naïve T cell sequestration in the bone marrow. No differences have been observed among Tregs.

The putative immunosuppressive phenotype of peripheral monocytes has been further corroborated by several groups. In mixed leukocyte reactions, monocytes from GBM patients are impaired in their capacity to stimulate T cell proliferation (Gustafson et al., 2010), and in a recent study, conditioned media from monocytes (monoCM) isolated from the blood of GBM patients could not inhibit the ability of allogeneic brain tumor initiating cells (BTIC) to form spheres in vitro, whereas monoCM from healthy donors profoundly inhibited sphere formation (Sarkar, Yang, et al., 2020). Notably, this suppressive function was reversed by adding Niacin (vitamin B3) to culture, which led the monocytes to increase secretion of IFNα14 – a type I interferon that impeded BTIC growth. In reverse translational studies using patient derived xenografts (PDX), *in vivo* delivery of vitamin B3 to tumor-bearing mice elevated the proportion of infiltrating $Iba1^+$ macrophages and their phagocytic capacity, significantly extending survival in a monocyte- and IFNAR-dependent manner (Sarkar, Yang, et al., 2020).

Other studies have aimed to repurpose drugs in the clinic that repolarize peripheral monocytes and endow them with antitumor properties. For example, demeclocycline (tetracycline antibiotic) was identified as a drug capable of stimulating monocytes to inhibit tumor sphere formation (Sarkar, Li, et al., 2020). Given that monocytes uptake foreign material and have such consequential a role in GBM immunology, other groups have focused on optimizing lipid nanocapsule parameters to preferentially target these circulating phagocytes (over other blood leukocytes) and deliver immune modifying therapeutics (Pinton et al., 2020). In mouse models, intravenously administered nanoparticles are preferentially taken up by border myeloid cells as opposed to those in the tumor core (where many of these once-circulating monocytes engraft and differentiate into macrophages) (Karimian-Jazi et al.,

2020). These data suggest that modifying monocytes peripherally prior to tumor entry offers an important therapeutic opportunity to interfere with GBM growth. Although the exact mechanisms by which peripheral monocyte dysregulation occurs in GBM patients are unknown, this circulating innate immune cell population can be easily manipulated and might prove useful in the fight against GBM.

1.1.1.3.2 THE MYELOD INFILTRATE IN THE GBM CORE IS MOSTLY MACROPHAGES

Bone marrow derived myeloid cells in the tumor microenvironment (referred to as 'macrophages' here) can comprise up to 80% of the GBM immune infiltrate **(Figure 1-3)** (Friebel et al., 2020; Gabrusiewicz et al., 2016; Goswami et al., 2020). The frequencies between GBM subsets (i.e., classical, mesenchymal, proneural) are by and large similar except for mesenchymal tumors, which have fewer macrophages and a greater proportion of microglia (Gabrusiewicz et al., 2016; Qianghu Wang et al., 2017). There are stark spatial differences in the myeloid landscape of GBM, in that macrophages preferentially occupy the tumor core and microglia the infiltrating margins (**Figure 1-3)** (Darmanis et al., 2017). There are also transcriptional differences between these two subsets, with single cell studies indicating that macrophages in the tumor core have elevated checkpoint molecule transcripts (e.g., *PDL1*, *PDL2*, *CTLA4*), as well as elevated *TGFβI*, *VEGFA*, and *IL1RN* transcripts, relative to their myeloid cousins at the tumor margins. The HIF-induced upregulation of TGFβ and VEGFA is a well-documented tenet of the hypoxic tumor core (Gabriely et al., 2017; Kaur et al., 2005; Pearson & Regad, 2017). Importantly, neurons, oligodendrocytes, and oligodendrocyte precursor cells were also analyzed in the tumor core and periphery at the single-cell level, but no significant transcriptional differences were found (Darmanis et

al., 2017). Taken together, these findings suggest that GBM myeloid cells are strongly influenced by their proximal surroundings.

Further supporting this gradient of inflammation, the tumor core has elevated *IL1RN* transcripts, whereas the periphery has elevated *IL1α/β* (Darmanis et al., 2017). *IL1RN,* which encodes the IL1 receptor antagonist, outcompetes the inflammatory cytokines(Di Paolo & Shayakhmetov, 2016) IL1α and IL1β for binding to their cognate receptor (Arend et al., 1998), suggesting immunosuppression in the core macrophages. In another study, in which macrophages and microglia were resected from the GBM core or margins using fluorescent and MRI-guided surgery, functional assays revealed that macrophages derived from the tumor core suppressed αCD3/CD28-stimulated autologous T cell proliferation significantly more than microglia from the core of either population from the tumor periphery (Pinton et al., 2019). Internally controlled experiments such as these underwrite the notion that proximal environmental niches can alter the function of the same myeloid population in strikingly different ways. Importantly, while these data suggest that the necrotic and hypoxic core of GBM (Hambardzumyan & Bergers, 2015) enhance the polarization of peripherally derived macrophages, they also indicate that myeloid cell functional tuning takes place *in vivo* and can potentially be manipulated for therapeutic purposes.

Macrophage polarization has long been reduced to an M1-M2 continuum, which describes M1 macrophages cells as “pro-inflammatory” and M2 as “anti-inflammatory.” Much of the M1/M2 literature over-indexes on *in vitro* experiments in which macrophages are perturbed by various exogenous stimuli (e.g., GM-CSF, IL-4) (Gabrusiewicz et al., 2015; Hambardzumyan et al., 2016; Pyonteck et al., 2013). However, in humans, macrophages can be polarized by a variety of cues in their physiological environment, such as DAMPs,

PAMPs, and cytokines, and the panoply of transcriptional and functional programs they undertake in response to those cues is not appropriately captured by the M1-M2 paradigm. Nonetheless, the GBM field has relied on phenotypic markers such as CD163, CD206, CSF-1R, IL-10, TGF-β, and pSTAT3 to define M2 macrophages and CD80, CD86, MHCII, TNF-α and pSTAT1 for M1, and concluded that GBM macrophages were largely M2(Gabrusiewicz et al., 2016). However, this dogma was challenged by findings that so-called MDSCs from human GBM, long regarded as M2-like, most commonly express pSTAT1, CD163, TNF-α, and have the highest expression of MHCII, CD80, CD86 (markers of immune activation and co-stimulation)(Gabrusiewicz et al., 2016). These data upheld previous findings that GBM macrophages express canonical markers from both M1 and M2 phenotypes (Muller et al., 2017; Takenaka et al., 2019). Interestingly, GBM macrophages have gene profiles most similar to nonpolarized PBMC-derived macrophages from an *in vitro* system (Gabrusiewicz et al., 2016). That infiltrating myeloid cells show a non-polarized phenotype is difficult to reconcile with studies that show profound changes in the cytokine secretion of microglia and splenic macrophages upon exposure to GBM-conditioned supernatant (Takenaka et al., 2019). Taken together, these findings underscore the importance of interpreting *in vitro* data with caution and the dangers of extrapolating these data to the far more complex *in vivo* context.

Importantly, functional *in vivo* studies of GBM immunology are rare namely due the myeloid-centric nature of the immune response elicited by GBM, which is not amenable to the plethora of tools available to those studying T-cell rich tumors; for instance, individual macrophage subsets within the GBM niche cannot be readily tracked or selectively depleted. Additionally, the field has historically been reliant on experimental techniques in which only

a select few markers can be investigated simultaneously. This has contributed to the perpetuation of simplistic *in vitro* paradigms being applied to *in vivo* settings, as evidenced by there being no direct link between M1 and M2 marker expression *in vivo* and macrophage function or clinical outcome. However, the advent of single-cell sequencing has the potential to change this status quo and shed more light on *in vivo* GBM immunology.

In one notable example of single-cell sequencing in GBM, a recent study found that, compared to several other cancers, GBM uniquely harbors a subset of $CD73^{hi}$ $CD68^{+}$ macrophages that persist following treatment with anti-PD-1 (Goswami et al., 2020). These macrophages express coinhibitory molecules such as VISTA and PD-1 and show elevated expression of hypoxia-associated genes. Reverse translational studies showed that antagonizing this subset may potentiate the response anti-PD-1 and anti-CTLA-4, but the mouse tumor model used was GL261, which is far more responsive to ICT than human GBM. To validate the relevance of this subset in human GBM, the authors stratified patients from The Cancer Genome Atlas (TCGA) dataset according to a "high" or "low" CD73 macrophage signature. Though the survival difference between the two groups was statistically significant, the effect size was negligible. Perhaps more importantly, the authors suggested that the persistence of these macrophages after ICT is indicative of their conferring therapeutic resistance. However, another study that evaluated GBM samples from the same open-label, single-arm phase II clinical trial revealed that the number of effector, cytotoxic, and memory T cells remained unchanged in the tumor after anti-PD-1 treatment (de Groot et al., 2020). These data indicate that a scarcity of intra-tumoral T cells also contributes to ICT resistance. Importantly, this study highlighted the overwhelming predominance of macrophages in the tumor (~76% of the immune infiltrate), the vast majority of which expressed at least one or more

immunoregulatory molecules that have the potential to impede T cell function. Macrophages can also negatively regulate T cells following activation by metabolites, such as kynurenine, secreted by glioblastoma cells (Takenaka et al., 2019). Kynurenine was recently shown to activate the aryl hydrocarbon receptor (AHR) on macrophages in murine GL261 tumors. This in turn promoted production of adenosine via CD39 that suppressed $CD8^+$ T cell function. In humans, CD39 and AHR were associated with high grade gliomas and worse outcomes. Thus, macrophages are equipped with multiple mechanisms that suppress anti-tumor immunity.

1.1.1.3.3 INFILTRATION BY MELOID CELLS INCONSISTENTLY CORRELATES WITH SURVIVAL

The finding that myeloid cell infiltration increases with tumor grade (Kong et al., 2010) has led to the assumption that myeloid cells are (i) monolithic and (ii) tumor promoting (Hambardzumyan et al., 2016). However, in some studies, high myeloid cell number in GBM tumors has been associated with increased survival when quantified as $CD33^+$ cells(Alban et al., 2018) or CD163, CD206, and CD68-positive cells (Zeiner et al., 2019). In another study, the opposite trend was observed with CD163 and TCGA data (Friebel et al., 2020), and no consistent association with survival has been noted when the tumor infiltrate is stratified according to Iba-1 levels[21]. Greater infiltration of tumors by MHC-$II^{neg/lo}$ myeloid cells (termed MDSCs by most groups) in recurrent GBM is associated with a poor prognosis (Alban et al., 2018). An important caveat of all these studies is that no one marker is representative of any unique myeloid cell type, and the quantification methods between studies varies significantly. Additionally, tumor sections from the same patient can harbor markedly different immune infiltrates (Martinez-Lage et al., 2019), and this heterogeneity will

certainly influence studies that rely on histological quantification of immune cells in tumor slices for correlative analyses. It will therefore be important in future studies to evaluate tumor-infiltrating myeloid cells using a combination of high parameter approaches (e.g., single cell RNAseq, multiplex immunohistochemistry, etc.) that more accurately reflect the diverse functional states that these cells acquire in the tumor microenvironment over time and in response to various treatments.

1.1.1.3.4 GBM SIGNALS TO THE PERIPHERY TO ATTRACT MONOCYTES

The considerable number of macrophages in GBM tumors has led many to define the chemoattractants that promote monocyte extravasation from the blood supply. On the other hand, the clear peripheral monocyte dysregulation in GBM patients has stimulated questions and research about how GBM signals to the periphery. GBM, like many other cancers, secretes exosomes into the blood supply, which can then exert immune modulating functions (Abels et al., 2019; Ebrahimkhani et al., 2018; Graner et al., 2009). Exosomes are most readily taken up by monocytes due to their intrinsic phagocytic nature, with phagocytosis being significantly more pronounced in monocytes derived from GBM patients relative to healthy donors (Gabrusiewicz et al., 2018). *In vitro*, glioma stem cell-derived exosomes modify cell surface expression and cytokine secretion of various canonical "M2" surface markers such as PD-L1, IL-6, CD163, CD206, and CD80 (in BM-derived macrophages), leading researchers to infer the transfer of an immunosuppressive function upon endocytosis. However, the queried markers also reflect states of general immune activation (De Vrij et al., 2015; Gabrusiewicz et al., 2018), and without additional functional studies, the degree to which GBM-derived exosomes regulate circulating myeloid cells remains unclear.

Osteopontin (OPN, *SPP1),* a glycophosphoprotein that binds to multiple integrins and certain variants of CD44, is thought to facilitate myeloid cell recruitment and/or influence their subsequent polarization (Ashkar et al., 2000; Ge et al., 2017; Kale et al., 2014). This protein is elevated in GBM tissue, which has stimulated interest in how it influences tumor myeloid cells (Wei et al., 2019). However, there are conflicting results in the literature regarding the role of OPN in GBM. For example, one murine GL261 study concluded that OPN produced by tumor and innate immune cells promotes recruitment of macrophages and maintains them in an alternatively activated "M2" state. OPN deficiency also rendered tumors more susceptible to $CD8^+$ T cell mediated killing and improved survival (Wei et al., 2019). By contrast, another study concluded that tumor associated myeloid cells (not GL261 cells) are the major source of OPN and removal of this protein from the host actually promoted tumor growth without altering recruitment of peripheral myeloid cells (Szulzewsky et al., 2018). Therefore, the role played by OPN in murine GBM models is unclear, and additional studies are required to determine how this protein influences the myeloid cell landscape and survival in human GBM.

Another relevant chemokine of interest is monocyte chemoattractant 1 (MCP-1) or CCL2. In human GBM, CCL2 expression is associated with reduced survival (Chang et al., 2016; Chen et al., 2017). Functional studies of CCL2 in the murine context have shown model-dependent differences in terms of the importance of CCL2 on survival and tumor development, whether the effect stems from tumor or host-derived CCL2, and whether there are associated changes in macrophage and T cell infiltration. Collectively, existing data suggest that tumor-derived CCL2 is propitious for both tumor growth and macrophage/Treg accumulation via CCR2 and CCR4 signaling, respectively (Chang et al., 2016; Chen et al.,

2017; Fujita et al., 2011; Zhu et al., 2011). However, the effect size is small, larger in slower growing tumors, and only present in T cell replete mice (Mohme et al., 2018), suggesting that the phenotype may have more to do with lymphoid rather than myeloid immunity. Importantly, there is a well-documented dearth of lymphoid immunity in human GBM, which suggests T cell-centric mechanisms may be an artifact of the model used. Nonetheless, several key findings regarding T cell suppression in GBM have emerged and will need to be considered as clinicians and scientists devise strategies to advance therapeutic outcomes.

1.1.2 NEUTROPHILS

1.1.2.1 NEUTROPHILS IN THE TUMOR NICHE ARE LIKLEY DELETERIOUS

Neutrophils are among the first cellular subsets to be called to an inflammatory milieu/damaged tissue. Neutrophils are increasingly considered important players in GBM immunity, making up approximately 10% of the immune infiltrate (Friebel et al., 2020). Necrotic cells, a hallmark of GBM, induce the expression of IL-8, the chief neutrophil chemoattractant (Ahn et al., 2016). Upon entering the highly inflamed and damaged tissue, neutrophils are induced to form neutrophil extracellular traps (NETs). *In vitro* studies have shown that co-incubation with neutrophils or NETs enhances GBM migration, drives GBM proliferation via NF-kB activation, and induces glioma cell secretion of IL-8 (Liang et al., 2014; Zha et al., 2020). Pre-clinical work using patient-derived xenograft models has demonstrated that irradiation induces the recruitment of neutrophils to the tumor niche, which are then found near newly de-differentiated glioma stem like cells. Notably, in one study, inhibiting neutrophils following radiotherapy increased survival (Jeon et al., 2019).

In addition, depleting neutrophils in the Sleeping Beauty-induced murine glioma model also significantly extended survival (Fujita et al., 2011; Fujita et al., 2010).

1.1.2.2 NEUTROPHILIA IS COMMON IN GBM PATIENTS

GBM patients, including treatment-naïve patients, present with neutrophilia, which is not uncommon in other cancers (Gabrusiewicz et al., 2016). Notably, almost 20% of GBM patient blood leukocytes are degranulated neutrophils, compared with nearly 0% in healthy donors (Sippel et al., 2011). This is potentially significant because arginase I is found in neutrophil granules and degranulation has been offered as an explanation for the elevated serum arginase I levels often seen in GBM patients. Arginase metabolizes L-arginine, a critical co-factor for sustaining CD3zeta expression in T cells, meaning increased arginase could potentially affect peripheral adaptive immune suppression. Elevated neutrophil to lymphocyte ratios has long been associated with poorer outcomes in patients, even if most of these neutrophils demonstrate an activated (IL-12^{+}) phenotype (Lei et al., 2019; Rahbar et al., 2016). Taken together, these data suggest that neutrophils may more be a measure of an aggressively growing GBM, rather than a contributor to tumor growth.

1.1.3 DENDRITIC CELLS (DCs)

Glioblastomas are unique among cancers for their lack of a tissue resident APC population capable of migrating to draining lymph nodes. DCs are capable of cross-presenting tumor antigen (Theisen et al., 2018), and they do so more effectively than any other myeloid cell found in tumor microenvironments (Lavin et al., 2017; Raeber et al., 2020; Salmon et al., 2016). DCs traffic antigen to the draining node, where they set off a tumor-specific T

cell response by presenting and co-stimulating anti-tumor T cells that can then productively traffic to the tumor. In fact, even those DCs whose functions have been subverted by the tumor can be effectively repolarized to drive T cell activation in certain contexts (Maier et al., 2020).

In GBM, zero to slightly above 2% of the immune infiltrate is comprised of DCs, including migratory, plasmacytoid DCs and conventional type I and II DCs (cDC1 and cDC2, respectively) as confirmed by a recent single-cell sequencing study in *de novo* and recurret GBM (Friebel et al., 2020; Fu et al., 2020; Pombo Antunes et al., 2021). Due to their rarity in the GBM context, however, functional data requiring their isolation is nearly non-existent (both in the tumor and cervical lymph node compartment). Monocytes have the capacity to differentiate into monocyte-derived DCs upon entering inflamed tissues, but the capacity of these DCs to efficiently cross-present tumor antigens and prime T cells *in vivo* is questionable. There have been enormous efforts over the last two decades to use DC-based vaccines in GBM, and these studies are elegantly reviewed elsewhere (Sampson et al., 2020). T cells activated by DCs would likely require local stimulation in the brain, and it is unclear if the dominant myeloid cell subsets in the GBM niche can provide this stimulation. In fact, it is likely that deficiencies tumor APCs and peripheral T cell responses in GBM patients (Weathers et al., 2020) explain why no DC trial has been successful to date in GBM patients.

1.1.4 T CELLS

1.1.4.1 EFFECTOR T CELLS

1.1.4.1.1 THE PHENOTYPE OF EFFECTOR T CELLS IN THE TUMOR SUGGESTS FEW ARE GBM-SPECIFIC

Studies differ in the reported percentage of T cells making up the GBM immune infiltrate, with some reporting a startling paucity and others up to 17% (Friebel et al., 2020; Fu et al., 2020; Goswami et al., 2020; Pinton et al., 2019). One study reported an even split between helper and cytotoxic T cells(Goswami et al., 2020), and another showed slightly more than half of $CD3^+$ cells are $CD8^+$ (Mohme et al., 2018). Early work in which 519 newly diagnosed GBM patients were binarized as short or long-term survivors showed that 38% of the latter but only 20% of the former were categorized as having intermediate or extensive T cell infiltrates(Yang et al., 2010). This study and others demonstrated (Lohr et al., 2011; Yang et al., 2010) the positive prognostic value of effector and cytotoxic T cells, but this finding has since been disputed, with a more recent study showing no relationship between CD8 infiltration and survival in GBM (Yue et al., 2014).

Unsurprisingly, T cells in the GBM tumor milieu have a unique profile relative to those found in matched patient and healthy blood samples (Fu et al., 2020; Mohme et al., 2018; Woroniecka et al., 2018): up to 90% of tumor infiltrating lymphocytes (TILs) were shown to be PD-1 positive. This likely indicates an activated state, as among TILs, PD-1+ T cells produced greater amounts of IL-2 upon stimulation relative to their PD1-negative counterparts (Woroniecka et al., 2018). The other ~10% of T cells in this same study were found to be triple-positive for PD-1, TIM-3, and LAG-3, and produced no cytokines following stimulation, indicating a hyporesponsive, exhausted state. CD39 has also been shown to be markedly elevated on TILs, and together with CD73 works to negatively regulate T cell activity (Goswami et al., 2020; Takenaka et al., 2019). TILs in GBM also have significantly

elevated levels of activation and memory markers, such as MHCII and CD45RO[69]. As a result of these and other phenotypic characterizations, some groups have classified TILs as effector memory T cells, differentiated, and antigen experienced (Mohme et al., 2018). Notably, unlike in matched blood samples, there are virtually no naïve or central memory T cells in the tumor milieu. The associated data regarding the function, clonality, and antigen specificity of these TILs are ambiguous, however.

One study showed that in response to αCD3/CD28 stimulation and relative to healthy donor T cells total TILs had comparable secretion of IFNγ and TNFα, elevated IL-17A, IL-5, IL-4, IL-9, and IL-21, and reduced IL-2. However, other groups have shown that following *in vitro* stimulation with PMA/ionomycin, GBM $CD8^+$ T cells produce virtually no IFN-γ, IL-2, or TNF-α, whereas T cells from patient blood and healthy donors (including $CD4^+$ TILS) show no difference in their capacity to respond accordingly(Chen et al., 2019; Woroniecka et al., 2018). The discrepancy in these studies may stem from the T cell stimulus used as well as whether the investigators chose to combine or separate the readout from $CD4^+$ and $CD8^+$ T cells.

As previously mentioned, most TILs are PD-1^+, but they express low levels of KLRG1, suggesting that they are not actively engaging cognate antigen in the tumor milieu (Mohme et al., 2018). Furthermore, studies have shown that GBM total TILs exhibit a restricted TCR repertoire, and in studies that differentiated between the two, $CD4^+$ T cells showed evidence of clonal expansion, whereas $CD8^+$ T cells did not (Mohme et al., 2018; Woroniecka et al., 2018). Collectively, these findings suggest that most TILs are likely bystander memory T cells that have trafficked to the tumor site due to general inflammatory

cues rather than specific antigens, and that *bona fide* tumor-specific T cells are very rare in GBM.

The trafficking of GBM-specific T cells into the tumor site is presumably reliant on ample and appropriate tumor antigen drainage to secondary lymphoid organs, where naïve T cells can be primed. The participation of lymphatics in the drainage of CNS antigen at steady state has been heavily debated in recent years (Ji Hoon Ahn et al., 2019; Iliff et al., 2012; Antoine Louveau et al., 2015). Despite the presence of lymphatics in the dura mater (Ji Hoon Ahn et al., 2019; Antoine Louveau et al., 2015) and leaky GBM vasculature (Hambardzumyan & Bergers, 2015), the degree of drainage from these tumors into secondary lymphoid tissues is vastly lower than that observed with peripheral tumors. In fact, it was posited in a recent study that GBM is particularly adept at evading immune engagement owing to limited lymphatic drainage of CNS antigens (Song et al., 2020). When meningeal lymphatic drainage was enhanced by ectopically expressing vascular endothelial growth factor C (VEGF-C) in the CSF, priming of cytotoxic T cells (CTL) was observed in the deep cervical lymph nodes. Importantly, these CTL migrated back to the tumor and engaged in clearance when ectopic VEGF-C treatment was combined with immune checkpoint therapy (Song et al., 2020). However, this study was limited by its reliance on the GL261 tumor model, which, unlike human GBM, is responsive to immune checkpoint therapy. Metastatic melanoma models unresponsive to immune checkpoint therapy were similarly not influenced by enhancement of lymphatic drainage with VEGF-C. These data confirm that enhancing T cell trafficking is a strategy conducive only for tumors amenable to productive T cell engagement. To date, little evidence suggests that human GBM falls into this category.

1.1.4.1.2 EFFECTOR T CELLS IN THE PERIPHERY ARE QUANTITATIVELY, BUT NOT QUALITATIVELY DIFFERENT IN GBM PATIENTS

As previously mentioned, circulating T cells from GBM patients are not phenotypically different from those of healthy donors: they show no real differences in terms of surface marker expression, and are just as responsive to external simulation (Mohme et al., 2018; Woroniecka et al., 2018). Quantitatively, however, GBM patients present with key differences in this compartment. Relative to healthy donors, even untreated GBM patients have fewer effector and cytotoxic T cells in the blood, as well as smaller spleens (Chen et al., 2019; Chongsathidkiet et al., 2018; Fu et al., 2020). Furthermore, 25% of patients have lymphopenia, with 15% presenting with T cell counts comparable to AIDS patients (Chongsathidkiet et al., 2018). Dexamethasone further decreases the percentage of lymphocytes in the blood(Gustafson et al., 2010). Within the T cell compartment, there is a greater proportion of $CD8^+$ T cells and a smaller proportion of $CD4^+$ T cells in the blood, an interesting finding considering the CD8-specific functional and clonal impairments described above (Mohme et al., 2018). Interestingly, in a recent seminal study, it was shown that naïve $CD4^+$ and $CD8^+$ T cells were sequestered in the bone marrow of GBM patients due to loss of S1P1 on the cell surface (Chongsathidkiet et al., 2018). S1P1 is the 'exit visa' for T cell egress into the blood stream. In animal models recapitulating this finding, rescuing of S1P1 internalization did not improve survival, despite increasing the numbers of activated tumor infiltrating T cells (Chongsathidkiet et al., 2018). Moreover, animals bearing any intracranial tumor (including models of metastasis) had decreased peripheral T cell counts, suggesting that this quantitative impairment is an anatomy-specific afferent effect of GBM. Thus, the extent of peripheral immune suppression in GBM patients must be carefully considered

when attempting to develop efficacious immunotherapies. Interestingly, long term survivors of GBM (>5 years) have an increased proportion of naïve $CD8^+$ T cells in circulation relative to healthy donors (Mohme et al., 2018), suggesting some capacity for overriding this peripheral immune suppression.

1.1.4.2 REGULATORY T CELLS

1.1.4.2.1 THE CURRENT LITERATURE SUGGESTS AN OVERSTATE ROLE FOR TREGS IN GBM

More than any other subset of lymphoid cells, T regulatory cells (Tregs) have been the subject of intense investigation and controversy in the GBM literature (Platten & Wick, 2015). This is due to their well-described capacity to secrete immunosuppressive factors such as IL-4, 10, and 13, and engage in negative regulatory crosstalk with other T cell and macrophage subsets. As with cytotoxic T cells, the prognostic value of Tregs in the blood and tumor differs based on the study and the quantification method. Some groups have shown no relationship between Treg blood percentage or Treg tumor infiltration and survival (Lohr et al., 2011; Thomas et al., 2015), others have shown that FoxP3 transcripts negatively associate with survival (Yue et al., 2014), while others still have shown that it is the *ratio* of cytotoxic T cells to Tregs that in fact correlates with survival, not just the quantification of one subset (Sayour et al., 2015). In stark contrast with peripheral myeloid cell and CD4/CD8 T cell dysregulation noted in GBM patients, there is no difference between the quantities of Tregs circulating in healthy donors or GBM patients (Alban et al., 2018). Tregs represent between 1 and 5% of tumor infiltrating T cells, compared with up to 15% in brain metastases (Friebel et al., 2020; Lohr et al., 2011). Notably, nearly all the Tregs infiltrating human

GBM have been shown to be Helios^{+} nTregs (thymus derived) as opposed to locally induced Tregs (iTregs) (Wainwright et al., 2011).

Results from reverse translational studies have differed based on the animal model used. In a Sleeping Beauty model of GBM, blocking Treg recruitment had no impact on survival (Fujita et al., 2010). In the GL261 model, it was demonstrated that Tregs rely more so on the chemokine receptor CCR4 for trafficking into gliomas than effector T cells, and inhibition of this receptor with a small molecule antagonist significantly improved survival (Chang et al., 2016). While these data suggest that Tregs impede antitumor immunity in the GL261 model, it remains unclear whether a similar Treg contribution exists in GBM patients.

1.1.5 NATURAL KILLER (NK) CELLS

1.1.5.1 NK CELLS HAVE YET TO FULFILL THEIR PROMISE IN KILLING GBM CELLS IN APPRECIABLE NUMBERS

In a TME lacking substantial numbers of APCs and whose response skews away from adaptive immunity, independence of NK cells from both antigen specificity and co-stimulation presents an exciting opportunity. NK cells comprise ~2.5% of the tumor immune infiltrate (Friebel et al., 2020). Importantly, loss of heterozygosity and downregulation of Human Leukocyte Antigen (HLA) Class I is a common genetic event in glioblastoma (Yeung et al., 2013). NK cells are known to kill cells "missing self"; however, HLA I loss/downregulation can also induce NK-cell tolerance depending on the inflammatory context (Bern et al., 2019). Furthermore, GBM is known to overexpress HLA-E (Wischhusen et al., 2005), which upon binding to its cognate receptor, NKG2A, on the NK-cell surface, inhibits NK effector function. Interestingly, PD-1^{+} CD8^{+} TILs also express NKG2A, and

upon engagement with HLA-E, their proliferation is inhibited (Abd Hamid et al., 2019). NKG2A expression is triggered by immunosuppressive cytokines commonly found in the GBM niche, namely IL-10 and TGFβ (van Montfoort et al., 2018; C. Zhang et al., 2019). Thus, although *in vitro* evidence demonstrates that pre-activated NK cells can kill GBM cells, existing *in vivo* data suggest NK cells are functionally impaired in the GBM milieu (Fu et al., 2020).

1.1.6 B CELLS

1.1.6.1 B CELLS HAVE UNTAPPED POTENTIAL IN GBM

When B cells and plasma cells are present, they appear to make up less than 1% of the immune infiltrate (Friebel et al., 2020). One study reported that B cells were found in ~4% of their GBM specimens (Martinez-Lage et al., 2019), whereas another study reported that 40% of patients showed evidence of B cell infiltration (Lee-Chang et al., 2019). In the latter study, tumor-derived B cells inhibited autologous $CD8^+$ T cell proliferation, and 80% of B cells were PD-$L1^+$, $TGF\beta^+$, and IL-10^+. In addition, treatment of CT2A-brain tumor bearing mice with an anti-CD20 antibody prolonged survival, suggesting a regulatory role for B cells in GBM (Lee-Chang et al., 2019). To overcome this regulatory activity, a recent study demonstrated a novel immunization strategy in mice that involved stimulating 4-1BBL+ B cells isolated from secondary lymphoid tissues with a CD40 agonist and IFNγ (Lee-Chang et al., 2021). These B cells promoted survival in tumor bearing mice in part by cross-presenting antigen to $CD8^+$ T cells. In fact, this B cell therapy was especially effective when combined with radiation and PD-L1 blockade. This study also showed that antibodies derived from the activated B cells alone were effective in extending survival when injected

intracranially into mice with CT2A tumors. While few GBM publications have focused on B cells, additional studies are warranted. If appropriately activated, B cells could play an important role in controlling GBM by presenting antigen to T cells (both $CD8^+$ and $CD4^+$) and secreting antitumor antibodies.

1.1.7 CONCLUDING REMARKS

The host response to GBM skews toward the innate and away from the adaptive immune system. This is a function of both GBM biology and the anatomical compartment in which this tumor is found. Relative to metastases in the brain, GBM is infiltrated by fewer T cells, suggesting that its myeloid cell-centricity is a response to tumor-specific characteristics(Friebel et al., 2020). However, the precise mechanisms by which the neoplastic cells of metastases versus those of GBM differ to attract disparate immune populations have not yet been elucidated.

Unlike in the periphery, there is little forgiveness for inflammation in the brain. To protect itself from fatal immunopathology, the brain has evolved mechanisms to induce antigenic ignorance and immune quiescence(Mohammad et al., 2014). Thus, in the neoplastic context, the brain becomes the ideal host. For instance, mouse studies have shown that when neoantigen-expressing melanoma cells are implanted intracranially as opposed to in the flank, the CNS draining lymph nodes of the tumor-bearing animals have significantly fewer specific T cells, and those that are present have impaired effector functions(Jackson et al., 2016). Furthermore, mice bearing intracranial tumors of any variety harbor significantly reduced naïve T cell counts in their blood (Chongsathidkiet et al., 2018). Thus, even under inflamed conditions or in the context of violated brain barriers, poor antigen drainage and the induction of peripheral immune suppression cooperate to prevent a peripheral immune

response to an intracranial tumor. Indeed, brain metastases can be controlled better than GBM, and this likely stems in part from the fact that in metastatic cancer, there is an existing peripheral immune response, enabling antigen-specific cells to better cross the various barriers protecting the parenchyma (Tawbi et al., 2018). The less remembered of Peter Medawar's experiments of the 1940s demonstrated that skin grafts failed to be rejected when implanted into the brain unless they were preceded by a heterotopic tissue graft elsewhere in the body. *De novo* immunity could not be mounted in the CNS but pre-existing immunity in the periphery could be harnessed to traverse the BBB and reject the foreign tissue(Medawar, 1948).

Another key consideration is that, at baseline, the brain parenchyma is home to a non-diverse resident immune population comprised almost completely of microglia. Sophisticated immune networks supported by functional studies have not been reproducibly identified in human GBM. For instance, while coordinated T cell-dendritic cell (DC) or natural killer (NK) cell-DC axes have been described extensively in other cancers (Barry et al., 2018; Binnewies et al., 2019; Böttcher et al., 2018; Hubert et al., 2020), with the exception of two single-cell studies (Darmanis et al., 2017; Pombo Antunes et al., 2021), most published studies don't even describe a cross-presenting DC infiltrate in the human GBM tumor microenvironment, nor can extract enough such DCs to assay their function (or impairments). While there is evidence that microglia can cross-present antigen under the right circumstances, they are brain tissue-resident cells that do not migrate to draining lymph nodes to present antigen (Moseman et al., 2020). In essence, GBM seemingly usurps the evolutionarily conserved immune quiescence of the brain. Thus, GBM is likely ignored or seen as

'self' until it is too late – when danger signals resulting from necrosing tissue and abundant microhemorrhages are released into the bloodstream.

Recent data from GBM trials show that following immunostimulation with neoantigen vaccination (Keskin et al., 2019) or immune checkpoint therapy(de Groot et al., 2020), the immune landscape of GBM is virtually unchanged. Though disheartening, these findings should motivate a more rigorous approach to studying the intersection of neuroimmunology and glioblastoma biology. The future design of efficacious GBM therapies requires consideration of both the local and distal immune cell networks that must be collectively activated to mount a robust response against this uniformly lethal cancer.

1.2 VIRUSES IN THE ETIOLOGY AND POTENTIAL TREATMENT OF GBM

As previously mentioned, with the exception of tumor-treating fields (application of low-intensity alternating electric fields) that have increased median survival from 16 to 21 months as well increased 5-year survival from 5% to 13% in exploratory studies (Stupp et al., 2017), virtually none of the many new therapies under investigation have materially prolonged GBM survival (Fisher & Adamson, 2021). Viral therapy, if further optimized and developed, may be one exception (Desjardins et al., 2018). The idea of using viruses (and other pathogens) to treat GBM was borne from the anecdotes of GBM patients contracting infections in the surgical site and surviving for years. In fact, a 2011 study of 200 GBM patients in Rome found that the 10 who contracted wound infections lived twice as long as their sterile counterparts (De Bonis et al., 2011). One neurosurgeon went on record with *The New Yorker* to say, "If I ever get a GBM, put your finger in your keister and put it in the wound." (Eakin, 2015) Admittedly this sounds less elegant than checkpoint blockade, but

for reasons that will be advanced below, such an approach (or an adjacent – more regulated – approach in the vein of deliberate viral infection) is likely to bear more fruit than typical immunotherapeutic strategies. Virotherapy can xenogenize a tumor that is deft at behaving like "self", triggering adaptive immune recognition in an otherwise immunologically quiet compartment. Viruses can also directly lyse tumor cells creating damage and further stimulating secondary immune reactions that are detrimental to tumor growth.

1.2.1 ENDOGENOUS VIRUSES FOUND IN GBM

GBM's vast intratumoral heterogeneity as well as its rank among the most lethal of all cancers has long prompted queries into its etiology. Viruses have captured the interests of investigators due to their role in the oncogenesis of other cancers, as well as the presence of viral nucleic acid and protein in GBM and the general state of immunosuppression in patients.

1.2.1.1 CYTOMEGALOVIRUS (CMV)

Human cytomegalovirus (CMV) is a beta herpes virus with a tropism for glial cells. CMV infects 50-90% of the adult population and seroprevalence increases with age(Cannon et al., 2010). In healthy individuals, CMV is a clinically irrelevant pathogen. In 2002, one of the first CMV studies in GBM showed that 27 of the 27 samples queried by immunohistochemistry and *in situ* hybridization expressed CMV genomic and protein material (Cobbs et al., 2002). Since then, a plethora of studies have both confirmed and denied these original findings in tumor tissue and blood (Mitchell et al., 2008; Poltermann et al., 2006; Sabatier

et al., 2005; Scheurer et al., 2008). Much of the variability has been attributed to assay sensitivity and type, as well as the age of the samples queried (Dziurzynski et al., 2012). Some groups have also shown that CMV expression was higher in GBM compared to low grade gliomas and epilepsy controls (Scheurer et al., 2008), and in newer samples compared with older ones (Ranganathan et al., 2012). In studies showing CMV gene products in tumor tissue, their absence in adjacent non-neoplastic tissue begged the question why lytic phase CMV did not spread. Further, investigators wondered whether CMV's presence was a product of the chaos in the tumor bed rather than a cause. Indeed, CMV primarily infects quiescent cells, pushes them to G_1 to induce viral gene expression, and arrests the cell cycle prior to host DNA synthesis in S phase – behavior not entirely conducive with oncogenesis(Spector, 2015). Furthermore, the prevalence of CMV in nearly 9 out of 10 adults does not match with the prevalence of GBM (1 out of 30,000). Thus, CMV has largely been ruled out as an oncogenic virus, though controversy remains as to whether it is an oncomodulator. According to this theory, CMV doesn't directly lead to malignant transformation but can perturb cellular processes in ways that promote oncogenic signaling and tumor growth. Treatment of GBM patients with the anti-viral drug Valganciclovir, in addition to standard of care GBM therapy, has been shown to improve median overall survival in newly diagnosed patients (Stragliotto et al., 2020). Reverse translational studies in syngeneic murine models revealed that tumor-bearing mice that had been perinatally infected with CMV fared worse than their uninfected counterparts, due in part to increased pericyte recruitment and enhanced angiogenesis in the tumor bed. Treating infected mice with antiviral therapy improved their survival by decreasing PDGF expression and impairing angiogenesis (Krenzlin et al., 2019).

Collectively, these data support the notion that CMV might promote GBM growth in humans, but additional studies are required to prove this definitively.

1.2.1.2 EPSTEIN-BARR VIRUS (EBV)

Another oncomodulatory virus with questionable links to GBM is Epstein Barr Virus (EBV). EBV is a ubiquitous gamma herpes virus that is present in approximately 90% of the adult population and manifests clinically as infectious mononucleosis during its acute lytic cycle. Following acute infection, EBV like CMV, establishes life-long persistence. In its latency, EBV exists in one of three programs each hallmarked by the expression of distinct RNA and proteins (Münz, 2019). One such protein produced during latency programs II and III is LMP1, an oncoprotein that is critical for the carcinogenesis of various subsets of lymphomas and carcinomas (Salahuddin et al., 2019). This is in line with data that show EBV's main cellular reservoir is memory B cells (Hatton et al., 2014; Heath et al., 2012). The CNS is also gaining interest as a potential reservoir for EBV latency. Indeed, compliment receptor 2 (CR2), the primary receptor for EBV, is expressed on astrocytes and upon viral entry, astrocytes demonstrate increased proliferation (Menet et al., 1999; Słońska et al., 2021). EBV's association with a plethora of CNS indications including but not limited to ataxia, encephalitis, and demyelinating diseases, as well as its frequent presence in CNS lymphomas has prompted inquiry into its role in gliomagenesis (Fujimoto et al., 2003; Soldan & Lieberman, 2020). However, results thus far have been discordant and point to no clear role for EBV in GBM (Strong et al., 2016).

1.2.1.3 HUMAN ENDOGENOUS RETROVIRUSES (HERVs)

Studies linking human endogenous retroviruses (HERVs) to GBM are sparse, but there appears to be active interest in determining if HERVs contribute to human cancers. HERVs, which are remnants of retroviral germline infections, make up ~8% of the human genome (Markovitz, 2014). The majority of HERVs are inactive and unable to replicate. However, certain HERVs, such as those in the HERV-K family, have retained open reading frames, and their viral products are translated during embryogenesis but typically silenced in healthy differentiated cells (Grow et al., 2015; Mayer et al., 1999). Due to genetic and epigenetic dysregulation in malignantly transformed cells, high levels of HERV products have been found in the following cancers: breast, lung, prostate, hepatocellular carcinoma, germ cell, melanoma, leukemia, lymphoma, and ovarian among others (Ishida et al., 2008; Kahyo et al., 2013; Kleiman et al., 2004; Ma et al., 2016; Serafino et al., 2009; Wang-Johanning et al., 2007; Wang-Johanning et al., 2008). Very recently, one study found that HERV transcripts (mostly from the ERV1 superfamily) were upregulated in GBM compared to adjacent tissue, though notably HERV-K was downregulated (Yuan et al., 2021). One other study reported that HERV-K could not be detected in GBM (Kessler et al., 2014). Given these conflicting reports and dearth of information, the role of HERVs in human GBM (if any) remains to be elucidated.

1.2.1.4 EXPLOITING ENDOGENOUS VIRUSES IN GBM FOR TREATMENT

One reason why GBM is such an intractable tumor is because it can grow relatively unseen by the adaptive immune system until too late (i.e., when the tumor mass is large)

(Song et al., 2020). This relative "invisibility" occurs at various steps of what should otherwise be the typical cancer immunity cycle: 1.) release of tumor antigens, 2.) antigen presentation by dendritic cells (DCs) and other professional antigen presenting cells (APCs), 3.) priming and activation of T cells in secondary lymphoid tissues, 4.) infiltration and engagement of the tumor by tumor-specific T cells (Chen & Mellman, 2013; Ozga et al., 2021). Given that GBM is thought to be driven primarily by canonical mutations rather than carcinogens or other environmental perturbations, it harbors a far smaller neoantigen burden than other cancers (Alexandrov et al., 2013; Lawrence et al., 2013; Neftel et al., 2019). Functionally, this means there are less altered self-antigens available for recognition by the immune system in steps 1 and 2 above. Furthermore, the brain lacks a population of migratory APCs to traffic tumor neoantigen to draining lymph nodes. There is also no evidence to date that lymphatic vessels directly contact and drain the brain parenchyma. Instead, parenchymal antigen is thought to drain along the 150nm wide basement membranes of capillaries and arteries, as well as along exiting neural sheaths (Carare et al., 2008; Kida et al., 1993; Ma et al., 2017). The little parenchymal antigen that does escape these tight barrier systems would enter the dura mater and potentially drain via its dedicated lymphatics (Ji Hoon Ahn et al., 2019; Antoine Louveau et al., 2015). However, we have observed in a murine model of GBM that drainage of tumor antigen into the cervical lymph nodes is negligible, which impinges on step 3 in the cancer immunity cycle, unless drainage can be enhanced (Song et al., 2020). Lastly, the blood-brain and CSF-brain barriers are designed to limit leukocyte migration into the brain to prevent immunopathology (Engelhardt & Ransohoff, 2012; Mastorakos & McGavern, 2019). In fact, CNS endothelium only support the migration of activated leukocytes, and even then, those that extravasate into the perivascular space are sequestered

there unless they recognize cognate antigen on perivascular APCs (Greter et al., 2005; Kawakami et al., 2005; Lodygin et al., 2013). The latter would only occur if appropriate tumor antigen drained in the first place. These features impede step 4 of the cancer immunity cycle. In concert, the unique anatomy and immunology of the CNS afford glioblastomas with the ability to remain well ensconced and hidden in the brain. Therefore, it might be incredibly useful to leverage endogenous viral infections against GBM.

CMV antigens in infected tumor cells could potentially be exploited as neoantigens worth targeting **(Figure 1-5, A).** Indeed, given the well-documented subclinical CMV viremia observed in GBM patients, there have been several adoptive T cell transfer and vaccine strategies employing CMV antigens as proxies for GBM-specific antigens and CMV-specific in place of tumor-specific T cells. A notable hallmark of CMV infection is its maintenance of outsized pools of oligoclonal memory T cells, which accumulate over time in a process called 'memory inflation'. Impressively, up to one quarter of the total CD8 T cell population of elderly CMV seropositive individuals is CMV-specific (Alejenef et al., 2014; Khan et al., 2002), and in contrast to other latent infections, CMV-specific T cells remain highly functional (Kim, Kim, et al., 2015). Such frequencies of oligoclonal T cells are rarely achieved even with vaccination. This, coupled with the high prevalence of CMV seropositivity in the adult population, makes co-opting this pre-existing pool of "tumor-specific" T cells attractive and pragmatic as a therapeutic.

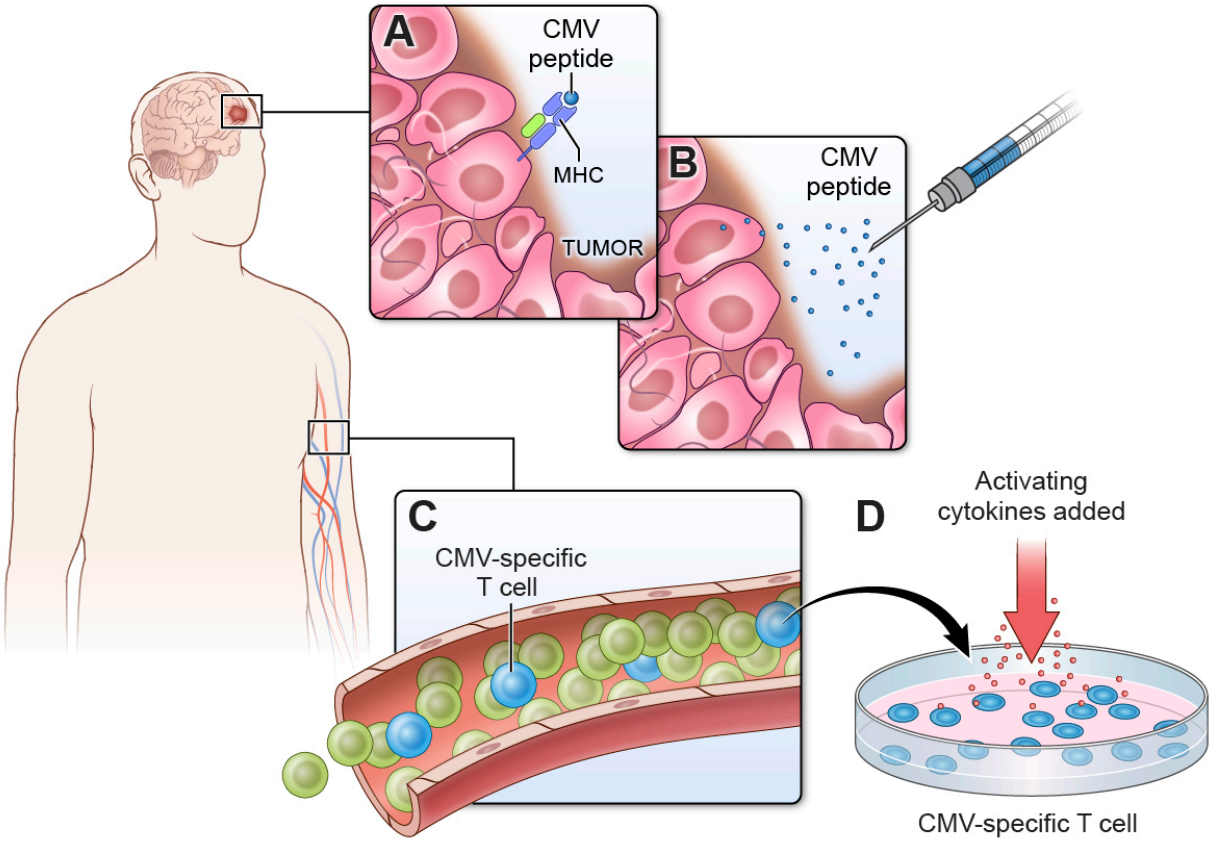

Figure 1-5: CMV xenogenization of glioblastoma. (**A)** GBM presents CMV peptide on the surface of MHC molecules. (**B)** CMV peptide injected either systemically or intratumorally can be used to activate CMV-specific T cells and route them to the tumor. **(C and D)** CMV-specific T cells can comprise up to 10% of the human T cell repertoire and represent a significant contingent of immune cells that can be harnessed for anti-GBM therapy. Many strategies currently involve transferring autologous T cells that have been stimulated ex vivo. *Abbreviations:* Major histocompatibility complex (MHC), cytomegalovirus (CMV)

The entire approach of rendering GBM antigenically foreign to an otherwise unperturbed host through endogenous viruses predicates on intact viral antigen presentation on the tumor cell surface **(Figure 1-5, A).** Though CMV has been detected in GBM, these assays do not test nor guarantee that CMV peptides are presented by major histocompatibility complexes (MHC), and there is adequate reason to doubt the extent to which appropriate antigen

presentation occurs. Over half of human GBM specimens show loss of HLA class I antigens and of the remaining fraction, half show faint staining, leaving only 20% of tumors with robust, intact membrane-bound MHC I expression(Castro et al., 2020; Facoetti et al., 2005). The assessment of MHC I expression should thus be routine in GBM care and should occur prior to the start of CD8 T cell-based immunotherapies. The absence of MHC can be irreversible, as in the case of loss of heterozygosity (LOH) mutations at 6p21 and 15q21, loci corresponding to HLA class I and β2-microglobulin (β2m), respectively, which are critical components of the MHC molecule (Yeung et al., 2013). This occurs in almost half of GBM cases and therapeutic strategies for these patients should be independent of MHC class I antigen presentation and CD8+ T cell engagement (Yeung et al., 2013). In other cases, the absence of surface MHC class I can be reversed with appropriate cytokine stimulation (e.g., type I and II interferons) provided the HLA-A, HLA-B, and HLA-C gene loci are intact(Satoh et al., 2006).

Patients with intact MHC loci might benefit from efforts underway to activate CMV-specific T cells and promote their subsequent engagement of brain tumors by injecting CMV peptides, and early reports demonstrate the safety and feasibility of this approach **(Figure 1-5, B).** (Cuburu et al., 2020; Thompson et al., 2020). Other methods to activate CMV-specific T cells **(Figure 1-5, C).** have included the transfer of autologous DCs pulsed *ex vivo* with CMV lower matrix protein pp65 as an adjuvant to standard of care chemoradiation. Across three sequential, independently-conducted clinical trials, nearly one third of GBM patients receiving pp65 DCs became 'exceptional long-term survivors (Batich et al., 2020; Mitchell et al., 2015). More recent efforts to treat patients with autologous CMV-specific T cells activated and expanded *ex vivo* **(Figure 1-5, D).** demonstrated safety as an adjuvant

therapy for primary and recurrent GBM and the potential to extend survival in part via epitope spreading (Ghazi et al., 2012; Schuessler et al., 2014; Smith et al., 2020). The latter is particularly important given how 'quiet' the adaptive immune response would otherwise be. GBM also has a well-documented history of antigenic escape following therapeutic pressure (Brown et al., 2016). Therefore, harnessing anti-viral immunity to wage an effective GBM response will likely require polyclonal T cell responses as well as epitope spreading to other antigens. The functional attributes of CMV-specific CD8 T cells are also important. To improve the polyfunctionality of therapeutic T cells, investigators recently combined the transfer of autologous CMV pp65-specific CD8+ T cells with pp65 RNA-loaded DCs. This combination improved frequencies of IFNγ, TNFα and CCL3 positive, polyfunctional CMV-specific T cells, which correlated with an increased overall survival(Reap et al., 2018). However, it remains to be determined how these functional attributes influenced the subsequent antitumor response.

The strategies summarized in **Figure 1-5** aim to combat the low immunogenicity of GBM and mount an adaptive antitumor immune response by harnessing CMV xenogenization of the tumor (Kobayashi, 1979). The efficacy of these strategies depends on there being sufficient cognate peptide-MHC I complexes on the surface of tumor cells for subsequent CD8+ T cell engagement and killing. However, MHC I loss is irreversible in nearly half of GBM patients (Yeung et al., 2013), and in the majority of the remaining half, MHC is significantly downregulated (Castro et al., 2020; Facoetti et al., 2005; Satoh et al., 2006). In patients with a loss of MHC I expression, immunotherapeutic strategies must rely on leukocyte-tumor interactions that are independent of MHC (e.g., NK cells or antibodies). On the other hand, patients with inducible MHC I expression should be treated with dual approaches

that first upregulate tumor antigen presentation (e.g., with type I or II interferons) and then promote cytolytic engagement of the tumor by anti-tumor (viral) CD8+ T cells.

1.2.2 ONCOLYTIC VIRAL THERAPY

Oncolytic viruses (OVs) are naturally occurring or genetically engineered viruses that selectively infect and lyse tumor cells, disseminating to adjacent malignant cells to repeat the process. OVs exploit the inherent dysregulation within the cancer cell – from cell signaling abnormalities to incapacitated antiviral machinery – as well as the cancer's own immune evasion pathways, to preferentially infect and reproduce in neoplastic cells (Kaufman et al., 2015). For this reason, oncolytic viruses do not necessarily rely on neoantigens at the tumor cell surface for their selective infection of tumor cells. OVs orchestrate antitumor activity through two distinct but related mechanisms. The first is their direct lysis of tumor cells, and the second is the concomitant innate and adaptive response mounted in response to damaged-associated molecular patterns (DAMPs) and viral pathogen-associated molecular patterns (PAMPs) released from dying tumor cells **(Figure 1-6).** The latter is thought to break immune tolerance against GBM. In fact, the molecular signals and cytokines induced by infection with OVs activate and attract a variety of APCs, as well as innate

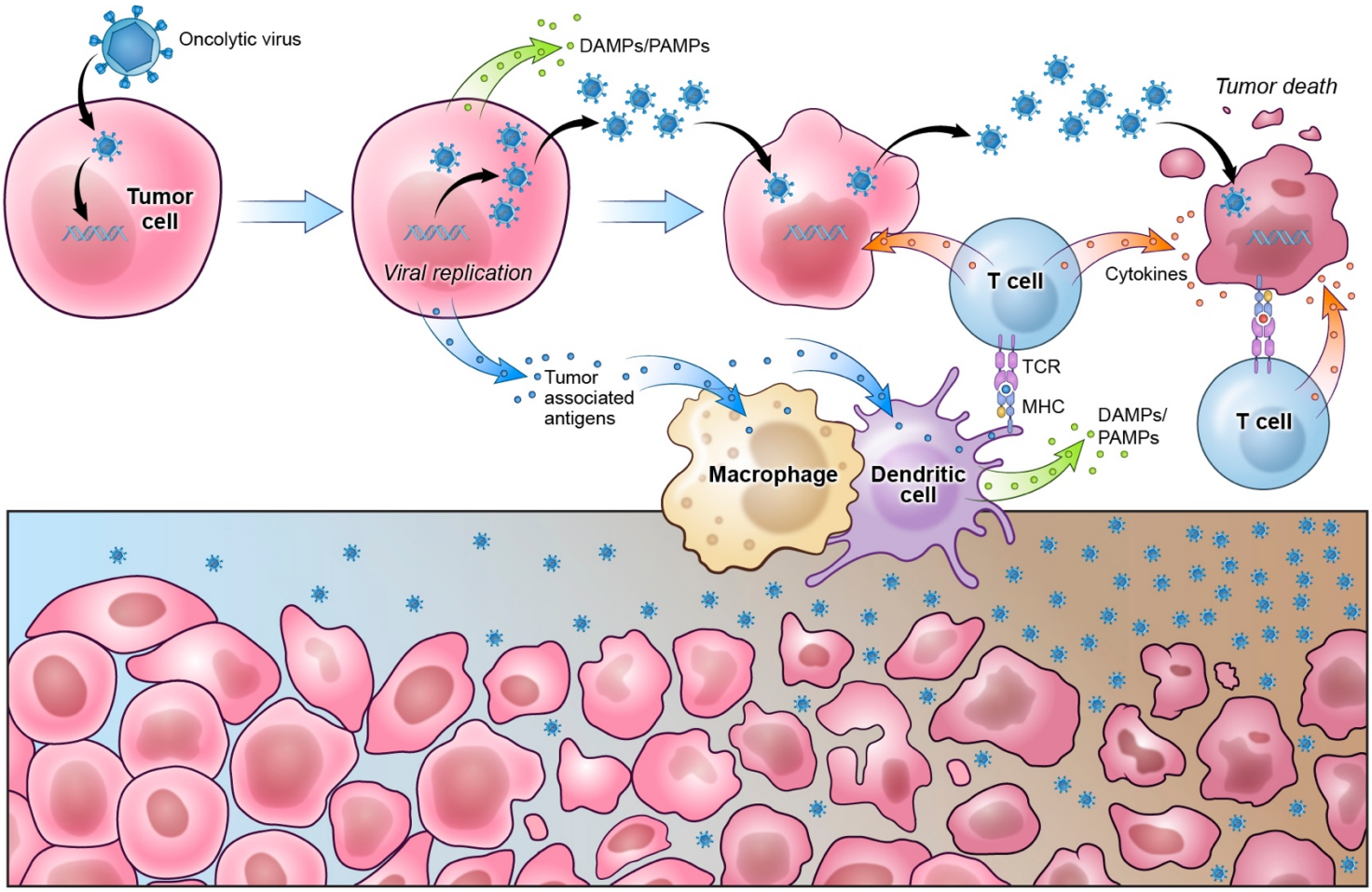

Figure 1-6: Viral oncolysis of glioblastoma. Oncolytic viruses are either naturally selected or engineered to preferentially infect tumor cells. Upon entry, viruses co-opt tumor cell machinery to support their own replication and lyse tumor cells in the process. Viral progeny are then released and continue infecting surrounding tumor cells. Secondary immune reactions develop in response to damage- and pathogen-associated molecular patterns (DAMPs and PAMPs), breaking immune tolerance against GBM. Increased antigen presentation facilitates the generation of both anti-viral and anti-tumor T cells that help destroy tumor cells. *Abbreviations:* T cell receptor (TCR), major histocompatibility complex (MHC)**.**

and adaptive immune cell subsets. Remarkably, induction of a pleiotropic anti-GBM response by OVs has promoted survival in a subset of GBM patients.

Among the most promising candidates is a prototype oncolytic poliovirus (PV) recombinant, PVSRIPO - a modified poliovirus lacking neurovirulence (Dobrikova et al., 2012). The tropism of PVSRIPO is based on CD155, which is type I transmembrane glycoprotein broadly upregulated on a variety of tumor cells, but not on normal adult neural cells, and on APCs (Chandramohan et al., 2017). Infection of DCs by PVSRIPO does not lyse them. Rather, it induces a strong type I interferon response, enhances antigen presentation, and promotes the ability of DCs to prime tumor-specific T cells that traffic to the tumor microenvironment (Brown et al., 2017; Mosaheb et al., 2020). In a recent Phase 2 dosing study, PVSRIPO delivered intratumorally via catheter modestly increased survival relative to a historical control group from 11.3 to 12.5 months. However, more impressive was the fact that survival plateaued at 21% in PVSRIP patients at 24 months and 36 months compared to 14% and 4%, respectively, in historical controls (Desjardins et al., 2018). These data suggest that a robust anti-tumor immune response was sustained in patients who responded to treatment, although additional studies into the HLA status and anti-tumor immune response in surviving patients are warranted. It will also be important to determine whether PVSRIPO promoted release of hidden tumor neoantigens. Though most patients experienced adverse events related to brain inflammation, a concern with OVs, edema was successfully managed in all cases. Some potential confounding variables in this exciting trial include the younger age of study participants as well their higher initial gross total resection rates and lower rates of prior bevacizumab (anti-VEGF) therapy than historical controls.

In other OV trials, subsets of patients have similarly experienced durable clinical responses. Following intratumoral inoculation of a tumor-specific adenovirus, DNX-2041, 20% of patients were alive at 36 months(Lang et al., 2018). Radiographic data in responders suggested immunogenic cell death, which is hypothesized to be the mechanism of action with OVs. G47Δ, a third-generation type I Herpes Simplex Virus (HSV-1) developed in Japan received 'Sakigake' breakthrough status and is expected to receive fast-track drug approval soon. Recent preliminary data from a Phase II study following six intratumoral injections of G47Δ showed a one year survival rate of 92.3% relative to the historical control rate of 15% (Todo, 2019). HSV-1 possesses a few advantageous properties. First, it is highly proliferative and thus can achieve high titers. Second, it does not integrate into the host genome. Third, anti-HSV-1 agents to which G47Δ is hypersensitive are readily available, providing a safety break if needed (Agarwalla & Aghi, 2012). Despite the capacity of HSV-1 to infect a variety of cells, deletion of ICP6, a ribonucleotide reductase (RR) required for viral DNA synthesis, in G47Δ renders the virus dependent on abundant RR in the cells it infects. Tumor cells, but not normal cells, express sufficient compensatory levels of RR to support G47Δ replication (Mineta et al., 1995).

Another virus that has attracted attention for its neurotropism is Zika Virus (ZIKV). It was recently reported that ZIKV preferentially lyses patient derived glioma stem cells (GSCs) over differentiated GBM cells or human neural precursors, due in part to increased surface integrin alpha chain V expression (Zhu et al., 2017; Zhu et al., 2020). GSCs are thought to drive tumor growth, immune evasion, and recurrence given their self-renewing multipotent nature, selective therapeutic resistance, and capacity to co-opt angiogenesis to self-sustain(Gimple et al., 2019). The use of ZIKV in GBM is still in the preclinical phase.

OVs offer the promise of not only warming an otherwise 'cold' tumor niche, but also of delivering therapeutic cargo encoded in the virus. This is of particular importance in GBM since the various barrier systems of the CNS passively and actively (via efflux pumps) work to prevent the infiltration of delivered drugs. Indeed, drug concentrations in the tumor microenvironment can be less than 20% of their concentration in the plasma **(Figure 1-7, A)** (Zhou et al., 2007). Arming OVs with immunostimulants provides another opportunity for this new class of therapeutics to break immune tolerance against GBM and control cargo delivery both spatially and temporally **(Figure 1-7, B)**. In pre-clinical studies using a fatal genetic model of GBM, an oncolytic HSV encoding IL-12 resulted in an unprecedented degree of protection and a 30% cure (Alessandrini et al., 2019).

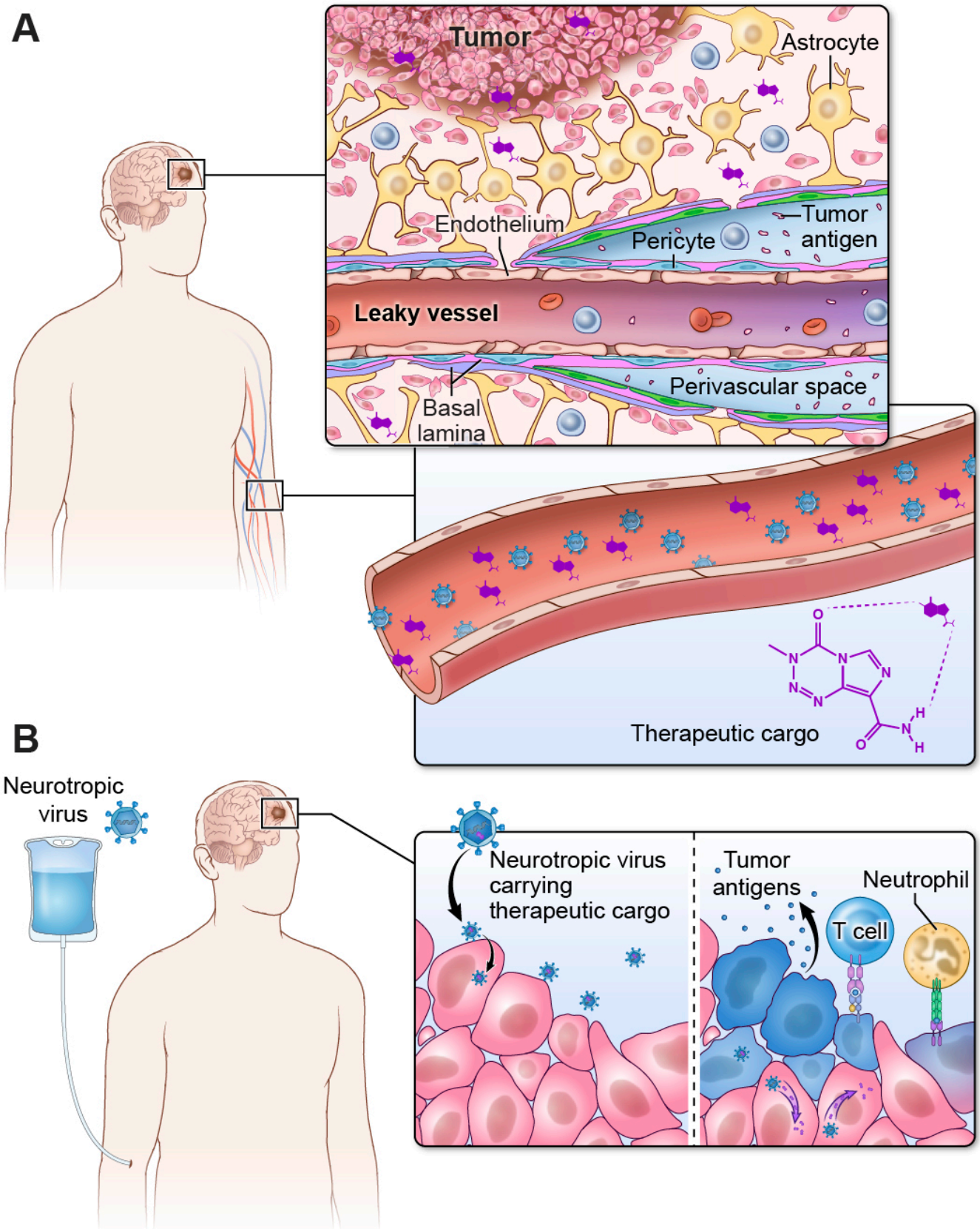
A
Tumor
Astrocyte
Endothelium
Pericyte
Tumor antigen
Leaky vessel
Perivascular space
Basal lamina
Therapeutic cargo
B
Neurotropic virus
Neurotropic virus carrying therapeutic cargo
Tumor antigens
Neutrophil
T cell

Figure 1-7: The blood-brain-barrier (BBB) makes it challenging to deliver drugs to GBM. (A) Approximately 20% of the delivered concentration of anticancer therapeutics reach the tumor bed despite the presence of leaky vessels. The BBB limits the degree to which therapeutics can access GBM. (B) Neurotropic viruses are naturally selected biologic agents that can traverse the BBB and infect the tumor bed. These viruses can be engineered to carry therapeutic cargo that is delivered directly to tumor cells, stimulating innate and adaptive immune responses.

1.2.3 CONCLUDING REMARKS

GBM remains one of the deadliest cancers, and its long-term survival rate has not changed in the last 50 years. There is a plethora of reasons for GBM's recalcitrance and lethality, a few of which include its striking heterogeneity, subset of stem cells, and capacity to induce systemic immune suppression. There are also significant limitations in the capacity of the brain to detect GBM antigens and support afferent as well as efferent immune responses. Few interventions can overcome all these hurdles except for virotherapy. Further studies are warranted to better understand the mechanisms by which these virotherapies work and improve upon their efficacy in all GBM patients. It will be important to map out determinants of long-term durable anti-tumor immune responses and identify other immunomodulatory therapies that provide synergistic combinatorial effects. Nonetheless, the rapid development of viral therapies for GBM starting at the turn of this century may ultimately have the greatest impact on improving life expectancy for GBM patients.

2 MATERIALS AND METHODS

2.1 *IN VIVO* EXPERIMENTS

2.1.1 MICE

Mice were bred and maintained in specific pathogen-free (SPF) conditions at the National Institutes of Health. The housing conditions were as follows: 22 degrees Celsius, 50% humidity, and a 12-hour light/dark cycle. If purchased or provided by collaborators, mice were transferred and then maintained under SPF conditions at the NIH. Mice used for the experiments in this thesis were 6-8 weeks of age and matched with age control groups. All mice were handled according to the NIH Animal Care and Use Committee guidelines and the recommendations set forth in the AAALAC Guide for the Care and Use of Laboratory Animals. Animal protocols were approved by the NINDS Animal Care and Use Committee.

2.1.1.1 MOUSE TRANSGENIC MODELS

C57BL/6J (B6), B6.129P- CX3CR1tm1 Litt/J ($CX3CR1^{GFP/GFP}$) (Jung et al., 2000), and B6.129(Cg)-Ccr2tm2.1Ifc/J ($CCR2^{RFP/RFP}$) (Saederup et al., 2010), and B6.Cg-Gt(ROSA)26Sortm14(CAG-tdTomato)Hze/J ($Stop^{fl/fl}$ tdTomato) (Madisen et al., 2010) mice were purchased from Jackson Laboratories. $CX3CR1^{GFP/WT}$ mice were generated from an F_1 cross of $CX3CR1^{GFP/GFP}$ and B6 mice. $CCR2^{RFP/WT}$ mice were generated from an F_1 cross of $CCR2^{RFP/RFP}$ and B6 mice. $CX3CR1^{GFP/WT}CCR2^{RFP/WT}$ Double Reporter mice were generated from an F_1 cross of $CX3CR1^{GFP/GFP}$ and $CCR2^{RFP/RFP}$ mice. B6.LysM $^{GFP/WT}$ (LysM $^{GFP/WT}$) mice were kindly provided by T. Graf (Albert Einstein College of Medicine,

Bronx, New York, USA) (Faust et al., 2000). LysM $^{GFP/GFP}$ mice were crossed with B6 to generated and maintain a colony of heterozygotes used for experiments. So-called Resident Red mice (i.e., enabling the visualization of resident CX3CR1+ mice, microglia) were generated from an F_1 cross of CX3CR1$^{CreER/WT}$ and Stop$^{fl/WT}$ TdTomato mice.

To enable CD8-T cell tracking of the dominant LCMV epitope, B6.Cg-Tcra^{tm1Mom}Tg(TcrLCMV)327Sdz/TacMmjax (P14) mice (Pircher et al., 1989) were bred and maintained at the NIH. To enable CD8-T cell tracking of the dominant Ovalbumin epitope, OT-I mice were used. Both reporter lines were crossed to a variety of fluorescent reporters (e.g., mTomato, Orange Fluorescent Protein (OFP)), and Calcium reporters (actin-GCamP6s), and in some cases triple crossed to enable tracking by color, epitope, and Calcium flux for intravital two-photon microscopy (Gossa et al., 2014; Moseman et al., 2016). This enabled the generation of P14 x OFP, P14 x m-Tomato, P14 x m-Tomato x GCamP6s, OTI x m-Tomato, and OTI x m-Tomato x GCamP6s mice.

2.1.1.2 INTRACEREBRAL TUMOR INJECTIONS

Mice were anesthetized with ketamine (85 mg/kg), xylazine (13 mg/kg) and acepromazine (2 mg/kg) in saline, and their body temperatures were maintained at 37°C. Hair covering the scalp was removed with clippers, and the area was cleaned with ethanol. Using a microsurgical blade, a clean incision was made to expose the skull, and the periosteum was subsequently removed. A metal bracket with an open circular area was secured onto the skull such that the center point of the exposed circle was 2mm lateral to the sagittal suture and 2mm anterior to the lambdoid suture. Very carefully, a cranial window in the skull measuring 2 x 2mm was thinned to 20-25μm using a microsurgical blade. Burr holes

were never used given the immense injury response caused by this commonly used technique; non-injurious skull thinning was based on previously documented techniques from the McGavern laboratory (Manglani & McGavern, 2018). Mice were immobilized on a Leica Angle Two Stereotaxic Instrument and using stereotactic guidance, a syringe gently pierced the thinned skulled and was lowered 500 microns below the surface. 5,000 tumor cells in a volume of 2µl of sterile saline were then injected at a rate of 7nl per second to avoid increasing intracranial pressure and causing second-order tissue damage to the tumor. Following slow removal of the inserted syringe, incisions were closed with wound clips and mice were injected with Buprenex (0.1 mg/kg) for subsequent pain management, and Antisedan (1mg/kg; Revertidine) for anesthetic reversal. Mice were maintained on heat pads to ensure optimal core body temperature until they were active and alert.

2.1.1.3 VIRAL INFECTIONS

Lymphocytic Choriomeningitis Virus (LCMV), a non-cytopathic arenavirus, was used in the majority of experiments for this thesis. Mice were infected with acute LCMV by intravenous (i.v.) administration of 2 x 10^6 Plaque Forming Units (PFU) Armstrong clone 53b 1 day after intracerebral tumor implantation. The virus was sourced from a colony of carrier mice (i.e., mice bred to maintain persistent LCMV infection following an initial intracerebral inoculation of parent mice at 1 day old (Oldstone et al., 1986). Viruses were propagated on singly passaged BHK-21 cells. The infectivity of each virus was quantified via limiting dilution plaque assay (infectious center assay) on green monkey kidney (Vero) cells as follows (Welsh & Seedhom, 2008). 100µL of serially diluted viral supernatant was placed on Vero monolayers growing 24-well flat plates and incubated for 3 hours. Then,

100µL of a 0.75% methylcellulose DMEM mixture (containing 10% FBS, 1% glutamine, and 1% Penicillin/Streptomycin) was added to each well and incubated for 48 hours in an incubator maintained at 37°C and 5% CO_2. Finally, cells were fixed with 4% neutral buffered formalin and stained with crystal violet for plaque enumeration.

For indicated experiments in which tumor cells were pre-infected prior to implantation, cells were infected *in vitro* by coating the cellular monolayer. Viral stock was diluted in cellular media for a final multiplicity of infection (MOI) of 1. Every 10 minutes for 1 hour the flask was gently rocked back and forth. At the end of the hour, the viral media was aspirated, and fresh media was applied.

2.1.1.4 SURVIVAL STUDIES

Following brain tumor surgery, mice were monitored daily for one week. Then, starting at 20 days post injury (dpi), mice were monitored daily for distress and weight loss. Those that lost greater than 25% of their originally-recorded weight or showed physical signs of distress reached endpoint and were sacrificed. The number of days since intracerebral surgery was performed was recorded.

2.1.1.5 T CELL ISOLATION AND ADOPTIVE TRANSFERS

To enable the tracking of either tumor-specific or virus-specific T cells, mice were pre-seeded 24h prior to intracerebral tumor implantation with adoptively transferred T cells from various donor mice i.e., P14 (CD8+ LCMV-Armstrong specific T cells) and OT-I (CD8+ Ovalbumin-specific T cells). Depending on the quantity needed for the experiment, CD8+ T cells were purified from the spleens or blood of naïve mice via negative selection

(EasySep, StemCell Technologies). Under sterile conditions, spleens were collected from 6–8-week-old donor mice into sterile Hanks' Balanced Salt Solution (HBSS) containing 2% fetal bovine serum (FBS). (Alternatively, a capillary tube of whole blood (~50µL volume) was collected and diluted in 1mL PBS. A small sample was stained to count the number of T cells by flow cytometry and transferred to recipient mice immediately thereafter). If a greater number of cells was needed, the spleen was mechanically disrupted through a 40µm mesh strainer to remove aggregates and debris. Following centrifugation at 300g for 10 minutes, a large pellet was formed and the sample was resuspended at a concentration of 1 x 10^8 cells/mL in EasySep Buffer (i.e., PBS free of Calcium and Magnesium ions, containing 2% FBS and 1mM EDTA). Rat serum at a concentration of 50µL/mL of sample was added to prevent non-specific antibody binding. The sample was then added to a 5ml polystyrene rounded-bottom tube and 50µL/mL of the Isolation Cocktail containing antibodies for negative selection was added to the tube. The sample was mixed and incubated at room temperature for 10 minutes. During this step, the Vortex RapidSpheres (magnetic beads) were vortexed for 30 seconds and 75µL/mL of sample was added to the tube. The sample was mixed and incubated at room temperature for 2.5 minutes. EasySep Buffer was added until the total volume reached 2.5mL and the sample was pipetted up and down 3 times. After removing the lid, the tube was placed into the EasySep magnet for 2.5 minutes. In one continuous fell swoop, the magnet was inverted, and the enriched cell suspension was poured into a new tube. The cells were counted, and 1 x 10^4 T cells were injected intravenously per recipient mouse.

2.1.2 INTRAVITAL TWO PHOTON MICROSCOPY (2P)

2.1.2.1 SKULL THINNING

Mice were anesthetized with ketamine (85 mg/kg), xylazine (13 mg/kg) and acepromazine (2 mg/kg) in saline, and their body temperatures were maintained at 37°C. Hair covering the scalp was removed with clippers, and the area was cleaned with ethanol. Using a microsurgical blade, a clean incision was made to expose the skull, and the periosteum was subsequently removed. A metal bracket with an open circular area was glued onto the skull such that the center point of the exposed circle was the site of tumor injection, 2mm lateral to the sagittal suture and 2mm anterior to the lambdoid suture. Very carefully, a cranial window in the skull measuring 2 x 2mm was thinned to 20-25µm using a microsurgical blade and the utmost care was taken to not disturb the area where the tumor was injected, but rather to thin around the site to ensure maximum visibility which required no bleeding under the surface of the previously injected skull.

2.1.2.2 INTRAVITAL IMAGING

The thinned skull described above served as the window through which live mice were imaged at various indicated time points following tumor implantation and/or viral infection. This method has been previously described and optimized by the McGavern lab (Manglani & McGavern, 2018). Mice were imaged using a Leica SP8 two-photon (2P) microscope equipped with the following: an 8,000-Hz resonant scanner, a 25x collar-corrected water-dipping objective (1.0 NA) or a 20x water-dipping objective (1.0 NA), a quad HyD external detector array, a Mai Tai HP DeepSee Laser (Spectra-Physics, Santa Clara, CA) tuned to a wavelength of 905 nm (for the detection of Green Fluorescent Protein (GFP), Alexa Fluor 488 (Af488), and Dylight 488 channels) and an Insight DS laser (Spectra-

Physics) tuned to 1,050 nm (for the detection of Evans blue (EB) and TdTomato channels) or to 1,100 nm (for the detection of Phycoerythrin (PE) and Allophycocyanin (APC) detection). Lenses were submerged into artificial cerebral spinal fluid (aCSF) (Harvard Apparatus, 597316) on the thinned skull. aCSF was maintained in the secured bracket at all times during imaging to ensure minimal dissonance between the refractive properties above and below the thinned skull bone.

Three-dimensional time-lapse movies were captured as Z stacks in 1-minute intervals using 20-70 planes of a 2.5-3um step size, depending on visibility conditions. For GCaMP imaging, stacks were acquired at 10-second intervals given the speed of Calcium flux. The signal to noise contrast was optimized by averaging 6-8 video frames per plane in resonance scanning mode. For the visualization of blood vessels, 70ul of Evans Blue (0.1mg/mL, Sigma, St. Louis, MO) diluted in PBS was injected retro-orbitally just before imaging. Alternatively, to visualize blood vessels in the GFP channel, 70ul of tomato lectin Dylight 488 (Vector Labs, Burlingame, CA) was injected retro-orbitally just before imaging. Tumor cells expressed either GFP or RFP enabling their clear visualization. CX3CR1$^{GFP/WT}$ mice enabled the visualization of brain myeloid cells. LysM $^{GFP/WT}$ were used to track infiltrating myelomonocytic cells.

For T cell tracking experiments, mice were pre-seeded with T cells expressing complementary fluorescent proteins to enable their discernment (i.e., GFP T cells with an RFP tumor, or vice versa). To measure the proportion of OT-I GCamP6s+ and P14 GCaMP6s+ T cells fluxing Calcium, as a proxy for T cell receptor/cognate ligand engagement, the percentage of flashing (i.e., GFP+ signal) vs non-flashing T cells fluxing at randomly selected

time points throughout a time lapse was calculated. During the grading process, group identities (i.e., control vs experimental) were blinded.

All imaging was acquired with Leica Application Suite X (LAS X) software v3.5.5.19976. The imaging was subsequently exported to Imaris version 9.6 (Bitplane, Concord, MA) for downstream analysis, and Adobe Premiere Pro 14.0 (Adobe systems, San Jose, CA) was used to edit final videos.

2.2 HIGH-PARAMETER FLOW CYTOMETRY (FACS)

2.2.1 CELL ISOLATION FROM THE BRAIN

At the indicated time points, mice were anesthetized, perfused with saline and their brains explanted. The following protocol was utilized for tumors through the 10dpi timepoint. To avoid diluting the preparation with naïve and unperturbed glial cells uninvolved in the tumor microenvironment (TME), a 2mm punch biopsy (MTP-33-34, Brain Tree Scientific) centered on the site of tumor injection was extracted. This punch biopsy was mechanically disrupted through a 70µm mesh strainer to remove aggregates and debris and washed with 20mL of FACS buffer (PBS containing 2% FBS). The samples were centrifuged at 500g for 5 minutes at 4 °C and the ensuing pellets were resuspended in 1mL FACS buffer and passed through a 35µm mesh strainer (352235, Corning). To create a 30% Percoll gradient, an additional 1mL of FACS buffer and 860µL of Percoll (GE17-5445-01, Sigma-Aldrich) were added to the filtered sample. Samples were centrifuged at 500g for 15 minutes at 4 °C with no deceleration. The myelin and debris remained at the top of the gradient, both

of which were aspirated. The final pellet was resuspended in 200µL and cells were then stained.

At timepoints later than 10dpi, the matrix in the tumor was too rigid to mechanically dissociate. Thus, the following enzymatic digestion protocol was used with the Tumor Dissociation Kit (130-096-730, Miltenyi Biotec). The enzyme mix was prepared by adding 2.35mL of RPMI 1640, 100µL of Enzyme D, 50µL of Enzyme R, and 12.5µL of Enzyme A in a gentleMACS C Tube. The tumor was minced with microsurgical scissors into small 1m x 1mm pieces and transferred to the gentleMACS C tube containing the enzyme mix. The mix was tightly closed and inverted on the sleeve of the automatic gentleMACS Dissociator and the "37C_m_TDK_1" program was selected. Following termination of the program, the C tube was detached from the Dissociator and the sample was strained through a 70µm mesh trainer placed on a 15mL Falcon tube. The strainer was washed with an additional 10mL of RPM1 1640 media. The cell suspension was centrifuged at 300g for 7 minutes and the pellet was resuspended in 200µL of FACS buffer and plated in a 96-well V bottom plate for staining.

2.2.2 CELL ISOLATION FROM THE SPLEEN AND LYMPH NODES

Spleens and lymph nodes were extracted from perfused mice and mechanically dissociated through a 70µm mesh strainer in a 50mL Falcon tube to remove aggregates and debris. The mesh strainer was washed with 20mL of FACS buffer to remove any remaining cells. The samples were centrifuged at 500g for 5 minutes at 4 °C and the ensuing pellets were resuspended in 1mL of FACS buffer. Cells were counted and 2 x 10^6 cells in 200µL of FACS buffer were transferred to a 96-well V bottom plate for staining.

2.2.3 CELL ISOLATION FROM THE BLOOD

Two heparinized micro-hematocrit tubes (Fisher 02-668-66) of blood were drawn from anesthetized mice prior to euthanasia and the blood was immediately emptied into an EDTA-coated collection tube. 1mL of Red Blood Cell (RBC) lysis buffer was added to the samples which were incubated on ice for 10 minutes. To neutralize the lysis reaction, FACS buffer was added, and samples were re-centrifuged at 500g for 5 minutes at 4 °C prior to plating in a 96-well V bottom plate for staining.

2.2.4 FACS STAINING

Cell suspensions in the 96-well V bottom plate were pelleted and resuspended in a 50µL master mix made of FACS buffer and the antibodies described in **Table 2-1** from either BioLegend (BioL) or BD at the indicated volume dilutions**.** Cells were kept in the dark and incubated for 15 minutes at 4 °C, then pipetted via multi-channel pipette and incubated in the dark at room temperature (22 °C) to enable certain chemokine staining. Cells were washed with 200µL of FACS before, centrifuged for 5 minutes, and then resuspended in 50µL of a PBS/LiveDead Fixable Blue Cell Staining mix for dead cell exclusion. Cells were kept in the dark and incubated for 10 minutes at 4 °C, washed, centrifuged, and fixed in 10% formalin for 10 minutes. Cell were washed, centrifuged, then resuspended in 250µL of FACS buffer and maintained in the dark at 4 °C prior to acquisition on a BD FACSymphony A-5 High Parameter Cell Analyzer.

For intracellular cytokine or growth factor staining, tissues were collected and processed in medium containing 1µL/mL of BD GolgiPlug (containing Brefeldin A, 555029).

Following fixation as described in the previous paragraph, cells were washed twice in 250µL of BD Perm/Wash Buffer. Cells were then stained in a 50µL solution of BD Perm/Wash Buffer containing the pre-determined concentration of antibody for intracellular staining and were incubated for 30 minutes at 4 °C in the dark. Cells were then washed twice in 250µL of BD Perm/Wash Buffer and resuspended in 200µL for FACS buffer for acquisition.

Table 2-1: Master Staining Panel for High Parameter Flow Cytometry.

Laser	Detector	Filters		Fluorochromes	Marker	Dilution	Vendor
Blue 488nm	**B515**	505LP	515/20	**FITC, A488, BB515, GFP, CFSE**	**CD11c**	200	BioL
	B780	750LP	780/60	**BB796**	**Ly6c**	200	BD
Violet 405nm	**V450**	**	450/50	**BV421, ViViD, Pac Bl, H450**	**CD103 BV421**	200	BD
	V510	450LP	474/25	**BV480, BV510, Aqua Bl, AmCyan, QD525**	**MHCII BV480**	450	BD
	V570	550LP	586/15	**BV570, QD565 (Cy3 acceptor)**	**CD11b BV570**	100	BioL
	V605	600LP	610/20	**BV605, QD585**	**TCR B BV605**	100	BioL
	V655	635LP	670/30**	**BV650, QD655**	**CD24 BV650**	300	BD
	V710	690LP	710/50	**BV711, QD705**	**CX3CR1 BV711**	100	BioL
Green 532nm	**G575**	**	575/26	**PE, Cy3, A532**	**P2ry12 PE**	200	BioL
	G660	635LP	670/30	**Cy5PE, A647PE, 7AAD**	**Ter119 PECy5**	2000	BioL
	G780	750LP	780/60	**Cy7PE, A750PE**	**CD206 PECy7**	400	BioL
UV 355nm	**U395**	**	379/20	**BUV395**	**CD45**	200	BD
	U450	410LP	450/50	**UV-Blue Viability**	**L/D blue**	1000	BD
	U500	450LP	515/30	**BUV490**	**CD4**	100	BD
	U570	550LP	586/15	**BUV550**	**Ly6G**	150	BD
	U670	635LP	670/30	**BUV680**	**CD19**	100	BD
	U740	690LP	740/35	**BUV737**	**CD44**	1400	BD
	U785	770LP	820/60	**BUV815**	**CD8**	100	BD
Red 628nm	**R670**	**	670/30	**APC, A647**	**VEGF or CD115**	100	BioL
	R730	690LP	710/50	**Cy55APC, A660, A680, A700, R700APC**	**F480**	500	BD
					Fc Block (CD16/32)	**200**	**BioL**

2.2.5 FACS ANALYSIS

Data were analyzed using FlowJo version 10. Date were first cleaned using the FlowAI algorithm and doublets and dead cells were removed. Samples were fully compensated and then subject to the PhenoGraph algorithm to identify cell populations and subpopulations in as unbiased and inclusive a manner as possible. UMAPs were generated with the UMAP plugin, onto which the identified cell clusters were mapped. Heatmaps and histograms of various markers were generated to define these cellular subsets according to their differential expression of over 20 proteins.

2.3 IMMUNOHISTOCHEMISTRY (IHC)

Mice were perfused intracardially with 4% paraformaldehyde (PFA). Their brains were explanted and incubated overnight at room temperature in 4% PFA. Brains were then sectioned in 100µm sections through the entire brain tumor lesion using a Compresstome (Precisionary).

2.3.1 STAINING

Sections were incubated on a shaker at room temperature for 30 minutes with Permeabilization and Blocking Buffer: 500µL PBS containing 0.1% Triton X-100 (AC215682, Thermo Fisher Scientific) and 3 drops per sample of Background Buster (NB306, Innovex Biosciences). To visualize microglial (Iba1+), brain sections were incubated with rabbit anti-Iba1 (1:500, 019-19741, Wako Chemicals). Alternatively, resident myeloid cells were labeled endogenously when using CX3CR1$^{GFP/WT}$ reporter mice and infiltrating myeloid cells

were labeled endogenously when using LysM$^{GFP/WT}$ reporter mice. Red blood cells were quantified using anti-Ter119 antibody conjugated to PE (1:500, BioLegend).

Primary antibody solutions were applied overnight on a shaker at 4 °C in the dark. Brain slices were then washed 3 times with PBS to remove any unbound antibody. Secondary antibodies were then applied in a buffer containing 0.1% Triton X-100 for 2 hours at room temperature with one of the following antibodies: goat anti–guinea pig Alexa Fluor 488 (1:500, A-11073, Thermo Fisher Scientific), donkey anti–rabbit Alexa Fluor 647 (1:500, A-31573, Thermo Fisher Scientific), or goat anti–mouse Alexa Fluor 488 (1:500, A-21131, Thermo Fisher Scientific). Where indicated, as a final step, DAPI was added for 10 minutes, and sections were washed. Slices were mounted on charged glass slides and 2 drops of FluorSave Reagent (Calbiochem) were added to each section before the final placement of a coverslip.

To stain for VL4 (LCMV nucleoprotein), brains with skulls attached were flash frozen in 2-methylbutane and then embedded intact in Tissue Freezing Medium (Triangle Biomedical Sciences). Coronal cryosections were cut using a Leica CM1850 cryostat at a thickness of 20-30 µm. Slices were briefly fixed for 10 minutes with 4% PFA at room temperature (RT), then incubated in anti-VL4 primary antibody for 1hr at RT, followed by a tagged secondary for 1 hour at RT.

2.3.2 IMAGE ACQUISITION AND ANALYSIS

Images were acquired using an Olympus FV1200 laser-scanning confocal microscope fitted with a 20X objective. Z stacks were 20µm. Confocal images were analyzed and edited using Imaris version 9.6 image analysis software. To enumerate the parameter of

interest, “surfaces” of “spots” were created based on signal thresholds from internal negative controls on the contralateral brain hemisphere, and the volumes or quantities enumerated.

2.4 SINGLE-CELL SEQUENCING

2.4.1 scRNA-SEQ LIBRAY PREPARATION, SEQUENCING, AND ANALYSIS

The following protocol was adapted from Kory Johnson, PhD, from the NINDS Bioinformatics core facility. I am grateful to Kory for analyzing the single-cell sequencing data in this thesis.

scRNA-Seq Libray Preparation, Sequencing, and Analysis. cDNA libraries were prepared from single-cell suspensions following the 10x Genomics 3' v3 protocol (www.10xgenomics.com) and sequenced on NovaSeq (www.illumina.com); returning an average of 8,066 reads per cell for an average of 8,602 cells per sample. Post sequencing, the 10x Genomics "cellranger" tool suite (v6.0.1) was used to generate expression counts per known gene (refdata-gex-mm10-2020-A) per sample. These counts were then imported into R (https://cran.r-project.org) for analysis using functions supported in the Monocle3 package (https://cole-trapnell-lab.github.io). For import, the "load_cellranger_data" function was used followed by the "combine_cds" function to collapse the count data across samples into one analysis-ready object. To select the number of principal components to use for analysis (n=50), the "plot_pc_variance_explained" function was used. To generate cell-level metrics, the "preprocess_cds" function was used. Cells observed to have a total number of features > 32,500 and/or total number of genes > 6,500 were removed from analysis as were cells having a total number of features < 250. Cells having a total percent read mapping to "mt-" genes greater than 15% were also removed. The "preprocess_cds" function was then used

again followed by use of the "align_cds" function with the "residual_model_formula_str" parameter included to correct for differences in total percent reads that map to "mt-" genes. To produce initial grouping of cells by partition and cluster, the "reduce_dimension" and "cluster_cells" functions were used. Doublet clusters and doublet cells were then tested for and removed using the "findDoubletClusters" and "computeDoubletDensity" functions supported in the "scDblFinder" package. The same functions used to generate the initial groupings of cells were then repeated, starting with the "preprocess_cds" function, producing final groupings of cells by partition and cluster. Annotation of these groupings per cell type was accomplished using the "SingleR" package in conjunction with the "MouseRNAseqData" and "ImmGenData" reference data sets. Visual inspection of the final groupings of cells was accomplished using the "plot_cells" function (reduction_method = "UMAP"). To describe the number of cells vs group vs sample, bar plots were generated using the "ggplot" function in conjunction with different options (position = "fill", position = "stack"). To identify markers per group, the "top_markers" function was used. To identify differential genes within a group between samples, the "fit_models" function was used. To visualize markers and differential genes, both dot plots and violin plots were generated using the "plot_genes_by_group" and "plot_genes_violin" functions respectively. To identify and visualize modules of co-regulated genes per group, the "graph_test", "find_gene_modules", "aggregate_gene_expression", and "pheatmap" functions were used. For groups of cells observed to have substructure, cells for the group were subset and the same functions used to generate the final groupings of cells repeated. Trajectory fitting was also explored for these subset groups of cells using the "learn_graph" and "order_cells" functions with the resulting

fits visualized using the prior mentioned "plot_cells" function (show_trajectory_graph = TRUE).

2.5 CELL CULTURE

SB28 cells were generously provided by Hideho Okada, MD, PhD at UCSF, Department of Neurosurgery. GL261 cells were purchased from the National Cancer Institute (NCI). SB28 and GL261 cells were cultured in monolayers with DMEM (Gibco) + 10% FBS and 1% L-glutamine (Sigma-Aldrich). All cells were confirmed to be mycoplasma free, and stocks were maintained in Liquid Nitrogen and -80°C. A new vial was thawed days before tumor cell implantation. One to two days after thawing, the cells were passaged. The day after passage (to capture exponential growth), the cells were collected and used for injections.

2.5.1 CELL LINE TRANSDUCTION

The following protocol was adapted from Vanja Lazarevic, PhD, from NCI. I am grateful to Vanja for generating the SB28-mTomato-Ova cell lines used in this thesis.

The membrane TdTomato-IRES element was amplified from pQC membrane TdTomato IX (https://www.addgene.org/37351/) by using cloning primers: TdTomato-IRES-BamHI-F:5'-agtcGGATCCatgctgtgctgtatgagaag-3' , and TdTomato-IRES-XbaI-R: 5'-agtcTCTAGAttatcatcgtgtttttcaaag-3', and then digested with BamHI and XbaI (New England Biolabs; NEB) to attain cohesive ends where respective restriction sites are shown in capital letters.

OVA was amplified from pcDNA3-OVA (https://www.addgene.org/64599/) by using the following primers: OVA-BamHI-XbaI-F: 5'-

agtcGGATCCTCTAGAatgggctccatcggtgcagc-3', and OVA-KpnI-R: 5'-agtcGGTAC-Cttaaggggaaacacatctgcc-3', and digested with XbaI and KpnI (NEB).

pLKO.1 puro (https://www.addgene.org/8453/) acceptor vector was digested with BamHI and KpnI (NEB) to remove the puromycin resistance cassette.

The three parts were mixed 1:1:1 and directionally ligated with T4 DNA ligase (NEB), and subsequently transformed in STBL-3 cells. Positive ampicillin- resistant colonies were selected, screened by restriction digestions, and the sequence was verified (Quintarabio) to attain the final pLKO.1-membrane TdTomato-IRES-OVA construct.

2.6 STATISTICAL ANALYSIS

Experiments involving 2 groups were analyzed with a 2-tailed Student's *t* test for parametric data and a ranked sum test for non-parametric data. Studies containing more than 2 groups were analyzed with a 1-way ANOVA (parametric) or a 1-way ANOVA on ranks (non-parametric). When comparing the means of more than 2 groups, multiple *t* tests with Holm-Sidak multiple comparisons correction was used. For survival studies, differences between curves were assessed using a log-rank test. *P* values are specified in all figure legends and statistical significance was determined as $P \leq 0.05$. Bar charts represent the mean ± standard deviation (SD). Data analysis was performed in GraphPad Prism 9.

3 CHAPTER 5: THE ANATOMY, IMMUNOLOGY, AND RELATIVE UTILITY OF TWO SYNGENEIC MURINE MODELS OF GBM

3.1 THE NEED FOR A HIGHER FIDELITY SYNGENEIC MODEL OF GBM

3.1.1 GL261 MODEL BACKGROUND

Glioblastoma multiforme (GBM) is intractable and among the most lethal human cancers. GBM is the most common tumor of the adult central nervous system (CNS) and is thought to arise from either neuroglial progenitors or de-differentiated glial cells(Gimple et al., 2019; Lee et al., 2018; Ostrom et al., 2015). GBM has a median survival of 14 months, and its 5-year survival rate has remained unchanged for nearly half a century, even in the face of new standards of care(Fukushima et al., 2013; Poon et al., 2020; Stupp et al., 2009). Many theories have been advanced for why GBM is universally lethal and intransigent. First, it harbors a bland mutagenomic profile and low neoantigen burden relative to other cancers, due in part to a few canonical mutations driving oncogenesis as opposed to carcinogens (Kim, Lee, et al., 2015). Second, GBM exhibits vast intra- and inter-individual heterogeneity at both the level of the tumor and immune cells (phenotypically, spatially, temporally, etc.) (Darmanis et al., 2017; Q. Wang et al., 2017). Third, GBM is an intrinsically infiltrative and migratory tumor akin to "sand in the grass," sitting behind both a blood-brain barrier and inside of a precious-real-estate organ that is unforgiving when it comes to supporting inflammation and immunity.

Standard of care including gross total resection, radiation, and chemotherapy has failed to improve life expectancy beyond 15 months. The 5-year survival rate has not changed in decades. Drug development efforts have largely been plagued – on the preclinical side – by a dearth of high-fidelity models.

GL261 has long been utilized as the gold standard for syngeneic murine modeling of GBM, but it does not recapitulate key tenets of the human disease. This orthotopic model was established in 1970 via intracranial chemical injection of the carcinogen, methylcholanthrene. Tumor fragments were subsequently transplanted subcutaneously and intracranially into C57BL/6 mice. Serially passaged and stable GL261 cells lines were established by the mid-1990s. GL261 harbors activations of the K-ras oncogene, mutations of the p53 tumor suppressor gene, and the subsequent elevation of the C-Myc oncogene which promotes aberrant cell cycle progression. Proponents of the GL261 model cite the aforementioned mutations, given that they have been shown to be critical to GBM oncogenesis and progression (Gururaj et al., 2013; Rajasekhar et al., 2003; Sidransky et al., 1992; Szatmári et al., 2006; Trent et al., 1986). However, there are important shortfalls of this model that need to be considered given that the vast majority of pre-clinical work on GBM has consisted of GL261 studies, and nearly all of it has failed to recapitulate promising results in human clinical trials.

First, GL261 is a homogenous tumor whereas GBM is famously heterogeneous, both intra- and inter-patient (Wiesner et al., 2005). Indeed, in the same tumor one can find as many as three different alleles of the *Trp53* tumor suppressor gene, as well as mixed expression of Epidermal Growth Factor Receptor (EGFR) (Cheng et al., 1999; Ren et al., 2007). Outside of such archetypical mutations however, GBM is among the least mutated of human cancers (likely due to it having no environmental etiology) (Vogelstein et al., 2013). GL261 is carcinogen-induced and therefore more mutated than human GBM and it responds to immune checkpoint therapy (ICT) and CSF1-R inhibition which is demonstrably not the case in humans (Butowski et al., 2016; Genoud et al., 2018; Quail et al., 2016; Reardon et al.,

2017). Owing to its 4932 non-synonymous exome mutations, GL261 expresses highly functional endogenous tumor-specific neoantigens, allowing the immune system to actually "see" the tumor in ways that human GBM would otherwise remain invisible (Haddad et al., 2021; Johanns et al., 2016). GL261 has high baseline MHCI expression whereas in human GBM, MHCI is expressed at low levels and nearly half of all patients have a loss of heterozygosity of HLA (Genoud et al., 2018; Yeung et al., 2013). Loss of HLA makes it functionally impossible for the tumor cell to present antigen to the immune system. The only alternative to salvage tumor antigen presentation to CD8 T cells would be if antigen were to be cross-presented. However, given the dearth of cross-presenting DCs in the brain at steady state (and their limited existence even in a compromised GBM TME, see section 2.1.6), and the fact that host immunity to GBM is clearly ineffective, we can reasonably assume that this compensatory mechanism is not overriding GBM-driven immune suppression. The evidence for cross-presenting microglia is nascent (see section 2.1.1.2.2). This lack of antigen presentation and immune "awareness" of human GBM is a core tenet that must be recapitulated in any animal model that seeks to be useful for the study of GBM.

3.1.2 SB28 MODEL BACKGROUND

In order to work with a model that more closely resembles human GBM, we explored SB28, a newer line that was originally generated by using Sleeping Beauty transposon-targeting of p53, NRAS, and Platelet Derived Growth Factor (PDGF), canonical mutations that drive human GBM. SB28 was generated in 2014 at UCSF in the lab of Hideho Okada via *in utero* electroporation of the aforementioned genes in the right lateral ventricle of neonates (Kosaka et al., 2014). This mechanism involves chromosomal integration and thus stable,

long-term expression of the delivered gene sequences (Wiesner et al., 2005). This *de novo* glioma tissue was then harvested, minced, and seeded in cell culture media. Cells were subsequently sub-cultured in a limiting dilution assay to select for clones with the highest luciferase activity.

Consistent with human trials of GBM, intracerebral SB28 is completely resistant to ICT and lacks constitutively active MHCI (and MHCII) (Genoud et al., 2018). Importantly, SB28 harbors a very low mutational burden and few neoepitopes much like human GBM. In line with these findings and SB28's complete resistance to ICT, SB28 was shown to be poorly infiltrated by CD8+ T cells, an immune "coldness" that is the norm in human GBM (Genoud et al., 2018). Importantly, SB28 has never been cured, according to private correspondence with the lab from which this line originates (Hideho Okada, UCSF). Given these initial observations of SB28, we were eager to explore this line and compare its differences to GL261 and assess its utility to better understand the neuro-immunology of GBM. To this end, we started by generating a trackable model of this tumor that would enable downstream phenotyping by high-parameter flow cytometry, immunohistochemistry, and intravital two photon microscopy.

3.2 OPTIMIZATION OF TUMOR MODEL FOR THIS THESIS

3.2.1 RECREATING THE POST-SURGERY INFLAMMATORY MILIEU

The standard of care for GBM starts with gross total resection (GTR) (Nam & de Groot, 2017). It is universally acknowledged that that GBM cells invariably remain in the tumor niche given GBM's highly infiltrative nature (Hambardzumyan & Bergers, 2015). Thus, we aimed to establish a model that mimic the two tenets of "time zero," the label we

gave to the earliest possible point of clinical intervention post surgery. A model that starts at "time zero" should therefore: (a) recapitulate the inflammatory and injured environment of a brain that just underwent surgery; (b) harbor the minimum number of tumor cells that properly engraft such that there is a window of opportunity to intervene with reasonable chance of success, mimicking the tumor cells that remain following GTR.

3.2.1.1 INFLAMMATION IN THE IMMEDIATE AFTERMATH OF "SURGERY"

Extant data from the McGavern lab documented the inflammatory response to a model of mild TBI (mTBI) (Roth et al., 2014). This model of mild TBI entailed thinning a 1mm2 are of the exposed skull bone (as though to prepare for 2P imaging) to a thickness of ~20–30 μm, over 1–2 minutes using a dental drill outfitted with a 500μm burr. Once thinned, a microsurgical blade was used to lightly compress the skull to compress the meninges. This mild injury has been shown to cause significant disturbances to the structural integrity of the glia limitans superficialis and cell death (Mason et al., 2021). The glia limitans is a barrier of surface-associated astrocytes crucial for the protection of the CNS parenchyma. Recognizing the extent of damage caused by such a light compression and application of pressure on an intact skull bone, we sought to limit the damage caused by tumor injection given that even the most delicate methodology of injection would induce a locally strong immune response hallmarked by the infiltration of myelomonocytics from the periphery, along with activated and inflamed resident microglia and cell death. The standard for orthotopic injection of tumor cells in syngeneic mouse models can be most generously described as blunt, and typically performed with little to no regard for the ensuing injury response (Abdelwahab et al., 2011). Burr holes are created using drill bits, thereby destroying the skull bone,

meninges, and underlying neocortex. We hypothesized that this wholesale destruction of tissue would generate secondary inflammatory responses that would both interfere with the inflammatory response to the tumor we aimed to study, and not mirror the extraordinary care and judiciousness neurosurgeons must exercise to leave intact brain parenchyma when operating. Thus, we generated a minimalistic model whereby I would very carefully thin a cranial window in the skull measuring 2 x 2mm and then gently lower a syringe into the thinned area into the neocortex, delivering 2µL of tumor cells in sterile saline infused over the course of 5 minutes (as opposed to the standard 2-3 minutes). As expected, an acute injury response was still observed given the invariable piercing of blood vessels in the meninges and concomitant infiltration / spill of the myelomonocytics, as shown in **Figure 3-1**.

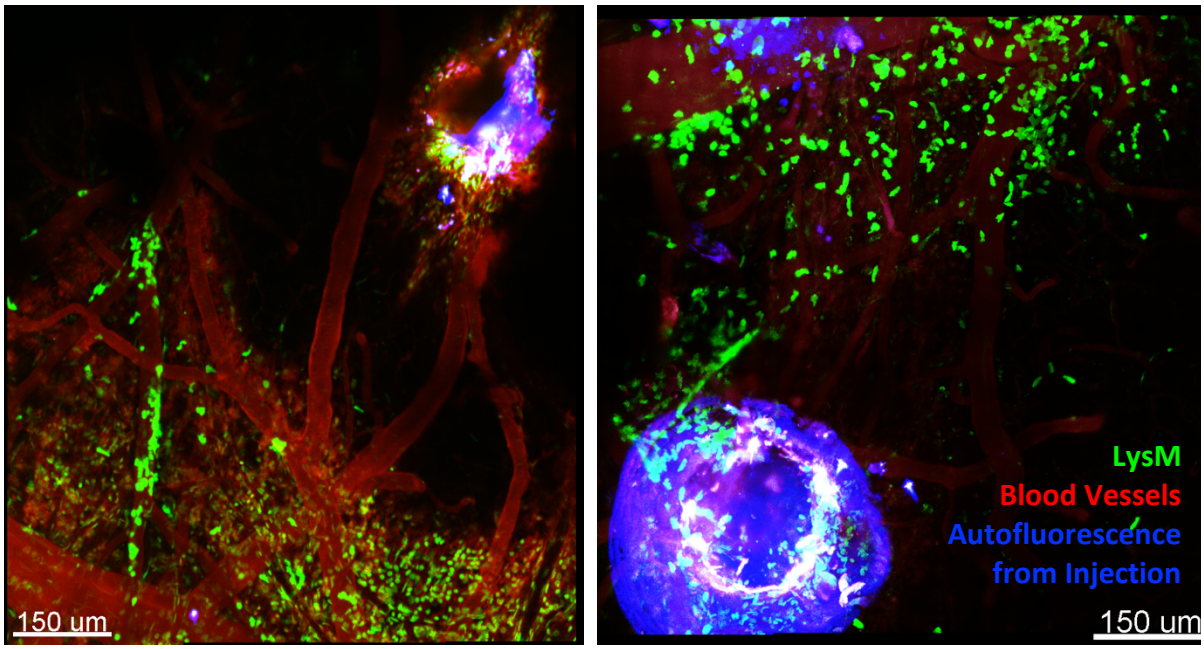

Figure 3-1: *XY* maximally projected Z stacks (100 µm depth) from two different mice show LysM+ myelomonocytic cells (green) and vasculature labeled with Evans Blue (red) in LysM $^{GFP/WT}$ reporter mice immediately after tumor cell injection.

3.2.1.2 ENABLING CONSISTENT TUMOR ENGRAFTMENT WITH THE MINIMUM NUMBER OF TUMOR CELLS

Given the high mitotic index of GBM (and its murine counterpart models), we hypothesized that any efficacious intervention in the clinical course of this disease would need to occur at "time zero," before the growth and absolute number of tumor cells hit escape velocity. We also sought to mimic the reality that residual tumor cells remain in the tumor niche (the percentage of which relative to the originally resected tumor bulk has not been quantified). Thus, we aimed to inject the minimum number of cells, identical across models, that would enable consistent engraftment and tracking capability. Given that 1 x 10^5 GL261 cells are typically implanted, versus 5 x 10^4 SB28 cells, we titrated the lowest possible dose in GL261 given the data that it is less aggressive and less consistent, testing the consistency of engraftment of 2.5 x 10^3, 5 x 10^3, and 1 x 10^4 GL261 cells and assaying consistency and visualization by 2P. We observed that 5 days after injection, 2.5 x 10^3 cells did not consistently form tumors, whereas both 5 x 10^3 and 1 x 10^4 GL261 cells did consistently form visible tumors by day 5 (**Figure 3-2**). Thus, we opted to inject 5,000 tumor cells in the model.

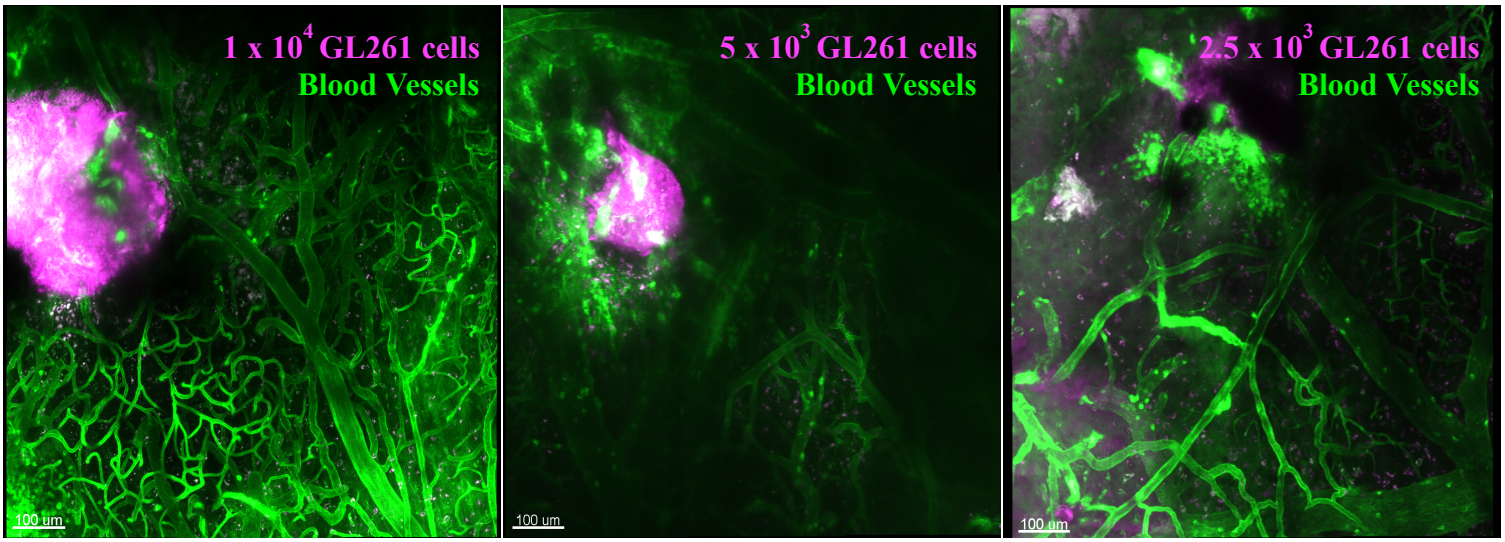

Figure 3-2: Representative *xy* maximally projected Z stack (70 µm depth) images (n=3) in C57BL/6 mice 5dpi. GL261 cells are shown in pink and Lectin-488 labeled blood vessels are shown in green. Injections of 5,000 and 10,000 cells consistently formed visible tumors at the 5-day timepoint, whereas an injection of 2,500 cells was assessed to be below the threshold level of consistent engraftment.

3.2.2 DEPTH OF INJECTION TO ENABLE CONSISTENT VISIBLITY BY TWO-PHOTON

Next, we titrated the depth of injection for the tumor cells that would enable visualization by 2P as well as analysis by flow cytometry and immunohistochemistry. Given the inflammation conferred by the tumor itself, visibility below the meninges was typically limited to a depth of 100µm. Thus, we aimed to optimize an injection depth that would allow the tumor to span the superficial neocortex. During surgeries, we observed that injecting 250µm below the thinned skull led to large amounts of backflow. Confocal microscopy in **Figure 3-3** confirmed that the majority of tumor cells injected 250µm below ultimately engrafted in the meninges, which was not the goal given that the immune landscape of the meninges differs sharply from that of the parenchyma, in that the meninges functionally behaves like a peripheral tissue (Fitzpatrick et al., 2020). Furthermore, GBM does not typically arise in the meninges, though leptomeningeal spread in advanced disease is a severe

complication that occurs in the late stages of the disease for 35% of patients and portends an abysmal 2-month survival (Birzu et al., 2020). Tumors injected 1mm below the thinned skull engrafted at a depth starting at ~500µm, which would be below the range of detection by 2P, whereas tumors injected at 500µm spanned the neocortex and were visible in the top 100µm of the brain and would thus be amenable to tracking by 2P (**Figure 3-3**).

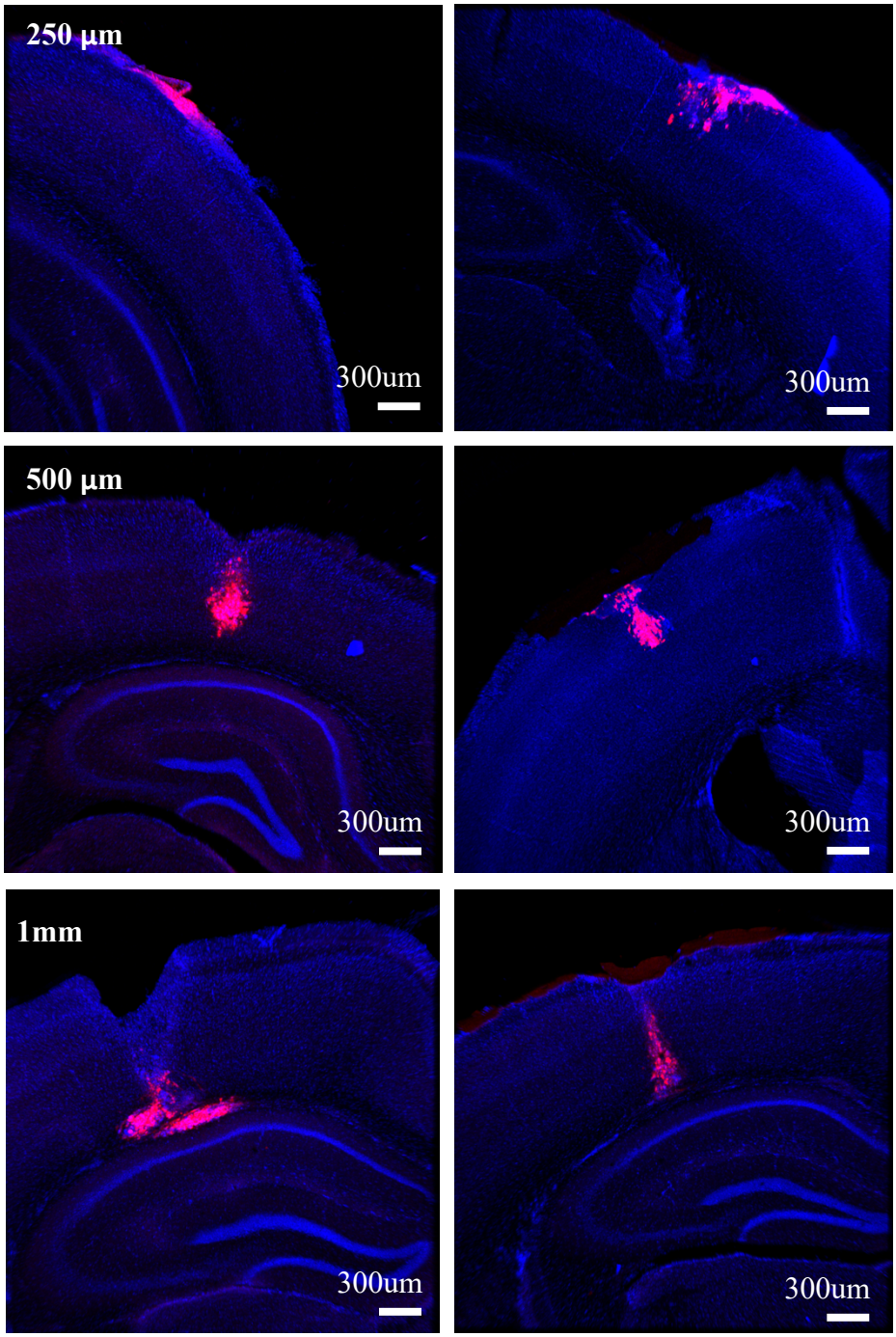

Figure 3-3: Representative confocal images (n=4) of GL261 tumors in a C57BL/6 mouse injected 5 days prior. GL261 is shown in pink. DAPI is shown in blue. Top row represents an injection depth of 250µm, middle row 500µm, and bottom row 1mm.

3.2.3 OPTIMIZING THE PUNCH BIOPSY FOR EARLY TIME POINT-FLOW CYTOMETRY

In initial experiments to optimize the master flow cytometry panel (see **FACS STAINING**), the right hemisphere was mechanically disrupted and processed for flow cytometric analysis 5 days after sham (saline) or GL261 injection. Completely unperturbed, naïve mice were used as an additional negative control to account for the immune reaction in response to the procedure. Briefly, mice were anesthetized, perfused with saline and their brains explanted. The tumor-bearing, right hemisphere was mechanically disrupted through a 70µm mesh strainer to remove aggregates and debris and washed with FACS buffer, centrifuged, and subject to a 30% Percoll gradient as described in **CELL ISOLATION FROM THE BRAIN**. Washed cells were isolated and stained. We used uniform manifold approximation and projection (UMAP) analysis to visualize the high dimensional data in 2 dimensions(Becht et al., 2019). These UMAPs revealed no significant differences between naïve, sham (saline)-injected, and GL261-bearing animals at this early day 5 time point (**Figure 3-4).**

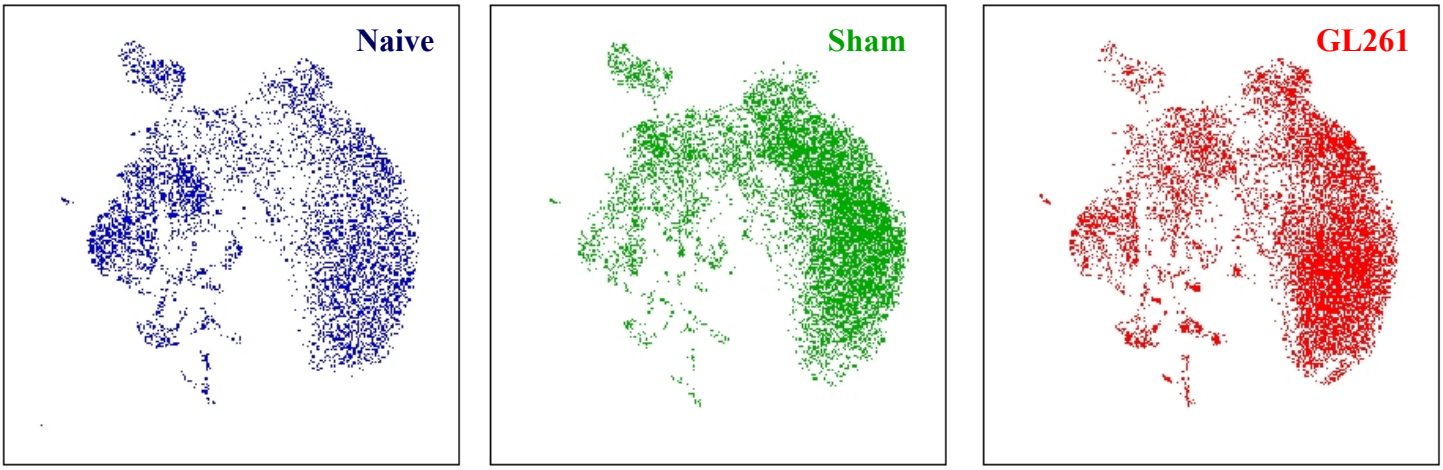

Figure 3-4: UMAP display of the immune infiltrate of naïve, sham (saline) injected, and GL261-bearing mice on day 5 post tumor implantation. Each dot represents a single cell. UMAPs reveal no significant differences between the three different experimental groups.

However, we knew that there was indeed an early immune response (even if we couldn't detect it initially by FACS), due to observations of microglial activation by two-photon. On day 5 post injection of GL261 in CX3CR1$^{GFP/WT}$ reporter mice, we surveilled the tumor milieu and adjacent brain parenchyma by 2P. Infiltrating myelomonocytics express CX3CR1 at much lower levels than brain resident microglia, therefore we assumed that the majority of CX3CR1+ (GFP+) myeloid cells were microglia. Those distal to the tumor site were ramified and have small cell bodies, indicating an inactive resting state and ignorance of the tumor in their milieu (**Figure 3-5**). Microglia in the tumor milieu and in direct contact with GL261 cells are morphologically distinct, as shown by their amoeboid appearance and larger, swollen cell bodies (Davis et al., 2017). Confirming this, two-photon imaging of these mice showed phagocytic microglia (in green) extending their processes to both surveil the surrounding tumor bed as well as ingest tumor material (GL261 shown in pink) **(Video 1).** These observations supported our hypothesis that immune activation could

be assayed at such an early time point, though perhaps the sensitivity of the FACS protocol was prohibitive when explanting an entire hemisphere for the cell preparation. In addition, we appreciated that detecting immunological differences by FACS had proved challenging in previous attempts in the McGavern lab from mTBI work, in which lesioned areas similar to the size of the tumor (<1mm^2) were assayed by FACS and no differences were detected between mTBI and naïve mice. In these experiments as well, immunological changes could *not* be detected through existing flow cytometry protocols, even though evidence of a strong, local immune response was well-documented by two-photon and immunohistochemistry.

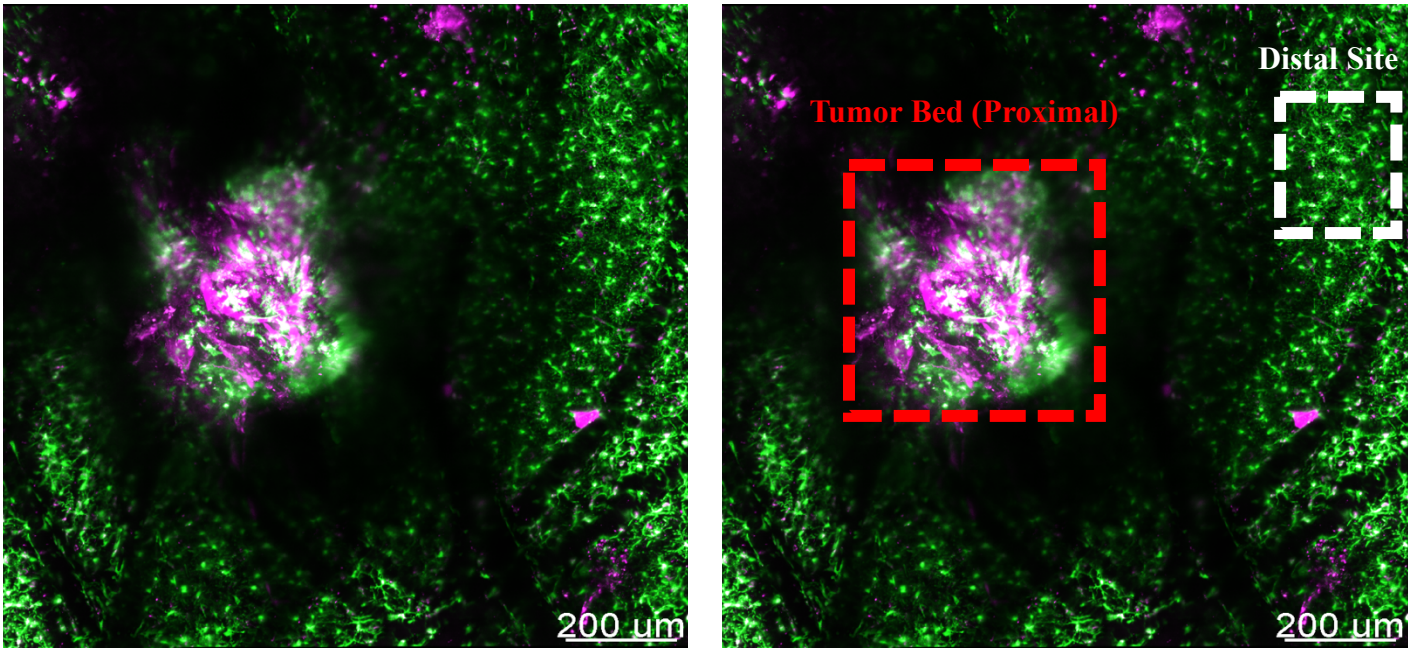

Figure 3-5: Representative *xy* maximally projected Z stacks (100 µm in depth) show CX3CR1-GFP+ myeloid cells (green) and GL261 cells (pink), 5 days after tumor implantation. Myeloid cells in the tumor bed (right, red box) display an activated state by dint of their amoeboid morphology, whereas those distal to the tumor have small cell bodies and ramified arborizations indicated a resting state (right, white box). See corresponding **Video 1** of microglia interacting with tumor cells in the red demarcated area. Images are representative of 2 independent experiments with 3 mice per group.

To troubleshoot what we posited to be a dilution issue, we developed a protocol of using a 2mm cortical punch biopsy as the cellular source for FACS preparations (see **CELL ISOLATION FROM THE BRAIN**). The subsequent data are shown in **HIGH-PARAMETER IMMUNE PHENOTYPING OF SB28 AND GL261**.

3.2.4 MODEL SYNTHESIS & EXPERIMENTAL WORKFLOW

To enable the depth of immune phenotyping we aimed to achieve, and to offer the possibility of triangulating between methods that could provide spatial, temporal, and genetic / phenotypic insights, the GBM model developed in this thesis need to be amenable to the workflow shown in **Figure 3-6.** In summary, the model developed achieved the following aims: (1) enable very early stage immune-phenotyping to mimic "time zero" in patients when clinical intervention begins, while minimizing the number of cells injected, reminiscent of those that invariably remain following Gross Total Resection; (b) recapitulate tenets of the post-surgical inflammatory milieu; (c) be situated in the superficial neocortex for two-photon imaging.

.

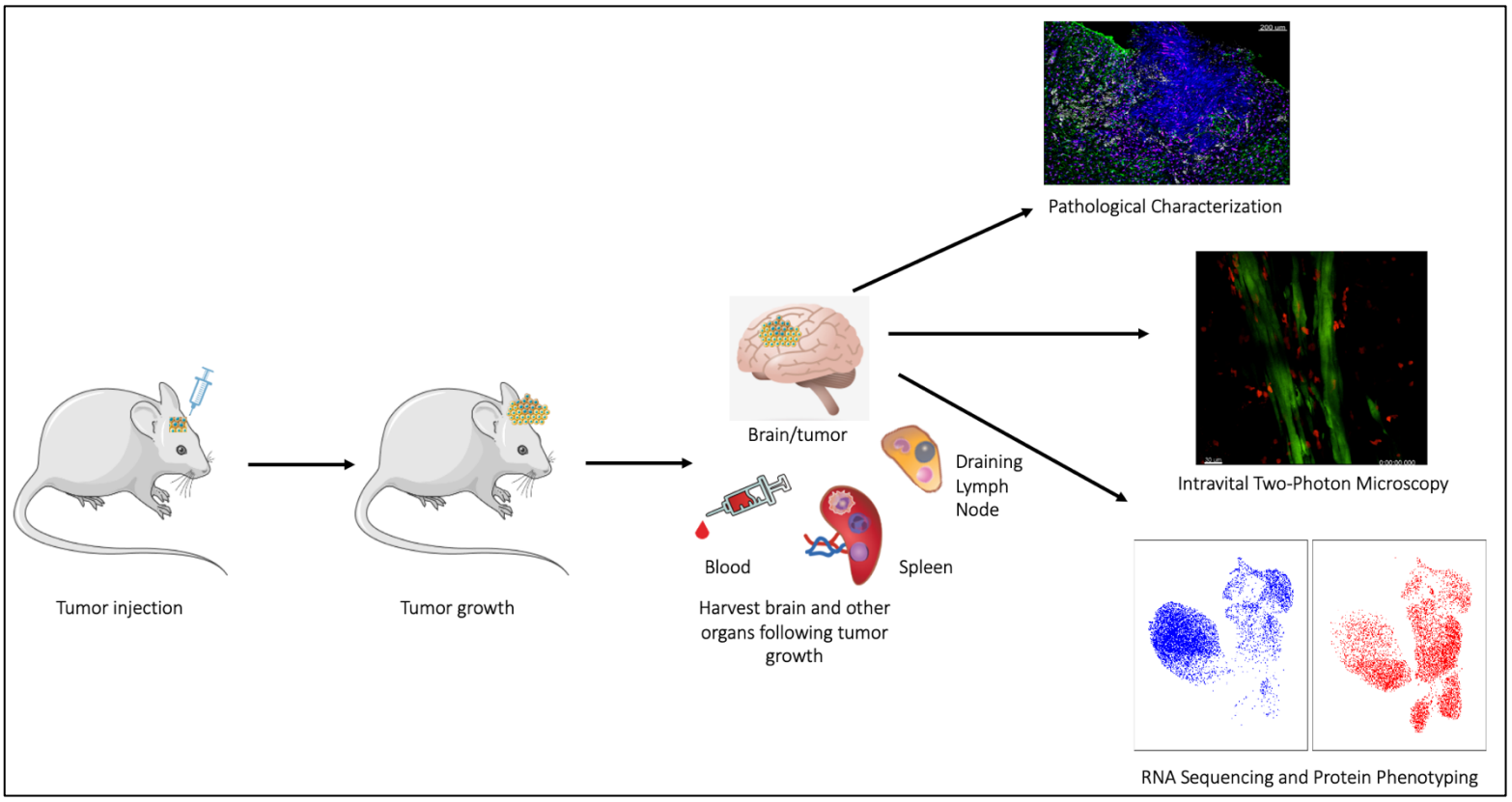

Figure 3-6: Experimental work flow to assay tumor growth and the immune response across space and time.

3.3 HIGH-PARAMETER IMMUNE PHENOTYPING OF SB28 AND GL261

Given the novelty of SB28, at the start of my thesis, there was limited information available on its immune profile, and surprisingly, we also found no high-parameter immune phenotyping of GL261 either. (In 2020, two years after the beginning of these experiments, a deep immune phenotyping of GL261 was published) (Khalsa et al., 2020). To fill these gaps, we defined the immune landscape of both GL261 and SB28 at two early time points: days 5 and 10.

3.3.1 EARLY TIME POINT FACS PROFILING: DAY 5

We performed high-parameter flow cytometry on 2mm punch biopsies of the tumor and surrounding area. To define the immune landscape into distinct cellular subsets (i.e., clusters), we used the PhenoGraph algorithm which elucidates phenotypes in high-dimensional data through a data-driven and unsupervised approach (Levine et al., 2015). We opted to "automate" the gating strategy rather than employ manual gating which depends on somewhat arbitrary cutoffs, two dimensions at a time, because this would subject our analysis to predefined and already well-documented cell subsets, but would not be suitable to identify novel and more fluid phenotypes that are distinct in their combinations of 2+ varying cell surface markers.

PhenoGraph clustering of high-parameter flow cytometric data yielded between 20 and 25 unique clusters depending on the experiment. To determine cluster identity, we compared the expression of canonical myeloid and lymphoid markers, the combinations of which were unique to resident microglia, infiltrating myelomonocytics (monocytes and neutrophils), and lymphocytes. Examination of these data revealed 11 different microglial subsets that primarily differed based on their expression of CX3CR1, CD11c, intracellular Vascular Endothelial Growth Factor (VEGF), and P2RY12. Both GL261 and SB28-bearing mice had greater numbers of $CX3CR1^{hi}$ microglia compared to sham-injected mice, indicating that early-on, the tumor was inducing the activation of microglia beyond the expected injury response **(Figure 3-7)**. Interestingly, a distinct subset of microglia (VEGF, CD11c, CD206-positive, and $P2RY12^{low}$) was found exclusively in SB28-bearing mice and not in their GL261-bearing counterparts, indicating an important divergence in the immune infiltrate between these two models at 5 days post injection. These data also revealed 3 different

clusters of monocytes, based on their Ly6C, CD45, CD44, CD11c, CD24, and CD206 expression, which we summarized as belonging to either the 'Inflammatory Monocyte' pool or the more heterogeneous CD11c+ monocytes **(Figure 3-7)**. The latter two subsets likely represent 'Classical' Ly6c^{Hi} and 'Non-Classical, Patrolling' Ly6c^{Lo} monocytes (Mildner et al., 2017). Both subsets we almost exclusively found in SB28-bearing mice indicating almost no input from the peripheral immune system in GL261-bearing or sham-injected mice. As shown in **Figure 3-1**, immediately following injection, LysM+ myelomonocytics are observed by two-photon at the tumor site. The fact that monocytes were virtually non-existent in sham or GL261-bearing mice indicates that the spill of these peripherally-derived myeloid cells from piercing vessels in the meninges was largely cleared by this day 5 time point, giving us confidence that day 5 allowed us to isolate tumor- and not injury-driven immune changes. Furthermore, the lack of any peripheral myeloid cell input in sham and GL261 mice indicated that few if any signals were being released to the periphery except for in SB28-bearing mice. In that same proverbial vein, in human GBM, chemoattractants and tumor-derived exosomes are known to promote monocyte extravasation from the blood supply (see **GBM SIGNALS TO THE PERIPHERY TO ATTRACT MONOCYTES**). This was the first clear indication of greater parallels between SB28 and human GBM than between GL261 and human GBM. Strikingly, at this early time point, SB28 was also infiltrated by putative monocytic "myeloid-derived suppressor cells (MDSCs)," denoted as such on the basis of their high side scatter (SSC) and typical monocyte marker expression **(Figure 3-7)**. Lymphocytes and neutrophils were also elevated in SB28-bearing mice and no differences in these populations were observed between sham and GL261-bearing mice **(Figure 3-7)**.

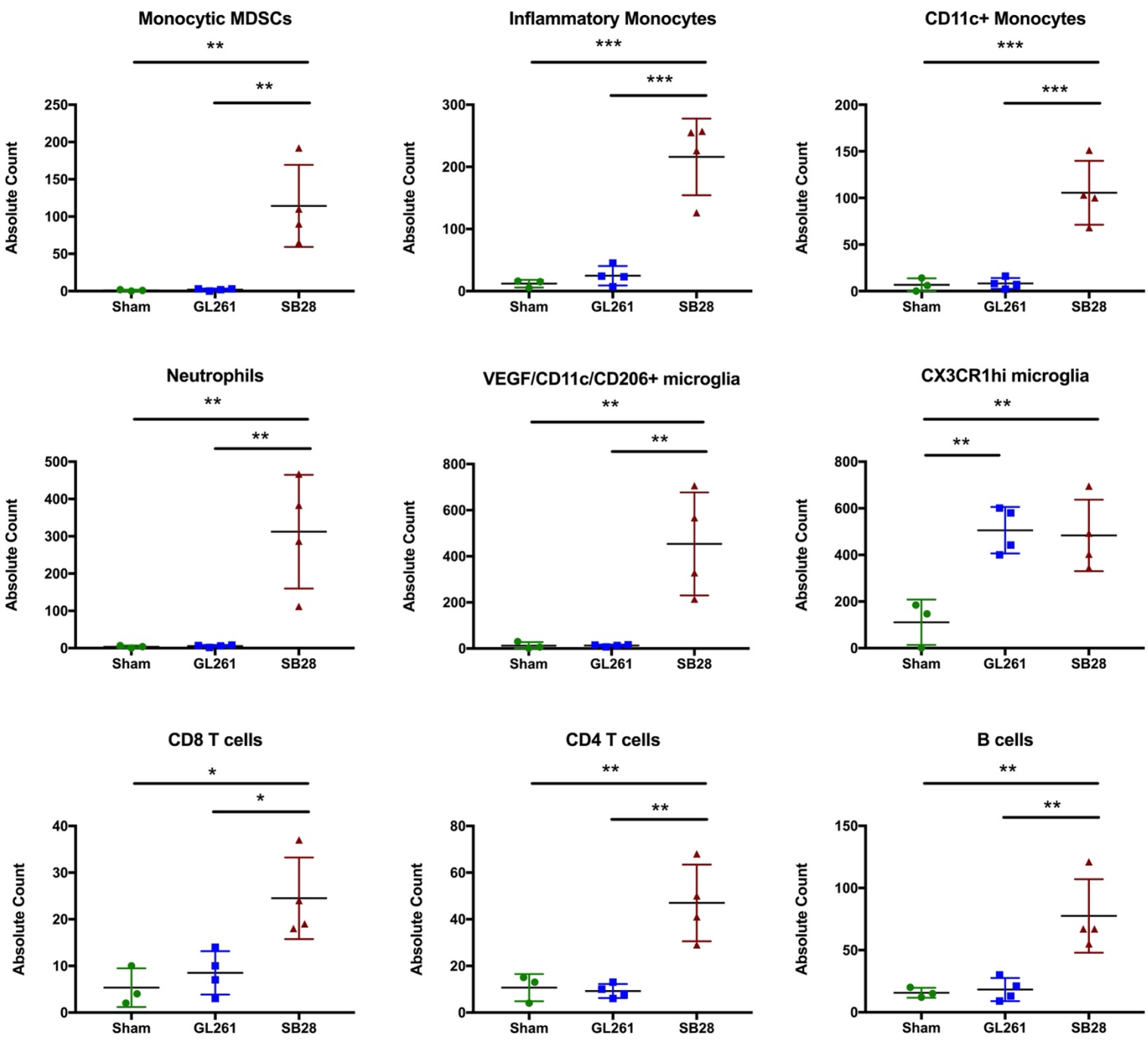

Figure 3-7: Representative flow cytometry bar graphs based on PhenoGraph clustering of disparate cell populations on day 5 post sham or tumor injection. Bar graphs indicate the absolute number of cells per experimental group, with each dot representing an individual mouse. Bar graphs are representative of 3 independent experiments with 3-4 mice per experimental group. Data are displayed as mean ± SD. Multiple t-tests with Holm-Sidak Multiple Comparisons Test were used to analyze statistical significance, with *$P \leq 0.05$, **$P \leq 0.01$, and ***$P \leq 0.001$.

Finally, we used uniform manifold approximation and projection (UMAP) analysis to visualize the high-dimensional data in two dimensions and to synthesize the above findings **(Figure 3-8)** (Becht et al., 2019). On day 5, the sham group was dominated by resting microglia as expected, GL261 showed a modest immune infiltrate from the periphery thought its immune landscape comprised largely resting microglia, whereas SB28 stood apart in its degree of infiltration by peripheral immune cells and the upregulation of VEGF in microglia, and the general diversity of its immune landscape **(Figure 3-9).**

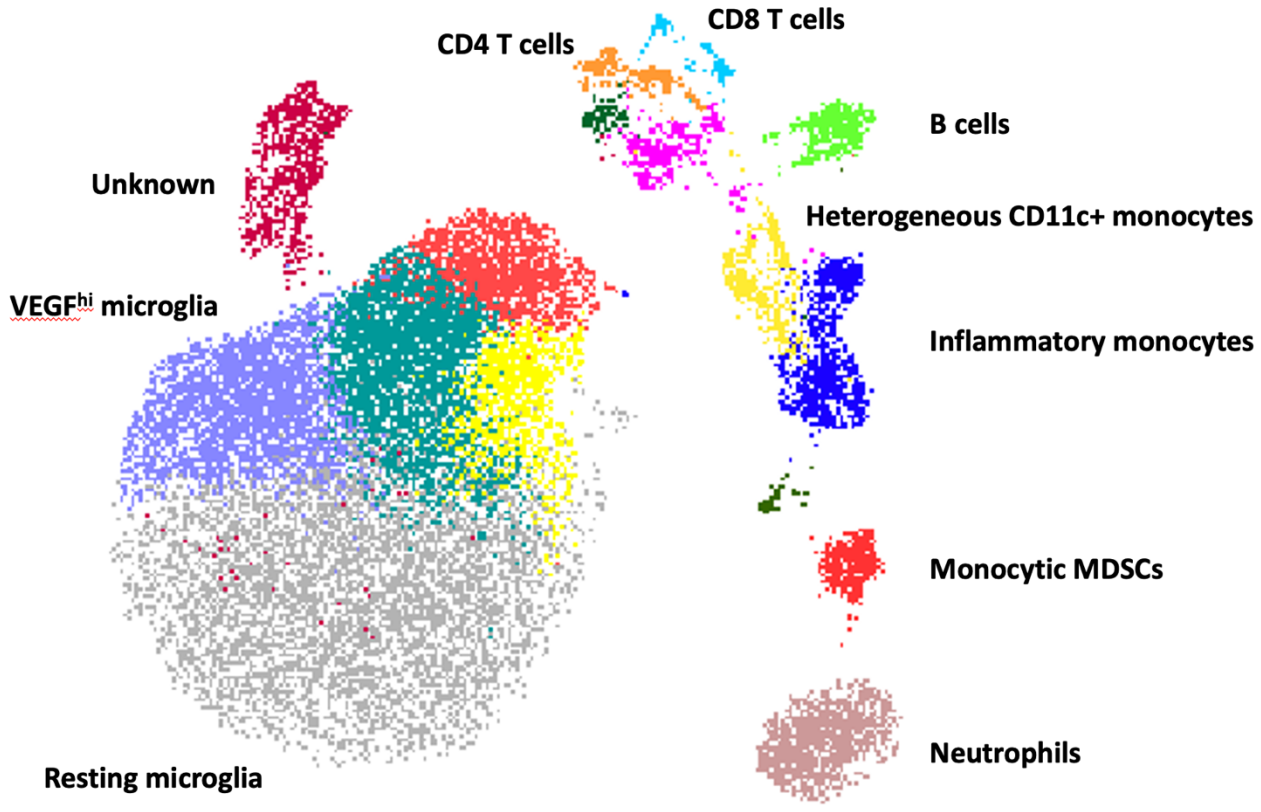

Figure 3-8: Concatenated UMAP display of the immune infiltrate of sham injected, GL261 and SB28-bearing mice on day 5 display the various PhenoGraph-identified cell clusters (**Figure 3-7**) present at this time point. Dots depict cellularity. UMAP is representative of 3 independent experiments with 3-4 mice per experimental group.

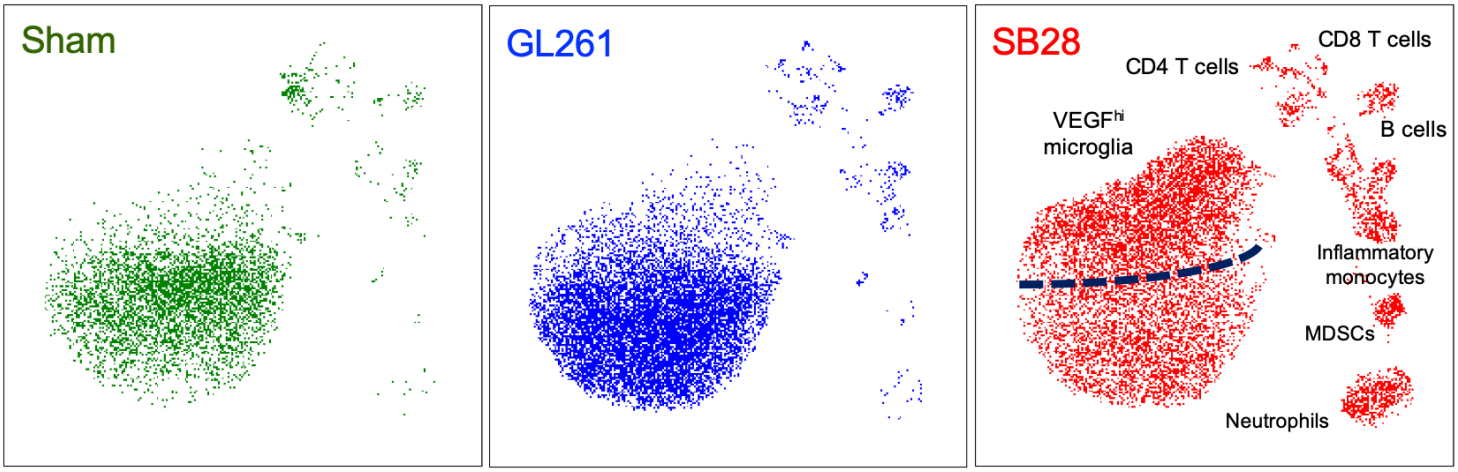

Figure 3-9: UMAP displays of the immune infiltrate of sham injected, GL261, or SB28-bearing mice on day 5 post injection. Data are from the same experiment as shown in **Figure 3-8**. Resting microglia comprise the majority of the immune infiltrate in sham-injected mice (green), as would be the case for homeostatic brain tissue. GL261-bearing mice (blue) have similar levels of peripheral immune inputs as the sham mice, indicating baseline levels of sample contamination from the meninges. By contrast, SB28-bearing mice (red) show robust myeloid immune cell infiltration, including MDSCs, inflammatory monocytes, and neutrophils, as well as microglia expressing high levels of VEGF.

3.3.2 MID TIME POINT FACS PROFILING: DAY 10

On day 10, GL261 tumors remained almost completely comprised of resting microglia, although they showed a greater infiltration by peripheral myelomonocytics compared to day 5. SB28 still stood out at this time point in that the majority of the microglia were VEGF+ and myelomonocytics displayed a highly activated phenotype (CD11c+ CD24+) **(Figure 3-10, A-B).** We identified a unique subset of microglia expressing high levels of VEGF and CD11c, and named them Repair Associated Microglia (RAMs). At the time of this experiment, this type of microglia had never been described in mice before. In parallel, I had been contributing to a lab-mate's project on the distinct myeloid cells responses that

mediate damage and repair following cerebral vascular injury (CVI). I had identified RAMs in my lab-mate's FACS data as well, and we later found that these microglia were pro-angiogenic and that their generation and subsequent wound-repair relied on crosstalk with infiltrating myelomonocytics (in the context of CVI, angiogenesis was an important repair response critical for survival following stroke) (Mastorakos, Mihelson, et al., 2021). However, in the context of GBM, ample human data paint a darker picture of the angiogenic signature of the tumor. Microglial samples show an upregulation of angiogenesis-associated genes such as VEGFA (Sankowski et al., 2019). GBM is known to be highly vascularized, and interfering with the formation of new vessels via anti-Ang2/VEGF antibodies or by targeting microglia has been shown to decrease GBM growth in animal models (Atzori et al., 2017; Brandenburg et al., 2016; Kloepper et al., 2016; Ricci-Vitiani et al., 2010; Turkowski et al., 2018). Unfortunately, anti-VEGF antibody therapy in human GBM (Bevacizumab) has not successfully increased overall survival due to a variety of compensatory and resistance mechanisms that result, along with dose-limiting toxicities of the drug (Ahn et al., 2016; Kloepper et al., 2016). The fact that RAMs were uniquely abundant in SB28 tumors **(Figure 3-10, B)** further corroborated our hypothesis that SB28 more closely approximated human GBM, and that SB28 harnesses a wound healing program that likely feeds its growth. Indeed, the global VEGF signature from SB28 was significantly greater than that of the sham and GL261 **(Figure 3-10, C).**

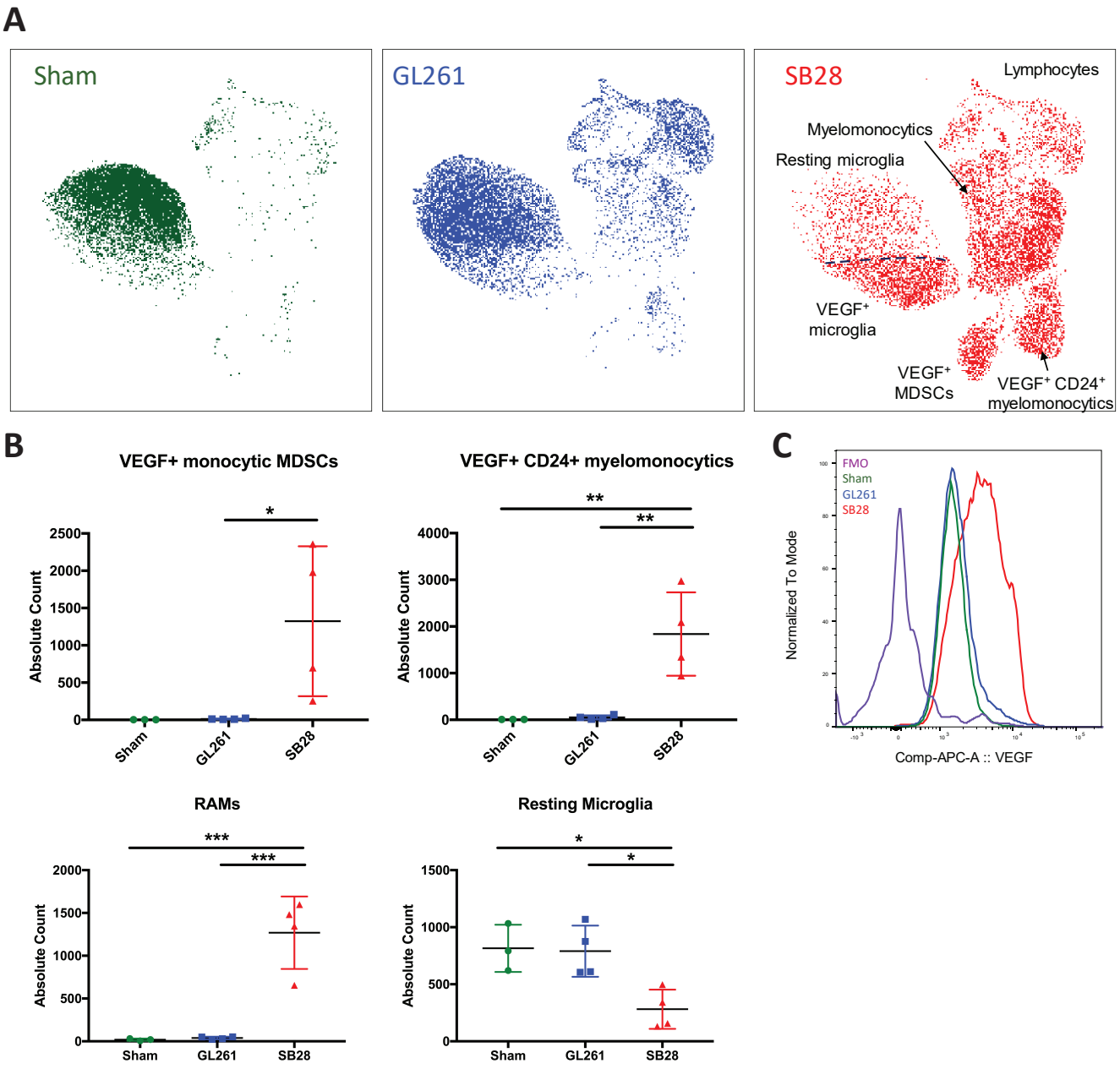

Figure 3-10: (A) UMAP display of the immune infiltrate of sham injected, GL261and SB28-bearing mice on day 10. UMAPs clearly show minimal baseline contamination in the Sham sample from any other cells other than resting microglia. GL261 immune infiltrate is primarily resting microglia and lymphocytes (top right of the UMAP). SB28 is richly enmeshed with activated myeloid cells. **(B)** Representative flow cytometry bar graphs based on PhenoGraph clustering of disparate cell populations on day 10. Data are displayed as mean ± SD. Multiple t-tests with Holm-Sidak Multiple Comparisons Test were used to analyze statistical significance, with *$P \leq 0.05$, **$P \leq 0.01$, and ***$P \leq 0.001$. **(C)** Representative flow cytometry histogram showing VEGF expression of CD45+ cells from 4 pooled samples within each group, comparing the FMO negative staining control to sham, GL261, and SB28 groups.

3.3.3 MORPHOLOGICAL DIFFERENCES BETWEEN GL261 AND SB28

3.3.3.1 HEMORRHAGE

The florid vascular proliferation that is well-documented in human GBM is accompanied by extensive pockets of hemorrhage. Over half of all glioblastomas show evidence of hypervascularization and blood pooling, the degree to which is associated with worse survival in patients (Puig et al., 2016). Given the findings of a pronounced VEGF signature in SB28 but not in GL261, we also sought to characterize and compare the extent of bleeding in both models. Given the possible error introduced in quantifying red blood cells (RBCs) by FACS (since fixation leads to erythrocyte lysis), we employed confocal microscopy to assess hemorrhage. Tumors were harvested at 10 dpi. Mice were not perfused to avoid any disruption of the vasculature or bursting of the vessels that could introduce noise into the assay. Brains were explanted and incubated overnight at room temperature in 4% PFA (which pilot data had shown me did not impact the visualization of blood pools), sectioned and stained with Ter-119. The volume of the blood pools was quantified by creating a 3-dimensional surface in Imaris of the entire Ter-119+ signal. As hypothesized, GL261 showed nearly no sign of inducing bleeding in the surrounding parenchyma, whereas SB28 showed significantly more bleeding **(Figure 3-11).**

A

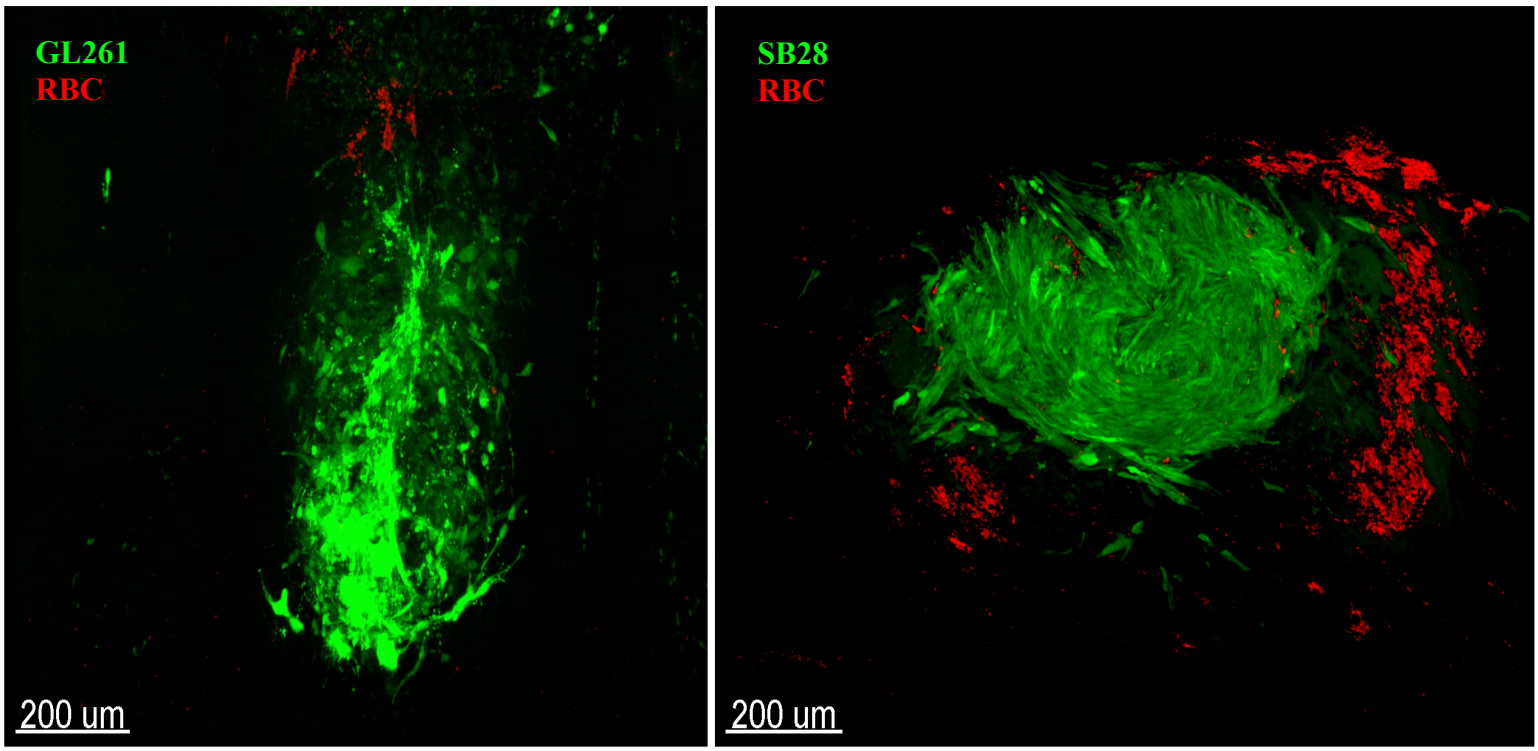

B

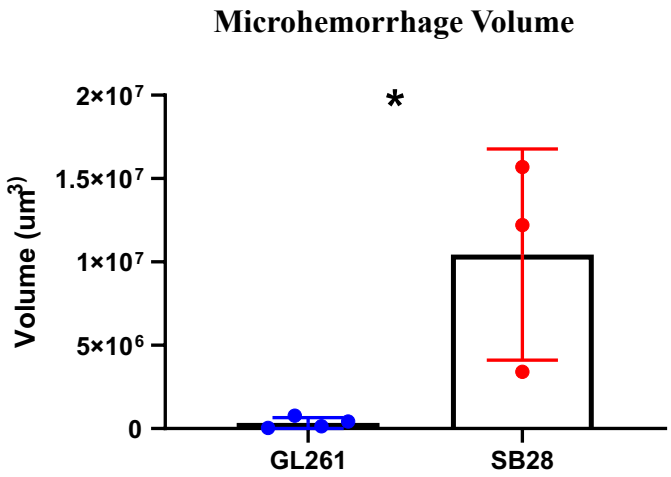

Figure 3-11: (A) Representative *xy* maximally projected Z stacks (100 µm in depth) show Ter-119+ RBCs (red) and tumor cells (green), with GL261 on the left and SB28 on the right, 10 days after tumor implantation. Images are representative of 2 independent experiments with 3-4 mice per group. **(B)** The volume of microhemorrhage was quantified using the Surfaces function in Imaris over the entire Ter-119 (red) signal. Data are displayed as mean ± SD. Multiple t-tests with Holm-Sidak Multiple Comparisons Test were used to analyze statistical significance, with *$P \leq 0.05$.

3.3.3.2 ANATOMICAL DIFFERENCES IN THE INTERPLAY BETWEEN TUMOR MODEL AND ITS MILIEU

GBM is notorious for its "sand-in-the-grass" quality, such that tumor cells enmesh themselves in the parenchyma rendering the first line of treatment – "Gross Total Resection" – more a goal and less a realistic outcome. That the brain is a precious real estate organ further adds to the complication of resecting the tumor, and there are obvious limitations to any efforts of resecting "wide margins." To qualitatively assess the degree to which GL261 and SB28 embed themselves in their surrounding milieu, we employed confocal and intravital two-photon microscopy to image the interplay of immune, glial, and tumor cells. Our FACS data showed minimal myelomoncytic infiltration in GL261 tumors relative to their SB28 counterparts, but we sought to gain a spatial understanding of this finding. We confirmed in brain slices from lysozyme M-GFP (LysM-GFP) reporter mice that GL261 is a more compartmentalized tumor with minimal LysM-GFP+ myelomonocytic input derived primarily from damaged vessels as opposed to any apparent tumor-myeloid cell cross talk. In **Figure 3-12**, myelomonocytics shown in green are entering via a broken vessel (left frame). By contrast, myelomonocytics are evenly dispersed throughout the more inflamed SB28 tumor, suggesting greater interplay between the tumor and its environment (**Figure 3-12**, right). Given how evenly dispersed the LysM+ cells are, we confirmed that the striking quantities of infiltrating myelomonocytes apparent in SB28 FACS samples are derived not from injury but from a coordinated tumor-myeloid cell axis, as has been described in humans and reviewed in this thesis in the section **GBM SIGNALS TO THE PERIPHERY TO ATTRACT MONOCYTES.**

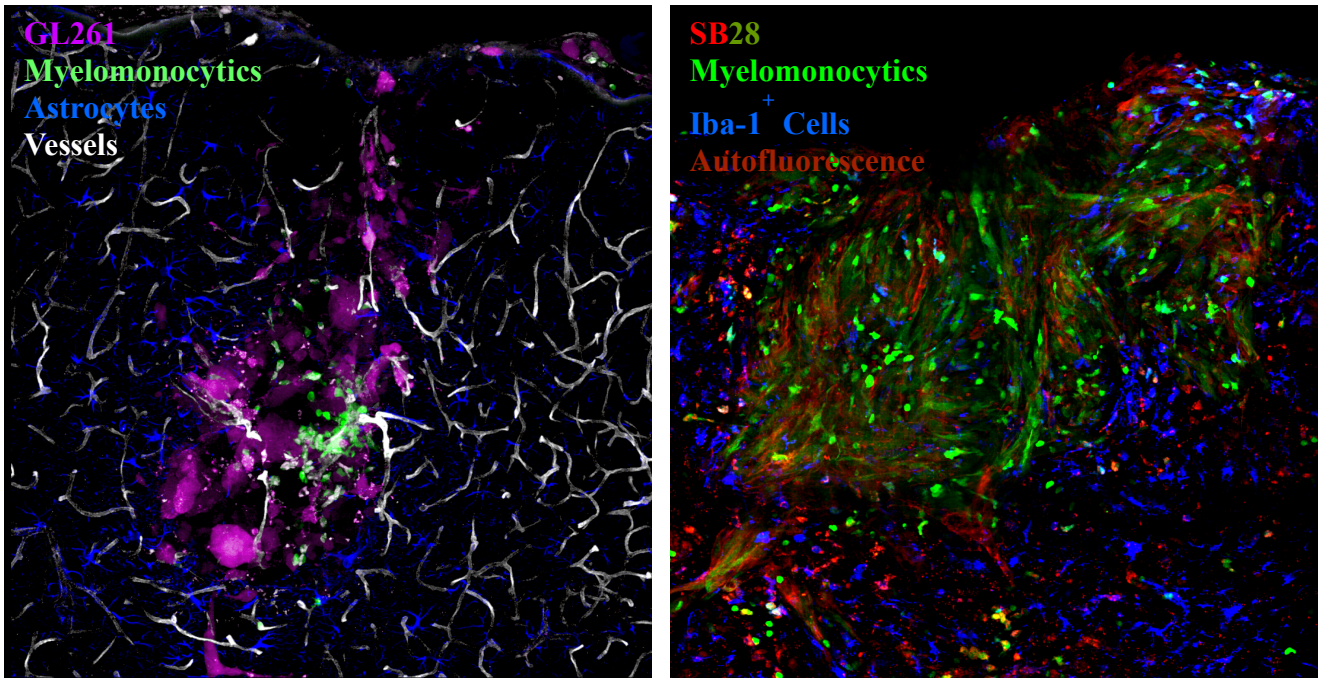

Figure 3-12: Representative *xy* maximally projected Z stacks (100 µm in depth) of GL261 tumors (left, in pink) or SB28 tumors (right, in green with red membranes) in LysM reporter mice. Myelomonocytics (bright green) enter via a broken vessel in GL261 tumors but otherwise show little interaction with the tumor. By contrast, these LysM+ cells are evenly present throughout SB28 tumors indicating tumor-monocyte cross talk and infiltration. Images are representative of 2 independent experiments with 3 mice per group.

Using two-photon microscopy, we also studied the dynamics of brain-resident microglia in GL261 and SB28 tumors. **Video 2** (snapshot in **Figure 3-13**) reveals that microglia adjacent to GL261 are ramified and have small cell bodies, indicating an inactive, resting state and ignorance of the tumor in their milieu (corroborating the 5dpi and 10dpi FACS data indicating that microglia in this model are primarily "resting"). SB28, conversely, enmeshes itself in the parenchyma and is actively surveilled by the microglia (**Video 3,** snapshot in **Figure 3-14**), all of which are clearly activated given their amoeboid appearance, swollen cell bodies, and the clear protruding and retracting of their processes as they sample the surrounding area. Vacuoles are also visible in the majority of the microglia suggesting a

phagocytic phenotype. Given the latter observation, we honed in on this observation and highlighted these phagocytic microglia (left box) and observed in real-time their tumor cell killing capacity (right box) in **Video 4** (snapshot in **Figure 3-15**). These striking differences in microglial and myelomonocytic spatial and behavioral patterns between the models are particularly relevant as up to one third of the GBM mass is comprised of myeloid cells.

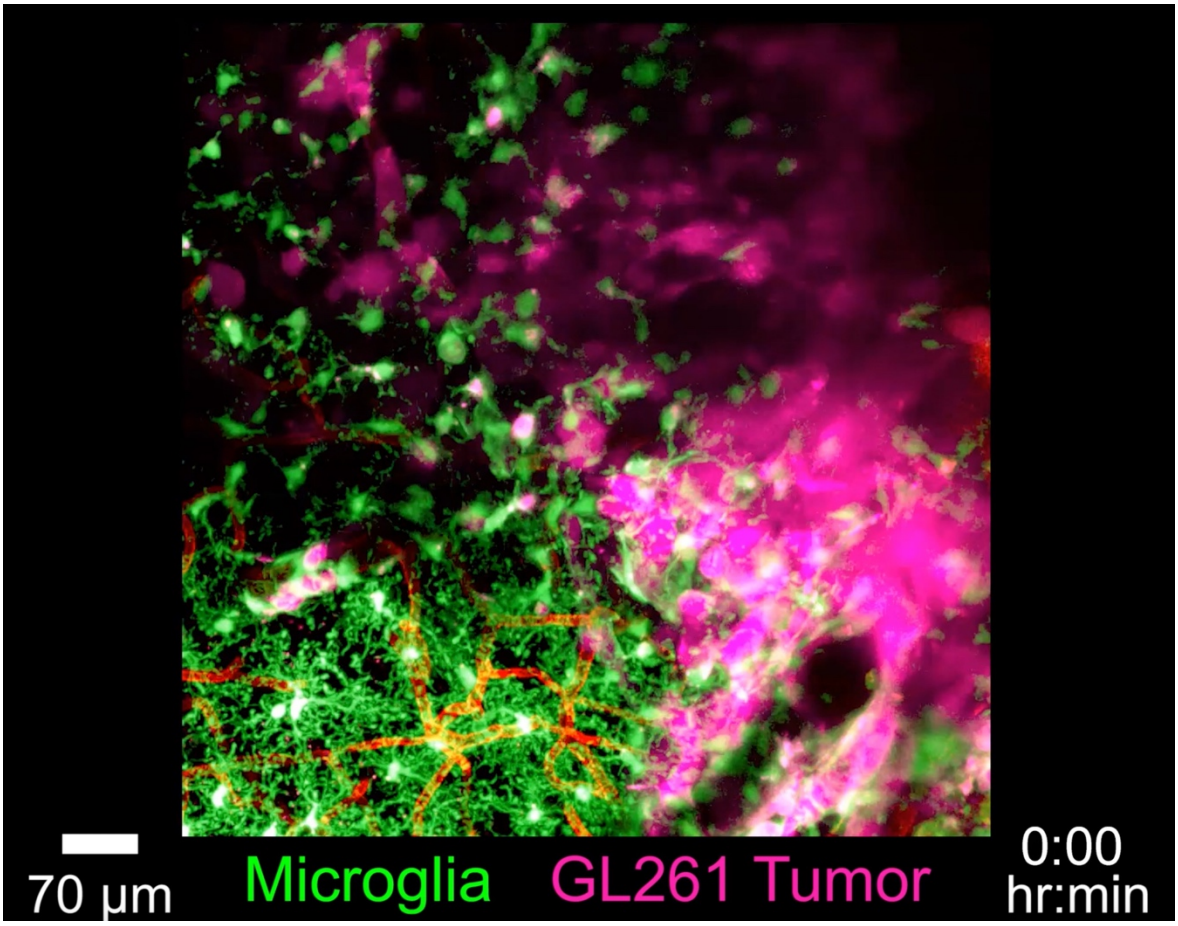

Figure 3-13: Snapshot of Video 2, Representative maximal projection of a two-photon z-stack viewed through the thinned skull of CX3CR1$^{GFP/WT}$ mice 7 days after GL261 implantation. GL261 is shown in pink, microglia in green, and blood vessels in red. The microglia in direct contact with the tumor are amoeboid and have larger cell bodies and no longer have the ramified processes that hallmark resting microglia. GL261 cells appear to be poorly infiltrated by microglia. Microglia just adjacent to the tumor but not in direct contact (lower left corner) appear to be completely unperturbed and naïve to the fact that a tumor is in the milieu. Their cell bodies are small and their processes highly ramified. This video is representative of 2 independent experiments of 4-5 mice each.

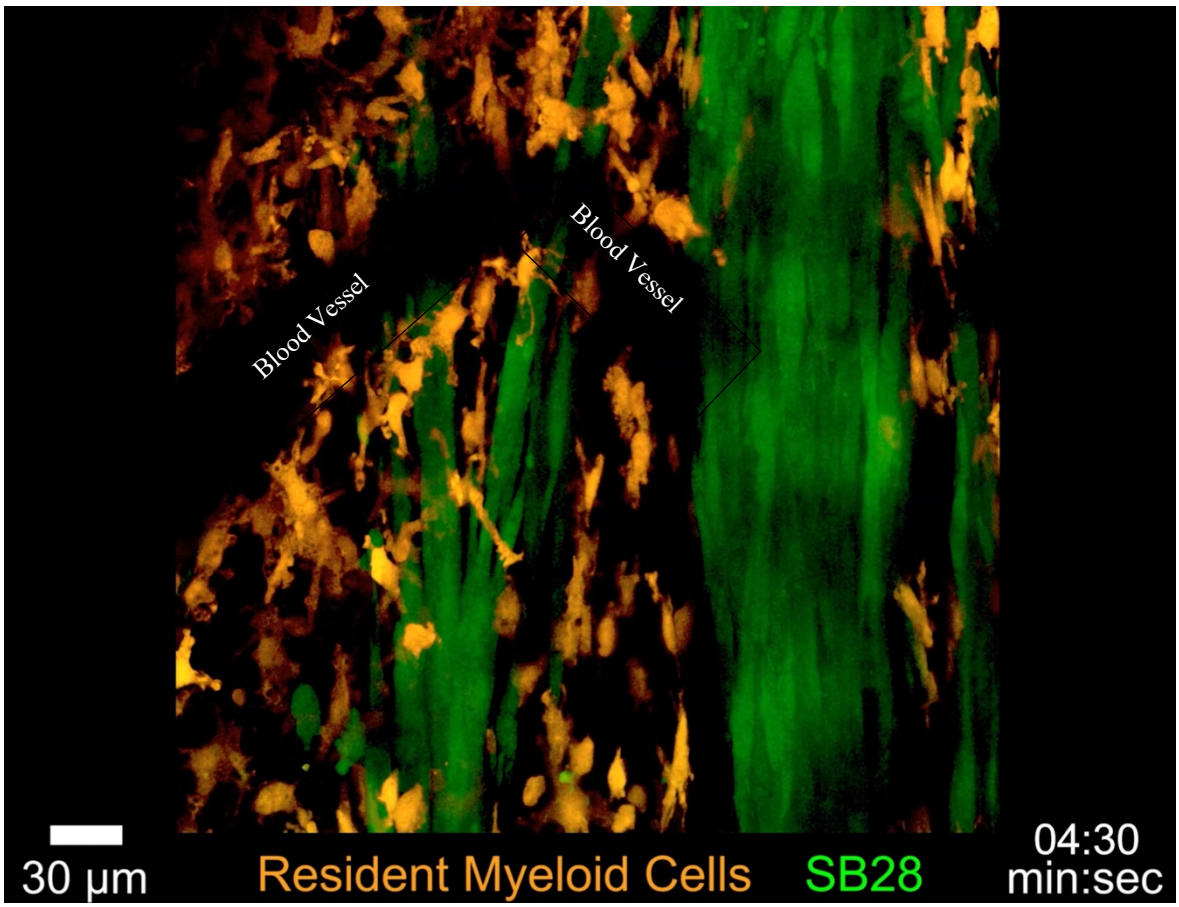

Figure 3-14: Snapshot of Video 3, Representative maximal projection of a two-photon z-stack viewed through the thinned skull of Resident Red mice 7 days after SB28 implantation. SB28 is shown in green, and resident myeloid cells (i.e., microglia) in orange. In stark contrast with the pattern observed in GL261-bearing mice, SB28 enmeshes itself in the brain parenchyma (reminiscent of human GBM's "sand-in-the-grass" quality) and all the microglia visible in the thinned skull window are activated and have clearly transformed into a phagocytic phenotype as evidenced by their swollen cell bodies and clear vacuoles. This video is representative of 2 independent experiments of 4-5 mice each.

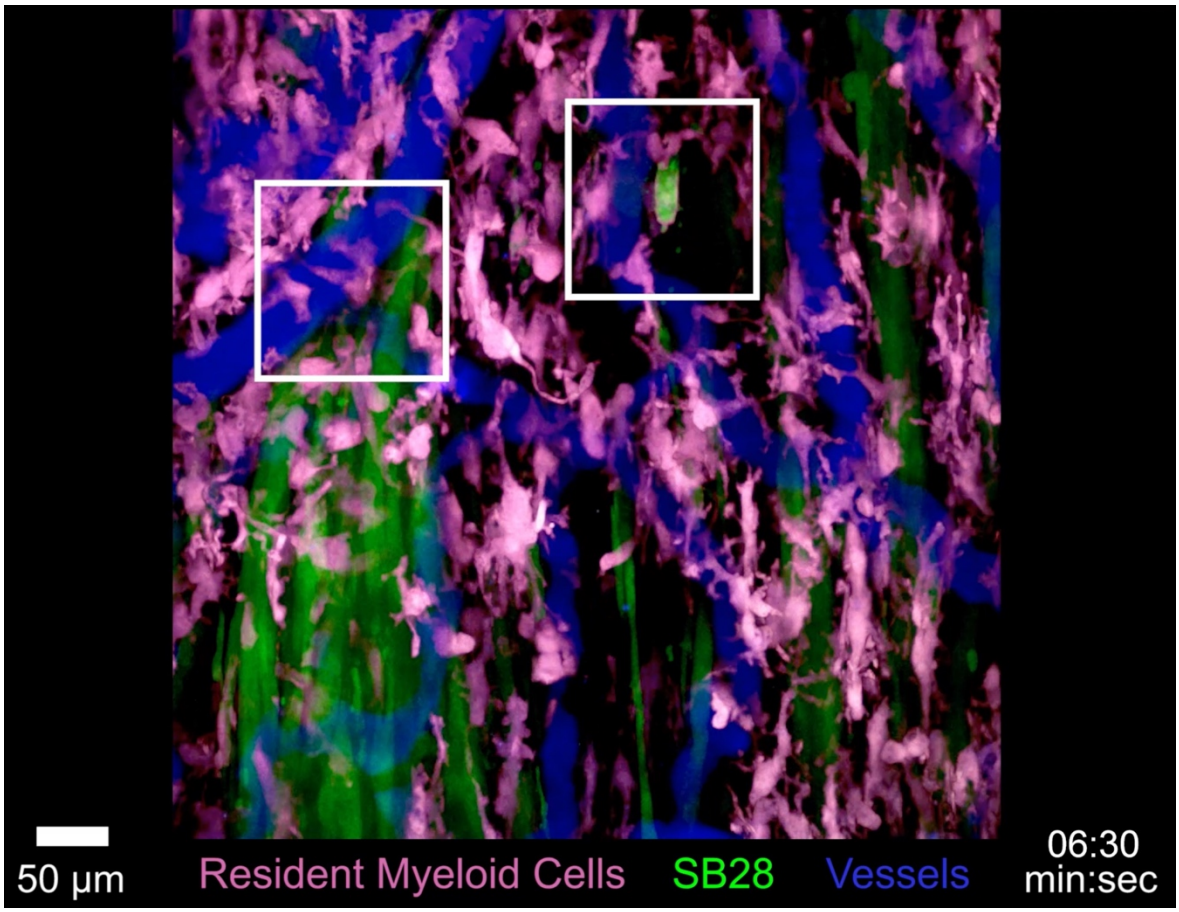

Figure 3-15: Snapshot of Video 4, Representative maximal projection of a two-photon z-stack viewed through the thinned skull of Resident Red mice 7 days after SB28 implantation illustrates phagocytic microglia ingesting tumor cells. SB28 is shown in green, blood vessels in blue, and resident myeloid cells (i.e., microglia) in pink. The white box on the *left* focuses on microglia with clear vacuoles, suggesting prior ingestions and processing of material in the microenvironment. The *right* box captures in real-time a microglia phagocytosing (and thereby killing) a tumor cell. This video is representative of 2 independent experiments of 4-5 mice each.

3.4 SUMMARY

The first priority of my DPhil was to establish a model that more closely approximated the immune response to human GBM. Almost every clinical intervention had been pre-clinically developed using the GL261 syngeneic murine model, yet none have gone on to materially improve the life expectancy of patients. This macro trend suggested that not

only is GBM supremely recalcitrant and complicated to treat for a number of reasons, but also that GL261 was over-simplifying the disease in ways that rendered it a low-integrity approach to testing new modalities. Prior to leveraging viral immunology to attack the tumor, we sought to improve upon this gold standard model. To this end, we employed two GBM models that recapitulate the highly inflamed environment observed in the brain following surgical resection and that enable tracking by intravital two-photon (2P) microscopy. By studying two different tumor cell lines (GL261 and SB28), we uncovered diverse patterns of pathology and immunity that underscore the challenges associated with treating all glioblastoma similarly. High-parameter phenotyping of the immune landscapes of these models, which at the time of these experiments and the start of my thesis had not ever been performed or published, revealed divergent patterns of immunity. SB28 demonstrated higher fidelity to human disease, inducing a sizable myelomonocytic response, perivascular hemorrhaging at sites both proximal and distal to the tumor, as well as a pronounced wound healing signature characterized by myeloid cell VEGF production. At 10dpi, GL261 did induce a peripheral immune response that was markedly lymphocytic, whereas human GBM is overwhelmingly myeloid in its immune landscape. In future studies, it will be important to more deeply phenotype the activation state of the myeloid and lymphocyte infiltrates, to understand their polarization. Studies pursuant to the latter may include *ex vivo* killing assays to understand what – if any – baseline pressure the immune system can exert on the two models, and how this differs. Further, it would be important to understand why SB28 engenders a richer immune infiltrate, and studying the supernatant of *ex vivo* SB28 vs GL261 at the corresponding 5 and 10 day timepoints may shed light on the signaling factors secreted by both lines.

SB28 appeared to also enmesh itself in the brain parenchyma whereas GL261 behaved more like a confined tumor mass that could easily be explanted. These findings were triangulated across several methodologies (i.e., FACS, IHC, 2P), further validating the hypothesis that SB28 tumor more closely approximates human GBM. Thus, the majority of subsequent studies were carried out using this model. We developed a paradigm that enabled to track the tumor-immune response across various methodologies so as to gain real time insights into the quantitative, spatial and temporal evolution of this response.

4 CHAPTER 4: MODULATION OF THE ANTI-TUMOR IMMUNE LANDSCAPE BY VIRAL INFECTION

4.1 THE PROMISE OF VIROTHERAPY AND THE RATIONALE BEHIND LCMV

The previously discussed FACS data showed that an immune response was clearly mounted in SB28 tumors. But given the universal lethality of this model, we concluded that ultimately the immune response was either insufficient or ineffective. Virotherapies are among the most promising opportunities to mount a lasting anti-GBM response. Anecdotally, patients who go on to contract infections at surgical sites fare better than those who do not (De Bonis et al., 2011) and to date the only therapeutic strategy (immune-related or otherwise) that moves the needle for long-term GBM survival is poliovirus therapy such that patients receiving treatment have a three-year survival of 21% compared to 4% in controls (Desjardins et al., 2018). The modified poliovirus used in these trials, PVSRIPO, preferentially targets GBM cells, and essentially xenogenizes them such that a targeted immune response against the tumor is mounted (indeed, antigen-specific cytotoxic T cells responses have been observed in the context of this therapy, which is an otherwise elusive finding in the GBM literature) (Brown et al., 2017). Nonetheless, current efforts are saddled by the need to infect tumors directly via cerebral catheters as well as patients' pre-existing immunity to many of the candidate virotherapies (Brown et al., 2017; Desjardins et al., 2018).

Thus, we sought to administer a systemic virus via circulation, with neurotropism, and to which natural immunity would be rare. Lymphocytic Choriomeningits Virus (LCMV) was a premier candidate that fulfills the aforementioned prerequisites, and about which there is a wealth of information known about the immune response it engenders as well as the

kinetics of infection based off nearly a century of immunological research (Oldstone et al., 1986).

LCMV is a positive single-stranded RNA virus, first discovered in the 1930s as the cause of meningitis in both humans and rodents (MUCKENFUSS et al., 1934). It has since been used as one of the most powerful tools in virology and immunology for 3 main reasons: First, as a non-cytopathic arenavirus (unlike PVSRIPO which is cytolytic, causing direct cancer cell killing), the pathology and tissue damage conferred by LCMV infection is almost exclusively due to the immune response. This has enabled LCMV to be a powerful tool in the study of various immune system phenomena. Secondly, nearly all the immunological findings stemming from pre-clinical LCMV work have been successfully extrapolated to human diseases (Oldstone, 2016). And lastly, there are a variety of LCMV strains that proffer distinct course of infection (and concomitant immunological phenomena). The first isolated strain, Armstrong, leads to inflammation of the meninges in the brain and spinal cord, as well as choroid plexus lining the ventricles. Acute LCMV Armstrong infection induces a fulminant CD8+ T cell response, which is indispensable for viral clearance within 7-10 days (Zinselmeyer et al., 2013). As much as 70% of these cytotoxic T lymphocytes (CTLs) are LCMV-specific (Murali-Krishna et al., 1998). Following their rapid expansion, the T cells enter a contraction phase, which is a followed by a memory phase during which a stable pool of memory T cells are maintained throughout the host's life. These memory cells rapidly proliferate in response to viral re-challenge (Murali-Krishna et al., 1998). At the opposite end of the spectrum is Clone 13, an LCMV strain derived from the parent Armstrong, and whose differences are driven by two critical amino acids from Armstrong (Matloubian et al., 1993). Clone 13 establishes a chronic infection by dint of its higher affinity cellular receptor

and polymerase-induced replicative advantage. These two mutations work in concert to establish persistence and ultimately T cell exhaustion via PD-1 and IL-10 pathways (Zinselmeyer et al., 2013).

Additionally, we were particularly interested in employing LCMV as a tool to engender productive anti-SB28 immunity given the VEGF+ wound repair signature observed **(Figure 3-10).** Extant data from the McGavern lab showed that LCMV infection impeded the meningeal wound healing response following mTBI, and blocked pro-angiogenic myeloid cell-mediated repair in the brain parenchyma following CVI (Mastorakos, Russo, et al., 2021). In the context of injuries such as mTBI and CVI, impeding wound repair meant blood-brain barrier leakage, long-term cognitive and motor dysfunction, and even death. However, we hypothesized that in the context of SB28 (and cancer in general) which seemed to co-opt wound repair programs to sustain its unfettered growth, blocking this process via LCMV introduction would be beneficial. Beyond its potential pre-clinical utility, and as noted above, LCMV has historically played an unrivaled role as a tool to decipher many immunological phenomena, from MHC restriction to immune checkpoint blockade and immune escape. And in the service of further deciphering the immune response to GBM (and its various failings), we appreciated that LCMV – whether or not therapeutically productive in this context– could help elucidate some of these mechanisms.

4.2 SYSTEMIC ADMINISTRATION OF LCMV IN TUMOR-BEARING MICE LEADS TO EXTENDED SURVIVAL AND TUMOR-SPECIFIC VIRAL INFECTION

To assess the effect of systemic infection on survival, we conducted a series of survival and imagine studies. We injected 2 x 10^6 Plaque Forming Units (PFU) of LCMV Armstrong intravenously, 24 hours after tumor injection. It is important to note that the infectivity of

each viral stock is quantified via limiting dilution plaque assay. However, there is a margin of error in this PFU quantification such that in the first few experiments, it became clear that some batches of virus led to fatal meningitis within 6-8 days whereas others did not (despite all doses being delivered at a putative dose 2 x 10^6 PFU per injection). We hypothesized that the reason for the fatal meningitis (as opposed to viral clearance within 7-10 days as would be typical for the i.v. administration of LCMV Armstrong) was because the injection of tumor 1 day prior opened up the barrier systems in the brain such that the i.v. administration more closely approximated intracerebral LCMV injection (which reliably results in fatal meningitis in exactly 6 days, and should be administered at a dose of 1 x 10^3 PFU). Depending on the exact titer of the Armstrong batch I delivered, there was likely some threshold of viral load, paired with some degree of openness in the brain parenchyma, that resulted in this administration behaving like the uniformly fatal intracerebral route. In experiments that did not result in meningitis-related fatality, it was clear however that LCMV Armstrong promoted greater survival in SB28-bearing mice compared to the control group (**Figure 4-1, A)**. We next asked whether the improvement in survival resulted from general inflammation in the meninges (to be expected) that forced the trafficking of non-tumor-specific T cells to the milieu, or whether the tumor itself could possibly be infected with the virus, thereby xenogenizing the SB28 cells and optimizing them for direct T cell-tumor cell engagement and subsequent killing. We were surprised to find near complete penetrance and infection of the tumor (**Figure 4-1, B)**. Perhaps more interestingly, viral nucleoprotein was exclusively detected in the tumor and not in the adjacent, healthy parenchyma. Given concerns around off-target viral infection when using viral therapies to treat cancer, this finding was of particular interest. We hypothesized that the dysregulated metabolism and cell division that

hallmarks SB28 made the tumor a particularly suitable and attractive niche for viral deposition and replication.

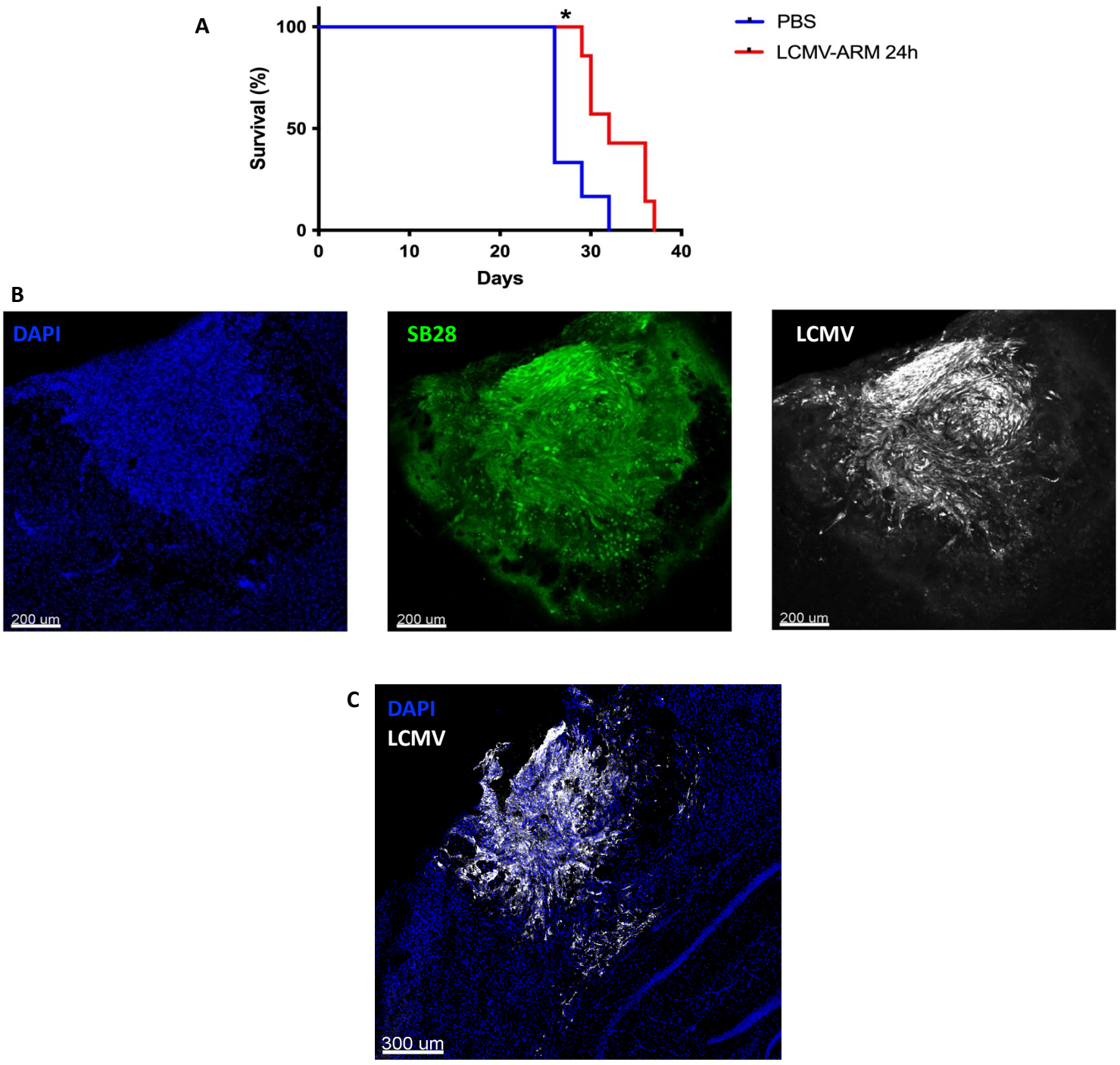

Figure 4-1: (A) Kaplan-Meier curve following tumor injection or tumor injection with LCMV Armstrong administration 24h later shows uniform tumor-related fatality in all mice. However, the median survival was 26 days in the control group and 32 days with LCMV. (*P*=0.0133; Log-rank test). Data are representative of over 10 experiments with 4-6 mice per group. **(B)** Four days following viral administration – at the peak of infection – (i.e., 5 days after tumor implantation), brains were harvested and slices were stained with an antibody targeting LCMV Nucleoprotein (Clone: VL4), shown in white. SB28-GFP cells are shown in green. DAPI cellular stain is shown in blue. B shows one representative mouse, with each fluorescent channel shown separately in the three panels. Images taken at 20x magnification. **(C)** Intravenously-administered LCMV Armstrong preferentially infects the SB28 tumor but not the surrounding parenchyma. Images taken at 4x magnification. All IHC images are representative of 2-3 experiments of 4 mice each.

4.2.1 LCMV INDUCES MARKEDLY ALTERS THE SB28 IMMUNE LANDSCAPE

To follow-up on the findings that systemically-administered LCMV Armstrong extended survival (but did not cure SB28), we sought to understand how the immune response to SB28 differed with and without LCMV Armstrong. Specifically, we asked whether tumor growth was abrogated by the virus' stimulation of a Type I anti-viral immune response that would deviate the previously-observed tumor supportive wound healing program **(Figure 3-10).** To triangulate these results with previously performed FACS experiments, we harvested mice 10 days after tumor implantation (9 days after viral administration – or saline for the controls). At this time point, the well-documented kinetics of Armstrong infection suggest that the virus should be cleared or in its final stages of clearance, and the CTL response should be contracting.

Flow cytometric analyses and the concomitant PhenoGraph and UMAP analyses identified over 29 immune cell subpopulations that could be visualized in 2 dimensions and broadly categorized into the previously identified immune subsets, including CD8 T cells, CD4 T cells, non-classical lymphocytes, microglia, monocytes, MDSCs, and neutrophils **(Figure 4-2)**. As shown in **Figure 4-3**, **A**, LCMV infection profoundly altered the SB28

immune landscape. Despite being in the contraction phase, a powerful CD8 T cell response was still observed (such that the numbers of brain resident microglia paled in comparison) in the LCMV group. The VEGF+ signature previously observed in SB28 samples was reproduced in the uninfected control group. Infection abrogated the VEGF response in both monocytes and MDSCs, as well as drastically reduced the number of MDSCs and neutrophils in the tumor milieu (**Figure 4-3**, **B).** The total VEGF signature based on the pre-gating of all CD45+ leukocytes was slightly reduced in the LCMV group (**Figure 4-3**, **C)**.

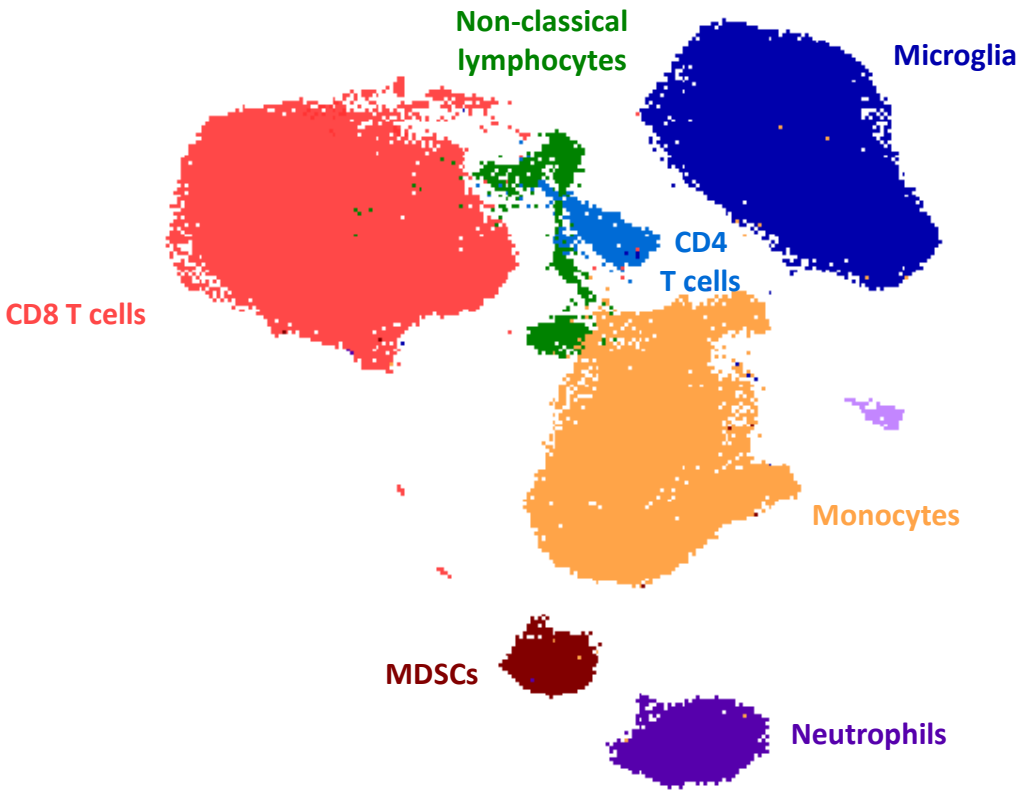

Figure 4-2: Concatenated UMAP display of the immune infiltrate of uninfected and LCMV-Armstrong mice on day 10 following SB28 injection display the broader PhenoGraph-identified cell clusters present at this time point. Dots depict cellularity. UMAP is representative of 2 independent experiments with 3-4 mice per group.

A

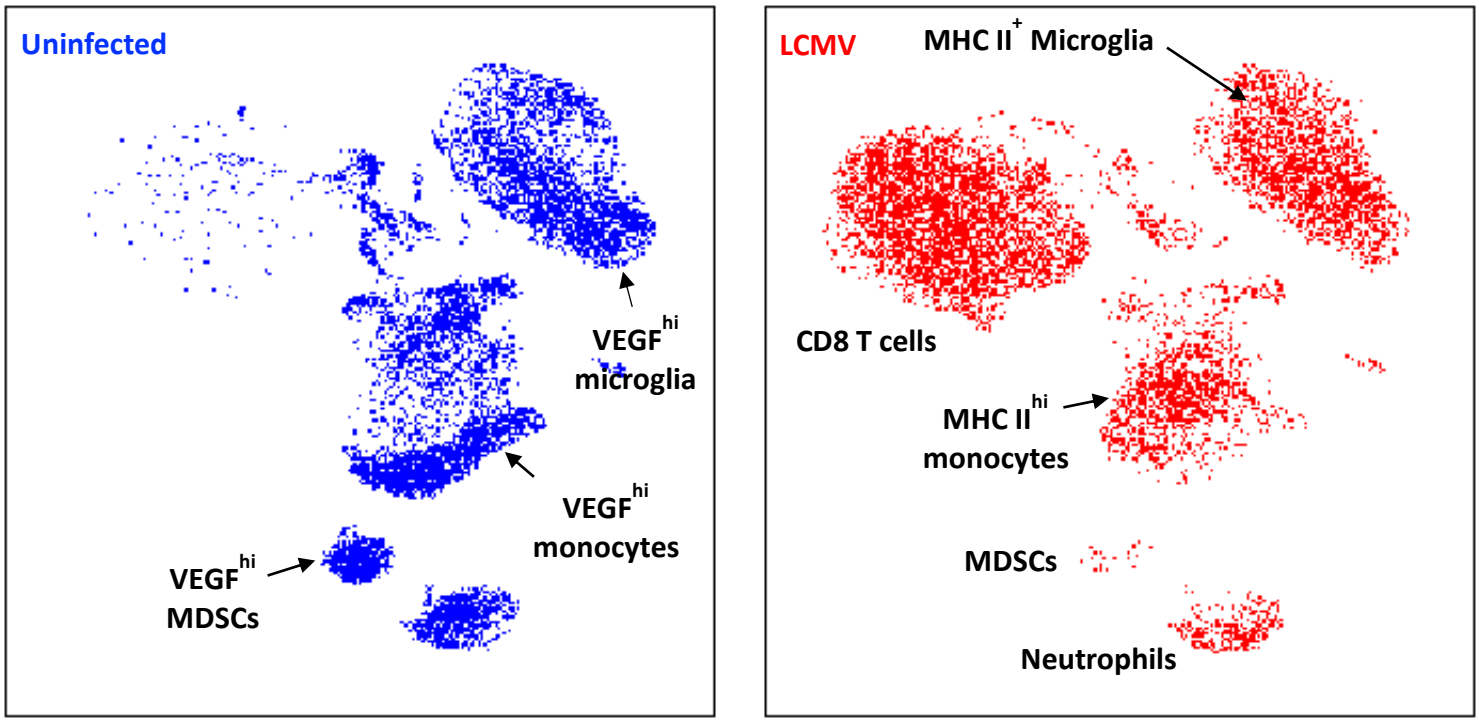
Uninfected
VEGF hi microglia
VEGF hi monocytes
VEGF hi MDSCs
LCMV
MHC II + Microglia
CD8 T cells
MHC II hi monocytes
MDSCs
Neutrophils

B

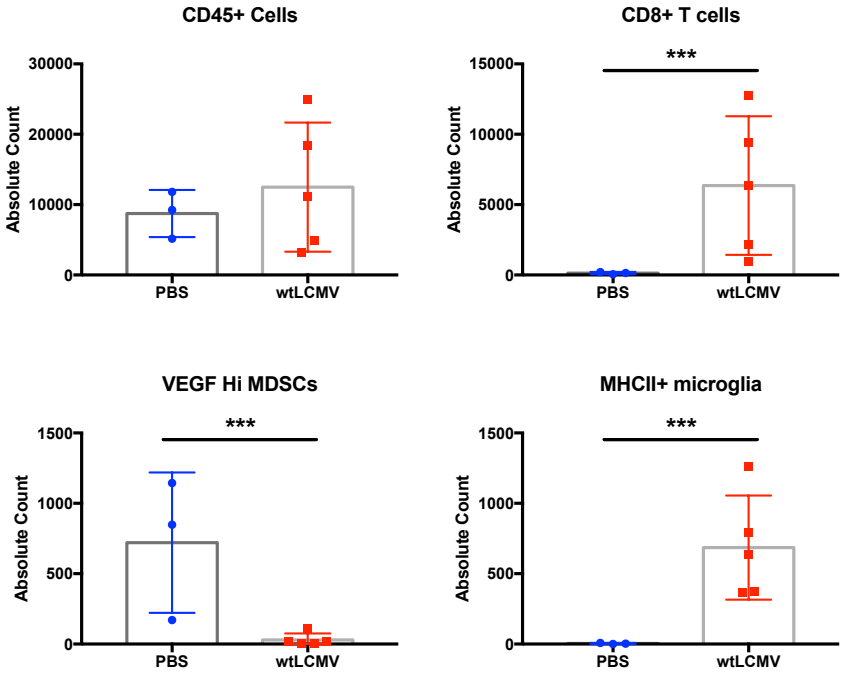
CD45+ Cells
Absolute Count
30000
20000
10000
0
PBS
wtLCMV
CD8+ T cells
***
15000
10000
5000
0
VEGF Hi MDSCs
1500
1000
500
MHCII+ microglia

C

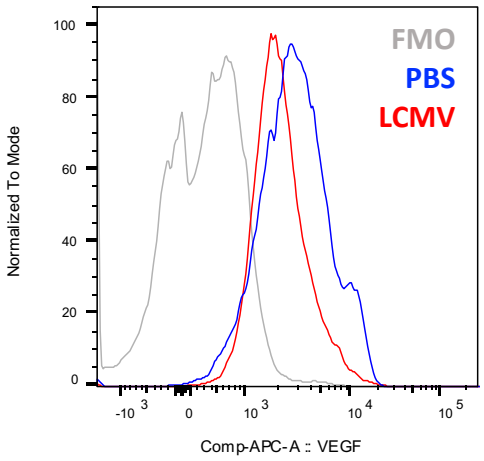
FMO
PBS
LCMV
Normalized To Mode
100
80
60
40
20
0
-10 3
0
10 3
10 4
10 5
Comp-APC-A :: VEGF

Figure 4-3: (A) UMAP display of the immune infiltrate 10 days following the injection of SB28 (i.e., 9 days following either saline or LCMV-Armstrong infection). UMAPs clearly show that LCMV Armstrong infection rearranges the tumor-immune landscape, such that a fulsome CD8+ T cell response is triggered, the phenotype of myelomoncytics shifts from VEGF+ to MHCII+ indicating an altered activation state, and MDSCs and neutrophils decrease drastically in number. **(B)** Representative flow cytometry bar graphs based on PhenoGraph clustering of disparate cell populations on day 10. Data are displayed as mean ± SD. Multiple t-tests with Holm-Sidak Multiple Comparisons Test were used to analyze statistical significance, with *P≤0.05, **P≤0.01, and ***P≤0.001. **(C)** Representative flow cytometry histogram showing VEGF expression of CD45+ cells from 4 pooled samples within each group, comparing the FMO negative staining control to uninfected and infected groups. LCMV Armstrong modestly decreases the global VEGF signature among leukocytes.

4.2.2 TUNING THE KINETICS AND STRENGTH OF THE LCMV-SB28 IMMUNE RESPONSE

4.2.2.1 TITRATING THE STRENGTH OF VIRAL INFECTION AND CTL RESPONSE

The findings of selective, nearly complete infection of the tumor **(Figure 4-1, C),** along with profound alteration of the immune landscape **(Figure 4-3)** led us to query why the survival benefit conferred was not more robust than a 23% increase in median survival time **(Figure 4-1, A).** Since early data using different batches of the same virus indicated that with potentially greater doses, the immune response may be overwhelming and lead to fatal inflammation, we sought to titrate the PFU delivered with the aim of finding the balance of a more robust (yet sublethal) immune reaction. Three cohorts of SB28-bearing mice were administered either 6.0×10^5, 1.8×10^6, or 2.5×10^6 PFU 24h following tumor implantation. Surprisingly, no differences in survival were observed **(Figure 4-4, A).**

Next, we asked whether the time it took to stimulate a CTL response allowed the tumor too much a window of opportunity to grow exponentially, such that the sheer number of tumor cells and their concomitant growth at escape velocity could not be controlled by a cytotoxic T cell response. Thus, we adoptively transferred CTL to provide the immune system with a head-start against the tumor. Donor B6 mice were infected with LCMV Armstrong and on day 8, at the peak of T cell expansion, CD8+ T cells were purified from their spleens via positive selection under sterile conditions (EasySep, StemCell Technologies).

LCMV Armstrong induces splenomegaly and up to 80% of splenic CD8 T cells at this time points are specific for ten LCMV-epitopes (Masopust et al., 2007). Mice received tumor injections on day 0, either saline or Armstrong infection on day 1, and either saline or 4 x 10^6 CTLs from infected donor mice on day 2. Despite stacking the deck in favor of the anti-viral/anti-tumor immune response by short-circuiting the time needed to develop the adaptive response, no differences in survival were observed between groups **(Figure 4-4, B).**

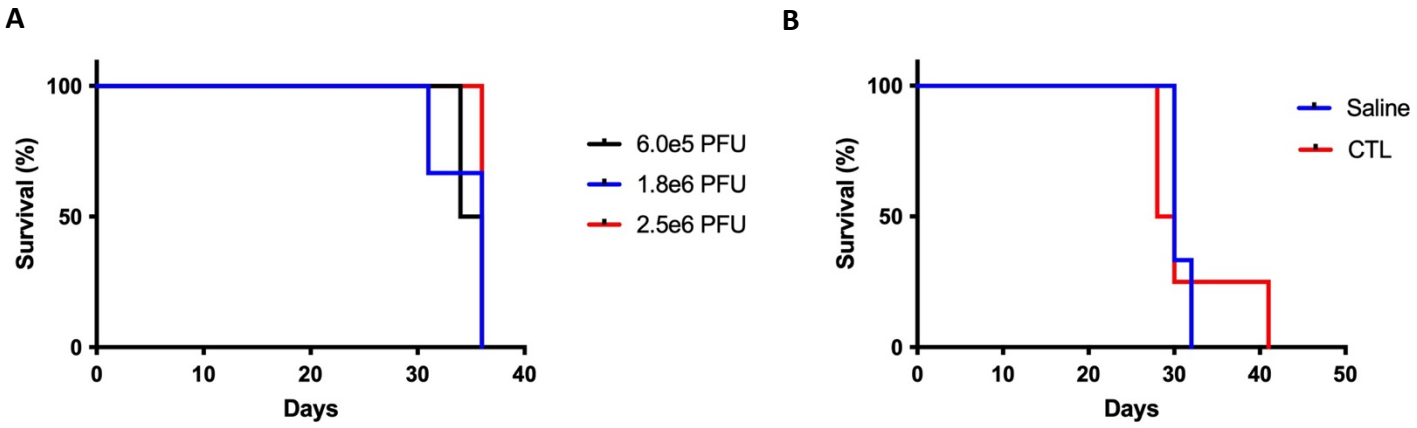

Figure 4-4: (A) Kaplan-Meier curve of various doses of LCMV Armstrong administered 24h following tumor injection. No survival differences were observed. (*P*=0.63; Log-rank test). **(B)** Kaplan-Meier curve of mice receiving either saline or adoptively transferred splenic CTL from Armstrong-infected donors 8 days post infection. Adoptive transfers occurred in tumor-bearing mice 24h following infection, 48h following tumor implantation. No survival differences were observed. (*P*=0.88; Log-rank test). Data in both **A** and **B** are representative of 2 experiments with 5-6 mice per group.

4.2.2.2 ANTI-VIRAL CTL IN THE BRAIN

The fact that pre-seeding mice with anti-LCMV CTL led us to ask whether the tumor was suppressing the efferent trafficking of virus-specific (and depending on the degree of antigen presentation on SB28, tumor-specific) T cells. Thus, we sought confirmation that the extraordinary T cell response in the brain shown in flow cytometric data was virus-

specific (as opposed to bystanders). 24 hours before tumor implantation, spleens from P14-Thy1.1 were extracted and T cells isolated. P14-Thy1.1 mice carry a re-arranged T-cell receptor specific for the immunodominant epitope of LCMV Armstrong infection, peptide P14, as well as a trackable Thy1.1 allele. Recipient mice received 1 x 10^3 T cells, SB28 tumor implantation 24h later, and half of all tumor-bearing mice were infected with LCMV 24h thereafter. Using P14 T cell expansion as a proxy for LCMV-specific T cell expansion writ large, flow cytometric analyses from brain tissue 8d post infection indeed revealed that in control mice, T cells comprised a mean of 5.9% of total CD45+ cells compared with 55.7% of total CD45+ cells in infected mice. In control mice, there was virtually no expansion of P14 T cells as expected, whereas 18.87% of T cells were P14 specific in the

Armstrong group, confirming that virus-specific expansion and subsequent trafficking to the infected tumor site occurred **(Figure 4-5).**

4.2.2.3 ANTI-PD1 THERAPY DOES NOT INCREASE SURVIVAL

After confirming that virus-specific CTLs were in the infected-tumor milieu, we hypothesized that immune cell exhaustion could be mediating the tumor's ability to ultimately surmount the immune onslaught. Thus, we queried whether PD1 inhibition would abrogate tumor growth. All tumor-bearing mice were infected with LCMV Armstrong 24h post tumor injection, and half the mice received either 200ug of IgG2a isotype control or 200ug of aPD1 antibody (BioXCell) on days 2, 4, and 6 following infection. No differences in survival were observed, suggesting that the PD1 T cell signaling was not ultimately responsible for the failed T cell response **(Figure 4-6).** The time points (i.e., 2, 4, and 6 days post infection)

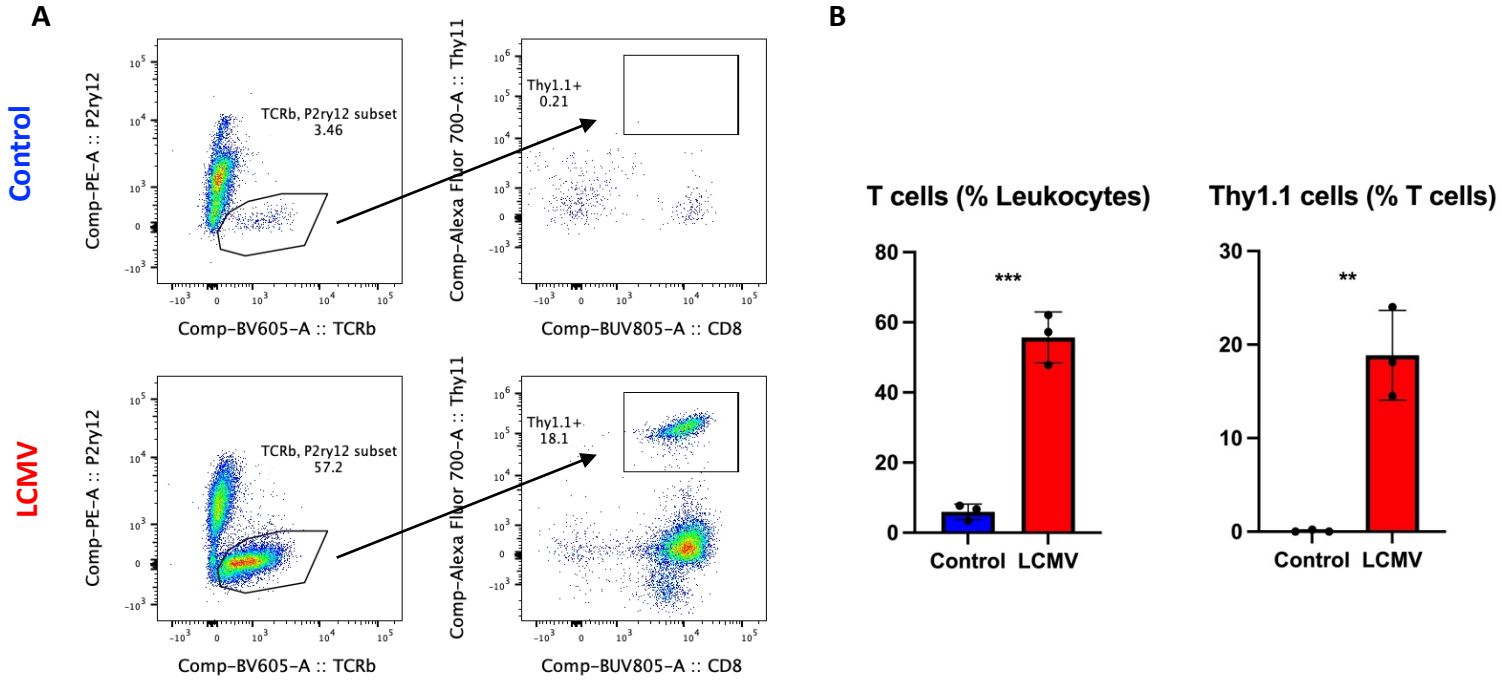

Figure 4-5: **(A)** Representative FACS pseudo color dot plots pre-gated on live single CD45+ cells from the brain 8 days post infection. LCMV group shows a significant T cell presence of which nearly 1/5th of all T cells are specific to the immunodominant epitope of LCMV. There is no expansion of Thy1.1 cells in control mice. **(B)** Bar graphs show the frequency of T cells (left) and epitope-specific P14-Thy1.1+ T cells (right). Bar graphs are representative of 2 independent experiments with 3 mice per experimental group. Data are displayed as mean ± SD. *P≤0.05, **P≤0.01, and ***P≤0.001.

were selected as these represented the peak expansion phase of the anti-viral T cell response. Future studies would require that we phenotype the infiltrating T cells for other inhibitory co-receptors as well as other markers related to activation state and function to identify potential pathways involved in their perceived inefficiency.

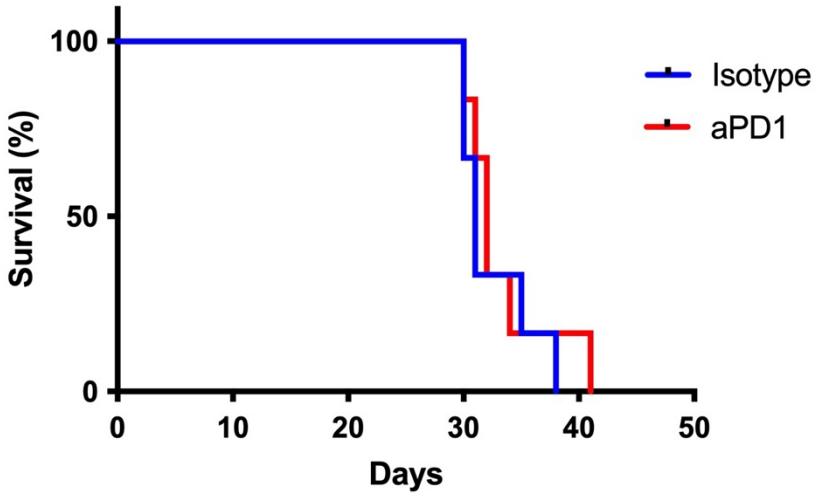

Figure 4-6: Kaplan-Meier curve of LCMV-infected, SB28-bearing mice that received either isotype control of 200ug of aPD1 antibody therapy 2, 4, and 6 days post infection. No survival differences were observed. (*P*=0.31; Log-rank test).

4.2.3 ANTIGEN PRESENTATION TO COGNATE CYTOTOXIC T CELLS

To gain additional insights into the interactions of T cells and tumors, we employed 2P microscopy. CD11c-YFP Reporter mice were pre-seeded with traceable T cells, constitutively expressing OFP under the actin promoter, prior to tumor implantation. 24h after SB28 was intracranially injected, half the mice were infected with Armstrong. As shown in **Videos 5** (left, uninfected control) **and 6** (right, infected)**,** with corresponding snapshot in **Figure 4-7**, infected mice showed a much greater degree of CD11c+ cells (in yellow)

infiltrating the tumor (in green). CD11c+ cells represent both activated microglia (i.e., RAMs and other activated phenotypes identified by previous FACS data) as well as certain subsets of non-classical monocytes. No expansion of the adoptively transferred P14 T cells (in red) was observed in control, uninfected mice. **Video 6** shows anti-viral P14 T cells interacting with tumor cells. Few of the T cells have suppressed locomotion on their tumor cell target, which is indicative of T cell engagement and the formation of the immunological synapse (IS), a ~15nm gap separating a T cell from its cognate peptide-MHC complex on its target cell surface (Dustin, 2014). The formation of an IS is critical for the T cell's subsequent actin cytoskeleton rearrangement and targeted delivery of cytotoxic granules (e.g., perforin and granzymes) which mediate cell killing. The observation of few T cells stopping on tumor cells suggested that T cells may be engaging non-cytolytically with tumor cells, which could explain the ultimate outgrowth of the tumor. To further study whether a lack of IS formation is driving the observed patterns in T cell motility, a key future objective is to conduct higher-end microscopy studies in which fluorescently-tagged proteins that accumulate at an IS (i.e., supramolecular activation complexes (SMACs), TCR/MHC:peptide complexes, co-stimulatory molecules such as CD80/CD28, and other supporting kinases and adhesion molecules such as ICAM-1/LFA-1) can be assayed (Wetzel et al., 2002). The reduction in interactions between co-stimulatory and adhesion molecules on the tumor and T cell may be partly responsible for a putative lack of IS formation, thus assessing the expression of these proteins on the surface of both APC and CTL will be critical.

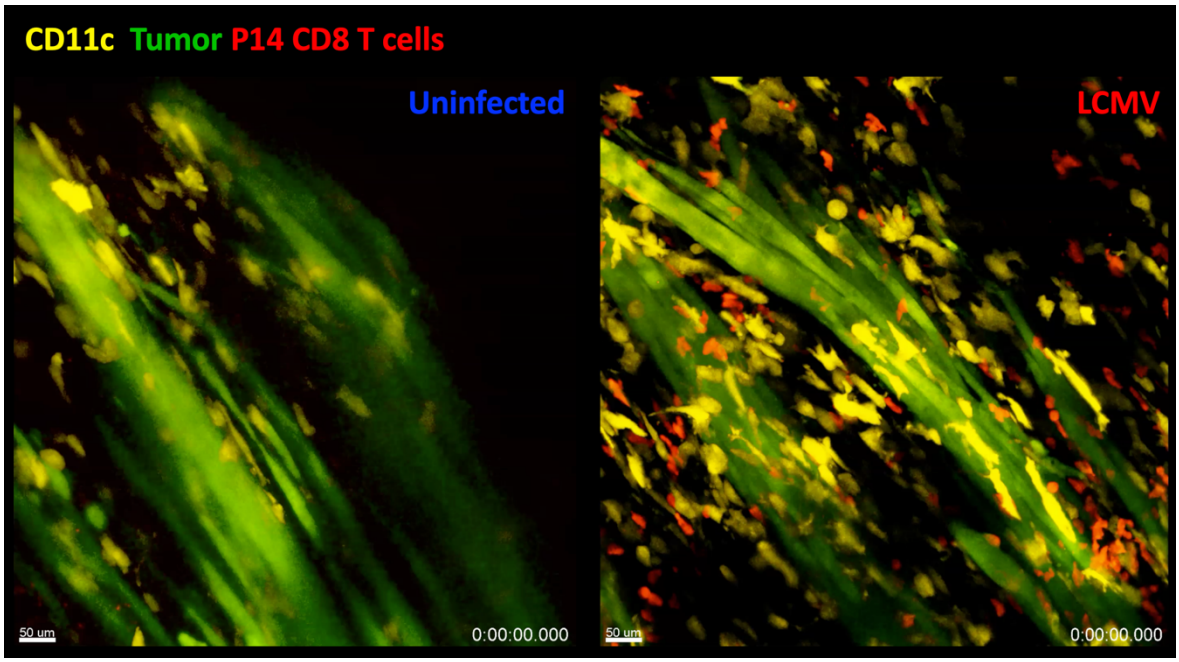

Figure 4-7: Snapshots of Videos 5 and 6, Representative maximal projection of a two-photon z-stack viewed through the thinned skull of tumor-bearing CD11c$^{YFP/WT}$ mice 7 days after LCMV infection. SB28 is shown in green, CD11c+ cells in yellow, and anti-viral P14 cells in red. In uninfected mice (left, Video 5), there are fewer CD11c cells infiltrating the tumor and they expand and retract processes more slowly. Conversely, those in infected mice (right, Video 6), actively surveil the tumor and show vacuoles indicating phagocytic activity as expected of activated myeloid cells in the niche. The majority of P14 cells move quickly around the tumor cells, with few stopping and locking to engage.

4.3 LCMV FAILS TO PROMOTE SUSTAINED ANTI-TUMOR IMMUNITY

4.3.1 LCMV IS CLEARED FROM THE TUMOR MILIEU BY DAY 14

In canonical LCV Armstrong paradigms, the virus is cleared within 10 days of infection, and the T cell response begins contracting by day 9. FACS data from the latter timepoint showed that a large number of T cells remained in the brain at this time point, and pilot 2P studies showed that anti-viral T cells could be found in the brain as late as 12-3d post infection. Thus, we queried whether we could detect viral nucleoprotein in the tumor milieu 14 days post infection (i.e., 15d post tumor implantation). At this time point, brains were

harvested and slices were stained with an antibody targeting LCMV Nucleoprotein (Clone: VL4), shown in white. No virus was detected in the tumor, shown in green (GFP+) **(Figure 4-8)**. As a positive control to ensure the VL4 staining protocol was effective, carrier mice (infected *in utero* and persistently harboring infection in the brain and body*)* were also stained. The fact that the virus was cleared but the tumor remained indicated that either (a) complete penetrance of infection in the tumor was not actually achieved, and uninfected tumor cells drove outgrowth following the killing of their infected counterparts and/or (b) anti-viral T cells engaged with the tumor, but only to clear the virus noncytopathically. Non-cytopathic clearance of infected CNS cells (or in this case, tumor cells mimicking CNS cells) is an evolutionarily conserved mechanism: the nonredundant and irreparable cells of the CNS require strict control of potentially lethal, efferent inflammation. Indeed, it has been shown that even antiviral T cells possessing granzymes can clear infected microglia (and bystander neurons) noncytopathically via IFNγ secretion (Herz et al., 2015). Non-cytopathic interactions between T cells and their targets may be influenced by the degree of antigen presentation, thus we hypothesized that the tumor may be favoring these interactions by downregulating MHC-I or other elements of the antigen processing and presentation path-

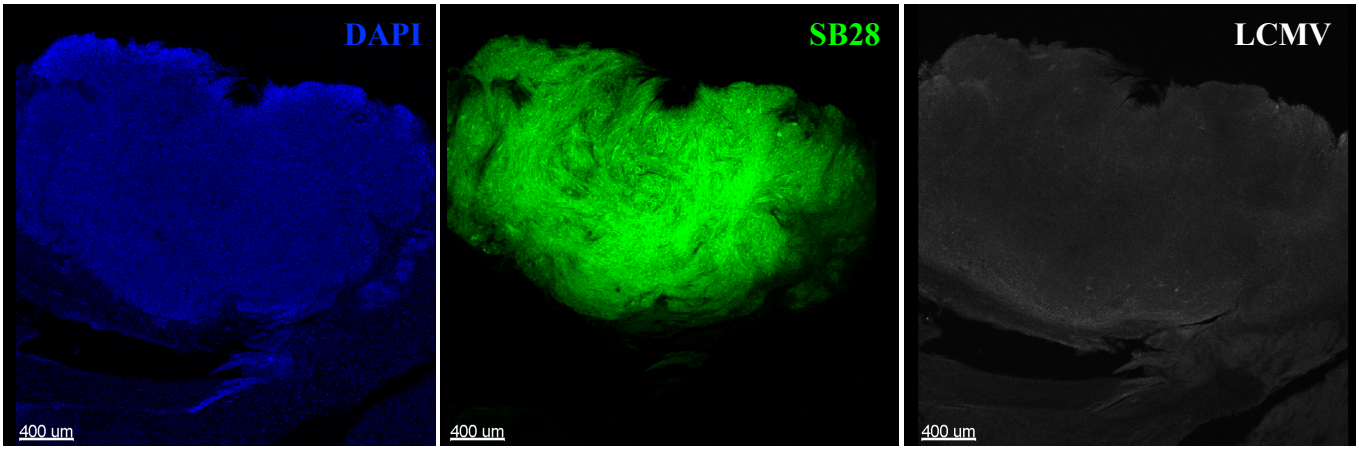

way.

Figure 4-8: Viral infection was assessed in SB28 tumors 14d following viral administration. SB28-GFP cells are shown in green, DAPI cellular stain in blue, and LCMV Nucleoprotein in white. Images taken at 10x magnification. At this time point, no viral infection of the tumor (nor surrounding parenchyma) could be detected).

4.3.2 SINGLE-CELL SEQUENCING OF CONTROL AND INFECTED SB28 TUMORS, AND THEIR IMMUNE COMPARTMENTS

To gain deeper insights into the differences between uninfected and infected tumors, as well as the decay of the anti-viral/tumor immune response, we analyzed gene expression by single-cell RNA sequencing of tumor and immune cells in uninfected and LCMV mice, at peak infection (i.e., 4 days), and once viral clearance had been achieved (i.e., 14 days and 15 days) **(Figures 4-9 – 4-15).** This sampling across treatment and time allowed us to phenotype the evolution of tumor and immune cells from equivalent injection batches of infection and tumor.

In the process of explanting 14dpi tumor-bearing brains for IHC staining, it became clear that at this time point the tumor showed increased stiffness such that it was no longer amenable to the punch biopsy protocol that had been used for any brain processing during all earlier time points. The tumor felt hard to the touch, so to fully dissociate it while avoiding excess damage to the immune cells within the tumor niche, we employed a protocol involving enzymatic digestion (Tumor Dissociation Kit, 130-096-730, Miltenyi Biotec). All samples in the single-cell sequencing experiment were processed identically. Data from this experiment were analyzed by Kory Johnson, PhD, from the NINDS Bioinformatics core facility.

4.3.2.1 WITHIN THE INFECTED TUMOR IMMUNE LANDSCAPE, CD8 T CELLS SHOW THE MOST PROFOUND CHANGE IN FUNCTION OVER TIME

scRNA-seq returned an average of 8,602 cells per sample and 8,066 reads per cell. Variance analysis indicated that 50 principal components effectively captured most of the variation in the data. Unsupervised clustering revealed 18 partitions, that were labeled with ImmGen Data and reference mouse RNA sequencing data and manually confirmed using known marker genes. We identified populations of immune, endothelial, glial, and tumor cells **(Figure 4-9).**

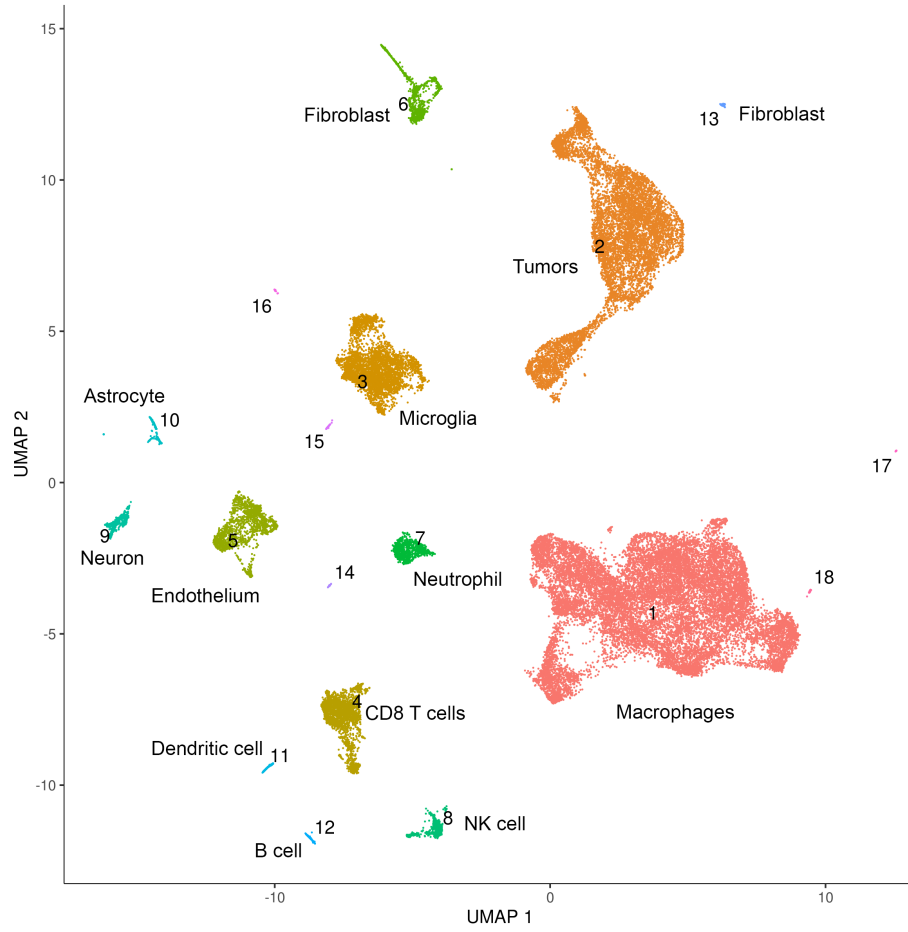

Figure 4-9: Uniform Manifold Approximation and Projection (UMAP) plot describing cell to partition relationships for a total of 39,608 cells and 18 partitions. Expression for 31,040 non-MT genes were used. Partitions were generated using monocle3 with annotations assigned based on majority cell types present therein using SingleR in conjunction with the ImmGenData and MouseRNAseqData celldx data sets.

We then asked which populations showed the greatest change across both time and treatment condition, to enable downstream trajectory analysis. We quantified the numbers of cells per partition that belonged to each experimental group, and visualized the percentages of cells from each experimental group by partition **(Figure 4-10).**

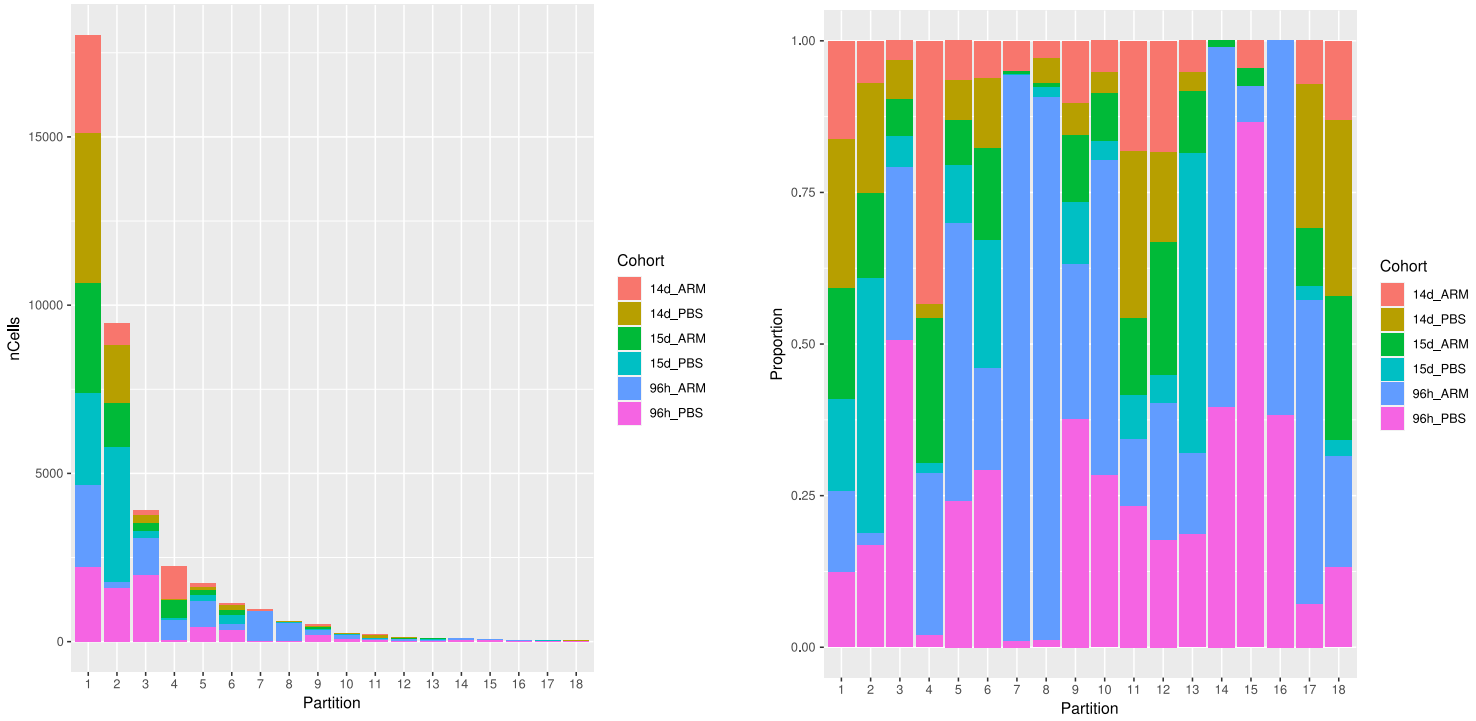

Figure 4-10: Number of cells per sample (y-axis) in each partition (x-axis) are described by stacked bar plot (left). Proportion of cells per sample (y-axis) in each partition (x-axis) are described by filled bar plot (right). Partitions 4, 7, and 8 – corresponding to CD8 T cells, Neutrophils, and NK cells respectively – show disproportionate frequencies with respect to either treatment (Armstrong vs PBS) or time (96h vs 14/15 days).

In T cells, NK cells, and neutrophils, there were disproportionate frequencies with respect to infection, clearly connecting their infiltration of the TME to the virus **(Figure 4-10)**. However, for neutrophils (partition 7) and NK cells (partition 8), there is virtually no

involvement at later time points; they are early responders at the 96h timepoint and then wane precipitously, such that they are not found at 14/15dpi **(Figure 4-11).**

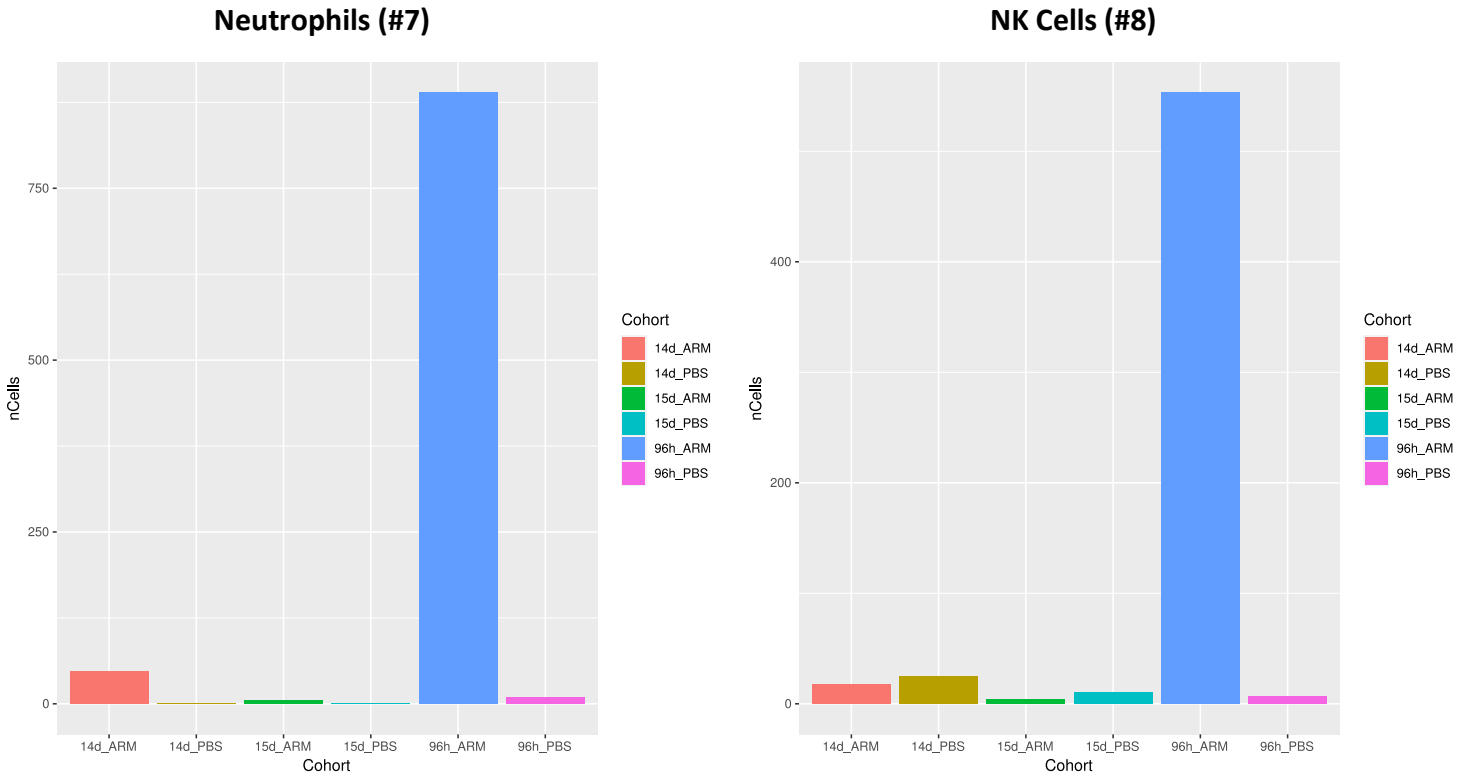

Figure 4-11: Number of cells (x-axis) per sample (y-axis) in partition 7 (Neutrophils) are described by bar plot (left). Number of cells (x-axis) per sample (y-axis) in partition 8 (NK cells) are described by bar plot (left). Both neutrophils and NK cells are found in the TME only transiently, 96h post infection (shown in blue).

T cell presence, on the other hand, remained unchanged over time in the infected groups (despite the clearance of the virus by 14dpi) **(Figure 4-12),** and thus we subjected the CD8 T cell partition to further sub-clustering to query evolving gene expression patterns over time **(Figure 4-13).**

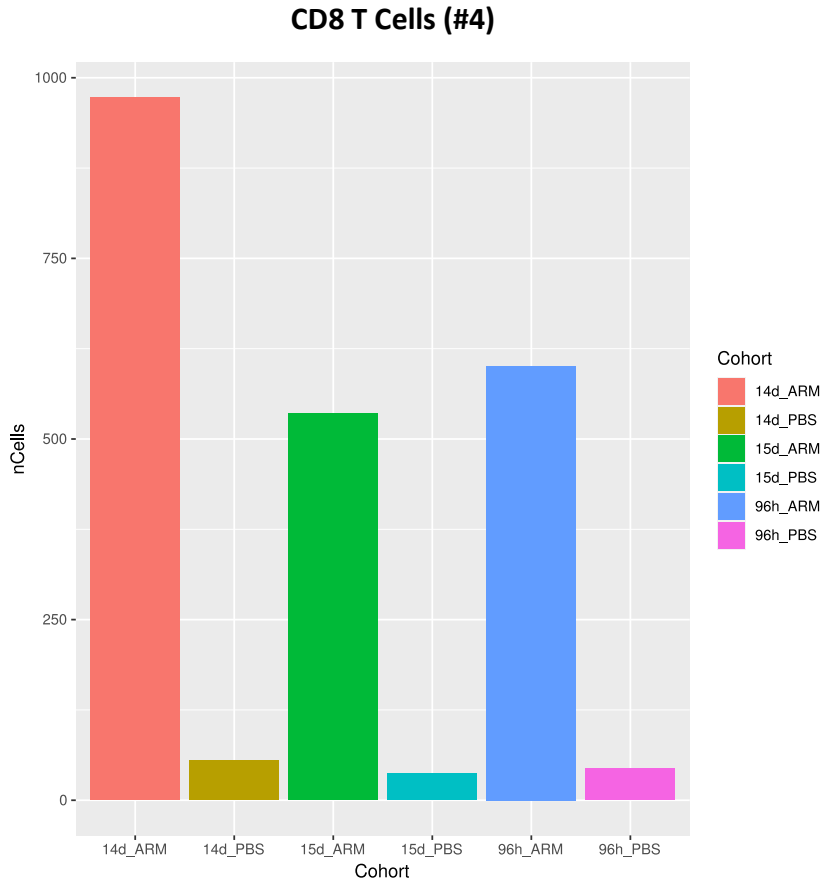

Figure 4-12: Number of cells (x-axis) per sample (y-axis) in partition 4 (CD8 T cells) are described by bar plot. CD8 T cells exist in the TME at all time points queried even though the virus is cleared by 14dpi.

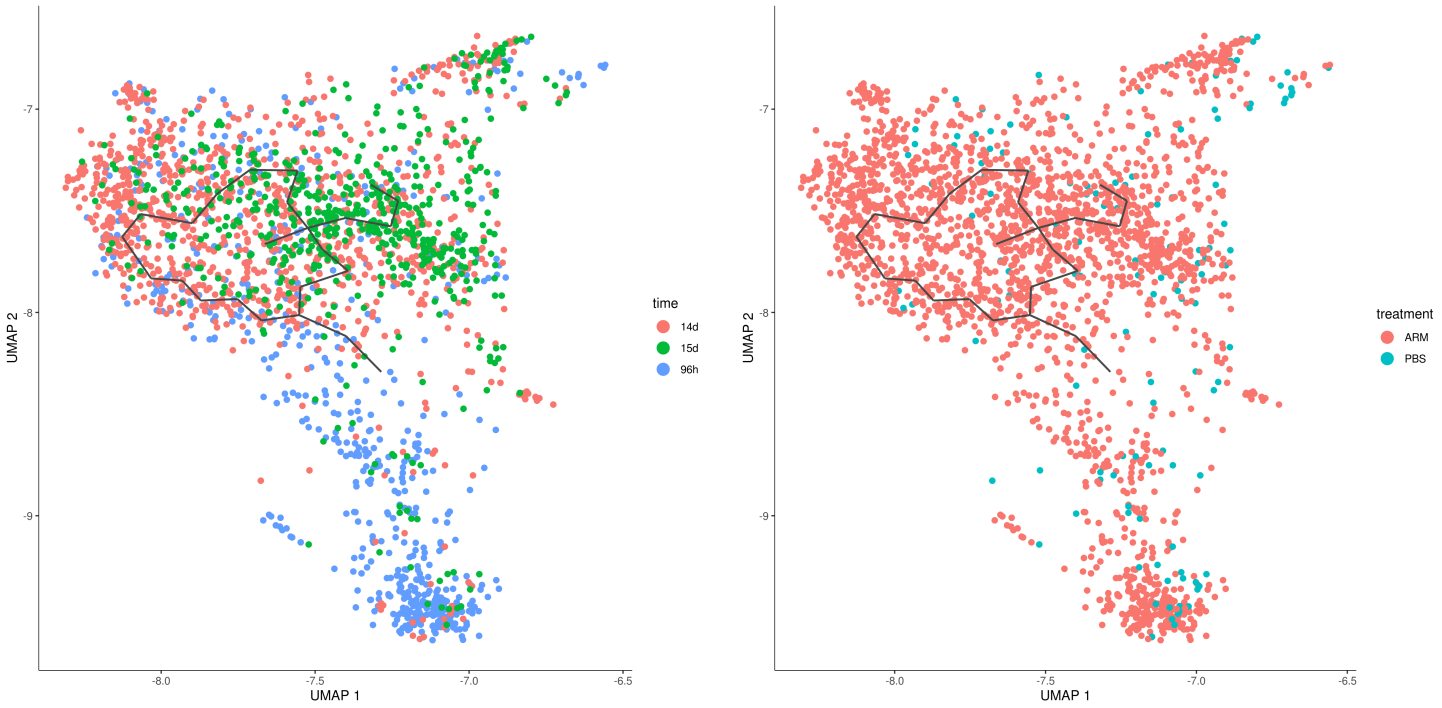

Figure 4-13: Uniform Manifold Approximation and Projection (UMAP) plot describing cell to cell relationships for CD8 T cells (partition 4) after subset, repeat clustering, and trajectory fitting using monocle3. Expression for 31,040 non-MT genes were used. Cells are colored by time (left), such that 96h is shown in blue, 14d in red, and 15d in green, and sub-cluster according to timepoint. Cells are colored by treatment (right), such that Armstrong is shown in red and PBS in blue.

Pseudotime analysis based on differentially expressed genes across time points confirmed the evolution of the T cell phenotype from 96h to 14/15 days **(Figure 4-14).**

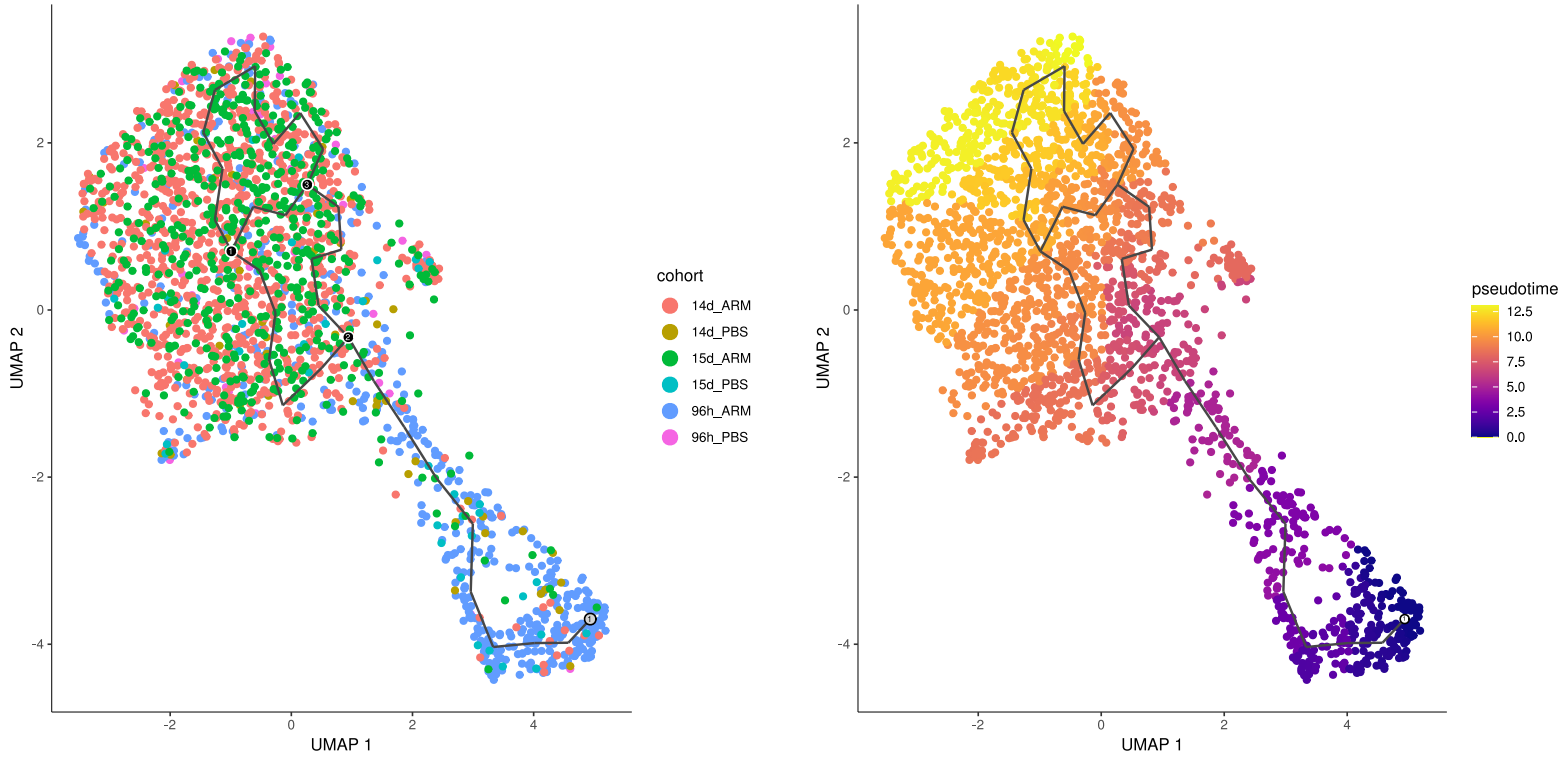

Figure 4-14: UMAP describing cell to cell relationships for CD8 T cells (partition 4) after subset, repeat clustering, and trajectory fitting using monocle3. Expression for 430 non-MT genes identified differential gene expression between 96h and subsequent time points (Wald test Benjamini and Hochberg q-value < 0.05). Cells are colored by sample (left) and separately colored by pseudotime (right).

Specifically, we found that effector function in the T cells was virtually nonexistent at later time points, such that at peak infection (96h) CTLs expressed high levels of proliferative marker *Ki67*, survival gene *Survivin*, and effector molecules Granzyme A and B. However, by 14 and 15dpi these transcripts were hardly detectable **(Figure 4-15).** This drastic decay in effector function and proliferative capacity may explain the overall failure of LCMV infection to provide long-lasting anti-tumor immunity.

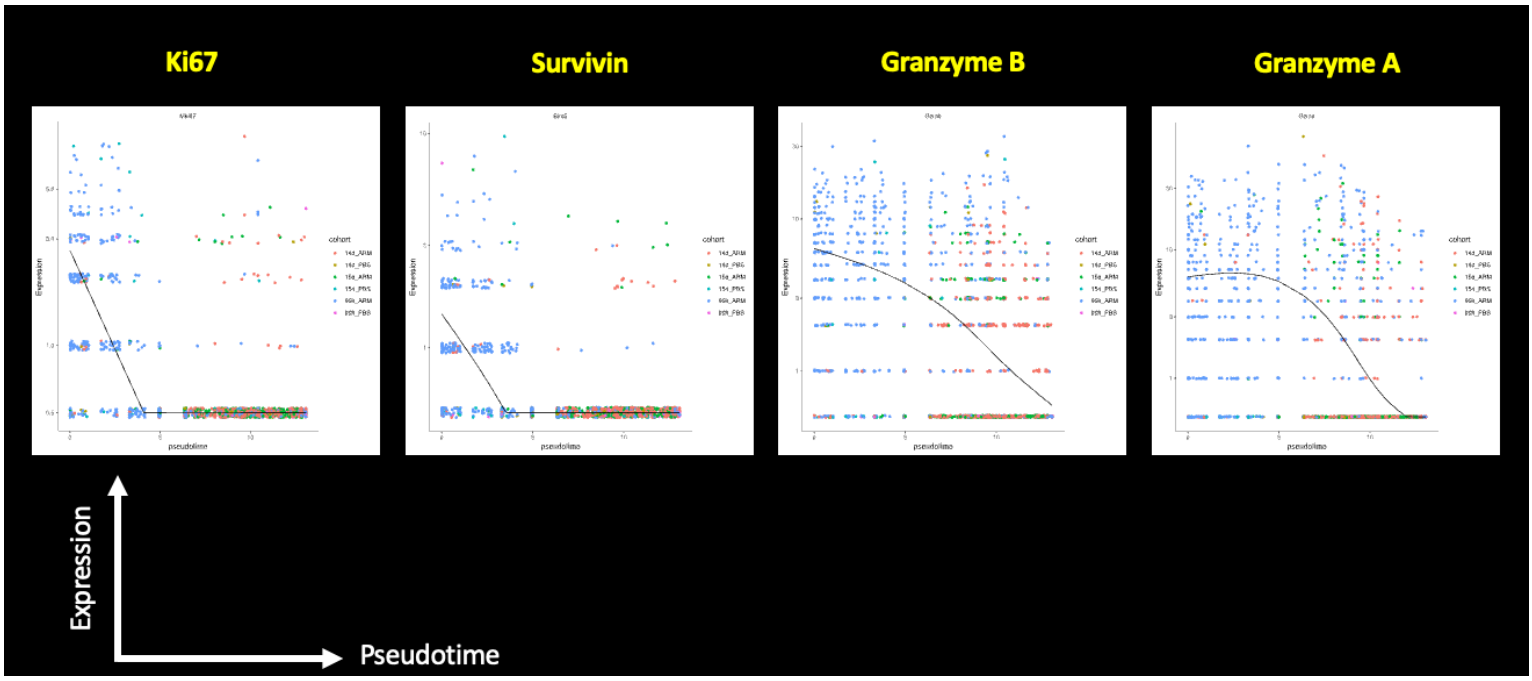

Figure 4-15: Scatter plots describing expression (y-axis) for *Mki67, Survivin, Gzmb, and Gzma* vs pseudotime (x-axis) for CD8 T cells after subset, repeat clustering, and trajectory fitting using monocle3. Expression for 430 non-MT genes identified differential gene expression between 96h and subsequent time points (Wald test Benjamini and Hochberg q-value < 0.05). Cells are colored by sample, such that 96h is shown in blue, 14d in red, and 15d in green.

4.4 SUMMARY

We administered LCMV Armstrong to tumor-bearing mice with the goal of co-opting the well-documented and fulminant CTL response for anti-tumor immunity. LCMV Armstrong infection preferentially infected SB28 tumors, leaving surrounding brain parenchyma uninfected. Infection profoundly altered the SB28 immune landscape, rerouting the myeloid response from a VEGF+ phenotype to an activated MHCII+ phenotype, abrogating MDSCs, and inducing – as expected – an overwhelming CD8+ T cell response. Additional profiling by single-cell RNA sequencing confirmed that of all immune cell types identified, the CD8 T cell response was most profoundly impacted by infection. Much like in clinical GBM which is poorly infiltrated by CTL, control samples showed almost no T cells. Despite the

virus being completely cleared and undetectable 2 weeks after infection, the number of T cells between 96h (peak infection) and 15d (post viral clearance) hardly differed. Instead, however, T cell effector function almost completely decayed. T cells at peak infection expressed high levels of proliferative and survival genes, along with effector molecules such as Granzymes. At later time points these transcripts were hardly detectable. This decay in function and proliferative programming may explain the ultimate outcome – that even infected mice succumb to tumor-related fatalities.

An important, yet outstanding question remains whether the T cells are engaging with what they believe is a reservoir of virus (but is a tumor). If this were the case, we would expect more cytopathic control as LCMV CTLs notably clear virus by killing infected host cells. In future work, we could leverage a recombinant strain of LCMV expressing Cre, and generate an SB28 line in which a fluorescent reporter protein (e.g., mCerulean) is floxed, such that infected tumor cells would permanently fluoresce Cerulean. If at endpoint, Cerulean SB28 cells remain, then it would be conclusive that T cells engaged with the tumor noncytopathically, and additional work on how to convert this interaction into a cytolytic one (be it by augmenting antigen presentation, or impinging on different pathways related to cytokine-mediated noncytopathic clearance) would be warranted.

5 CHAPTER 4: PARADIGM TO SIMULTANESOULY TRACK ANTI-VIRAL AND ANTI-TUMOR IMMUNITY

5.1 SB28-OVA ENABLES TRACKING OF THE TUMOR-SPECIFIC T CELL RESPONSE

LCMV-Armstrong administration led to an acute and robust anti-viral immune response as evidenced by FACS and 2P imaging. The selective infection of the tumor, its subsequent expression of viral nucleoprotein, and the observation of anti-viral T cells interacting directly with tumor cells suggested that the so-called anti-viral response doubled as an anti-tumor response. Thus, we posited that the aforementioned molecular mimicry drove the statistically significant increase in survival conferred by infection. Single-cell sequencing revealed that anti-viral CTLs were becoming less efficient per unit time, so we aimed to accelerate the killing efficiency of CTLs before their total decay in function and energetics.

Our 2P imaging showed P14 T cells engaging with the LCMV-infected tumor (**Figure 4-7**), yet the majority of T cells, even if they were recognizing cognate ligand on the surface of the tumor, did not stop and lock long enough to form a tumor-T cell synapse, a requirement for the rearrangement of CTLs' actin cytoskeletons and delivery of effector molecules such as perforin and granzyme. Instead, the CTLs' "drive-by" behavior suggested short-lived kinaptic interactions with the tumor, which would favor non-cytopathic clearance of the tumor via cytokine secretion, its masking as a reservoir of virus notwithstanding. Non-cytolytic clearance of the tumor would explain its ultimate outgrowth. We needed to devise a system in which CTL cognate antigen remained present on the surface of the tumor cell, past the point when the virus would inevitably be cleared. We collaborated with Vanja Lazarevic, PhD, from the National Cancer Institute, who transduced our parent SB28-GFP tumor line with a TdTomato-Ova transgene (**Figure 5-1**).

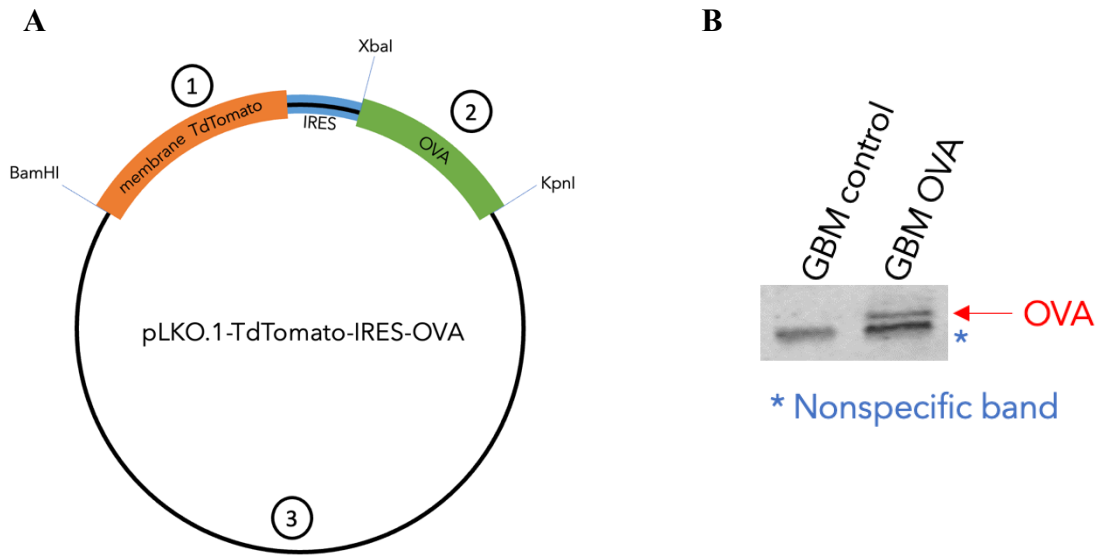

Figure 5-1: (A) The SB28-TdT-Ova cell line was generated by transducing the parent SB28-GFP line with a pLKO.1-TdTomato-IRES-OVA lentivirus. **(B)** Western Blot confirmed Ovalbumin expression in the newly generated SB28-TdT line.

5.1.1 SB28-GFP AND SB28-OVA HAVE IDENTICAL SURVIVAL PROFILES

To assess whether SB28-Ova could be used in place of the SB28-GFP line with which all prior experiments were conducted, and to ensure that the more famously immunogenic Ova did not lead to any differences in immune rejection of the tumor (or SB28's universal fatality), we compared the survivals of both cell lines. No differences in survival were observed **(Figure 5-2)**.

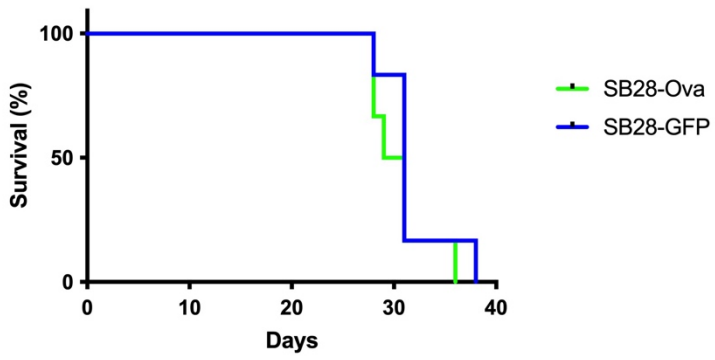

Figure 5-2: Kaplan-Meier curve of mice receiving either SB28-GFP (parent line) or SB28-TdT-Ova (transduced). Data are representative of 2 experiments with 4-6 mice per group. No survival differences were observed. (*P*=0.29; Log-rank test).

5.1.2 SB28-OVA ENABLES TRACKING OF ANTIGEN DRAINAGE AND PERIPHERAL IMMUNE RESPONSE

5.1.2.1 ABSENT VIRAL INFECTION, THERE IS VIRTUALLY NO ANTIGEN DRAINED NOR ANTI-TUMOR IMMUNE RESPONSE

The Cancer-Immunity cycle, canonized by Chen and Mellman **(Figure 5-3),** identifies the release of cancer cell antigens as the first step in mounting an anti-tumor immune response. Particularly in the context of GBM (and any intracranial tumor for that matter), the degree to which antigen is drained is limited. The brain is among a few unique tissues (i.e., eyes and testes) that does not participate in conventional efferent and afferent modes of immune surveillance (Engelhardt et al., 2017) (**Figure 1-1**). While conventional lymphatic vessels exist along the venous sinuses in the dura mater – the outermost layer of the meninges (Ji Hoon Ahn et al., 2019; Andres et al., 1987; Antoine Louveau et al., 2015; Waggener & Beggs, 1967), the same has not yet been shown in the brain parenchyma.

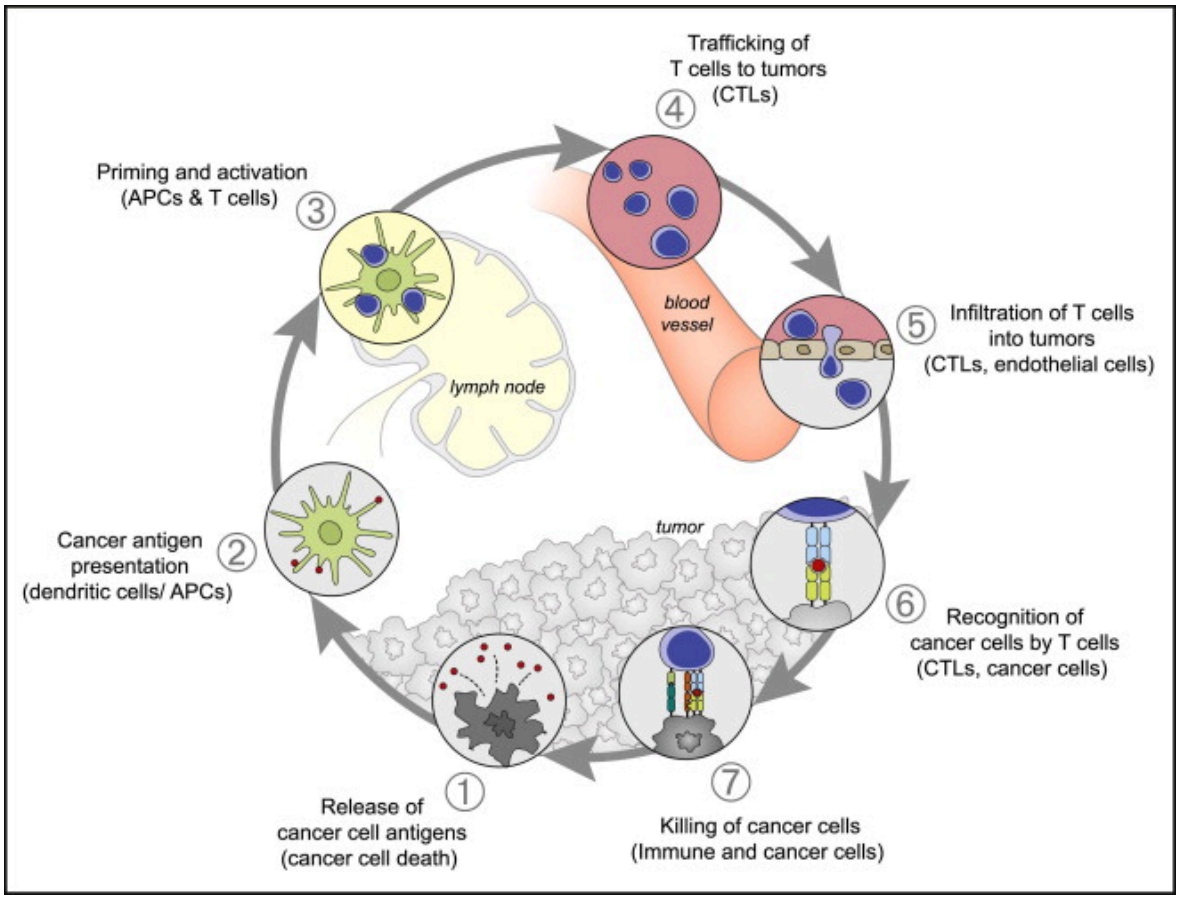

Figure 5-3: The Cancer Immunity Cycle. Reproduced from *Oncology Meets Immunology: The Cancer-Immunity Cycle, Chen and Mellman, Immunity 2013.*

At the start of my thesis, we aimed to understand the baseline level of host immune surveillance of a developing SB28 tumor, however, the only trackable neoantigen in this tumor line is GFP. B6 mice are an H-2K^{b}/D^{b} haplotype, and the only available anti-GFP trackable T cells recognize the immunodominant epitope of GFP when presented on H-2K^{d}. Thus, we were unable to conduct an experiment assessing the extent of antigen release and subsequent presentation by APCs, and priming and activation of T cells in the draining cervical lymph nodes. The use of SB28-Ova presented an opportunity to measure the baseline efficacy of the aforementioned steps 1-3 in the Cancer Immunity Cycle for our model of GBM.

B6 mice were pre-seeded with 10,000 naïve, donor mTomato-OTI T cells that recognize the immunodominant epitope of Ovalbumin. 24h later, all mice were injected with SB28-Ova cells. As a positive control, half the mice were infected 24h following tumor implantation with recombinant LCMV-Ova (rLCMV-Ova). To generate recombinant LCMV virus, the parent glycoprotein is replaced with the antigen of choice, in this case Ova (Wingerath et al., 2017). The result is a replication-deficient form of LCMV that does not produce infective progeny and in this context, does not lead to fatal meningitis.

7 days following either rLCMV-Ova or saline control infection, tumor-bearing mice were sacrificed, and their deep and superficial cervical lymph nodes and spleens explanted. These lymphoid tissues were mechanically dissociated and subject to flow cytometric analysis. In uninfected mice, there was no expansion of tumor-specific OTI T cells in the draining nodes or spleen, indicating a complete failure of the host immune system to detect a tumor within one week of its implantation (representing ~25% of the entire clinical course) **(Figure 5-4).**

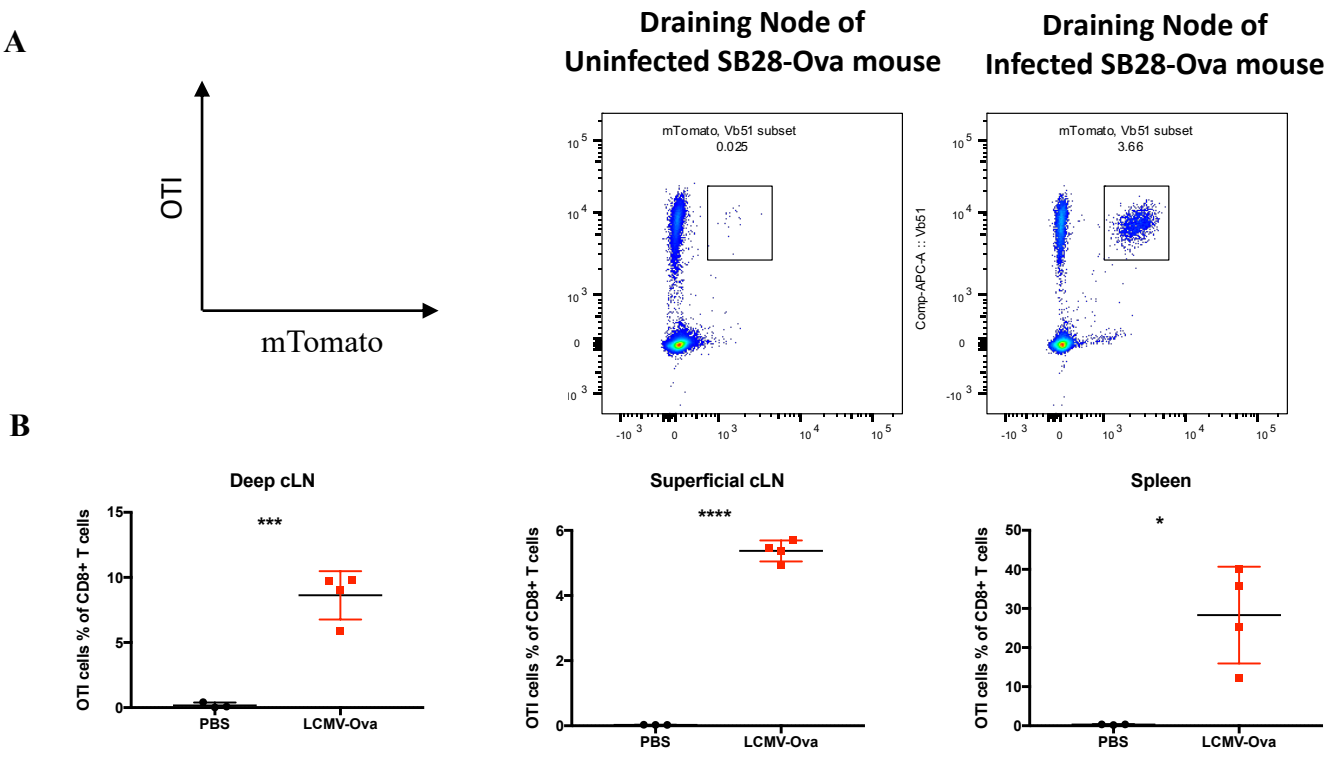

Figure 5-4: FACS plots from the lymphoid tissues of mice 7d after either rLCMV-Ova infection or saline injection. **(A)** Pseudocolor FACS plots pre-gated on live, CD45+ cells show the gating strategy for identifying mTomato-OTI cells, which were double positive for mTomato (PE channel) and stained positive for the variable beta 5.1 chain, present only on the TCR of adoptively transferred OTI cells. **(B)** Bar graphs indicate the frequency of OTI T cells. Data are representative of 2 independent experiments with 4 mice per experimental group. Data are displayed as mean ± SD. Multiple t-tests with Holm-Sidak Multiple Comparisons Test were used to analyze statistical significance, with *P≤0.05, **P≤0.01, and ***P≤0.001.

To confirm these findings in another system, we injected SB28 tumors in genetically mismatched mice, in which foreign grafts (such as tumors) should be rejected 100% of the time provided there is immune surveillance of the anatomical compartment into which the graft is injected. We compared the rejection of SB28 tumors in B6 mice (in which the model had been originally developed) versus DBA/2J mice, an immunocompetent strain with a different MHCI haplotype. DBA/2J mice failed to consistently reject SB28 tumors. Only

25% of injected mice survived the implantation **(Figure 5-5, A).** These 25% likely experienced enough injury during the tumor injection to irreversibly open up the BBB and allow for constant antigen drainage.

The B6 vs DBA2 experiments recalled those of Pete Medawar in the 1940s, in which Medawar implanted skin grafts in the brain and periphery, to find that those in the periphery were universally rejected while those in the brain were not. The notion of the brain's immune privilege was borne of these experiments. However, the less remembered of Medawar's experiments demonstrated that skin grafts were indeed rejected from the brain when they were preceded by a heterotopic tissue graft elsewhere in the body. *De novo* immunity could not be mounted in the CNS but pre-existing immunity in the periphery could be harnessed to traverse the BBB and reject the foreign tissue (Medawar, 1948). We sought to recreate this system by inducing memory against the tumor neoantigen, Ova. Mice were either injected with saline or infected with rLCMV-Ova. 45 days later, following the clearance of the virus and establishment of immunological memory, mice were injected with SB28-Ova. Surprisingly, SB28-Ova tumors were not eradicated in hosts with Ova-specific memory, and no survival differences were observed **(Figure 5-5, B).**

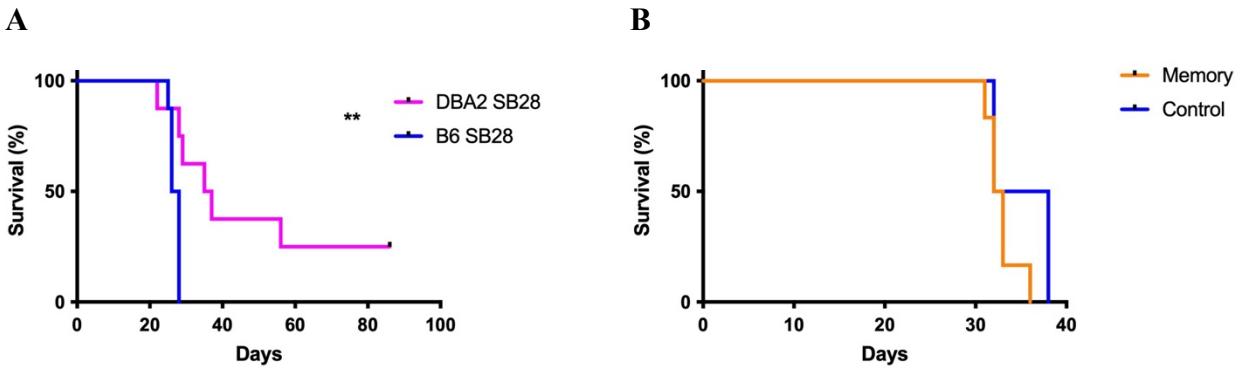

Figure 5-5: (A) Kaplan-Meier curve following tumor injection in either B6 (matched) or DBA2 (genetically mismatched) mice. 25% of DBA2 mice survived. Median survival in B6 mice was 27 days and median survival in DBA2 mice was 36 days (*P*=0.007; Log-rank test). Data are representative of 2 with 6 mice per group. **(B)** Kaplan-Meier curve following tumor injection in either naïve or Memory mice. Memory mice had been infected with LCMV-Ova 45d prior to tumor implantation. No survival differences were observed (*P*=0.29; Log-rank test).

5.2 LCMV INFECTION POSSESSING A TUMOR ANTIGEN MIMIC

The FACS data on OTI T cell expansion in secondary lymphoid organs of SB28-Ova-bearing mice indicated that although at baseline, Steps 1-3 of the Cancer-Immunity cycle were not occurring, we could short-circuit the process of antigen release, presentation, and T cell priming and expansion by employing rLCMV carrying a direct tumor antigen mimic (i.e., rLCMV-Ova) **(Figure 5-4).** The survival data from genetically mismatched mice as well as mice harboring memory immunity against the tumor antigen also made clear that to profoundly improve SB28 survival, we needed a peripheral instigator of acute and tumor-specific immunity.

5.2.1 rLCMV-Ova INFECTION EXTENDS SURVIVAL IN SB28-OVA-BEARING MICE

Mice received intracranial injections of 5,000 SB28-Ova tumor cells, and 24h later, were administered eithered saline (control), rLCMV-Ova, or LCMV-Armstrong intravenously. rLCMV-Ova is an attenuated recombinant of LCMV-Armstrong that instigates a less robust immune response and thus does not result in any fatal meningitis (Emonet et al., 2009). Infection with rLCMV-Ova conferred the greater survival benefit **(Figure 5-6, A).** We then queried whether rLCMV-Ova infected the tumor tissue, in the same way LCMV-Armstrong did. At 96h post infection (representing peak infection), rLCMV-Ova infected mice bearing SB28-Ova tumors were sacrificed and brains explanted. Slices were stained for VL4 nucleoprotein and none could be detected in the tumors of infected mice (even though some could be detected in the meninges and skull fragments) **(Figure 5-6, B).** These data suggested that peripheral infection with rLCMV-Ova was enough to send tumor- (i.e., Ova-) specific CTLs to the brain, where they could be reprimed by engaging with either APCs or tumors presenting cognate antigen, and that these interactions were leading to some level of tumor-cell killing that exceeded the tumor cell killing that occurred when antiviral P14 CTLs interacted with SB28-GFP tumors expressing Armstrong's dominant epitope. Alternatively, these data indicated that even if one assumed the P14 killing efficiency of Armstrong-infected SB28-GFP equaled the OTI killing efficiency of SB28-Ova, then the CTL cognate antigen was presented for longer in the Ova system given that it was constitutively expressed by the tumor, and could not simply be cleared once the virus was cleared, as was the case in the Armstrong system.

A

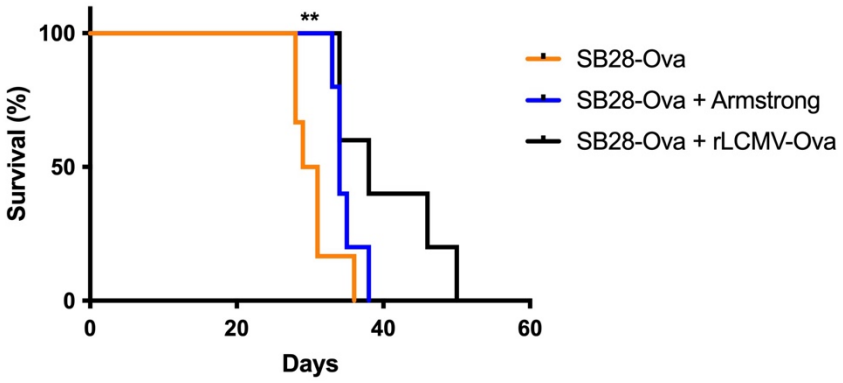
**
100
50
0
Survival (%)
0
20
40
60
Days
SB28-Ova
SB28-Ova + Armstrong
SB28-Ova + rLCMV-Ova

B

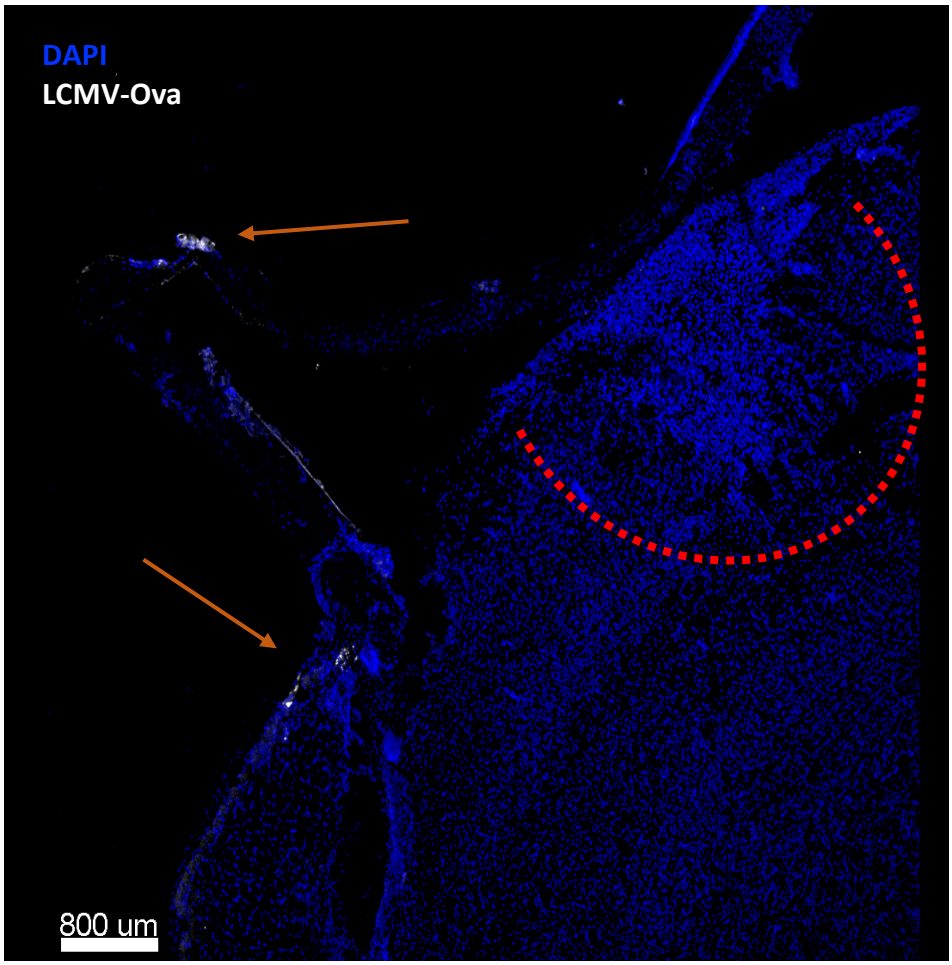
DAPI
LCMV-Ova
800 um

Figure 5-6: (A) Kaplan-Meier curve following tumor injection and saline administration (orange), wild-type LCMV-Armstrong infection (blue), or recombinant LCMV-Ova infection (black) 24h later. Median survival was 30, 34, and 38 days in the control, Armstrong, and LCMV-Ova groups resepctively. (*P*=0.007; Log-rank test). Data are representative of 4 experiments with 4-6 mice per group. **(B)** IHC stain from an SB28-Ova tumor slice at 96h post rLCMV-Ova infection. DAPI is shown in blue, the tumor is demarcated in a red dotted line, and VL4 nucleoprotein indicative of infection is shown in white. Orange arrows indicated areas of the meninges and skull fragment in which infection was detected, serving as an internal positive control for the stain. SB28-Ova tumor was not infected with the peripherally administered rLCMV-Ova.

5.2.1.1 AUGMENTING PRESENTATION OF TUMOR NEOANTIGEN ON THE CELL SURFACE

scRNA-seq data from the SB28-GFP/Armstrong system had shown that acute LCMV infection led to an early increase in MHCI-related transcript levels at 96h. These transcripts included *H2-K*, *H2-D*, and β2-microglobulin *(B2m)*. *H2-K* and *H2-D* are alleles of the MHCI gene. *β2m* is a component of the MHCI protein. In PBS control samples, the levels observed in LCMV at 96h, were roughly equivalent to those in PBS samples by 14/15 days. While the increase in MHCI-related transcripts did not continue to increase over time in the LCMV samples, we hypothesized that this initial jumpstart in antigen presentation could be related to the ultimate increase in survival in this group **(Figure 5-7).** Along this same thread, the extended survival following increased presentation of the viral antigen on the tumor cell surface via the SB28-Ova / rLMCV-Ova system led us to wonder how we could additionally augment the Ova's visibility on SB28-Ova cells, given the correlations between presentation and survival **(Figure 5-6, A).**

H2-K1
Q = 9.77-31

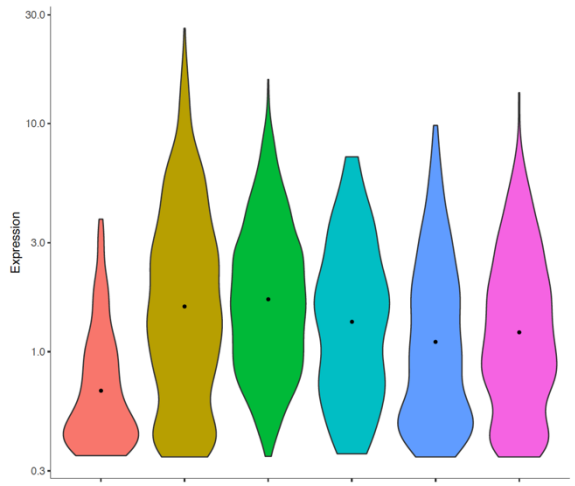

PBS 4d PBS 14d PBS 15d LCMV 4d LCMV 14d LCMV 15d

H2-D1
Q = 2.61-29

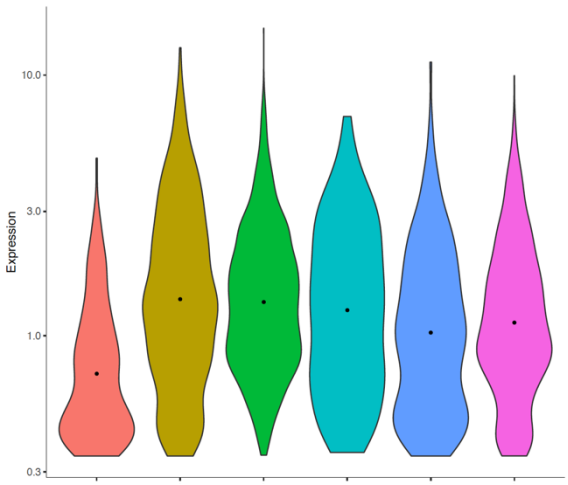

PBS 4d PBS 14d PBS 15d LCMV 4d LCMV 14d LCMV 15d

B2m
Q = 1.71^{-14}

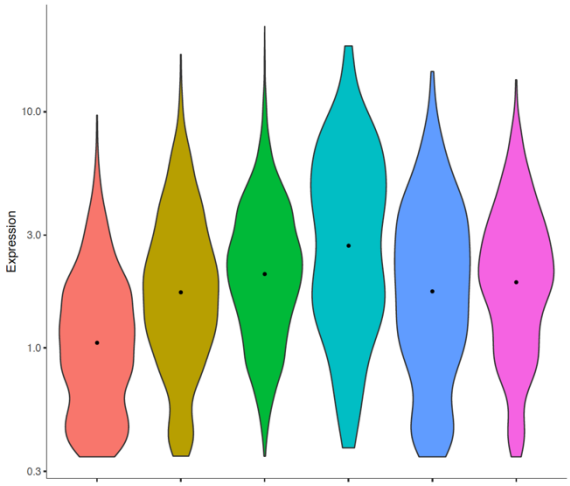

PBS 4d PBS 14d PBS 15d LCMV 4d LCMV 14d LCMV 15d

Figure 5-7: Violin plots describing gene expression for H2-K1, H2-D1, and B2m across samples (y-axis) in SB28 cells (partition 2) by treatment/time sample (x-axis). Corresponding q-value is indicated post regression fit (expression~time+treatment) and coefficient testing via Wald test under Benjamini and Hochberg multiple comparison condition = 1.

Thus, we sought ways to infect with SB28-Ova tumor with LCMV-Ova. Given that peripheral administration of the recombinant virus did not infect the tumor **(Figure 5-6, B)**, we pre-infected tumor cells *in vitro* such that they harbored virus on implantation. Briefly, SB28-Ova cells were thawed, and once recovered, cells were passaged on day 0. 24h later cells were infected by coating the cellular monolayer with rLCMV-Ova at an MOI of 1. Virus as diluted in cell media and the flask was gently rocked for an hour. At the end of the hour, the viral media was aspirated, and fresh media was applied. 24h following infection, and while cells were still in a period of exponential growth, cells were collected and 5,000 were implanted into B6 mice **(Figure 5-8, A).**

Beyond the augmentation of antigen presentation, there was an adiditonal benefit to this pre-infection paradigm. In the SB28-GFP/Armstrong system, we could not be certain (though IHC seemed to suggest) that there was 100% infection of the tumor cells. Thus, it remained an open question whether the ultimate tumor outgrowth stemmed from (a) noncytopathic clearance of infected tumor cells that survived the CTL onslaught or (b) the outgrowth of uninfected cells that were not killed by CTL that were in fact efficient at cytopathically clearing tumor cells masking as reservoirs of virus. We could not simply measure VL4 expression by FACS in Armstrong-infected SB28-GFP cells *ex vivo* given that the tumor digestion protocol would have introduced significant variability for this particular stain.

Following *in vitro* infection of SB28-Ova cells with rLCMV-Ova, and just before implantation, an aliquot of tumor cells were stained for VL4. 100% of injected cells were found

to be infected with rLCMV-Ova, obviating any concerns that tumor outgrowth resulted from uninfected cells **(Figure 5-8, A).**

B6 mice were injected with SB28-Ova cells. 24h later, the control group received i.v. saline, Armstrong infection, or peripheral rLCMV-Ova infection. One group received pre-infected SB28-Ova/rLCMV-Ova cells and saline injected 24h later i.v. The latter group showed the greatest increase in median survival observed up until this point. Control mice survived for a median of 30 days, and those receiving pre-infected SB28-Ova tumors survived for a median of 45 days, increasing median survival by 50% **(Figure 5-8, B).**

A

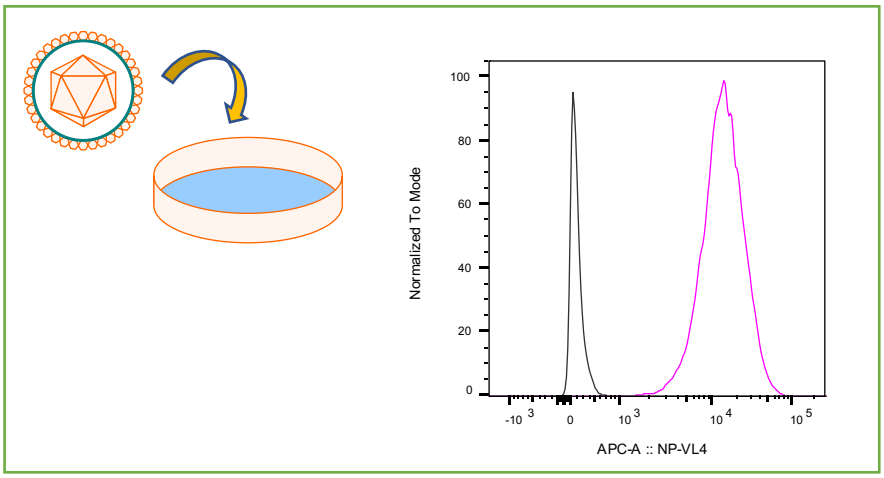

B

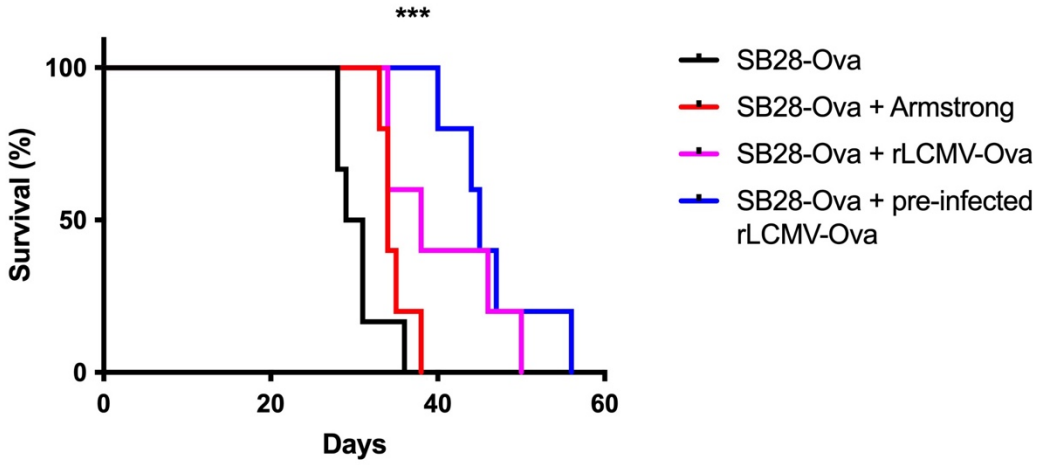

Figure 5-8: (A) Schematic describing how SB28-Ova cells were infected at an MOI of 1 with rLCMV-Ova *in vitro* 24h prior to implantation. Flow cytometric staining for VL4 nucleoprotein confirmed that 100% of the tumor cells were infected. **(B)** Kaplan-Meier curve following SB28-Ova implantation in 4 groups of mice. Shown in black are the controls that received saline 24h post implantation. LCMV-Armstrong infection is shown in red, rLCMV-Ova peripheral infection in pink, and rLCMV-Ova *in vitro* pre-infection shown in blue. The latter extended median survival by 50% compared to saline controls (30d vs 45d). (*P*=0.001; Log-rank test).

5.2.2 MONITORING TUMOR-T CELL ENGAGEMENT IN THE SB28-OVA/LCMV-OVA PARADIGM

To investigate whether tumor-specific CTL antigen encounters drove the significant increase in survival of pre-infected SB28-Ova mice, we leveraged 2P microscopy to monitor T cell calcium flux. When T cells recognize cognate peptide-MHC complexes, a rapid increase in intracellular calcium ensues (Oh-hora & Rao, 2008). We used OTI cells expressing mTomato (for visual labeling of the plasma membrane) and GCamP6s, a fluorescent Calcium indicator. Upon recognizing cognate MHC-ligand, these red T cells flux green. We compared the calcium activity in these triple reporter OTI-mTomato-GCamP6s T cells in SB28-Ova bearing mice that were either infected peripherally with rLCMV-Ova or intratumorally via *in vitro* infection **(Figure 5-9).** 24h prior to tumor implantation, mice received a transfer of 10,000 T cells. 7 days following tumor injection, calcium flux was clearly visible in all mice, though significantly more so in the pre-infected group **(Figure 5-10).** These data clearly indicate that by augmenting tumor antigen presentation on the cell surface of target cells, cognate T cells more efficiently recognize peptide bound to MHC, which is associated with a 50% extension in median survival, which to date, is an uncurable murine model of GBM.

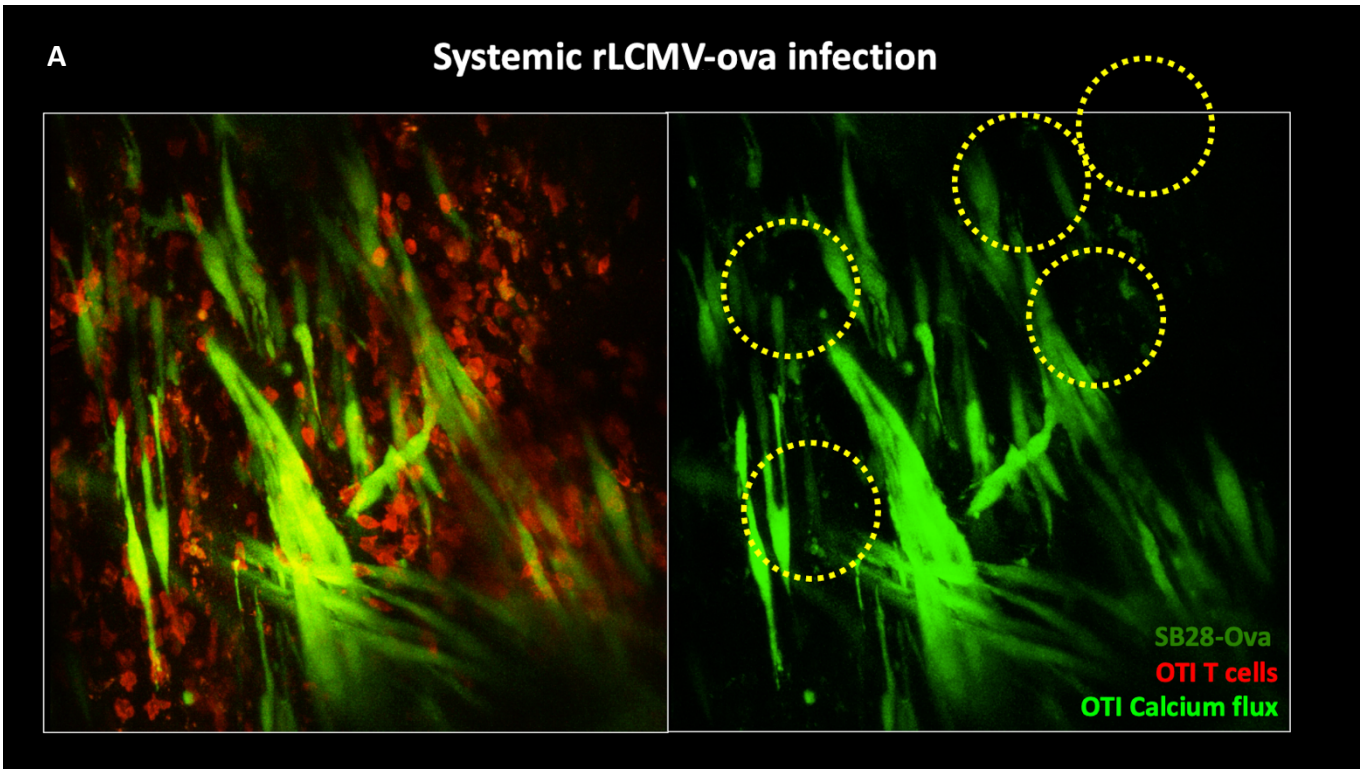
A
Systemic rLCMV-ova infection
SB28-Ova
OTI T cells
OTI Calcium flux

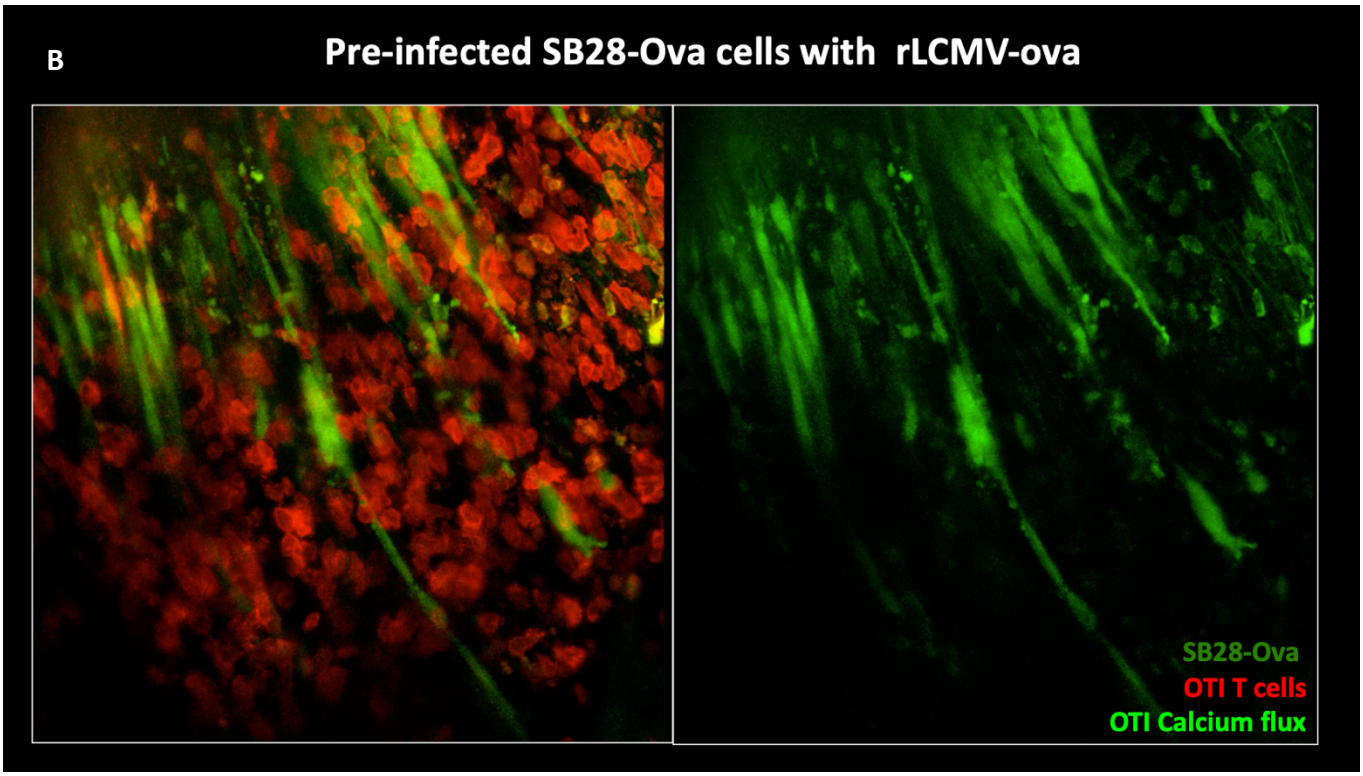
B
Pre-infected SB28-Ova cells with rLCMV-ova
SB28-Ova
OTI T cells
OTI Calcium flux

Figure 5-9: Snapshots of Video 7 (A, left), Video 8 (A, right), Video 9 (B, left), and Video 10 (B, right). Representative maximal projections of two-photon z-stacks viewed through the thinned skull of B6 mice bearing SB28-Ova tumor in green, and OTI-mTomato- GCamP6s T cells in red, which flux Calcium (transient green) upon recognizing MHC-bound Ova epitope. Z stacks were acquired at 10 second intervals to capture the Calcium flux. **(A)** Video 7 (left) represents a mouse that was systemically infected with rLCMV-Ova, thus the tumor was not infected. Calcium fluxing is more subtle, thus yellow demarcated circles focus on the T cells that recognize their cognate ligand. Video 8 (right) is the same mouse shown in Video 7, with the red channel removed for easier visualization. **(B)** Video 9 (left) represents a mouse that received pre-infected SB28-Ova cells with rLCMV-Ova. Calcium fluxing is overwhelming and easily visualized in Video 10 (right) with the red channel removed. All videos are representative of 2 independent experiments with 5-6 mice each.

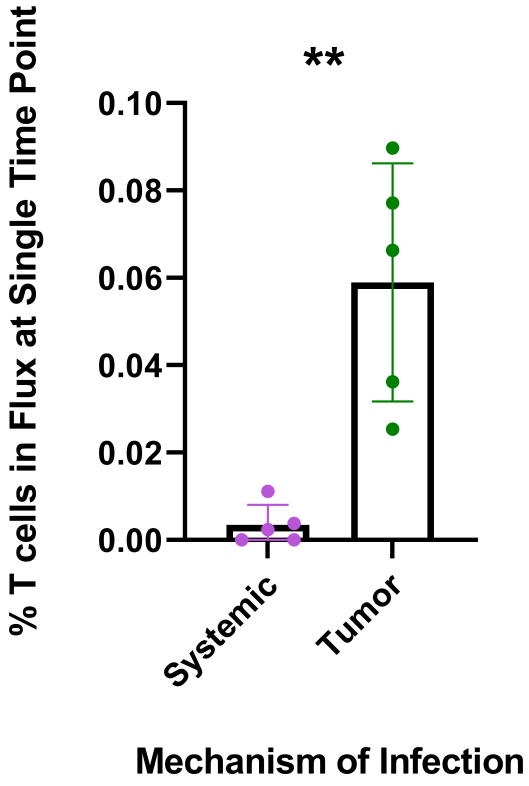

Figure 5-10: Calcium flux frequency of SB28-Ova and rLCMV-Ova-specific OT-I mTomato+ GCaMP6s+ T cells in systemically infected mice (in which the tumor is not infected with virus) versus pre-infected tumor-bearing mice (in which the tumor is infected with virus). Data were quantified from the experiment shown in **Figure 5-8**; **p<0.01)

5.3 SUMMARY

The Cancer-Immunity Cycle **(Figure 5-3)** outlines the necessary steps to mount a productive anti-tumor immune response. First, tumor antigen must be released, most commonly through cancer cell death. These antigens must be processed and then presented on the surface of APCs, which must then drain to the local lymph node to prime T cells. Following tumor-specific T cell expansion, T cells traffic to the tumor site, recognize their cognate ligand on the surface of tumor cells, and mediate tumor cell death.

Our experiments in mice maintaining memory to the dominant tumor neoantigen, and in genetically mismatched mice such that the tumor tissue should be considered a completely foreign tissue graft, show that there is near complete silence in the immune system. The first steps of the Cancer Immunity Cycle are not initiated, as shown by the undetectable expansion of tumor-specific T cells in the drain cervical nodes. Infection with recombinant LCMV expressing tumor antigen short-circuits this failure, and not only leads to tumor-specific T cell in the node, but also their efficient trafficking back to the tumor site and recognition of cognate antigen as well as subsequent cancer cell killing. This resulted in the longest extension of survival in the SB28 model reported to date and to the best of our knowledge.

6 DISCUSSION

6.1 THE CANCER IMMUNITY CYCLE REVISTED

In the last decade and particularly in the last 5 years, immunotherapy has cataclysmically changed cancer treatment options. Certain cancers such as leukemias, lymphomas, melanomas, and breast cancers (among other previously recalcitrant late-stage cancers) have been shown to be responsive and in some cases cured by strategies ranging from CAR-T cell therapy to immune checkpoint blockade. Whereas in the past, cancer was largely thought to be a cell-intrinsic disease – a series of genetic failures that drove aberrant growth – cancer is now often viewed through the prism of the immune system, and its failure to recognize, target, and kill the aberrancy. The recent advances in immunotherapeutic strategies are borne of this paradigm shift in how cancer is studied. These advances show the promise of leveraging the immune system to effectively treat tumors and provide long-term protection, yet GBM has largely been excluded from these successes.

Glioblastoma stands apart from the panoply of other human cancers not only due to its universal fatality and unchanging 5-year survival rate, but also because of the way its anatomical confines interact with its bland mutagenomic profile, making it nearly impossible for the immune system to detect the growing mass.

Unlike breast, skin, and lung cancers which have well-defined carcinogenic etiologies, GBM is driven by a few canonical mutations instead of environmental perturbations. It thus harbors a much lower neoantigen burden (Alexandrov et al., 2013; Lawrence et al., 2013; Neftel et al., 2019). With fewer antigens available for recognition by the immune system, the host anti-tumor immune response already provides a relatively poor baseline.

However, even if one were to assume that the low neoantigen burden were not an obstacle, or were an obstacle that could be overcome, the Cancer-Immunity cycle outlines the seven basic steps to mounting a productive anti-tumor response, and the anatomical barriers of the CNS preclude nearly every step in this cycle **(Figure 6-1).** This cycle includes: (1) the release of cancer cell antigens; (2) cancer cell antigen presentation; (3) priming and activation by APCs and T cells; (4) trafficking of CTLs to tumors; (5) T cell infiltration of the tumor; (6) T cell recognition of cancer cells; (7) CTL killing of cancer cells.

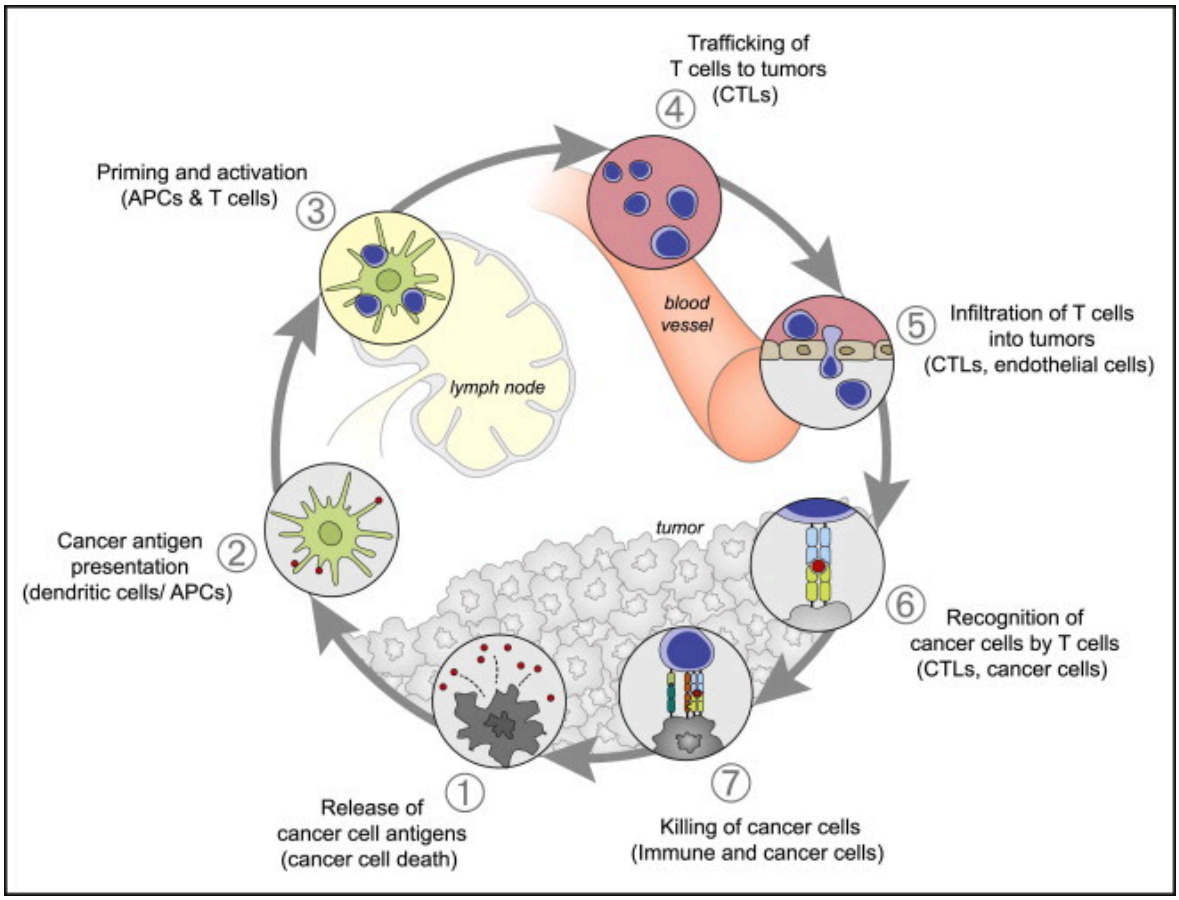

Figure 6-1: Reproduced from *Oncology Meets Immunology: The Cancer-Immunity Cycle, Chen and Mellman, Immunity 2013.*

The host is at a disadvantage starting with steps 1 and 2. The release of cancer cell antigens and their presentation relies on both lymphatic drainage of antigen from the tissue in which the tumor resides, as well as a population of migratory APCs that can effectively present antigen in the draining node ahead of step 3. Notably, however, the brain parenchyma lacks both lymphatic drainage and a resident population of migratory APCs that could traffic tumor antigen to the draining nodes. Parenchymal antigen is thought to drain along the 150nm wide basement membranes of capillaries and arteries, as well as along exiting neural sheaths (Carare et al., 2008; Kida et al., 1993; Ma et al., 2017). The little parenchymal antigen that does escape these tight barrier systems would enter the dura mater and potentially drain via its dedicated lymphatics (J. H. Ahn et al., 2019; A. Louveau et al., 2015). In our own SB28 model, there was no detectable antigen drainage and subsequent priming and expansion of tumor-specific T cells, despite the fact that we pierced the aforementioned barrier systems upon injection of the tumor, and the antigen (Ova) was highly immunogenic. These findings alone would suggest that any immunotherapies reliant on peripheral recognition of GBM would be better served by first guaranteeing antigen release and presentation, and then employing the immunotherapy (such as checkpoint blockade) as an adjuvant. Without the required foundation, such therapies are unlikely to prove fruitful. Other groups have also investigated ways to enhance lymphatic drainage by administering supraphysiologic levels of VEGF-C, a known modulator of lymphatic pumping. Delivery of VEGF-C was shown to enhance the priming of CTLs in the draining nodes, support their migration to the tumor, and led to clearance of the tumor via synergy with anti-PD1 therapy (albeit in the GL261 model). The model notwithstanding, this important study similarly confirmed that absent any intervention and due to the intracranial confines of GBM, CD8 involvement is

limited, and any strategies aiming to leverage CTLs will need to first consider the immunological limitation conferred by the anatomy of the CNS.

6.2 LCMV AS A TOOL TO OVERCOME GBM-IMMUNE RESPONSE CHALLENGES

Given the described anatomy-induced limitations on afferent and efferent immunity to the brain, as well as GBM-intrinsic immune suppressive mechanisms, we devised an immune-based strategy that would (a) localize to the glioblastoma niche in a tunable manner, (b) stimulate the peripheral immune system in a manner so robust as to override GBM and anatomy-driven suppression, and (c) demonstrate efficacy in a high-fidelity immunocompetent model.

We started by interrogating the standard model used in nearly all GBM pre-clinical studies: GL261. GL261 has long been the gold standard used in nearly all murine syngeneic work, yet its limitations are well-documented and no therapeutic successfully trialed in GL261 has gone on to ameliorate the human disease. At the start of my DPhil, our lab learned of a newer model from UCSF and we first sought to compare the immune profile of both. Extant studies had shown that SB28 is universally fatal, does not respond to ICT, and at baseline has much lower MHC-I levels, thus we hypothesized that given these similarities to human GBM, the immune infiltrate may be similarly relevant (Genoud et al., 2018; Yeung et al., 2013).

High-parameter flow cytometric analysis of the both models' immune landscapes had not yet been performed at the start of my thesis, thus establishing these baseline data was of paramount importance. SB28 and GL261 demonstrated divergent patterns of immune infiltration. Whereas GL261 at two timepoints primarily showed a lymphocytic infiltrate

(unlike human GBM), SB28 induced a sizeable myelomonocytic response. (Up to one third of a human GBM mass is comprised of macrophages/microglia). SB28 also induced a VEGF+ signature in these myelomonocytic cells, reminiscent of how the GBM TME displays florid vascularization and elevated levels of VEGF, which has led to various therapeutic attempts to inhibit VEGF signaling (though all unfortunately unsuccessful) (Weathers & de Groot, 2015). 2P microscopy also revealed divergent morphological patterns, such that SB28 enmeshed itself in the brain parenchyma whereas GL261 appeared more like a confined tumor mass that could easily be explanted. GBM's diffusely infiltrative pattern of invasion could not be overlooked, and thus SB28 was further validated as the model of choice with which to proceed on all subsequent experiments. As part of the model setup, we developed a paradigm that enabled us to track the tumor-immune response across various methodologies so as to gain real time insights into the quantitative, spatial and temporal evolution of this response, using intravital 2P microscopy, FACS, single-cell sequencing, and IHC.

To reprogram the immune landscape, subvert wound healing, and stimulate anti-tumor immunity, we administered a recombinant noncytopathic arenavirus (LCMV) into circulation. LCMV is a neurotropic virus whose pathology is exclusively mediated by the overwhelming immune response. We immediately observed a survival benefit to infection with the wildtype acute strain, Armstrong. This survival benefit was observed alongside a dramatic shift in the immune landscape: an overwhelming CTL response, an abrogation of MDSCs, and a more activated phenotype in myelomonocytics hallmarked by MHCII expression instead of the previously elevated VEGF expression. Excitingly, Armstrong selectively penetrated and infected the tumor mass, and we observed P14 T cells interacting with the tumor by 2P. However, two weeks post infection, the tumor was cleared of virus and

ultimately all mice still succumbed. These data suggested one of two explanations: (1) The virus was cleared noncytopathically by CTLs such that T cells could engage kinaptically with the tumor cell, and never deliver a "kill-shot" of perforin/granzyme. Noncytopathic intracellular mechanisms of LCMV clearance, such as those employed by liver hepatocytes, are well documented and depend on antiviral pathways that upregulate interferon and tumor necrosis factor (Guidotti et al., 1999). In a different model of noncytopathic clearance following anti-viral immunotherapy, infected microglia in the brains of chronically infected mice were cleared noncytopathically despite engagement by antiviral CTLs that possessed granzymes. This clearance depended in part on the antiviral cytokine IFNγ (Herz et al., 2015). (2) CTLs could have killed every infected tumor cell, but outgrowth resulted from the few that were not infected and then proceeded to grow exponentially, hence the extension in survival yet a lack of cure. Indeed, single-cell sequencing data showed that in T cells, there was a significant decay in function and energetics over a two-week period, which could have resulted from either suppressive tumor-T cell signaling or a natural decrease in the availability of CTL cognate antigen as infected tumor cells were killed.

To minimize the number of variables in our hypotheses, we developed a system in which there would be molecular mimicry between tumor and viral antigen, such that in the case of noncytopathic viral clearance, cognate antigen would still be available on the surface of tumor cells for T cells to engage. Alternatively, in the case of outgrowth of uninfected cells, we ensured 100% infection prior to implantation. Further, we sought to amplify antigen presentation as a means to promote the formation of an Immunological Synapse between the T cell and tumor cell.

To this end, we employed a line of SB28 cells constitutively expressing Ova, and pre-infected the tumor cells with rLCMV-Ova prior to implantation, which generated a robust anti-viral/anti-tumor CTL response. In this paradigm, we significantly increased T cell – tumor direct engagement, as quantified by Calcium flux on 2P, and increased survival by 50%.

6.3 FUTURE DIRECTIONS

Even in a model in which all aspects of the cancer immunity cycle were optimized – starting from antigen drainage and ending with T cell killing of cancer cells, SB28 still proved universally fatal. This was a particularly interesting finding given the optimization of the paradigm, in light of previous concerns around using Armstrong. First, 100% of tumor cells were infected with rLCMV-Ova prior to implantation, thus the notion that the uninfected cells could spearhead outgrowth no longer applied. Second, even following viral clearance, ample viral (i.e., tumor) antigen should have remained on the surface of the tumor cell (and an immunogenic antigen no less). The wide and continued availability of MHC-peptide should have provided reason enough for T cells to remain engaged and in the milieu. However, in preliminary experiments that would serve as the basis for future directions to explore the mechanism of recalcitrance, we assessed whether SB28 engaged in immunoediting as a compensatory immunosuppressive response. We implanted SB28-GFP, SB28-TdTomato, SB28-TdTomato-Ova, and pre-infected SB28-TdTomato-Ova with rLCMV-Ova to compare the selective pressures on these 4 lines to downregulated TdTomato. (The GFP line served as a negative control for the identification of TdT signal by FACS). Prior to implantation, an aliquot of each of the 4 cell lines was assayed for TdT expression. 21

days post implantation we measured this signal and found a significant decrease in TdT expression exclusively in the pre-infected line, relative to the signal of the same line pre-implantation **(Figure 6-2).**

Indeed, in human trials targeting specific antigens such as the often-mutated EGFRvIII via CAR-T therapy, antigenic deletion is well documented (O'Rourke et al., 2017). As in our study, these investigators observed that CART-EGFRvIII trafficked to the GBM mass and exerted antigen-specific activity. However, following treatment, this group noted an even more immunosuppressive environment hallmarked by Treg infiltration and the upregulation of immunoinhibitory molecules on the tumor cells surface (e.g., IDO1, PD-L1, and IL-10).

Tukey's multiple comparisons test	Mean Diff.	95.00% CI of diff.	Significant?	Summary	Adjusted P Value	
GFP vs. TDT	-0.2142	-114.2 to 113.8	No	ns	>0.9999	A-B
GFP vs. SB-Ova	-15.32	-137.2 to 106.6	No	ns	0.9796	A-C
GFP vs. SB-Ova preinfected	-246.3	-360.3 to -132.3	Yes	***	0.0003	A-D
TDT vs. SB-Ova	-15.1	-129.1 to 98.9	No	ns	0.9763	B-C
TDT vs. SB-Ova preinfected	-246.1	-351.7 to -140.6	Yes	***	0.0002	B-D
SB-Ova vs. SB-Ova preinfected	-231	-345 to -117	Yes	***	0.0005	C-D

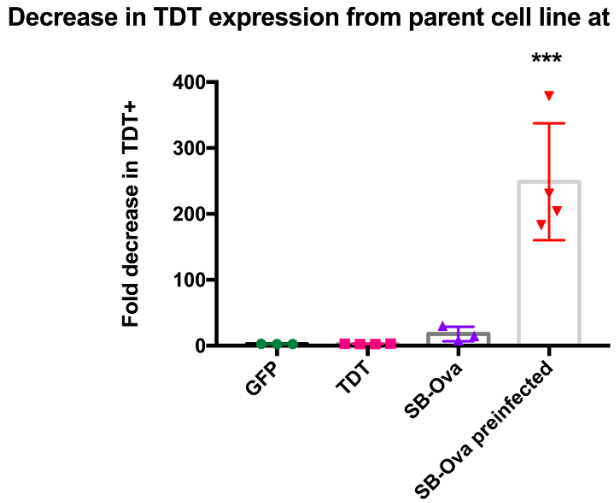

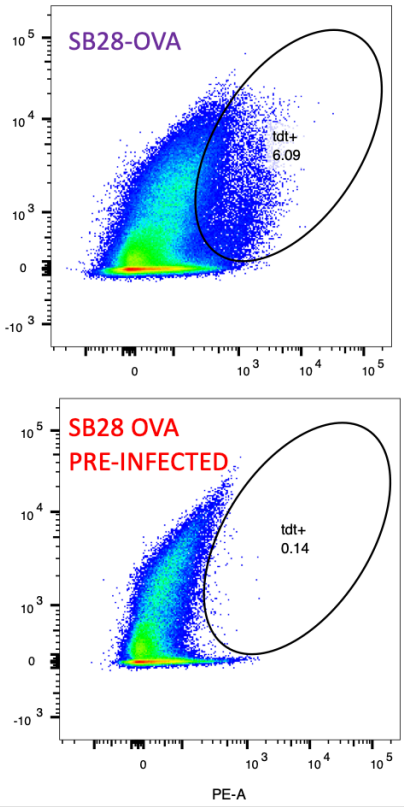

Figure 6-2: At 21dpi, tumors from four different SB28 lines: GFP, TdTomato, TdTomato-Ova, and rLCMV-Ova infected TdTomato-Ova were assayed for their TdT expression. Threshold for TdT expression was based on GFP negative controls. The percentage of TdT+ cells per sample was compared to the same cells' expression prior to tumor implantation, and the fold decrease in the frequency of TdT+ cells was plotted. Only the pre-infected SB28-Ova sample showed a significant decreased in TdT expression, indicating selective pressure on the tumor to induce antigenic escape as a compensatory mechanism to prevent immune engagement.

Our own data, as well as data from human clinical trials, indicate that immune escape – via HLA downregulation or immunoediting to produce antigen-null tumor cells – is a likely response to immunotherapeutics targeting a specific epitope on the tumor cell. In light of this reality, synergistic efforts with therapies that optimize and increase the efficiency of T cell killing during the limited window of opportunity, are warranted. In our own paradigm, we observed a significant decay in the function and energetics of T cells following tumor

infection with LCMV over a two-week period. We also observed by 2P that most T cell-tumor interactions were “drive-by” engagements, as opposed to T cells stopping, locking, and killing tumor cells. While increasing antigen expression by pre-infecting tumor cells prior to implantation resulted in more synaptic interactions and longer survival, future studies should investigate the use of biologics that stabilize the Immunological Synapse. A variety of factors may contribute to the type of motility we observed in T cells, ranging from high extracellular concentrations of Potassium, to aberrant chemokine receptor signaling (Dustin, 2014). Strategies that promote IS formation should be considered as adjuvants with immunotherapies seeking to leverage a CTL anti-tumor response.

Outside of direct tumor-T cell engagement, an important remaining question is how indispensable different APCs in the tumor niche are for presentation and re-priming of T cells, and whether these interactions confer the observed survival benefit. Upon interaction with antiviral T cells, microglia upregulate CD11c expression and transform into robust APCs (Herz et al., 2015). Given our imaging data showing antiviral T cell engagement with microglia, we hypothesize that this interaction polarizes the microglia into the activated, phagocytic APCs visualized by two-photon microscopy, and that this transformation is in part responsible for the subsequent tumor growth inhibition. To interrogate whether antigen presentation on these infected cells is required for tumor restraint, future studies would include a variety of mice with different floxed genes that can be deleted following infection with an LCMV recombinant that expresses Cre recombinase (rLCMV-Cre). Some examples include floxed β2-microglobulin mice (used to remove MHC-I from infected cells) and floxed interferon alpha/beta receptor mice (used to remove type I interferon signaling). The advantage of this rLCMV-Cre paradigm is that the anti-tumor role of any floxed gene of

interest can be studied. Further studies would also include additional high-parameter flow cytometric analysis experiments to compare the immune landscape, and more specifically, the myeloid cell phenotype between the various successful and failed paradigms (as measured by survival benefit). This would enable us to identify critical immune cell subsets and activation states that may be conferring anti-tumor immunity.

6.4 CLINICAL RELEVANCE

In many ways, it is the less remembered of Medawar's experiments that inspired our current work. Skin grafts failed to be rejected when implanted into the brain unless they were preceded by a heterotopic tissue graft elsewhere in the body. De novo immunity could not be mounted in the CNS but pre-existing immunity in the periphery could be harnessed to traverse the BBB and reject the foreign tissue (Medawar, 1948). Timing, in glioblastoma, is taking center stage. While aPD1 therapy has failed in past trials, recent data showed a near doubling in the median survival of patients who received just one neoadjuvant dose prior to surgical resection, owing to antecedent T cell activation (Cloughesy et al., 2019). In this thesis, we similarly extended median survival by kickstarting a robust anti-LCMV response peripherally. LCMV was employed as a tool to lure the host's immune system to what should be seen – like in Medawar's experiments – as a foreign tissue, a glioblastoma.

While a clear limitation of this work is that GBM cannot be engineered to express an antigen of choice, and further amplified by intratumoral LCMV infection expressing said antigen, there are two use cases for derivatives of our paradigm. First, vaccination strategies using tumor cells infected *in vitro* with several rLMCV strains engineered to express various tumor antigens may offer a solution to the inevitable antigenic deletion escape mechanism, while mounting a robust (and pleiotropic) immune response against GBM.

Second, recombinant LCMV is in fact safe for human administration (Wingerath et al., 2017) and is currently being investigated for use in Phase 1/2 clinical trials for the treatment of Human Papillomavirus (HPV)-associated head and neck cancers (ClinicalTrials.gov Identifier: NCT04180215). In November 2021, the United States FDA granted Fast Track status for the biologic under investigation called HB-201, a recombinant LCMV vector expressing a highly antigenic fusion protein from HPV. And as of June 2022, positive Phase I results were announced by the biotechnology company developing this vector, Hookipa Pharma. HB-201induced a robust tumor-specific T cell response and displayed anti-tumor activity in metastatic and treatment-refractory head and neck cancer patients. Hookipa is developing additional recombinant LCMV backbones to treat other cancers – for example, rLCMV expressing PSA to target metastatic castration-resistant prostate cancer, or rLCMV expressing KRAS mutants to target colorectal, pancreatic, and lung cancers. Our work provides an important basis for the potential use of recombinant LCMV as a mechanism to infect patients with mapped GBM epitopes. With additional development, a future immunotherapeutic strategy may employ the systemic vaccination of rLCMV carrying a cassette of tumor neoantigen, which would stimulate an important peripheral immune response that could effectively traffic to the GBM TME, as well as overcome many of the practical challenges of needing to deliver GBM therapy locally and consistently.

Cancer used to be thought of us a cell-intrinsic disease, studied through the prism of disordered genetic events. However, in the last two decades the scientific community has increasingly appreciated that cancer is not just a cell-intrinsic disease, but also a cell-extrinsic manifestation of immune failures. Given the dearth of baseline immune involvement in GBM, few investigators have studied GBM through the prism of neuro-immunology, and

have instead sought to apply therapeutic modalities from other cancers to the treatment of GBM, and to no success.

6.5 CONCLUDING SYNTHESIS

The work in this thesis represents an important advancement in our understanding of how GBM should be modeled in pre-clinical work and considered in the context of the specific confines and immune landscape of the CNS. We first uncovered divergent patterns of immunology, injury, and morphology between the often-used GL261 model and the newer SB28. Every clinical intervention that has been pre-clinically developed using the GL261 has gone on to fail in patients, thus a new model is warranted. Injection of SB28 cells allowed us to recapitulate the highly inflamed environment observed in the brain following surgical resection. SB28 demonstrated higher fidelity to human disease, enmeshing itself into the brain parenchyma, and inducing a sizable myelomonocytic response, perivascular hemorrhaging at sites both proximal and distal to the tumor, and a pronounced wound healing signature characterized by myeloid cell VEGF production, all of which phenocopy human GBM. We were able to track this evolution over time by FACS, IHC, and 2P microscopy. We then administered LCMV Armstrong to tumor-bearing mice with the goal of co-opting the well-documented and fulminant CTL response for anti-tumor immunity. LCMV Armstrong infection preferentially infected SB28 tumors, leaving surrounding brain parenchyma uninfected. Infection altered the SB28 immune landscape, rerouting the myeloid response from a VEGF+ phenotype to an activated MHCII+ phenotype, abrogating MDSCs, and inducing – as expected – an overwhelming CD8+ T cell response. However, the virus was cleared within 2 weeks and the concomitant CTL response was profoundly impacted by

time. T cells remained in the tumor niche following viral clearance, yet their effector function and proliferative capacity almost completely decayed. We thus established a paradigm in which viral and tumor antigen were exact mimics, so that even following viral clearance, antigen would remain. We also obviated any concerns around a lack of complete tumor infection, by pre-infecting tumor cells with rLCMV carrying a cassette of tumor antigen (e.g., Ova). We successfully demonstrated activation of each step in the Cancer-Immunity Cycle and augmented direct tumor-T cell engagement, and extended survival by 50% in a completely uncurable and recalcitrant model of GBM. Future clinical interventions in GBM should consider the limitations our work uncovered – first, there should be no expectation of peripheral immune recognition of GBM, nor antigen drainage. Our findings from genetically mismatched mice, and mice harboring peripheral memory made clear that the periphery is functionally ignorant of a growing tumor in the brain. Routing tumor-specific immune cells (in appreciable numbers and quality) to the brain would first require a systemic response that targets not one – but several – tumor antigens. Recombinant LCMV holds the promise to do so in a way that is safe, robust, and durable.

7 REFERENCES

References

Abd Hamid, M., Wang, R. Z., Yao, X., Fan, P., Li, X., Chang, X. M., Feng, Y., Jones, S., Maldonado-Perez, D., Waugh, C., Verrill, C., Simmons, A., Cerundolo, V., McMichael, A., Conlon, C., Wang, X., Peng, Y., & Dong, T. (2019). Enriched HLA-E and CD94/NKG2A Interaction Limits Antitumor CD8(+) Tumor-Infiltrating T Lymphocyte Responses. *Cancer Immunol Res*, *7*(8), 1293-1306. https://doi.org/10.1158/2326-6066.CIR-18-0885

Abdelwahab, M. G., Sankar, T., Preul, M. C., & Scheck, A. C. (2011). Intracranial implantation with subsequent 3D in vivo bioluminescent imaging of murine gliomas. *J Vis Exp*(57), e3403. https://doi.org/10.3791/3403

Abels, E. R., Maas, S. L. N., Nieland, L., Wei, Z., Cheah, P. S., Tai, E., Kolsteeg, C. J., Dusoswa, S. A., Ting, D. T., Hickman, S., El Khoury, J., Krichevsky, A. M., Broekman, M. L. D., & Breakefield, X. O. (2019). Glioblastoma-Associated Microglia Reprogramming Is Mediated by Functional Transfer of Extracellular miR-21. *Cell Rep*, *28*(12), 3105-3119 e3107. https://doi.org/10.1016/j.celrep.2019.08.036

Agarwalla, P. K., & Aghi, M. K. (2012). Oncolytic herpes simplex virus engineering and preparation. *Methods Mol Biol*, *797*, 1-19. https://doi.org/10.1007/978-1-61779-340-0_1

Ahn, J. H., Cho, H., Kim, J. H., Kim, S. H., Ham, J. S., Park, I., Suh, S. H., Hong, S. P., Song, J. H., Hong, Y. K., Jeong, Y., Park, S. H., & Koh, G. Y. (2019). Meningeal lymphatic vessels at the skull base drain cerebrospinal fluid. *Nature*, *572*, 62-66. https://doi.org/10.1038/s41586-019-1419-5

Ahn, J. H., Cho, H., Kim, J. H., Kim, S. H., Ham, J. S., Park, I., Suh, S. H., Hong, S. P., Song, J. H., Hong, Y. K., Jeong, Y., Park, S. H., & Koh, G. Y. (2019). Meningeal lymphatic vessels at the skull base drain cerebrospinal fluid. *Nature*, *572*(7767), 62-66. https://doi.org/10.1038/s41586-019-1419-5

Ahn, S. H., Park, H., Ahn, Y. H., Kim, S., Cho, M. S., Kang, J. L., & Choi, Y. H. (2016). Necrotic cells influence migration and invasion of glioblastoma via NF-κB/AP-1-mediated IL-8 regulation. *Scientific Reports*, *6*, 1-12. https://doi.org/10.1038/srep24552

Alban, T. J., Alvarado, A. G., Sorensen, M. D., Bayik, D., Volovetz, J., Serbinowski, E., Mulkearns-Hubert, E. E., Sinyuk, M., Hale, J. S., Onzi, G. R., McGraw, M., Huang, P., Grabowski, M. M., Wathen, C. A., Ahluwalia, M. S., Radivoyevitch, T., Kornblum, H. I., Kristensen, B. W., Vogelbaum, M. A., & Lathia, J. D. (2018). Global immune fingerprinting in glioblastoma patient peripheral blood reveals immune-suppression signatures associated with prognosis. *JCI Insight*, *3*. https://doi.org/10.1172/jci.insight.122264

Alejenef, A., Pachnio, A., Halawi, M., Christmas, S. E., Moss, P. A., & Khan, N. (2014). Cytomegalovirus drives Vδ2neg γδ T cell inflation in many healthy virus carriers with increasing age. *Clin Exp Immunol*, *176*(3), 418-428. https://doi.org/10.1111/cei.12297

Alessandrini, F., Menotti, L., Avitabile, E., Appolloni, I., Ceresa, D., Marubbi, D., Campadelli-Fiume, G., & Malatesta, P. (2019). Eradication of glioblastoma by immuno-virotherapy with a retargeted oncolytic HSV in a preclinical model. *Oncogene*, *38*(23), 4467-4479. https://doi.org/10.1038/s41388-019-0737-2

Alexandrov, L. B., Nik-Zainal, S., Wedge, D. C., Aparicio, S. A., Behjati, S., Biankin, A. V., Bignell, G. R., Bolli, N., Borg, A., Børresen-Dale, A. L., Boyault, S., Burkhardt, B., Butler, A. P., Caldas, C., Davies, H. R., Desmedt, C., Eils, R., Eyfjörd, J. E., Foekens, J. A., . . . Stratton, M. R. (2013). Signatures of mutational processes in human cancer. *Nature*, *500*(7463), 415-421. https://doi.org/10.1038/nature12477

Andres, K. H., von During, M., Muszynski, K., & Schmidt, R. F. (1987). Nerve fibres and their terminals of the dura mater encephali of the rat. *Anat Embryol (Berl)*, *175*(3), 289-301. https://doi.org/10.1007/BF00309843

Arend, W. P., Malyak, M., Guthridge, C. J., & Gabay, C. (1998). Interleukin-1 receptor antagonist: role in biology. *Annu Rev Immunol*, *16*, 27-55. https://doi.org/10.1146/annurev.immunol.16.1.27

Ashkar, S., Weber, G. F., Panoutsakopoulou, V., Sanchirico, M. E., Jansson, M., Zawaideh, S., Rittling, S. R., Denhardt, D. T., Glimcher, M. J., & Cantor, H. (2000). Eta-1 (osteopontin): An early component of type-1 (cell-mediated) immunity. *Science*, *287*, 860-864. https://doi.org/10.1126/science.287.5454.860

Atzori, M. G., Tentori, L., Ruffini, F., Ceci, C., Lisi, L., Bonanno, E., Scimeca, M., Eskilsson, E., Daubon, T., Miletic, H., Ricci Vitiani, L., Pallini, R., Navarra, P., Bjerkvig, R., D'Atri, S., Lacal, P. M., & Graziani, G. (2017). The anti-vascular endothelial growth factor receptor-1 monoclonal antibody D16F7 inhibits invasiveness of human glioblastoma and glioblastoma stem cells. *J Exp Clin Cancer Res*, *36*(1), 106. https://doi.org/10.1186/s13046-017-0577-2

Barry, K. C., Hsu, J., Broz, M. L., Cueto, F. J., Binnewies, M., Combes, A. J., Nelson, A. E., Loo, K., Kumar, R., Rosenblum, M. D., Alvarado, M. D., Wolf, D. M., Bogunovic, D., Bhardwaj, N., Daud, A. I., Ha, P. K., Ryan, W. R., Pollack, J. L., Samad, B., . . . Krummel, M. F. (2018). A natural killer–dendritic cell axis defines checkpoint therapy–responsive tumor microenvironments. *Nature Medicine*, *24*, 1178-1191. https://doi.org/10.1038/s41591-018-0085-8

Batich, K. A., Mitchell, D. A., Healy, P., Herndon, J. E., & Sampson, J. H. (2020). Once, Twice, Three Times a Finding: Reproducibility of Dendritic Cell Vaccine Trials Targeting Cytomegalovirus in Glioblastoma. *Clinical Cancer Research*, *26*(20), 5297. https://doi.org/10.1158/1078-0432.CCR-20-1082

Becht, E., McInnes, L., Healy, J., Dutertre, C.-A., Kwok, I. W. H., Ng, L. G., Ginhoux, F., & Newell, E. W. (2019). Dimensionality reduction for visualizing single-cell data using UMAP. *Nature Biotechnology*, *37*(1), 38-44. https://doi.org/10.1038/nbt.4314

Bern, M. D., Parikh, B. A., Yang, L., Beckman, D. L., Poursine-Laurent, J., & Yokoyama, W. M. (2019). Inducible down-regulation of MHC class I results in natural killer cell tolerance. *Journal of Experimental Medicine*, *216*, 99-116. https://doi.org/10.1084/jem.20181076

Binnewies, M., Mujal, A. M., Pollack, J. L., Combes, A. J., Hardison, E. A., Barry, K. C., Tsui, J., Ruhland, M. K., Kersten, K., Abushawish, M. A., Spasic, M., Giurintano, J. P.,

Chan, V., Daud, A. I., Ha, P., Ye, C. J., Roberts, E. W., & Krummel, M. F. (2019). Unleashing Type-2 Dendritic Cells to Drive Protective Antitumor CD4 + T Cell Immunity. *Cell*, *177*, 556-571.e516. https://doi.org/10.1016/j.cell.2019.02.005

Birzu, C., Tran, S., Bielle, F., Touat, M., Mokhtari, K., Younan, N., Psimaras, D., Hoang-Xuan, K., Sanson, M., Delattre, J. Y., & Idbaih, A. (2020). Leptomeningeal Spread in Glioblastoma: Diagnostic and Therapeutic Challenges. *Oncologist*, *25*(11), e1763-e1776. https://doi.org/10.1634/theoncologist.2020-0258

Böttcher, J. P., Bonavita, E., Chakravarty, P., Blees, H., Cabeza-Cabrerizo, M., Sammicheli, S., Rogers, N. C., Sahai, E., Zelenay, S., & Reis e Sousa, C. (2018). NK Cells Stimulate Recruitment of cDC1 into the Tumor Microenvironment Promoting Cancer Immune Control. *Cell*, *172*, 1022-1037.e1014. https://doi.org/10.1016/j.cell.2018.01.004

Brandenburg, S., Muller, A., Turkowski, K., Radev, Y. T., Rot, S., Schmidt, C., Bungert, A. D., Acker, G., Schorr, A., Hippe, A., Miller, K., Heppner, F. L., Homey, B., & Vajkoczy, P. (2016). Resident microglia rather than peripheral macrophages promote vascularization in brain tumors and are source of alternative pro-angiogenic factors. *Acta Neuropathol*, *131*(3), 365-378. https://doi.org/10.1007/s00401-015-1529-6

Brandes, A. A., Carpentier, A. F., Kesari, S., Sepulveda-Sanchez, J. M., Wheeler, H. R., Chinot, O., Cher, L., Steinbach, J. P., Capper, D., Specenier, P., Rodon, J., Cleverly, A., Smith, C., Gueorguieva, I., Miles, C., Guba, S. C., Desaiah, D., Lahn, M. M., & Wick, W. (2016). A Phase II randomized study of galunisertib monotherapy or galunisertib plus lomustine compared with lomustine monotherapy in patients with recurrent glioblastoma. *Neuro-Oncology*, *18*, 1146-1156. https://doi.org/10.1093/neuonc/now009

Brown, C. E., Alizadeh, D., Starr, R., Weng, L., Wagner, J. R., Naranjo, A., Ostberg, J. R., Blanchard, M. S., Kilpatrick, J., Simpson, J., Kurien, A., Priceman, S. J., Wang, X., Harshbarger, T. L., D'Apuzzo, M., Ressler, J. A., Jensen, M. C., Barish, M. E., Chen, M., . . . Badie, B. (2016). Regression of Glioblastoma after Chimeric Antigen Receptor T-Cell Therapy. *New England Journal of Medicine*, *375*(26), 2561-2569. https://doi.org/10.1056/NEJMoa1610497

Brown, M. C., Holl, E. K., Boczkowski, D., Dobrikova, E., Mosaheb, M., Chandramohan, V., Bigner, D. D., Gromeier, M., & Nair, S. K. (2017). Cancer immunotherapy with recombinant poliovirus induces IFN-dominant activation of dendritic cells and tumor antigen-specific CTLs. *Sci Transl Med*, *9*(408). https://doi.org/10.1126/scitranslmed.aan4220

Butowski, N., Colman, H., De Groot, J. F., Omuro, A. M., Nayak, L., Wen, P. Y., Cloughesy, T. F., Marimuthu, A., Haidar, S., Perry, A., Huse, J., Phillips, J., West, B. L., Nolop, K. B., Hsu, H. H., Ligon, K. L., Molinaro, A. M., & Prados, M. (2016). Orally administered colony stimulating factor 1 receptor inhibitor PLX3397 in recurrent glioblastoma: An Ivy Foundation Early Phase Clinical Trials Consortium phase II study. *Neuro-Oncology*, *18*, 557-564. https://doi.org/10.1093/neuonc/nov245

Cannon, M. J., Schmid, D. S., & Hyde, T. B. (2010). Review of cytomegalovirus seroprevalence and demographic characteristics associated with infection. *Rev Med Virol*, *20*(4), 202-213. https://doi.org/10.1002/rmv.655

Carare, R. O., Bernardes-Silva, M., Newman, T. A., Page, A. M., Nicoll, J. A., Perry, V. H., & Weller, R. O. (2008). Solutes, but not cells, drain from the brain parenchyma along basement membranes of capillaries and arteries: significance for cerebral amyloid angiopathy and neuroimmunology. *Neuropathol Appl Neurobiol*, *34*(2), 131-144. https://doi.org/10.1111/j.1365-2990.2007.00926.x

Castro, M., Sipos, B., Pieper, N., & Biskup, S. (2020). Major histocompatibility complex class 1 (MHC1) loss among patients with glioblastoma (GBM). *Journal of Clinical Oncology*, *38*(15_suppl), e14523-e14523. https://doi.org/10.1200/JCO.2020.38.15_suppl.e14523

Chandramohan, V., Bryant, J. D., Piao, H., Keir, S. T., Lipp, E. S., Lefaivre, M., Perkinson, K., Bigner, D. D., Gromeier, M., & McLendon, R. E. (2017). Validation of an Immunohistochemistry Assay for Detection of CD155, the Poliovirus Receptor, in Malignant Gliomas. *Arch Pathol Lab Med*, *141*(12), 1697-1704. https://doi.org/10.5858/arpa.2016-0580-OA

Chang, A. L., Miska, J., Wainwright, D. A., Dey, M., Rivetta, C. V., Yu, D., Kanojia, D., Pituch, K. C., Qiao, J., Pytel, P., Han, Y., Wu, M., Zhang, L., Horbinski, C. M., Ahmed, A. U., & Lesniak, M. S. (2016). CCL2 Produced by the Glioma Microenvironment Is Essential for the Recruitment of Regulatory T Cells and Myeloid-Derived Suppressor Cells. *Cancer Res*, *76*(19), 5671-5682. https://doi.org/10.1158/0008-5472.CAN-16-0144

Chen, Daniel S., & Mellman, I. (2013). Oncology Meets Immunology: The Cancer-Immunity Cycle. *Immunity*, *39*(1), 1-10. https://doi.org/https://doi.org/10.1016/j.immuni.2013.07.012

Chen, P. Y., Wu, C. Y., Fang, J. H., Chen, H. C., Feng, L. Y., Huang, C. Y., Wei, K. C., Fang, J. Y., & Lin, C. Y. (2019). Functional Change of Effector Tumor-Infiltrating CCR5(+)CD38(+)HLA-DR(+)CD8(+) T Cells in Glioma Microenvironment. *Front Immunol*, *10*, 2395. https://doi.org/10.3389/fimmu.2019.02395

Chen, Z., Feng, X., Herting, C. J., Garcia, V. A., Nie, K., Pong, W. W., Rasmussen, R., Dwivedi, B., Seby, S., Wolf, S. A., Gutmann, D. H., & Hambardzumyan, D. (2017). Cellular and Molecular Identity of Tumor-Associated Macrophages in Glioblastoma. *Cancer Res*, *77*(9), 2266-2278. https://doi.org/10.1158/0008-5472.CAN-16-2310

Cheng, Y., Ng, H. K., Ding, M., Zhang, S. F., Pang, J. C., & Lo, K. W. (1999). Molecular analysis of microdissected de novo glioblastomas and paired astrocytic tumors. *J Neuropathol Exp Neurol*, *58*(2), 120-128. https://doi.org/10.1097/00005072-199902000-00002

Chongsathidkiet, P., Jackson, C., Koyama, S., Loebel, F., Cui, X., Farber, S. H., Woroniecka, K., Elsamadicy, A. A., Dechant, C. A., Kemeny, H. R., Sanchez-Perez, L., Cheema, T. A., Souders, N. C., Herndon, J. E., Coumans, J. V., Everitt, J. I., Nahed, B. V., Sampson, J. H., Gunn, M. D., . . . Fecci, P. E. (2018). Sequestration of T cells in bone

marrow in the setting of glioblastoma and other intracranial tumors. *Nat Med*, *24*(9), 1459-1468. https://doi.org/10.1038/s41591-018-0135-2

Cloughesy, T. F., Mochizuki, A. Y., Orpilla, J. R., Hugo, W., Lee, A. H., Davidson, T. B., Wang, A. C., Ellingson, B. M., Rytlewski, J. A., Sanders, C. M., Kawaguchi, E. S., Du, L., Li, G., Yong, W. H., Gaffey, S. C., Cohen, A. L., Mellinghoff, I. K., Lee, E. Q., Reardon, D. A., . . . Prins, R. M. (2019). Neoadjuvant anti-PD-1 immunotherapy promotes a survival benefit with intratumoral and systemic immune responses in recurrent glioblastoma. *Nat Med*, *25*(3), 477-486. https://doi.org/10.1038/s41591-018-0337-7

Cobbs, C. S., Harkins, L., Samanta, M., Gillespie, G. Y., Bharara, S., King, P. H., Nabors, L. B., Cobbs, C. G., & Britt, W. J. (2002). Human cytomegalovirus infection and expression in human malignant glioma. *Cancer Res*, *62*(12), 3347-3350.

Cuburu, N., Bialkowski, L., Pontejo, S. M., Bell, A., Kim, R., Thompson, C. D., Lowy, D. R., & Schiller, J. T. (2020). Abstract 5563: Harnessing pre-existing viral immunity for development of a broadly applicable tumor immunotherapy. *Cancer Research*, *80*(16 Supplement), 5563. https://doi.org/10.1158/1538-7445.AM2020-5563

Darmanis, S., Sloan, S. A., Croote, D., Mignardi, M., Chernikova, S., Samghababi, P., Zhang, Y., Neff, N., Kowarsky, M., Caneda, C., Li, G., Chang, S. D., Connolly, I. D., Li, Y., Barres, B. A., Gephart, M. H., & Quake, S. R. (2017). Single-Cell RNA-Seq Analysis of Infiltrating Neoplastic Cells at the Migrating Front of Human Glioblastoma. *Cell Reports*, *21*, 1399-1410. https://doi.org/10.1016/j.celrep.2017.10.030

Davis, B. M., Salinas-Navarro, M., Cordeiro, M. F., Moons, L., & De Groef, L. (2017). Characterizing microglia activation: a spatial statistics approach to maximize information extraction. *Scientific Reports*, *7*(1), 1576. https://doi.org/10.1038/s41598-017-01747-8

De Bonis, P., Albanese, A., Lofrese, G., de Waure, C., Mangiola, A., Pettorini, B. L., Pompucci, A., Balducci, M., Fiorentino, A., Lauriola, L., Anile, C., & Maira, G. (2011). Postoperative infection may influence survival in patients with glioblastoma: simply a myth? *Neurosurgery*, *69*(4), 864-868; discussion 868-869. https://doi.org/10.1227/NEU.0b013e318222adfa

de Groot, J., Penas-Prado, M., Alfaro-Munoz, K., Hunter, K., Pei, B. L., O'Brien, B., Weathers, S. P., Loghin, M., Kamiya Matsouka, C., Yung, W. K. A., Mandel, J., Wu, J., Yuan, Y., Zhou, S., Fuller, G. N., Huse, J., Rao, G., Weinberg, J. S., Prabhu, S. S., . . . Heimberger, A. B. (2020). Window-of-opportunity clinical trial of pembrolizumab in patients with recurrent glioblastoma reveals predominance of immune-suppressive macrophages. *Neuro Oncol*, *22*(4), 539-549. https://doi.org/10.1093/neuonc/noz185

De Vrij, J., Niek Maas, S. L., Kwappenberg, K. M. C., Schnoor, R., Kleijn, A., Dekker, L., Luider, T. M., De Witte, L. D., Litjens, M., Van Strien, M. E., Hol, E. M., Kroonen, J., Robe, P. A., Lamfers, M. L., Schilham, M. W., & Broekman, M. L. D. (2015). Glioblastoma-derived extracellular vesicles modify the phenotype of monocytic cells. *International Journal of Cancer*, *137*, 1630-1642. https://doi.org/10.1002/ijc.29521

Desjardins, A., Gromeier, M., Herndon, J. E., 2nd, Beaubier, N., Bolognesi, D. P., Friedman, A. H., Friedman, H. S., McSherry, F., Muscat, A. M., Nair, S., Peters, K. B., Randazzo, D., Sampson, J. H., Vlahovic, G., Harrison, W. T., McLendon, R. E., Ashley, D., & Bigner, D. D. (2018). Recurrent Glioblastoma Treated with Recombinant Poliovirus. *N Engl J Med*, *379*(2), 150-161. https://doi.org/10.1056/NEJMoa1716435

Di Paolo, N. C., & Shayakhmetov, D. M. (2016). Interleukin 1α and the inflammatory process. *Nature Immunology*, *17*, 906-913. https://doi.org/10.1038/ni.3503

Dirkse, A., Golebiewska, A., Buder, T., Nazarov, P. V., Muller, A., Poovathingal, S., Brons, N. H. C., Leite, S., Sauvageot, N., Sarkisjan, D., Seyfrid, M., Fritah, S., Stieber, D., Michelucci, A., Hertel, F., Herold-Mende, C., Azuaje, F., Skupin, A., Bjerkvig, R., . . . Niclou, S. P. (2019). Stem cell-associated heterogeneity in Glioblastoma results from intrinsic tumor plasticity shaped by the microenvironment. *Nat Commun*, *10*(1), 1787. https://doi.org/10.1038/s41467-019-09853-z

Dobrikova, E. Y., Goetz, C., Walters, R. W., Lawson, S. K., Peggins, J. O., Muszynski, K., Ruppel, S., Poole, K., Giardina, S. L., Vela, E. M., Estep, J. E., & Gromeier, M. (2012). Attenuation of neurovirulence, biodistribution, and shedding of a poliovirus:rhinovirus chimera after intrathalamic inoculation in Macaca fascicularis. *J Virol*, *86*(5), 2750-2759. https://doi.org/10.1128/jvi.06427-11

Dustin, M. L. (2014). The immunological synapse. *Cancer Immunol Res*, *2*(11), 1023-1033. https://doi.org/10.1158/2326-6066.Cir-14-0161

Dziurzynski, K., Chang, S. M., Heimberger, A. B., Kalejta, R. F., McGregor Dallas, S. R., Smit, M., Soroceanu, L., & Cobbs, C. S. (2012). Consensus on the role of human cytomegalovirus in glioblastoma. *Neuro Oncol*, *14*(3), 246-255. https://doi.org/10.1093/neuonc/nor227

Eakin, E. (2015, December 7, 2015). Bacteria on the Brain. *The New Yorker*, *Annals of Medicine*.

Ebrahimkhani, S., Vafaee, F., Hallal, S., Wei, H., Lee, M. Y. T., Young, P. E., Satgunaseelan, L., Beadnall, H., Barnett, M. H., Shivalingam, B., Suter, C. M., Buckland, M. E., & Kaufman, K. L. (2018). Deep sequencing of circulating exosomal microRNA allows non-invasive glioblastoma diagnosis. *NPJ Precis Oncol*, *2*, 28. https://doi.org/10.1038/s41698-018-0071-0

Emonet, S. F., Garidou, L., McGavern, D. B., & de la Torre, J. C. (2009). Generation of recombinant lymphocytic choriomeningitis viruses with trisegmented genomes stably expressing two additional genes of interest. *Proc Natl Acad Sci U S A*, *106*(9), 3473-3478. https://doi.org/10.1073/pnas.0900088106

Engelhardt, B., & Ransohoff, R. M. (2012). Capture, crawl, cross: the T cell code to breach the blood-brain barriers. *Trends Immunol*, *33*(12), 579-589. https://doi.org/10.1016/j.it.2012.07.004

Engelhardt, B., Vajkoczy, P., & Weller, R. O. (2017). The movers and shapers in immune privilege of the CNS. *Nat Immunol*, *18*(2), 123-131. https://doi.org/10.1038/ni.3666

Facoetti, A., Nano, R., Zelini, P., Morbini, P., Benericetti, E., Ceroni, M., Campoli, M., & Ferrone, S. (2005). Human leukocyte antigen and antigen processing machinery

component defects in astrocytic tumors. *Clin Cancer Res*, *11*(23), 8304-8311. https://doi.org/10.1158/1078-0432.Ccr-04-2588

Faust, N., Varas, F., Kelly, L. M., Heck, S., & Graf, T. (2000). Insertion of enhanced green fluorescent protein into the lysozyme gene creates mice with green fluorescent granulocytes and macrophages. *Blood*, *96*(2), 719-726.

Filley, A. C., Henriquez, M., & Dey, M. (2017). Recurrent glioma clinical trial, CheckMate-143: the game is not over yet. *Oncotarget*, *8*(53), 91779-91794. https://doi.org/10.18632/oncotarget.21586

Fisher, J. P., & Adamson, D. C. (2021). Current FDA-Approved Therapies for High-Grade Malignant Gliomas. *Biomedicines*, *9*(3). https://doi.org/10.3390/biomedicines9030324

Fitzpatrick, Z., Frazer, G., Ferro, A., Clare, S., Bouladoux, N., Ferdinand, J., Tuong, Z. K., Negro-Demontel, M. L., Kumar, N., Suchanek, O., Tajsic, T., Harcourt, K., Scott, K., Bashford-Rogers, R., Helmy, A., Reich, D. S., Belkaid, Y., Lawley, T. D., McGavern, D. B., & Clatworthy, M. R. (2020). Gut-educated IgA plasma cells defend the meningeal venous sinuses. *Nature*, *587*(7834), 472-476. https://doi.org/10.1038/s41586-020-2886-4

Friebel, E., Kapolou, K., Unger, S., Núñez, N. G., Utz, S., Rushing, E. J., Regli, L., Weller, M., Greter, M., Tugues, S., Neidert, M. C., & Becher, B. (2020). Single-Cell Mapping of Human Brain Cancer Reveals Tumor-Specific Instruction of Tissue-Invading Leukocytes. *Cell*. https://doi.org/10.1016/j.cell.2020.04.055

Fu, W., Wang, W., Li, H., Jiao, Y., Huo, R., Yan, Z., Wang, J., Wang, S., Wang, J., Chen, D., Cao, Y., & Zhao, J. (2020). Single-Cell Atlas Reveals Complexity of the Immunosuppressive Microenvironment of Initial and Recurrent Glioblastoma. *Front Immunol*, *11*, 835. https://doi.org/10.3389/fimmu.2020.00835

Fujimoto, H., Asaoka, K., Imaizumi, T., Ayabe, M., Shoji, H., & Kaji, M. (2003). Epstein-Barr virus infections of the central nervous system. *Intern Med*, *42*(1), 33-40. https://doi.org/10.2169/internalmedicine.42.33

Fujita, M., Kohanbash, G., Fellows-Mayle, W., Hamilton, R. L., Komohara, Y., Decker, S. A., Ohlfest, J. R., & Okada, H. (2011). COX-2 blockade suppresses gliomagenesis by inhibiting myeloid-derived suppressor cells. *Cancer Res*, *71*, 2664-2674. https://doi.org/10.1158/0008-5472.CAN-10-3055

Fujita, M., Scheurer, M. E., Decker, S. A., McDonald, H. A., Kohanbash, G., Kastenhuber, E. R., Kato, H., Bondy, M. L., Ohlfest, J. R., & Okada, H. (2010). Role of type 1 IFNs in antiglioma immunosurveillance--using mouse studies to guide examination of novel prognostic markers in humans. *Clin Cancer Res*, *16*(13), 3409-3419. https://doi.org/10.1158/1078-0432.CCR-10-0644

Fukushima, S., Narita, Y., Miyakita, Y., Ohno, M., Takizawa, T., Takusagawa, Y., Mori, M., Ichimura, K., Tsuda, H., & Shibui, S. (2013). A case of more than 20 years survival with glioblastoma, and development of cavernous angioma as a delayed complication of radiotherapy. *Neuropathology*, *33*(5), 576-581. https://doi.org/10.1111/neup.12022

Gabriely, G., Wheeler, M. A., Takenaka, M. C., & Quintana, F. J. (2017). Role of AHR and HIF-1alpha in Glioblastoma Metabolism. *Trends Endocrinol Metab*, *28*(6), 428-436. https://doi.org/10.1016/j.tem.2017.02.009

Gabrusiewicz, K., Hossain, M. B., Cortes-Santiago, N., Fan, X., Kaminska, B., Marini, F. C., Fueyo, J., & Gomez-Manzano, C. (2015). Macrophage Ablation Reduces M2-Like Populations and Jeopardizes Tumor Growth in a MAFIA-Based Glioma Model. *Neoplasia*, *17*, 374-384. https://doi.org/10.1016/j.neo.2015.03.003

Gabrusiewicz, K., Li, X., Wei, J., Hashimoto, Y., Marisetty, A. L., Ott, M., Wang, F., Hawke, D., Yu, J., Healy, L. M., Hossain, A., Akers, J. C., Maiti, S. N., Yamashita, S., Shimizu, Y., Dunner, K., Zal, M. A., Burks, J. K., Gumin, J., . . . Heimberger, A. B. (2018). Glioblastoma stem cell-derived exosomes induce M2 macrophages and PD-L1 expression on human monocytes. *OncoImmunology*, *7*, e1412909. https://doi.org/10.1080/2162402X.2017.1412909

Gabrusiewicz, K., Rodriguez, B., Wei, J., Hashimoto, Y., Healy, L. M., Maiti, S. N., Thomas, G., Zhou, S., Wang, Q., Elakkad, A., Liebelt, B. D., Yaghi, N. K., Ezhilarasan, R., Huang, N., Weinberg, J. S., Prabhu, S. S., Rao, G., Sawaya, R., Langford, L. A., . . . Heimberger, A. B. (2016). Glioblastoma-infiltrated innate immune cells resemble M0 macrophage phenotype. *JCI Insight*, *1*(2). https://doi.org/10.1172/jci.insight.85841

Ge, Q., Ruan, C. C., Ma, Y., Tang, X. F., Wu, Q. H., Wang, J. G., Zhu, D. L., & Gao, P. J. (2017). Osteopontin regulates macrophage activation and osteoclast formation in hypertensive patients with vascular calcification. *Scientific Reports*, *7*, 1-9. https://doi.org/10.1038/srep40253

Genoud, V., Marinari, E., Nikolaev, S. I., Castle, J. C., Bukur, V., Dietrich, P. Y., Okada, H., & Walker, P. R. (2018). Responsiveness to anti-PD-1 and anti-CTLA-4 immune checkpoint blockade in SB28 and GL261 mouse glioma models. *OncoImmunology*, *7*(12), e1501137. https://doi.org/10.1080/2162402x.2018.1501137

Ghazi, A., Ashoori, A., Hanley, P. J., Brawley, V. S., Shaffer, D. R., Kew, Y., Powell, S. Z., Grossman, R., Grada, Z., Scheurer, M. E., Hegde, M., Leen, A. M., Bollard, C. M., Rooney, C. M., Heslop, H. E., Gottschalk, S., & Ahmed, N. (2012). Generation of polyclonal CMV-specific T cells for the adoptive immunotherapy of glioblastoma. *J Immunother*, *35*(2), 159-168. https://doi.org/10.1097/CJI.0b013e318247642f

Gielen, P. R., Schulte, B. M., Kers-Rebel, E. D., Verrijp, K., Petersen-Baltussen, H. M. J. M., Ter Laan, M., Wesseling, P., & Adema, G. J. (2015). Increase in Both CD14-Positive and CD15-Positive Myeloid-Derived Suppressor Cell Subpopulations in the Blood of Patients with Glioma but Predominance of CD15-Positive Myeloid-Derived Suppressor Cells in Glioma Tissue. *Journal of Neuropathology and Experimental Neurology*, *74*, 390-400. https://doi.org/10.1097/NEN.0000000000000183

Gimple, R. C., Bhargava, S., Dixit, D., & Rich, J. N. (2019). Glioblastoma stem cells: lessons from the tumor hierarchy in a lethal cancer. *Genes Dev*, *33*(11-12), 591-609. https://doi.org/10.1101/gad.324301.119

Gossa, S., Nayak, D., Zinselmeyer, B. H., & McGavern, D. B. (2014). Development of an immunologically tolerated combination of fluorescent proteins for in vivo two-photon imaging. *Sci Rep*, *4*, 6664. https://doi.org/10.1038/srep06664

Goswami, S., Walle, T., Cornish, A. E., Basu, S., Anandhan, S., Fernandez, I., Vence, L., Blando, J., Zhao, H., Yadav, S. S., Ott, M., Kong, L. Y., Heimberger, A. B., de Groot, J., Sepesi, B., Overman, M., Kopetz, S., Allison, J. P., Pe'er, D., & Sharma, P. (2020). Immune profiling of human tumors identifies CD73 as a combinatorial target in glioblastoma. *Nat Med*, *26*(1), 39-46. https://doi.org/10.1038/s41591-019-0694-x

Graner, M. W., Alzate, O., Dechkovskaia, A. M., Keene, J. D., Sampson, J. H., Mitchell, D. A., & Bigner, D. D. (2009). Proteomic and immunologic analyses of brain tumor exosomes. *FASEB J*, *23*(5), 1541-1557. https://doi.org/10.1096/fj.08-122184

Greter, M., Heppner, F. L., Lemos, M. P., Odermatt, B. M., Goebels, N., Laufer, T., Noelle, R. J., & Becher, B. (2005). Dendritic cells permit immune invasion of the CNS in an animal model of multiple sclerosis. *Nat Med*, *11*(3), 328-334. https://doi.org/10.1038/nm1197

Grow, E. J., Flynn, R. A., Chavez, S. L., Bayless, N. L., Wossidlo, M., Wesche, D. J., Martin, L., Ware, C. B., Blish, C. A., Chang, H. Y., Pera, R. A., & Wysocka, J. (2015). Intrinsic retroviral reactivation in human preimplantation embryos and pluripotent cells. *Nature*, *522*(7555), 221-225. https://doi.org/10.1038/nature14308

Guidotti, L. G., Borrow, P., Brown, A., McClary, H., Koch, R., & Chisari, F. V. (1999). Noncytopathic clearance of lymphocytic choriomeningitis virus from the hepatocyte. *J Exp Med*, *189*(10), 1555-1564. https://doi.org/10.1084/jem.189.10.1555

Gururaj, A. E., Gibson, L., Panchabhai, S., Bai, M., Manyam, G., Lu, Y., Latha, K., Rojas, M. L., Hwang, Y., Liang, S., & Bogler, O. (2013). Access to the nucleus and functional association with c-Myc is required for the full oncogenic potential of ΔEGFR/EGFRvIII. *J Biol Chem*, *288*(5), 3428-3438. https://doi.org/10.1074/jbc.M112.399352

Gustafson, M. P., Lin, Y., New, K. C., Bulur, P. A., O'Neill, B. P., Gastineau, D. A., & Dietz, A. B. (2010). Systemic immune suppression in glioblastoma: The interplay between CD14 +HLA-DR lo/neg monocytes, tumor factors, and dexamethasone. *Neuro-Oncology*, *12*, 631-644. https://doi.org/10.1093/neuonc/noq001

Haddad, A. F., Young, J. S., Amara, D., Berger, M. S., Raleigh, D. R., Aghi, M. K., & Butowski, N. A. (2021). Mouse models of glioblastoma for the evaluation of novel therapeutic strategies. *Neurooncol Adv*, *3*(1), vdab100. https://doi.org/10.1093/noajnl/vdab100

Hambardzumyan, D., & Bergers, G. (2015). Glioblastoma: Defining Tumor Niches. *Trends Cancer*, *1*(4), 252-265. https://doi.org/10.1016/j.trecan.2015.10.009

Hambardzumyan, D., Gutmann, D. H., & Kettenmann, H. (2016). The role of microglia and macrophages in glioma maintenance and progression. *Nat Neurosci*, *19*(1), 20-27. https://doi.org/10.1038/nn.4185

Harshyne, L. A., Nasca, B. J., Kenyon, L. C., Andrews, D. W., & Hooper, D. C. (2016). Serum exosomes and cytokines promote a T-helper cell type 2 environment in the peripheral blood of glioblastoma patients. *Neuro-Oncology*, *18*, 206-215. https://doi.org/10.1093/neuonc/nov107

Hatton, O. L., Harris-Arnold, A., Schaffert, S., Krams, S. M., & Martinez, O. M. (2014). The interplay between Epstein-Barr virus and B lymphocytes: implications for

infection, immunity, and disease. *Immunol Res*, *58*(2-3), 268-276. https://doi.org/10.1007/s12026-014-8496-1

Heath, E., Begue-Pastor, N., Chaganti, S., Croom-Carter, D., Shannon-Lowe, C., Kube, D., Feederle, R., Delecluse, H. J., Rickinson, A. B., & Bell, A. I. (2012). Epstein-Barr virus infection of naïve B cells in vitro frequently selects clones with mutated immunoglobulin genotypes: implications for virus biology. *PLoS Pathog*, *8*(5), e1002697. https://doi.org/10.1371/journal.ppat.1002697

Herz, J., Johnson, K. R., & McGavern, D. B. (2015). Therapeutic antiviral T cells noncytopathically clear persistently infected microglia after conversion into antigen-presenting cells. *J Exp Med*, *212*(8), 1153-1169. https://doi.org/10.1084/jem.20142047

Hubert, M., Gobbini, E., Couillault, C., Manh, T. V., Doffin, A. C., Berthet, J., Rodriguez, C., Ollion, V., Kielbassa, J., Sajous, C., Treilleux, I., Tredan, O., Dubois, B., Dalod, M., Bendriss-Vermare, N., Caux, C., & Valladeau-Guilemond, J. (2020). IFN-III is selectively produced by cDC1 and predicts good clinical outcome in breast cancer. *Sci Immunol*, *5*(46). https://doi.org/10.1126/sciimmunol.aav3942

Hussain, S. F., Yang, D., Suki, D., Aldape, K., Grimm, E., & Heimberger, A. B. (2006). The role of human glioma-infiltrating microglia/macrophages in mediating antitumor immune responses. *Neuro Oncol*, *8*(3), 261-279. https://doi.org/10.1215/15228517-2006-008

Hutter, G., Theruvath, J., Graef, C. M., Zhang, M., Schoen, M. K., Manz, E. M., Bennett, M. L., Olson, A., Azad, T. D., Sinha, R., Chan, C., Assad Kahn, S., Gholamin, S., Wilson, C., Grant, G., He, J., Weissman, I. L., Mitra, S. S., & Cheshier, S. H. (2019). Microglia are effector cells of CD47-SIRPalpha antiphagocytic axis disruption against glioblastoma. *Proc Natl Acad Sci U S A*, *116*(3), 997-1006. https://doi.org/10.1073/pnas.1721434116

Iliff, J. J., Wang, M., Liao, Y., Plogg, B. A., Peng, W., Gundersen, G. A., Benveniste, H., Vates, G. E., Deane, R., Goldman, S. A., Nagelhus, E. A., & Nedergaard, M. (2012). A paravascular pathway facilitates CSF flow through the brain parenchyma and the clearance of interstitial solutes, including amyloid beta. *Sci Transl Med*, *4*(147), 147ra111. https://doi.org/10.1126/scitranslmed.3003748

Ishida, T., Obata, Y., Ohara, N., Matsushita, H., Sato, S., Uenaka, A., Saika, T., Miyamura, T., Chayama, K., Nakamura, Y., Wada, H., Yamashita, T., Morishima, T., Old, L. J., & Nakayama, E. (2008). Identification of the HERV-K gag antigen in prostate cancer by SEREX using autologous patient serum and its immunogenicity. *Cancer Immun*, *8*, 15.

Jackson, C. M., Kochel, C. M., Nirschl, C. J., Durham, N. M., Ruzevick, J., Alme, A., Francica, B. J., Elias, J., Daniels, A., Dubensky, T. W., Jr., Lauer, P., Brockstedt, D. G., Baxi, E. G., Calabresi, P. A., Taube, J. M., Pardo, C. A., Brem, H., Pardoll, D. M., Lim, M., & Drake, C. G. (2016). Systemic Tolerance Mediated by Melanoma Brain Tumors Is Reversible by Radiotherapy and Vaccination. *Clin Cancer Res*, *22*(5), 1161-1172. https://doi.org/10.1158/1078-0432.CCR-15-1516

Jeon, H. Y., Ham, S. W., Kim, J. K., Jin, X., Lee, S. Y., Shin, Y. J., Choi, C. Y., Sa, J. K., Kim, S. H., Chun, T., Jin, X., Nam, D. H., & Kim, H. (2019). Ly6G(+) inflammatory cells

enable the conversion of cancer cells to cancer stem cells in an irradiated glioblastoma model. *Cell Death Differ*, *26*(10), 2139-2156. https://doi.org/10.1038/s41418-019-0282-0

Johanns, T. M., Ward, J. P., Miller, C. A., Wilson, C., Kobayashi, D. K., Bender, D., Fu, Y., Alexandrov, A., Mardis, E. R., Artyomov, M. N., Schreiber, R. D., & Dunn, G. P. (2016). Endogenous Neoantigen-Specific CD8 T Cells Identified in Two Glioblastoma Models Using a Cancer Immunogenomics Approach. *Cancer Immunol Res*, *4*(12), 1007-1015. https://doi.org/10.1158/2326-6066.Cir-16-0156

Jung, S., Aliberti, J., Graemmel, P., Sunshine, M. J., Kreutzberg, G. W., Sher, A., & Littman, D. R. (2000). Analysis of fractalkine receptor CX(3)CR1 function by targeted deletion and green fluorescent protein reporter gene insertion. *Mol Cell Biol*, *20*(11), 4106-4114. https://doi.org/10.1128/mcb.20.11.4106-4114.2000

Kahyo, T., Tao, H., Shinmura, K., Yamada, H., Mori, H., Funai, K., Kurabe, N., Suzuki, M., Tanahashi, M., Niwa, H., Ogawa, H., Tanioka, F., Yin, G., Morita, M., Matsuo, K., Kono, S., & Sugimura, H. (2013). Identification and association study with lung cancer for novel insertion polymorphisms of human endogenous retrovirus. *Carcinogenesis*, *34*(11), 2531-2538. https://doi.org/10.1093/carcin/bgt253

Kale, S., Raja, R., Thorat, D., Soundararajan, G., Patil, T. V., & Kundu, G. C. (2014). Osteopontin signaling upregulates cyclooxygenase-2 expression in tumor-associated macrophages leading to enhanced angiogenesis and melanoma growth via α9β1 integrin. *Oncogene*, *33*, 2295-2306. https://doi.org/10.1038/onc.2013.184

Karimian-Jazi, K., Munch, P., Alexander, A., Fischer, M., Pfleiderer, K., Piechutta, M., Karreman, M. A., Solecki, G. M., Berghoff, A. S., Friedrich, M., Deumelandt, K., Kurz, F. T., Wick, W., Heiland, S., Bendszus, M., Winkler, F., Platten, M., & Breckwoldt, M. O. (2020). Monitoring innate immune cell dynamics in the glioma microenvironment by magnetic resonance imaging and multiphoton microscopy (MR-MPM). *Theranostics*, *10*(4), 1873-1883. https://doi.org/10.7150/thno.38659

Kaufman, H. L., Kohlhapp, F. J., & Zloza, A. (2015). Oncolytic viruses: a new class of immunotherapy drugs. *Nature Reviews Drug Discovery*, *14*(9), 642-662. https://doi.org/10.1038/nrd4663

Kaur, B., Khwaja, F. W., Severson, E. A., Matheny, S. L., Brat, D. J., & Van Meir, E. G. (2005). Hypoxia and the hypoxia-inducible-factor pathway in glioma growth and angiogenesis. *Neuro Oncol*, *7*(2), 134-153. https://doi.org/10.1215/S1152851704001115

Kawakami, N., Nägerl, U. V., Odoardi, F., Bonhoeffer, T., Wekerle, H., & Flügel, A. (2005). Live imaging of effector cell trafficking and autoantigen recognition within the unfolding autoimmune encephalomyelitis lesion. *J Exp Med*, *201*(11), 1805-1814. https://doi.org/10.1084/jem.20050011

Keskin, D. B., Anandappa, A. J., Sun, J., Tirosh, I., Mathewson, N. D., Li, S., Oliveira, G., Giobbie-Hurder, A., Felt, K., Gjini, E., Shukla, S. A., Hu, Z., Li, L., Le, P. M., Allesoe, R. L., Richman, A. R., Kowalczyk, M. S., Abdelrahman, S., Geduldig, J. E., . . . Reardon, D. A. (2019). Neoantigen vaccine generates intratumoral T cell responses in phase

Ib glioblastoma trial. *Nature*, *565*(7738), 234-239. https://doi.org/10.1038/s41586-018-0792-9

Kessler, A. F., Wiesner, M., Denner, J., Kämmerer, U., Vince, G. H., Linsenmann, T., Löhr, M., Ernestus, R. I., & Hagemann, C. (2014). Expression-analysis of the human endogenous retrovirus HERV-K in human astrocytic tumors. *BMC Res Notes*, *7*, 159. https://doi.org/10.1186/1756-0500-7-159

Khalsa, J. K., Cheng, N., Keegan, J., Chaudry, A., Driver, J., Bi, W. L., Lederer, J., & Shah, K. (2020). Immune phenotyping of diverse syngeneic murine brain tumors identifies immunologically distinct types. *Nature Communications*, *11*(1), 3912. https://doi.org/10.1038/s41467-020-17704-5

Khan, N., Shariff, N., Cobbold, M., Bruton, R., Ainsworth, J. A., Sinclair, A. J., Nayak, L., & Moss, P. A. (2002). Cytomegalovirus seropositivity drives the CD8 T cell repertoire toward greater clonality in healthy elderly individuals. *J Immunol*, *169*(4), 1984-1992. https://doi.org/10.4049/jimmunol.169.4.1984

Kida, S., Pantazis, A., & Weller, R. O. (1993). CSF drains directly from the subarachnoid space into nasal lymphatics in the rat. Anatomy, histology and immunological significance. *Neuropathol Appl Neurobiol*, *19*(6), 480-488. https://doi.org/10.1111/j.1365-2990.1993.tb00476.x

Kim, J., Kim, A. R., & Shin, E. C. (2015). Cytomegalovirus Infection and Memory T Cell Inflation. *Immune Netw*, *15*(4), 186-190. https://doi.org/10.4110/in.2015.15.4.186

Kim, J., Lee, I. H., Cho, H. J., Park, C. K., Jung, Y. S., Kim, Y., Nam, S. H., Kim, B. S., Johnson, M. D., Kong, D. S., Seol, H. J., Lee, J. I., Joo, K. M., Yoon, Y., Park, W. Y., Lee, J., Park, P. J., & Nam, D. H. (2015). Spatiotemporal Evolution of the Primary Glioblastoma Genome. *Cancer Cell*, *28*(3), 318-328. https://doi.org/10.1016/j.ccell.2015.07.013

Kleiman, A., Senyuta, N., Tryakin, A., Sauter, M., Karseladze, A., Tjulandin, S., Gurtsevitch, V., & Mueller-Lantzsch, N. (2004). HERV-K(HML-2) GAG/ENV antibodies as indicator for therapy effect in patients with germ cell tumors. *Int J Cancer*, *110*(3), 459-461. https://doi.org/10.1002/ijc.11649

Kloepper, J., Riedemann, L., Amoozgar, Z., Seano, G., Susek, K., Yu, V., Dalvie, N., Amelung, R. L., Datta, M., Song, J. W., Askoxylakis, V., Taylor, J. W., Lu-Emerson, C., Batista, A., Kirkpatrick, N. D., Jung, K., Snuderl, M., Muzikansky, A., Stubenrauch, K. G., . . . Jain, R. K. (2016). Ang-2/VEGF bispecific antibody reprograms macrophages and resident microglia to anti-tumor phenotype and prolongs glioblastoma survival. *Proc Natl Acad Sci U S A*, *113*(16), 4476-4481. https://doi.org/10.1073/pnas.1525360113

Kobayashi, M. (1979). Viral Xenogenization of Intact Tumor Cells. In G. Klein & S. Weinhouse (Eds.), *Advances in Cancer Research* (Vol. 30, pp. 279-299). Academic Press. https://doi.org/https://doi.org/10.1016/S0065-230X(08)60899-4

Komohara, Y., Ohnishi, K., Kuratsu, J., & Takeya, M. (2008). Possible involvement of the M2 anti-inflammatory macrophage phenotype in growth of human gliomas. *J Pathol*, *216*(1), 15-24. https://doi.org/10.1002/path.2370

Kong, L. Y., Wu, A. S., Doucette, T., Wei, J., Priebe, W., Fuller, G. N., Qiao, W., Sawaya, R., Rao, G., & Heimberger, A. B. (2010). Intratumoral mediated immunosuppression is prognostic in genetically engineered murine models of glioma and correlates to

immunotherapeutic responses. *Clin Cancer Res*, *16*(23), 5722-5733. https://doi.org/10.1158/1078-0432.CCR-10-1693

Kosaka, A., Ohkuri, T., & Okada, H. (2014). Combination of an agonistic anti-CD40 monoclonal antibody and the COX-2 inhibitor celecoxib induces anti-glioma effects by promotion of type-1 immunity in myeloid cells and T-cells. *Cancer Immunol Immunother*, *63*(8), 847-857. https://doi.org/10.1007/s00262-014-1561-8

Krenzlin, H., Behera, P., Lorenz, V., Passaro, C., Zdioruk, M., Nowicki, M. O., Grauwet, K., Zhang, H., Skubal, M., Ito, H., Zane, R., Gutknecht, M., Griessl, M. B., Ricklefs, F., Ding, L., Peled, S., Rooj, A., James, C. D., Cobbs, C. S., . . . Lawler, S. E. (2019). Cytomegalovirus promotes murine glioblastoma growth via pericyte recruitment and angiogenesis. *J Clin Invest*, *129*(4), 1671-1683. https://doi.org/10.1172/jci123375

Lang, F. F., Conrad, C., Gomez-Manzano, C., Yung, W. K. A., Sawaya, R., Weinberg, J. S., Prabhu, S. S., Rao, G., Fuller, G. N., Aldape, K. D., Gumin, J., Vence, L. M., Wistuba, I., Rodriguez-Canales, J., Villalobos, P. A., Dirven, C. M. F., Tejada, S., Valle, R. D., Alonso, M. M., . . . Fueyo, J. (2018). Phase I Study of DNX-2401 (Delta-24-RGD) Oncolytic Adenovirus: Replication and Immunotherapeutic Effects in Recurrent Malignant Glioma. *Journal of Clinical Oncology*, *36*(14), 1419-1427. https://doi.org/10.1200/JCO.2017.75.8219

Lavin, Y., Kobayashi, S., Leader, A., Amir, E. a. D., Elefant, N., Bigenwald, C., Remark, R., Sweeney, R., Becker, C. D., Levine, J. H., Meinhof, K., Chow, A., Kim-Shulze, S., Wolf, A., Medaglia, C., Li, H., Rytlewski, J. A., Emerson, R. O., Solovyov, A., . . . Merad, M. (2017). Innate Immune Landscape in Early Lung Adenocarcinoma by Paired Single-Cell Analyses. *Cell*, *169*, 750-765.e717. https://doi.org/10.1016/j.cell.2017.04.014

Lawrence, M. S., Stojanov, P., Polak, P., Kryukov, G. V., Cibulskis, K., Sivachenko, A., Carter, S. L., Stewart, C., Mermel, C. H., Roberts, S. A., Kiezun, A., Hammerman, P. S., McKenna, A., Drier, Y., Zou, L., Ramos, A. H., Pugh, T. J., Stransky, N., Helman, E., . . . Getz, G. (2013). Mutational heterogeneity in cancer and the search for new cancer-associated genes. *Nature*, *499*(7457), 214-218. https://doi.org/10.1038/nature12213

Lee, J. H., Lee, J. E., Kahng, J. Y., Kim, S. H., Park, J. S., Yoon, S. J., Um, J. Y., Kim, W. K., Lee, J. K., Park, J., Kim, E. H., Lee, J. H., Lee, J. H., Chung, W. S., Ju, Y. S., Park, S. H., Chang, J. H., Kang, S. G., & Lee, J. H. (2018). Human glioblastoma arises from subventricular zone cells with low-level driver mutations. *Nature*, *560*(7717), 243-247. https://doi.org/10.1038/s41586-018-0389-3

Lee-Chang, C., Miska, J., Hou, D., Rashidi, A., Zhang, P., Burga, R. A., Jusue-Torres, I., Xiao, T., Arrieta, V. A., Zhang, D. Y., Lopez-Rosas, A., Han, Y., Sonabend, A. M., Horbinski, C. M., Stupp, R., Balyasnikova, I. V., & Lesniak, M. S. (2021). Activation of 4-1BBL+ B cells with CD40 agonism and IFNgamma elicits potent immunity against glioblastoma. *J Exp Med*, *218*(1). https://doi.org/10.1084/jem.20200913

Lee-Chang, C., Rashidi, A., Miska, J., Zhang, P., Pituch, K. C., Hou, D., Xiao, T., Fischietti, M., Kang, S. J., Appin, C. L., Horbinski, C., Platanias, L. C., Lopez-Rosas, A., Han, Y., Balyasnikova, I. V., & Lesniak, M. S. (2019). Myeloid-Derived Suppressive Cells

Promote B cell-Mediated Immunosuppression via Transfer of PD-L1 in Glioblastoma. *Cancer Immunol Res*, *7*(12), 1928-1943. https://doi.org/10.1158/2326-6066.CIR-19-0240

Lei, Y. Y., Li, Y. T., Hu, Q. L., Wang, J., & Sui, A. X. (2019). Prognostic impact of neutrophil-to-lymphocyte ratio in gliomas: a systematic review and meta-analysis. *World J Surg Oncol*, *17*(1), 152. https://doi.org/10.1186/s12957-019-1686-5

Lenting, K., Verhaak, R., Ter Laan, M., Wesseling, P., & Leenders, W. (2017). Glioma: experimental models and reality. *Acta Neuropathol*, *133*(2), 263-282. https://doi.org/10.1007/s00401-017-1671-4

Levine, Jacob H., Simonds, Erin F., Bendall, Sean C., Davis, Kara L., Amir, E.-ad D., Tadmor, Michelle D., Litvin, O., Fienberg, Harris G., Jager, A., Zunder, Eli R., Finck, R., Gedman, Amanda L., Radtke, I., Downing, James R., Pe'er, D., & Nolan, Garry P. (2015). Data-Driven Phenotypic Dissection of AML Reveals Progenitor-like Cells that Correlate with Prognosis. *Cell*, *162*(1), 184-197. https://doi.org/10.1016/j.cell.2015.05.047

Liang, J., Piao, Y., Holmes, L., Fuller, G. N., Henry, V., Tiao, N., & de Groot, J. F. (2014). Neutrophils promote the malignant glioma phenotype through S100A4. *Clin Cancer Res*, *20*(1), 187-198. https://doi.org/10.1158/1078-0432.CCR-13-1279

Lim, M., Xia, Y., Bettegowda, C., & Weller, M. (2018). Current state of immunotherapy for glioblastoma. *Nat Rev Clin Oncol*, *15*(7), 422-442. https://doi.org/10.1038/s41571-018-0003-5

Lodygin, D., Odoardi, F., Schläger, C., Körner, H., Kitz, A., Nosov, M., van den Brandt, J., Reichardt, H. M., Haberl, M., & Flügel, A. (2013). A combination of fluorescent NFAT and H2B sensors uncovers dynamics of T cell activation in real time during CNS autoimmunity. *Nat Med*, *19*(6), 784-790. https://doi.org/10.1038/nm.3182

Lohr, J., Ratliff, T., Huppertz, A., Ge, Y., Dictus, C., Ahmadi, R., Grau, S., Hiraoka, N., Eckstein, V., Ecker, R. C., Korff, T., von Deimling, A., Unterberg, A., Beckhove, P., & Herold-Mende, C. (2011). Effector T-cell infiltration positively impacts survival of glioblastoma patients and is impaired by tumor-derived TGF-beta. *Clin Cancer Res*, *17*(13), 4296-4308. https://doi.org/10.1158/1078-0432.CCR-10-2557

Lopez-Bertoni, H., Lal, B., Michelson, N., Guerrero-Cázares, H., Quinõnes-Hinojosa, A., Li, Y., & Laterra, J. (2016). Epigenetic modulation of a miR-296-5p:HMGA1 axis regulates Sox2 expression and glioblastoma stem cells. *Oncogene*, *35*, 4903-4913. https://doi.org/10.1038/onc.2016.22

Louveau, A., Smirnov, I., Keyes, T. J., Eccles, J. D., Rouhani, S. J., Peske, J. D., Derecki, N. C., Castle, D., Mandell, J. W., Lee, K. S., Harris, T. H., & Kipnis, J. (2015). Structural and functional features of central nervous system lymphatic vessels. *Nature*, *523*, 337-341. https://doi.org/10.1038/nature14432

Louveau, A., Smirnov, I., Keyes, T. J., Eccles, J. D., Rouhani, S. J., Peske, J. D., Derecki, N. C., Castle, D., Mandell, J. W., Lee, K. S., Harris, T. H., & Kipnis, J. (2015). Structural and functional features of central nervous system lymphatic vessels. *Nature*, *523*(7560), 337-341. https://doi.org/10.1038/nature14432

Ma, Q., Ineichen, B. V., Detmar, M., & Proulx, S. T. (2017). Outflow of cerebrospinal fluid is predominantly through lymphatic vessels and is reduced in aged mice. *Nat Commun*, *8*(1), 1434. https://doi.org/10.1038/s41467-017-01484-6

Ma, W., Hong, Z., Liu, H., Chen, X., Ding, L., Liu, Z., Zhou, F., & Yuan, Y. (2016). Human Endogenous Retroviruses-K (HML-2) Expression Is Correlated with Prognosis and Progress of Hepatocellular Carcinoma. *Biomed Res Int*, *2016*, 8201642. https://doi.org/10.1155/2016/8201642

Madisen, L., Zwingman, T. A., Sunkin, S. M., Oh, S. W., Zariwala, H. A., Gu, H., Ng, L. L., Palmiter, R. D., Hawrylycz, M. J., Jones, A. R., Lein, E. S., & Zeng, H. (2010). A robust and high-throughput Cre reporting and characterization system for the whole mouse brain. *Nat Neurosci*, *13*(1), 133-140. https://doi.org/10.1038/nn.2467

Maier, B., Leader, A. M., Chen, S. T., Tung, N., Chang, C., LeBerichel, J., Chudnovskiy, A., Maskey, S., Walker, L., Finnigan, J. P., Kirkling, M. E., Reizis, B., Ghosh, S., D'Amore, N. R., Bhardwaj, N., Rothlin, C. V., Wolf, A., Flores, R., Marron, T., . . . Merad, M. (2020). A conserved dendritic-cell regulatory program limits antitumour immunity. *Nature*, *580*, 257-262. https://doi.org/10.1038/s41586-020-2134-y

Manglani, M., & McGavern, D. B. (2018). Intravital Imaging of Neuroimmune Interactions Through a Thinned Skull. *Curr Protoc Immunol*, *120*, 24.22.21-24.22.12. https://doi.org/10.1002/cpim.46

Markert, J. M., Razdan, S. N., Kuo, H. C., Cantor, A., Knoll, A., Karrasch, M., Nabors, L. B., Markiewicz, M., Agee, B. S., Coleman, J. M., Lakeman, A. D., Palmer, C. A., Parker, J. N., Whitley, R. J., Weichselbaum, R. R., Fiveash, J. B., & Gillespie, G. Y. (2014). A phase 1 trial of oncolytic HSV-1, G207, given in combination with radiation for recurrent GBM demonstrates safety and radiographic responses. *Mol Ther*, *22*(5), 1048-1055. https://doi.org/10.1038/mt.2014.22

Markovitz, D. M. (2014). "Reverse genomics" and human endogenous retroviruses. *Trans Am Clin Climatol Assoc*, *125*, 57-62; discussion 62-53.

Martinez-Lage, M., Lynch, T. M., Bi, Y., Cocito, C., Way, G. P., Pal, S., Haller, J., Yan, R. E., Ziober, A., Nguyen, A., Kandpal, M., O'Rourke, D. M., Greenfield, J. P., Greene, C. S., Davuluri, R. V., & Dahmane, N. (2019). Immune landscapes associated with different glioblastoma molecular subtypes. *Acta Neuropathol Commun*, *7*(1), 203. https://doi.org/10.1186/s40478-019-0803-6

Mason, H. D., Johnson, A. M., Mihelson, N. A., Mastorakos, P., & McGavern, D. B. (2021). Glia limitans superficialis oxidation and breakdown promote cortical cell death after repetitive head injury. *JCI Insight*, *6*(19). https://doi.org/10.1172/jci.insight.149229

Masopust, D., Murali-Krishna, K., & Ahmed, R. (2007). Quantitating the Magnitude of the Lymphocytic Choriomeningitis Virus-Specific CD8 T-Cell Response: It Is Even Bigger than We Thought. *Journal of Virology*, *81*(4), 2002-2011. https://doi.org/doi:10.1128/JVI.01459-06

Mastorakos, P., & McGavern, D. (2019). The anatomy and immunology of vasculature in the central nervous system. *Sci Immunol*, *4*(37). https://doi.org/10.1126/sciimmunol.aav0492

Mastorakos, P., Mihelson, N., Luby, M., Burks, S. R., Johnson, K., Hsia, A. W., Witko, J., Frank, J. A., Latour, L., & McGavern, D. B. (2021). Temporally distinct myeloid cell responses mediate damage and repair after cerebrovascular injury. *Nat Neurosci*, *24*(2), 245-258. https://doi.org/10.1038/s41593-020-00773-6

Mastorakos, P., Russo, M. V., Zhou, T., Johnson, K., & McGavern, D. B. (2021). Antimicrobial immunity impedes CNS vascular repair following brain injury. *Nat Immunol*, *22*(10), 1280-1293. https://doi.org/10.1038/s41590-021-01012-1

Matloubian, M., Kolhekar, S. R., Somasundaram, T., & Ahmed, R. (1993). Molecular determinants of macrophage tropism and viral persistence: importance of single amino acid changes in the polymerase and glycoprotein of lymphocytic choriomeningitis virus. *J Virol*, *67*(12), 7340-7349. https://doi.org/10.1128/jvi.67.12.7340-7349.1993

Mayer, J., Sauter, M., Rácz, A., Scherer, D., Mueller-Lantzsch, N., & Meese, E. (1999). An almost-intact human endogenous retrovirus K on human chromosome 7. *Nat Genet*, *21*(3), 257-258. https://doi.org/10.1038/6766

Medawar, P. B. (1948). Immunity to homologous grafted skin; the fate of skin homografts transplanted to the brain, to subcutaneous tissue, and to the anterior chamber of the eye. *Br J Exp Pathol*, *29*(1), 58-69. https://www.ncbi.nlm.nih.gov/pubmed/18865105

Menet, A., Speth, C., Larcher, C., Prodinger, W. M., Schwendinger, M. G., Chan, P., Jäger, M., Schwarzmann, F., Recheis, H., Fontaine, M., & Dierich, M. P. (1999). Epstein-Barr virus infection of human astrocyte cell lines. *J Virol*, *73*(9), 7722-7733. https://doi.org/10.1128/jvi.73.9.7722-7733.1999

Mihelson, N., & McGavern, D. B. (2021). Viral Control of Glioblastoma. *Viruses*, *13*(7). https://doi.org/10.3390/v13071264

Mildner, A., Schönheit, J., Giladi, A., David, E., Lara-Astiaso, D., Lorenzo-Vivas, E., Paul, F., Chappell-Maor, L., Priller, J., Leutz, A., Amit, I., & Jung, S. (2017). Genomic Characterization of Murine Monocytes Reveals C/EBPβ Transcription Factor Dependence of Ly6C− Cells. *Immunity*, *46*(5), 849-862.e847. https://doi.org/https://doi.org/10.1016/j.immuni.2017.04.018

Mineta, T., Rabkin, S. D., Yazaki, T., Hunter, W. D., & Martuza, R. L. (1995). Attenuated multi-mutated herpes simplex virus-1 for the treatment of malignant gliomas. *Nat Med*, *1*(9), 938-943. https://doi.org/10.1038/nm0995-938

Mitchell, D. A., Batich, K. A., Gunn, M. D., Huang, M. N., Sanchez-Perez, L., Nair, S. K., Congdon, K. L., Reap, E. A., Archer, G. E., Desjardins, A., Friedman, A. H., Friedman, H. S., Herndon, J. E., 2nd, Coan, A., McLendon, R. E., Reardon, D. A., Vredenburgh, J. J., Bigner, D. D., & Sampson, J. H. (2015). Tetanus toxoid and CCL3 improve dendritic cell vaccines in mice and glioblastoma patients. *Nature*, *519*(7543), 366-369. https://doi.org/10.1038/nature14320

Mitchell, D. A., Xie, W., Schmittling, R., Learn, C., Friedman, A., McLendon, R. E., & Sampson, J. H. (2008). Sensitive detection of human cytomegalovirus in tumors and peripheral blood of patients diagnosed with glioblastoma. *Neuro Oncol*, *10*(1), 10-18. https://doi.org/10.1215/15228517-2007-035

Mohammad, M. G., Tsai, V. W., Ruitenberg, M. J., Hassanpour, M., Li, H., Hart, P. H., Breit, S. N., Sawchenko, P. E., & Brown, D. A. (2014). Immune cell trafficking from the brain maintains CNS immune tolerance. *J Clin Invest*, *124*(3), 1228-1241. https://doi.org/10.1172/JCI71544

Mohme, M., Schliffke, S., Maire, C. L., Runger, A., Glau, L., Mende, K. C., Matschke, J., Gehbauer, C., Akyuz, N., Zapf, S., Holz, M., Schaper, M., Martens, T., Schmidt, N. O., Peine, S., Westphal, M., Binder, M., Tolosa, E., & Lamszus, K. (2018). Immunophenotyping of Newly Diagnosed and Recurrent Glioblastoma Defines Distinct Immune Exhaustion Profiles in Peripheral and Tumor-infiltrating Lymphocytes. *Clin Cancer Res*, *24*(17), 4187-4200. https://doi.org/10.1158/1078-0432.CCR-17-2617

Morimura, T., Neuchrist, C., Kitz, K., Budka, H., Scheiner, O., Kraft, D., & Lassmann, H. (1990). Monocyte subpopulations in human gliomas: expression of Fc and complement receptors and correlation with tumor proliferation. *Acta Neuropathol*, *80*(3), 287-294. https://doi.org/10.1007/BF00294647

Morris, A. W., Sharp, M. M., Albargothy, N. J., Fernandes, R., Hawkes, C. A., Verma, A., Weller, R. O., & Carare, R. O. (2016). Vascular basement membranes as pathways for the passage of fluid into and out of the brain. *Acta Neuropathol*, *131*(5), 725-736. https://doi.org/10.1007/s00401-016-1555-z

Mosaheb, M. M., Dobrikova, E. Y., Brown, M. C., Yang, Y., Cable, J., Okada, H., Nair, S. K., Bigner, D. D., Ashley, D. M., & Gromeier, M. (2020). Genetically stable poliovirus vectors activate dendritic cells and prime antitumor CD8 T cell immunity. *Nat Commun*, *11*(1), 524. https://doi.org/10.1038/s41467-019-13939-z

Moseman, E. A., Blanchard, A. C., Nayak, D., & McGavern, D. B. (2020). T cell engagement of cross-presenting microglia protects the brain from a nasal virus infection. *Sci Immunol*, *5*(48). https://doi.org/10.1126/sciimmunol.abb1817

Moseman, E. A., Wu, T., de la Torre, J. C., Schwartzberg, P. L., & McGavern, D. B. (2016). Type I interferon suppresses virus-specific B cell responses by modulating CD8(+) T cell differentiation. *Sci Immunol*, *1*(4). https://doi.org/10.1126/sciimmunol.aah3565

MUCKENFUSS, R. S., ARMSTRONG, C., & WEBSTER, L. T. (1934). ETIOLOGY OF THE 1933 EPIDEMIC OF ENCEPHALITIS. *Journal of the American Medical Association*, *103*(10), 731-733. https://doi.org/10.1001/jama.1934.02750360007004

Muller, S., Kohanbash, G., Liu, S. J., Alvarado, B., Carrera, D., Bhaduri, A., Watchmaker, P. B., Yagnik, G., Di Lullo, E., Malatesta, M., Amankulor, N. M., Kriegstein, A. R., Lim, D. A., Aghi, M., Okada, H., & Diaz, A. (2017). Single-cell profiling of human gliomas reveals macrophage ontogeny as a basis for regional differences in macrophage activation in the tumor microenvironment. *Genome Biol*, *18*(1), 234. https://doi.org/10.1186/s13059-017-1362-4

Münz, C. (2019). Latency and lytic replication in Epstein-Barr virus-associated oncogenesis. *Nat Rev Microbiol*, *17*(11), 691-700. https://doi.org/10.1038/s41579-019-0249-7

Murali-Krishna, K., Altman, J. D., Suresh, M., Sourdive, D. J., Zajac, A. J., Miller, J. D., Slansky, J., & Ahmed, R. (1998). Counting antigen-specific CD8 T cells: a

reevaluation of bystander activation during viral infection. *Immunity*, *8*(2), 177-187. https://doi.org/10.1016/s1074-7613(00)80470-7

Murphy, J. B., & Sturm, E. (1923). Conditions determining the transplantability of tissues in the brain. *J Exp Med*, *38*, 183-197. https://doi.org/10.1084/jem.38.2.183

Nam, J. Y., & de Groot, J. F. (2017). Treatment of Glioblastoma. *Journal of Oncology Practice*, *13*(10), 629-638. https://doi.org/10.1200/JOP.2017.025536

Neftel, C., Laffy, J., Filbin, M. G., Hara, T., Shore, M. E., Rahme, G. J., Richman, A. R., Silverbush, D., Shaw, M. L., Hebert, C. M., Dewitt, J., Gritsch, S., Perez, E. M., Gonzalez Castro, L. N., Lan, X., Druck, N., Rodman, C., Dionne, D., Kaplan, A., . . . Suvà, M. L. (2019). An Integrative Model of Cellular States, Plasticity, and Genetics for Glioblastoma. *Cell*, *178*(4), 835-849.e821. https://doi.org/10.1016/j.cell.2019.06.024

O'Rourke, D. M., Nasrallah, M. P., Desai, A., Melenhorst, J. J., Mansfield, K., Morrissette, J. J. D., Martinez-Lage, M., Brem, S., Maloney, E., Shen, A., Isaacs, R., Mohan, S., Plesa, G., Lacey, S. F., Navenot, J. M., Zheng, Z., Levine, B. L., Okada, H., June, C. H., . . . Maus, M. V. (2017). A single dose of peripherally infused EGFRvIII-directed CAR T cells mediates antigen loss and induces adaptive resistance in patients with recurrent glioblastoma. *Sci Transl Med*, *9*(399). https://doi.org/10.1126/scitranslmed.aaa0984

Oh-hora, M., & Rao, A. (2008). Calcium signaling in lymphocytes. *Curr Opin Immunol*, *20*(3), 250-258. https://doi.org/10.1016/j.coi.2008.04.004

Oldstone, M. B. (2016). An Odyssey to Viral Pathogenesis. *Annu Rev Pathol*, *11*, 1-19. https://doi.org/10.1146/annurev-pathol-012615-044107

Oldstone, M. B., Blount, P., Southern, P. J., & Lampert, P. W. (1986). Cytoimmunotherapy for persistent virus infection reveals a unique clearance pattern from the central nervous system. *Nature*, *321*(6067), 239-243. https://doi.org/10.1038/321239a0

Ostrom, Q. T., Gittleman, H., Fulop, J., Liu, M., Blanda, R., Kromer, C., Wolinsky, Y., Kruchko, C., & Barnholtz-Sloan, J. S. (2015). CBTRUS Statistical Report: Primary Brain and Central Nervous System Tumors Diagnosed in the United States in 2008-2012. *Neuro Oncol*, *17 Suppl 4*(Suppl 4), iv1-iv62. https://doi.org/10.1093/neuonc/nov189

Ozga, A. J., Chow, M. T., & Luster, A. D. (2021). Chemokines and the immune response to cancer. *Immunity*, *54*(5), 859-874. https://doi.org/https://doi.org/10.1016/j.immuni.2021.01.012

Pearson, J. R. D., & Regad, T. (2017). Targeting cellular pathways in glioblastoma multiforme. *Signal Transduct Target Ther*, *2*, 17040. https://doi.org/10.1038/sigtrans.2017.40

Phuphanich, S., Wheeler, C. J., Rudnick, J. D., Mazer, M., Wang, H., Nuno, M. A., Richardson, J. E., Fan, X., Ji, J., Chu, R. M., Bender, J. G., Hawkins, E. S., Patil, C. G., Black, K. L., & Yu, J. S. (2013). Phase I trial of a multi-epitope-pulsed dendritic cell vaccine for patients with newly diagnosed glioblastoma. *Cancer Immunol Immunother*, *62*(1), 125-135. https://doi.org/10.1007/s00262-012-1319-0

Pinton, L., Magri, S., Masetto, E., Vettore, M., Schibuola, I., Ingangi, V., Marigo, I., Matha, K., Benoit, J. P., Della Puppa, A., Bronte, V., Lollo, G., & Mandruzzato, S. (2020).

Targeting of immunosuppressive myeloid cells from glioblastoma patients by modulation of size and surface charge of lipid nanocapsules. *J Nanobiotechnology*, *18*(1), 31. https://doi.org/10.1186/s12951-020-00589-3

Pinton, L., Masetto, E., Vettore, M., Solito, S., Magri, S., D'Andolfi, M., Del Bianco, P., Lollo, G., Benoit, J. P., Okada, H., Diaz, A., Della Puppa, A., & Mandruzzato, S. (2019). The immune suppressive microenvironment of human gliomas depends on the accumulation of bone marrow-derived macrophages in the center of the lesion. *J Immunother Cancer*, *7*(1), 58. https://doi.org/10.1186/s40425-019-0536-x

Pircher, H., Bürki, K., Lang, R., Hengartner, H., & Zinkernagel, R. M. (1989). Tolerance induction in double specific T-cell receptor transgenic mice varies with antigen. *Nature*, *342*(6249), 559-561. https://doi.org/10.1038/342559a0

Platten, M., & Wick, W. (2015). Tregs in gliomas - The jury is still out. *Neuro-Oncology*, *17*, 769-770. https://doi.org/10.1093/neuonc/nov034

Poltermann, S., Schlehofer, B., Steindorf, K., Schnitzler, P., Geletneky, K., & Schlehofer, J. R. (2006). Lack of association of herpesviruses with brain tumors. *J Neurovirol*, *12*(2), 90-99. https://doi.org/10.1080/13550280600654573

Pombo Antunes, A. R., Scheyltjens, I., Lodi, F., Messiaen, J., Antoranz, A., Duerinck, J., Kancheva, D., Martens, L., De Vlaminck, K., Van Hove, H., Kjølner Hansen, S. S., Bosisio, F. M., Van der Borght, K., De Vleeschouwer, S., Sciot, R., Bouwens, L., Verfaillie, M., Vandamme, N., Vandenbroucke, R. E., . . . Movahedi, K. (2021). Single-cell profiling of myeloid cells in glioblastoma across species and disease stage reveals macrophage competition and specialization. *Nature Neuroscience*, *24*(4), 595-610. https://doi.org/10.1038/s41593-020-00789-y

Poon, M. T. C., Sudlow, C. L. M., Figueroa, J. D., & Brennan, P. M. (2020). Longer-term (≥ 2 years) survival in patients with glioblastoma in population-based studies pre- and post-2005: a systematic review and meta-analysis. *Scientific Reports*, *10*(1), 11622. https://doi.org/10.1038/s41598-020-68011-4

Prosniak, M., Harshyne, L. A., Andrews, D. W., Kenyon, L. C., Bedelbaeva, K., Apanasovich, T. V., Heber-Katz, E., Curtis, M. T., Cotzia, P., & Hooper, D. C. (2013). Glioma grade is associated with the accumulation and activity of cells bearing M2 monocyte markers. *Clin Cancer Res*, *19*(14), 3776-3786. https://doi.org/10.1158/1078-0432.CCR-12-1940

Puig, J., Blasco, G., Daunis, I. E. J., Alberich-Bayarri, A., Essig, M., Jain, R., Remollo, S., Hernández, D., Puigdemont, M., Sánchez-González, J., Mateu, G., Wintermark, M., & Pedraza, S. (2016). High-resolution blood-pool-contrast-enhanced MR angiography in glioblastoma: tumor-associated neovascularization as a biomarker for patient survival. A preliminary study. *Neuroradiology*, *58*(1), 17-26. https://doi.org/10.1007/s00234-015-1599-0

Pyonteck, S. M., Akkari, L., Schuhmacher, A. J., Bowman, R. L., Sevenich, L., Quail, D. F., Olson, O. C., Quick, M. L., Huse, J. T., Teijeiro, V., Setty, M., Leslie, C. S., Oei, Y., Pedraza, A., Zhang, J., Brennan, C. W., Sutton, J. C., Holland, E. C., Daniel, D., & Joyce, J. A. (2013). CSF-1R inhibition alters macrophage polarization and blocks glioma progression. *Nature Medicine*, *19*, 1264-1272. https://doi.org/10.1038/nm.3337

Quail, D. F., Bowman, R. L., Akkari, L., Quick, M. L., Schuhmacher, A. J., Huse, J. T., Holland, E. C., Sutton, J. C., & Joyce, J. A. (2016). The tumor microenvironment underlies acquired resistance to CSF-1R inhibition in gliomas. *Science*, *352*(6288), aad3018. https://doi.org/10.1126/science.aad3018

Raeber, M. E., Rosalia, R. A., Schmid, D., Karakus, U., & Boyman, O. (2020). Interleukin-2 signals converge in a lymphoid-dendritic cell pathway that promotes anticancer immunity. *Sci Transl Med*, *12*(561). https://doi.org/10.1126/scitranslmed.aba5464

Rahbar, A., Cederarv, M., Wolmer-Solberg, N., Tammik, C., Stragliotto, G., Peredo, I., Fornara, O., Xu, X., Dzabic, M., Taher, C., Skarman, P., & Söderberg-Nauclér, C. (2016). Enhanced neutrophil activity is associated with shorter time to tumor progression in glioblastoma patients. *OncoImmunology*, *5*. https://doi.org/10.1080/2162402X.2015.1075693

Rajasekhar, V. K., Viale, A., Socci, N. D., Wiedmann, M., Hu, X., & Holland, E. C. (2003). Oncogenic Ras and Akt Signaling Contribute to Glioblastoma Formation by Differential Recruitment of Existing mRNAs to Polysomes. *Molecular Cell*, *12*(4), 889-901. https://doi.org/https://doi.org/10.1016/S1097-2765(03)00395-2

Ranganathan, P., Clark, P. A., Kuo, J. S., Salamat, M. S., & Kalejta, R. F. (2012). Significant association of multiple human cytomegalovirus genomic Loci with glioblastoma multiforme samples. *J Virol*, *86*(2), 854-864. https://doi.org/10.1128/jvi.06097-11

Reap, E. A., Suryadevara, C. M., Batich, K. A., Sanchez-Perez, L., Archer, G. E., Schmittling, R. J., Norberg, P. K., Herndon, J. E., Healy, P., Congdon, K. L., Gedeon, P. C., Campbell, O. C., Swartz, A. M., Riccione, K. A., Yi, J. S., Hossain-Ibrahim, M. K., Saraswathula, A., Nair, S. K., Dunn-Pirio, A. M., . . . Sampson, J. H. (2018). Dendritic Cells Enhance Polyfunctionality of Adoptively Transferred T Cells That Target Cytomegalovirus in Glioblastoma. *Cancer Research*, *78*(1), 256. https://doi.org/10.1158/0008-5472.CAN-17-0469

Reardon, D. A., Omuro, A., Brandes, A. A., Rieger, J., Wick, A., Sepulveda, J., Phuphanich, S., de Souza, P., Ahluwalia, M. S., Lim, M., Vlahovic, G., & Sampson, J. (2017). OS10.3 Randomized Phase 3 Study Evaluating the Efficacy and Safety of Nivolumab vs Bevacizumab in Patients With Recurrent Glioblastoma: CheckMate 143. *Neuro-Oncology*, *19*, iii21-iii21. https://doi.org/10.1093/neuonc/nox036.071

Ren, Z. P., Olofsson, T., Qu, M., Hesselager, G., Soussi, T., Kalimo, H., Smits, A., & Nistér, M. (2007). Molecular genetic analysis of p53 intratumoral heterogeneity in human astrocytic brain tumors. *J Neuropathol Exp Neurol*, *66*(10), 944-954. https://doi.org/10.1097/nen.0b013e318156bc05

Ricci-Vitiani, L., Pallini, R., Biffoni, M., Todaro, M., Invernici, G., Cenci, T., Maira, G., Parati, E. A., Stassi, G., Larocca, L. M., & De Maria, R. (2010). Tumour vascularization via endothelial differentiation of glioblastoma stem-like cells. *Nature*, *468*, 824-830. https://doi.org/10.1038/nature09557

Roggendorf, W., Strupp, S., & Paulus, W. (1996). Distribution and characterization of microglia/macrophages in human brain tumors. *Acta Neuropathologica*, *92*, 288-293. https://doi.org/10.1007/s004010050520

Roth, T. L., Nayak, D., Atanasijevic, T., Koretsky, A. P., Latour, L. L., & McGavern, D. B. (2014). Transcranial amelioration of inflammation and cell death after brain injury. *Nature*, *505*(7482), 223-228. https://doi.org/10.1038/nature12808

Sabatier, J., Uro-Coste, E., Pommepuy, I., Labrousse, F., Allart, S., Trémoulet, M., Delisle, M. B., & Brousset, P. (2005). Detection of human cytomegalovirus genome and gene products in central nervous system tumours. *Br J Cancer*, *92*(4), 747-750. https://doi.org/10.1038/sj.bjc.6602339

Saederup, N., Cardona, A. E., Croft, K., Mizutani, M., Cotleur, A. C., Tsou, C. L., Ransohoff, R. M., & Charo, I. F. (2010). Selective chemokine receptor usage by central nervous system myeloid cells in CCR2-red fluorescent protein knock-in mice. *PLoS One*, *5*(10), e13693. https://doi.org/10.1371/journal.pone.0013693

Salahuddin, S., Fath, E. K., Biel, N., Ray, A., Moss, C. R., Patel, A., Patel, S., Hilding, L., Varn, M., Ross, T., Cramblet, W. T., Lowrey, A., Pagano, J. S., Shackelford, J., & Bentz, G. L. (2019). Epstein-Barr Virus Latent Membrane Protein-1 Induces the Expression of SUMO-1 and SUMO-2/3 in LMP1-positive Lymphomas and Cells. *Scientific Reports*, *9*(1), 208. https://doi.org/10.1038/s41598-018-36312-4

Salmon, H., Idoyaga, J., Rahman, A., Leboeuf, M., Remark, R., Jordan, S., Casanova-Acebes, M., Khudoynazarova, M., Agudo, J., Tung, N., Chakarov, S., Rivera, C., Hogstad, B., Bosenberg, M., Hashimoto, D., Gnjatic, S., Bhardwaj, N., Palucka, A. K., Brown, B. D., . . . Merad, M. (2016). Expansion and Activation of CD103+ Dendritic Cell Progenitors at the Tumor Site Enhances Tumor Responses to Therapeutic PD-L1 and BRAF Inhibition. *Immunity*, *44*, 924-938. https://doi.org/10.1016/j.immuni.2016.03.012

Sampson, J. H., Gunn, M. D., Fecci, P. E., & Ashley, D. M. (2020). Brain immunology and immunotherapy in brain tumours. *Nat Rev Cancer*, *20*(1), 12-25. https://doi.org/10.1038/s41568-019-0224-7

Sankowski, R., Bottcher, C., Masuda, T., Geirsdottir, L., Sagar, Sindram, E., Seredenina, T., Muhs, A., Scheiwe, C., Shah, M. J., Heiland, D. H., Schnell, O., Grun, D., Priller, J., & Prinz, M. (2019). Mapping microglia states in the human brain through the integration of high-dimensional techniques. *Nat Neurosci*, *22*(12), 2098-2110. https://doi.org/10.1038/s41593-019-0532-y

Sarkar, S., Li, Y., Mirzaei, R., Rawji, K. S., Poon, C. C., Wang, J., Kumar, M., Bose, P., & Yong, V. W. (2020). Demeclocycline Reduces the Growth of Human Brain Tumor-Initiating Cells: Direct Activity and Through Monocytes. *Front Immunol*, *11*. https://doi.org/10.3389/fimmu.2020.00272

Sarkar, S., Yang, R., Mirzaei, R., Rawji, K., Poon, C., Mishra, M. K., Zemp, F. J., Bose, P., Kelly, J., Dunn, J. F., & Yong, V. W. (2020). Control of brain tumor growth by reactivating myeloid cells with niacin. *Sci Transl Med*, *12*, eaay9924. https://doi.org/10.1126/scitranslmed.aay9924

Sarkaria, J. N., Hu, L. S., Parney, I. F., Pafundi, D. H., Brinkmann, D. H., Laack, N. N., Giannini, C., Burns, T. C., Kizilbash, S. H., Laramy, J. K., Swanson, K. R., Kaufmann, T. J., Brown, P. D., Agar, N. Y. R., Galanis, E., Buckner, J. C., & Elmquist, W. F. (2018). Is the blood–brain barrier really disrupted in all glioblastomas? A critical

assessment of existing clinical data. *Neuro-Oncology*, *20*, 184-191. https://doi.org/10.1093/neuonc/nox175

Satoh, E., Mabuchi, T., Satoh, H., Asahara, T., Nukui, H., & Naganuma, H. (2006). Reduced expression of the transporter associated with antigen processing 1 molecule in malignant glioma cells, and its restoration by interferon-gamma and -beta. *J Neurosurg*, *104*(2), 264-271. https://doi.org/10.3171/jns.2006.104.2.264

Sayour, E. J., McLendon, P., McLendon, R., De Leon, G., Reynolds, R., Kresak, J., Sampson, J. H., & Mitchell, D. A. (2015). Increased proportion of FoxP3+ regulatory T cells in tumor infiltrating lymphocytes is associated with tumor recurrence and reduced survival in patients with glioblastoma. *Cancer Immunol Immunother*, *64*(4), 419-427. https://doi.org/10.1007/s00262-014-1651-7

Scheurer, M. E., Bondy, M. L., Aldape, K. D., Albrecht, T., & El-Zein, R. (2008). Detection of human cytomegalovirus in different histological types of gliomas. *Acta Neuropathol*, *116*(1), 79-86. https://doi.org/10.1007/s00401-008-0359-1

Schuessler, A., Smith, C., Beagley, L., Boyle, G. M., Rehan, S., Matthews, K., Jones, L., Crough, T., Dasari, V., Klein, K., Smalley, A., Alexander, H., Walker, D. G., & Khanna, R. (2014). Autologous T-cell therapy for cytomegalovirus as a consolidative treatment for recurrent glioblastoma. *Cancer Res*, *74*(13), 3466-3476. https://doi.org/10.1158/0008-5472.Can-14-0296

Serafino, A., Balestrieri, E., Pierimarchi, P., Matteucci, C., Moroni, G., Oricchio, E., Rasi, G., Mastino, A., Spadafora, C., Garaci, E., & Vallebona, P. S. (2009). The activation of human endogenous retrovirus K (HERV-K) is implicated in melanoma cell malignant transformation. *Exp Cell Res*, *315*(5), 849-862. https://doi.org/10.1016/j.yexcr.2008.12.023

Sidransky, D., Mikkelsen, T., Schwechheimer, K., Rosenblum, M. L., Cavanee, W., & Vogelstein, B. (1992). Clonal expansion of p53 mutant cells is associated with brain tumour progression. *Nature*, *355*(6363), 846-847. https://doi.org/10.1038/355846a0

Sippel, T. R., White, J., Nag, K., Tsvankin, V., Klaassen, M., Kleinschmidt-DeMasters, B. K., & Waziri, A. (2011). Neutrophil degranulation and immunosuppression in patients with GBM: restoration of cellular immune function by targeting arginase I. *Clin Cancer Res*, *17*(22), 6992-7002. https://doi.org/10.1158/1078-0432.CCR-11-1107

Słońska, A., Cymerys, J., Chodkowski, M., Bąska, P., Krzyżowska, M., & Bańbura, M. W. (2021). Human herpesvirus type 2 infection of primary murine astrocytes causes disruption of the mitochondrial network and remodeling of the actin cytoskeleton: an in vitro morphological study. *Arch Virol*, *166*(5), 1371-1383. https://doi.org/10.1007/s00705-021-05025-x

Smith, C., Lineburg, K. E., Martins, J. P., Ambalathingal, G. R., Neller, M. A., Morrison, B., Matthews, K. K., Rehan, S., Crooks, P., Panikkar, A., Beagley, L., Le Texier, L., Srihari, S., Walker, D., & Khanna, R. (2020). Autologous CMV-specific T cells are a safe adjuvant immunotherapy for primary glioblastoma multiforme. *J Clin Invest*, *130*(11), 6041-6053. https://doi.org/10.1172/jci138649

Soldan, S. S., & Lieberman, P. M. (2020). Epstein-Barr Virus Infection in the Development of Neurological Disorders. *Drug Discov Today Dis Models*, *32*(Pt A), 35-52. https://doi.org/10.1016/j.ddmod.2020.01.001

Song, E., Mao, T., Dong, H., Boisserand, L. S. B., Antila, S., Bosenberg, M., Alitalo, K., Thomas, J. L., & Iwasaki, A. (2020). VEGF-C-driven lymphatic drainage enables immunosurveillance of brain tumours. *Nature*, *577*, 689-694. https://doi.org/10.1038/s41586-019-1912-x

Spector, D. H. (2015). Human cytomegalovirus riding the cell cycle. *Medical Microbiology and Immunology*, *204*(3), 409-419. https://doi.org/10.1007/s00430-015-0396-z

Stragliotto, G., Pantalone, M. R., Rahbar, A., Bartek, J., & Söderberg-Naucler, C. (2020). Valganciclovir as Add-on to Standard Therapy in Glioblastoma Patients. *Clin Cancer Res*, *26*(15), 4031-4039. https://doi.org/10.1158/1078-0432.Ccr-20-0369

Strong, M. J., Blanchard, E. t., Lin, Z., Morris, C. A., Baddoo, M., Taylor, C. M., Ware, M. L., & Flemington, E. K. (2016). A comprehensive next generation sequencing-based virome assessment in brain tissue suggests no major virus - tumor association. *Acta Neuropathol Commun*, *4*(1), 71. https://doi.org/10.1186/s40478-016-0338-z

Stupp, R., Hegi, M. E., Mason, W. P., van den Bent, M. J., Taphoorn, M. J., Janzer, R. C., Ludwin, S. K., Allgeier, A., Fisher, B., Belanger, K., Hau, P., Brandes, A. A., Gijtenbeek, J., Marosi, C., Vecht, C. J., Mokhtari, K., Wesseling, P., Villa, S., Eisenhauer, E., . . . Mirimanoff, R. O. (2009). Effects of radiotherapy with concomitant and adjuvant temozolomide versus radiotherapy alone on survival in glioblastoma in a randomised phase III study: 5-year analysis of the EORTC-NCIC trial. *Lancet Oncol*, *10*(5), 459-466. https://doi.org/10.1016/s1470-2045(09)70025-7

Stupp, R., Taillibert, S., Kanner, A., Read, W., Steinberg, D., Lhermitte, B., Toms, S., Idbaih, A., Ahluwalia, M. S., Fink, K., Di Meco, F., Lieberman, F., Zhu, J. J., Stragliotto, G., Tran, D., Brem, S., Hottinger, A., Kirson, E. D., Lavy-Shahaf, G., . . . Ram, Z. (2017). Effect of Tumor-Treating Fields Plus Maintenance Temozolomide vs Maintenance Temozolomide Alone on Survival in Patients With Glioblastoma: A Randomized Clinical Trial. *JAMA*, *318*(23), 2306-2316. https://doi.org/10.1001/jama.2017.18718

Szatmári, T., Lumniczky, K., Désaknai, S., Trajcevski, S., Hídvégi, E. J., Hamada, H., & Sáfrány, G. (2006). Detailed characterization of the mouse glioma 261 tumor model for experimental glioblastoma therapy. *Cancer Sci*, *97*(6), 546-553. https://doi.org/10.1111/j.1349-7006.2006.00208.x

Szulzewsky, F., Schwendinger, N., Guneykaya, D., Cimino, P. J., Hambardzumyan, D., Synowitz, M., Holland, E. C., & Kettenmann, H. (2018). Loss of host-derived osteopontin creates a glioblastoma-promoting microenvironment. *Neuro Oncol*, *20*(3), 355-366. https://doi.org/10.1093/neuonc/nox165

Takenaka, M. C., Gabriely, G., Rothhammer, V., Mascanfroni, I. D., Wheeler, M. A., Chao, C. C., Gutierrez-Vazquez, C., Kenison, J., Tjon, E. C., Barroso, A., Vandeventer, T., de Lima, K. A., Rothweiler, S., Mayo, L., Ghannam, S., Zandee, S., Healy, L., Sherr, D., Farez, M. F., . . . Quintana, F. J. (2019). Control of tumor-associated

macrophages and T cells in glioblastoma via AHR and CD39. *Nat Neurosci*, *22*(5), 729-740. https://doi.org/10.1038/s41593-019-0370-y

Tawbi, H. A., Forsyth, P. A., Algazi, A., Hamid, O., Hodi, F. S., Moschos, S. J., Khushalani, N. I., Lewis, K., Lao, C. D., Postow, M. A., Atkins, M. B., Ernstoff, M. S., Reardon, D. A., Puzanov, I., Kudchadkar, R. R., Thomas, R. P., Tarhini, A., Pavlick, A. C., Jiang, J., . . . Margolin, K. (2018). Combined Nivolumab and Ipilimumab in Melanoma Metastatic to the Brain. *N Engl J Med*, *379*(8), 722-730. https://doi.org/10.1056/NEJMoa1805453

Theisen, D. J., Davidson, J. T., Briseño, C. G., Gargaro, M., Lauron, E. J., Wang, Q., Desai, P., Durai, V., Bagadia, P., Brickner, J. R., Beatty, W. L., Virgin, H. W., Gillanders, W. E., Mosammaparast, N., Diamond, M. S., Sibley, L. D., Yokoyama, W., Schreiber, R. D., Murphy, T. L., & Murphy, K. M. (2018). WDFY4 is required for cross-presentation in response to viral and tumor antigens. *Science*, *362*, 694-699. https://doi.org/10.1126/science.aat5030

Thomas, A. A., Fisher, J. L., Rahme, G. J., Hampton, T. H., Baron, U., Olek, S., Schwachula, T., Rhodes, C. H., Gui, J., Tafe, L. J., Tsongalis, G. J., Lefferts, J. A., Wishart, H., Kleen, J., Miller, M., Whipple, C. A., De Abreu, F. B., Ernstoff, M. S., & Fadul, C. E. (2015). Regulatory T cells are not a strong predictor of survival for patients with glioblastoma. *Neuro Oncol*, *17*(6), 801-809. https://doi.org/10.1093/neuonc/nou363

Thompson, E., Landi, D., Thompson, E., Lipp, E., Balajonda, B., Herndon, J., II, Buckley, E., Flahiff, C., Jaggers, D., Schroeder, K., Randazzo, D., Desjardins, A., Johnson, M., Peters, K., Khasraw, M., Malinzak, M., Mitchell, D., Ashley, D., & Sampson, J. (2020). CTIM-21. Peptide vaccine directed to CMV pp65 for treatment of recurrent malignant glioma and medulloblastoma in children and young adults: preliminary results of a phase I trial. *Neuro-Oncology*, *22*(Supplement_2), ii37-ii37. https://doi.org/10.1093/neuonc/noaa215.155

Todo, T. (2019). ATIM-14. Results of phase II clinical trial of oncolytic herpes virus G47Δ in patients with glioblastoma. *Neuro-Oncology*, *21*(Supplement_6), vi4-vi4. https://doi.org/10.1093/neuonc/noz175.014

Trent, J., Meltzer, P., Rosenblum, M., Harsh, G., Kinzler, K., Mashal, R., Feinberg, A., & Vogelstein, B. (1986). Evidence for rearrangement, amplification, and expression of c-myc in a human glioblastoma. *Proc Natl Acad Sci U S A*, *83*(2), 470-473. https://doi.org/10.1073/pnas.83.2.470

Tsui, K., Gajjar, A., Li, C., Srivastava, D., Broniscer, A., Wetmore, C., Kun, L. E., Merchant, T. E., Ellison, D. W., Orr, B. A., Boop, F. A., Klimo, P., Ross, J., Robison, L. L., & Armstrong, G. T. (2012015). Subsequent neoplasms in survivors of childhood central nervous system tumors: risk after modern multimodal therapy. *Neuro-Oncology*, *17*, 448-456. https://doi.org/10.1093/NEUONC

Turkowski, K., Brandenburg, S., Mueller, A., Kremenetskaia, I., Bungert, A. D., Blank, A., Felsenstein, M., & Vajkoczy, P. (2018). VEGF as a modulator of the innate immune response in glioblastoma. *GLIA*, *66*, 161-174. https://doi.org/10.1002/glia.23234

van Montfoort, N., Borst, L., Korrer, M. J., Sluijter, M., Marijt, K. A., Santegoets, S. J., van Ham, V. J., Ehsan, I., Charoentong, P., André, P., Wagtmann, N., Welters, M. J. P.,

Kim, Y. J., Piersma, S. J., van der Burg, S. H., & van Hall, T. (2018). NKG2A Blockade Potentiates CD8 T Cell Immunity Induced by Cancer Vaccines. *Cell*, *175*, 1744-1755.e1715. https://doi.org/10.1016/j.cell.2018.10.028

Vogelstein, B., Papadopoulos, N., Velculescu, V. E., Zhou, S., Diaz, L. A., Jr., & Kinzler, K. W. (2013). Cancer genome landscapes. *Science*, *339*(6127), 1546-1558. https://doi.org/10.1126/science.1235122

Waggener, J. D., & Beggs, J. (1967). The membranous coverings of neural tissues: an electron microscopy study. *J Neuropathol Exp Neurol*, *26*(3), 412-426. https://doi.org/10.1097/00005072-196707000-00005

Wainwright, D. A., Sengupta, S., Han, Y., & Lesniak, M. S. (2011). Thymus-derived rather than tumor-induced regulatory T cells predominate in brain tumors. *Neuro Oncol*, *13*(12), 1308-1323. https://doi.org/10.1093/neuonc/nor134

Wang, Q., Hu, B., Hu, X., Kim, H., Squatrito, M., Scarpace, L., deCarvalho, A. C., Lyu, S., Li, P., Li, Y., Barthel, F., Cho, H. J., Lin, Y. H., Satani, N., Martinez-Ledesma, E., Zheng, S., Chang, E., Sauvé, C. E. G., Olar, A., . . . Verhaak, R. G. W. (2017). Tumor Evolution of Glioma-Intrinsic Gene Expression Subtypes Associates with Immunological Changes in the Microenvironment. *Cancer Cell*, *32*, 42-56.e46. https://doi.org/10.1016/j.ccell.2017.06.003

Wang, Q., Hu, B., Hu, X., Kim, H., Squatrito, M., Scarpace, L., deCarvalho, A. C., Lyu, S., Li, P., Li, Y., Barthel, F., Cho, H. J., Lin, Y. H., Satani, N., Martinez-Ledesma, E., Zheng, S., Chang, E., Sauvé, C. G., Olar, A., . . . Verhaak, R. G. W. (2017). Tumor Evolution of Glioma-Intrinsic Gene Expression Subtypes Associates with Immunological Changes in the Microenvironment. *Cancer Cell*, *32*(1), 42-56.e46. https://doi.org/10.1016/j.ccell.2017.06.003

Wang, R., Chadalavada, K., Wilshire, J., Kowalik, U., Hovinga, K. E., Geber, A., Fligelman, B., Leversha, M., Brennan, C., & Tabar, V. (2010). Glioblastoma stem-like cells give rise to tumour endothelium. *Nature*, *468*, 829-835. https://doi.org/10.1038/nature09624

Wang, X., Prager, B. C., Mack, S. C., Bao, S., & Correspondence, J. N. R. (2018). Reciprocal Signaling between Glioblastoma Stem Cells and Differentiated Tumor Cells Promotes Malignant Progression. *Stem Cell*, *22*, 514-528.e515. https://doi.org/10.1016/j.stem.2018.03.011

Wang-Johanning, F., Liu, J., Rycaj, K., Huang, M., Tsai, K., Rosen, D. G., Chen, D. T., Lu, D. W., Barnhart, K. F., & Johanning, G. L. (2007). Expression of multiple human endogenous retrovirus surface envelope proteins in ovarian cancer. *Int J Cancer*, *120*(1), 81-90. https://doi.org/10.1002/ijc.22256

Wang-Johanning, F., Radvanyi, L., Rycaj, K., Plummer, J. B., Yan, P., Sastry, K. J., Piyathilake, C. J., Hunt, K. K., & Johanning, G. L. (2008). Human endogenous retrovirus K triggers an antigen-specific immune response in breast cancer patients. *Cancer Res*, *68*(14), 5869-5877. https://doi.org/10.1158/0008-5472.Can-07-6838

Weathers, S. P., & de Groot, J. (2015). VEGF Manipulation in Glioblastoma. *Oncology (Williston Park)*, *29*(10), 720-727.

Weathers, S. P., Penas-Prado, M., Pei, B. L., Ling, X., Kassab, C., Banerjee, P., Bdiwi, M., Shaim, H., Alsuliman, A., Shanley, M., de Groot, J. F., O'Brien, B. J., Harrison, R., Majd, N., Kamiya-Matsuoka, C., Fuller, G. N., Huse, J. T., Chi, L., Rao, G., . . . Heimberger, A. B. (2020). Glioblastoma-mediated Immune Dysfunction Limits CMV-specific T Cells and Therapeutic Responses: Results from a Phase I/II Trial. *Clin Cancer Res*, *26*(14), 3565-3577. https://doi.org/10.1158/1078-0432.CCR-20-0176

Wei, J., Gabrusiewicz, K., & Heimberger, A. (2013). The controversial role of microglia in malignant gliomas. *Clin Dev Immunol*, *2013*, 285246. https://doi.org/10.1155/2013/285246

Wei, J., Marisetty, A., Schrand, B., Gabrusiewicz, K., Hashimoto, Y., Ott, M., Grami, Z., Kong, L. Y., Ling, X., Caruso, H., Zhou, S., Wang, Y. A., Fuller, G. N., Huse, J., Gilboa, E., Kang, N., Huang, X., Verhaak, R., Li, S., & Heimberger, A. B. (2019). Osteopontin mediates glioblastoma-associated macrophage infiltration and is a potential therapeutic target. *J Clin Invest*, *129*(1), 137-149. https://doi.org/10.1172/JCI121266

Welsh, R. M., & Seedhom, M. O. (2008). Lymphocytic choriomeningitis virus (LCMV): propagation, quantitation, and storage. *Curr Protoc Microbiol*, *Chapter 15*, Unit 15A.11. https://doi.org/10.1002/9780471729259.mc15a01s8

Wetzel, S. A., McKeithan, T. W., & Parker, D. C. (2002). Live-Cell Dynamics and the Role of Costimulation in Immunological Synapse Formation. *The Journal of Immunology*, *169*(11), 6092-6101. https://doi.org/10.4049/jimmunol.169.11.6092

Wiesner, S. M., Freese, A., & Ohlfest, J. R. (2005). Emerging concepts in glioma biology: implications for clinical protocols and rational treatment strategies. *Neurosurg Focus*, *19*(4), E3. https://doi.org/10.3171/foc.2005.19.4.4

Wingerath, J., Ostroumov, D., Woller, N., Manns, M. P., Pinschewer, D. D., Orlinger, K., Berka, U., Kühnel, F., & Wirth, T. C. (2017). Recombinant LCMV Vectors Induce Protective Immunity following Homologous and Heterologous Vaccinations. *Mol Ther*, *25*(11), 2533-2545. https://doi.org/10.1016/j.ymthe.2017.07.012

Wischhusen, J., Friese, M. A., Mittelbronn, M., Meyermann, R., & Weller, M. (2005). HLA-E Protects Glioma Cells from NKG2D-Mediated Immune Responses In Vitro: Implications for Immune Escape In Vivo. *Journal of Neuropathology & Experimental Neurology*, *64*, 523-528. https://doi.org/10.1093/jnen/64.6.523

Woroniecka, K., Chongsathidkiet, P., Rhodin, K., Kemeny, H., Dechant, C., Farber, S. H., Elsamadicy, A. A., Cui, X., Koyama, S., Jackson, C., Hansen, L. J., Johanns, T. M., Sanchez-Perez, L., Chandramohan, V., Yu, Y. A., Bigner, D. D., Giles, A., Healy, P., Dranoff, G., . . . Fecci, P. E. (2018). T-Cell Exhaustion Signatures Vary with Tumor Type and Are Severe in Glioblastoma. *Clin Cancer Res*, *24*(17), 4175-4186. https://doi.org/10.1158/1078-0432.CCR-17-1846

Wu, A., Wei, J., Kong, L.-Y., Wang, Y., Priebe, W., Qiao, W., Sawaya, R., & Heimberger, A. B. (2010). Glioma cancer stem cells induce immunosuppressive macrophages/microglia. *Neuro-Oncology*, *12*, 1113-1125. https://doi.org/10.1093/neuonc/noq082

Yang, I., Tihan, T., Han, S. J., Wrensch, M. R., Wiencke, J., Sughrue, M. E., & Parsa, A. T. (2010). CD8+ T-cell infiltrate in newly diagnosed glioblastoma is associated with long-term survival. *Journal of Clinical Neuroscience*, *17*, 1381-1385. https://doi.org/10.1016/j.jocn.2010.03.031

Yeung, J. T., Hamilton, R. L., Ohnishi, K., Ikeura, M., Potter, D. M., Nikiforova, M. N., Ferrone, S., Jakacki, R. I., Pollack, I. F., & Okada, H. (2013). LOH in the HLA class I region at 6p21 is associated with shorter survival in newly diagnosed adult glioblastoma. *Clin Cancer Res*, *19*(7), 1816-1826. https://doi.org/10.1158/1078-0432.CCR-12-2861

Yuan, Z., Yang, Y., Zhang, N., Soto, C., Jiang, X., An, Z., & Zheng, W. J. (2021). Human Endogenous Retroviruses in Glioblastoma Multiforme. *Microorganisms*, *9*(4). https://doi.org/10.3390/microorganisms9040764

Yue, Q., Zhang, X., Ye, H. X., Wang, Y., Du, Z. G., Yao, Y., & Mao, Y. (2014). The prognostic value of Foxp3+ tumor-infiltrating lymphocytes in patients with glioblastoma. *Journal of Neuro-Oncology*, *116*, 251-259. https://doi.org/10.1007/s11060-013-1314-0

Zeiner, P. S., Preusse, C., Golebiewska, A., Zinke, J., Iriondo, A., Muller, A., Kaoma, T., Filipski, K., Müller-Eschner, M., Bernatz, S., Blank, A. E., Baumgarten, P., Ilina, E., Grote, A., Hansmann, M. L., Verhoff, M. A., Franz, K., Feuerhake, F., Steinbach, J. P., . . . Mittelbronn, M. (2019). Distribution and prognostic impact of microglia/macrophage subpopulations in gliomas. *Brain Pathology*, *29*, 513-529. https://doi.org/10.1111/bpa.12690

Zha, C., Meng, X., Li, L., Mi, S., Qian, D., Li, Z., Wu, P., Hu, S., Zhao, S., Cai, J., & Liu, Y. (2020). Neutrophil extracellular traps mediate the crosstalk between glioma progression and the tumor microenvironment via the HMGB1/RAGE/IL-8 axis. *Cancer Biol Med*, *17*(1), 154-168. https://doi.org/10.20892/j.issn.2095-3941.2019.0353

Zhang, C., Wang, X. M., Li, S. R., Twelkmeyer, T., Wang, W. H., Zhang, S. Y., Wang, S. F., Chen, J. Z., Jin, X., Wu, Y. Z., Chen, X. W., Wang, S. D., Niu, J. Q., Chen, H. R., & Tang, H. (2019). NKG2A is a NK cell exhaustion checkpoint for HCV persistence. *Nat Commun*, *10*(1), 1507. https://doi.org/10.1038/s41467-019-09212-y

Zhang, J., Caruso, F. P., Sa, J. K., Justesen, S., Nam, D. H., Sims, P., Ceccarelli, M., Lasorella, A., & Iavarone, A. (2019). The combination of neoantigen quality and T lymphocyte infiltrates identifies glioblastomas with the longest survival. *Commun Biol*, *2*, 135. https://doi.org/10.1038/s42003-019-0369-7

Zhou, Q., Guo, P., Kruh, G. D., Vicini, P., Wang, X., & Gallo, J. M. (2007). Predicting human tumor drug concentrations from a preclinical pharmacokinetic model of temozolomide brain disposition. *Clin Cancer Res*, *13*(14), 4271-4279. https://doi.org/10.1158/1078-0432.Ccr-07-0658

Zhu, X., Fujita, M., Snyder, L. A., & Okada, H. (2011). Systemic delivery of neutralizing antibody targeting CCL2 for glioma therapy. *Journal of Neuro-Oncology*, *104*, 83-92. https://doi.org/10.1007/s11060-010-0473-5

Zhu, Z., Gorman, M. J., McKenzie, L. D., Chai, J. N., Hubert, C. G., Prager, B. C., Fernandez, E., Richner, J. M., Zhang, R., Shan, C., Tycksen, E., Wang, X., Shi, P.-Y., Diamond, M.

S., Rich, J. N., & Chheda, M. G. (2017). Zika virus has oncolytic activity against glioblastoma stem cells. *Journal of Experimental Medicine*, *214*(10), 2843-2857. https://doi.org/10.1084/jem.20171093

Zhu, Z., Mesci, P., Bernatchez, J. A., Gimple, R. C., Wang, X., Schafer, S. T., Wettersten, H. I., Beck, S., Clark, A. E., Wu, Q., Prager, B. C., Kim, L. J. Y., Dhanwani, R., Sharma, S., Garancher, A., Weis, S. M., Mack, S. C., Negraes, P. D., Trujillo, C. A., . . . Rich, J. N. (2020). Zika Virus Targets Glioblastoma Stem Cells through a SOX2-Integrin αvβ5 Axis. *Cell Stem Cell*, *26*(2), 187-204.e110. https://doi.org/https://doi.org/10.1016/j.stem.2019.11.016

Zinselmeyer, B. H., Heydari, S., Sacristán, C., Nayak, D., Cammer, M., Herz, J., Cheng, X., Davis, S. J., Dustin, M. L., & McGavern, D. B. (2013). PD-1 promotes immune exhaustion by inducing antiviral T cell motility paralysis. *Journal of Experimental Medicine*, *210*(4), 757-774. https://doi.org/10.1084/jem.20121416